



Norwegian University of  
Science and Technology

# The Kværnerdammen F1 project - A comparison of constitutive models in PLAXIS and GeoSuite Excavation to in- situ measurements

**Bernhard Naglestad**  
**Michal Sperre**

Geotechnology

Submission date: June 2018

Supervisor: Bjørn Frengstad, IGP

Co-supervisor: Steinar Nordal, IBM  
Anders Ulvestad, Multiconsult  
Corneliu Athanasiu, Multiconsult

Norwegian University of Science and Technology  
Department of Geoscience and Petroleum





Report Title: <b>The Kværnerdammen F1 project – A comparison of constitutive models in PLAXIS and GeoSuite Excavation to in-situ measurements</b>	Dato: <b>14.06.2018</b>
	Number of pages (incl. appendix): 260
	Master Thesis   x
Names: Bernhard Naglestad and Michal Sperre	
Professor in charge/supervisor: Steinar Nordal	
Other external professional contacts/supervisors: Anders Ulvestad, Corneliu Athanasiu, Bjørn Frengstad	

**Abstract:**

The project Kværnerdammen F1 in Oslo comprises a seven-story building at the toe of a slope, partly consisting of quick clay. Multiconsult is the geotechnical consultant on the project and designed a multi-anchored sheet pile wall (SPW) bolted to bedrock, securing the building pit. Lime cement columns (LCC) was used in front of the SPW to increase stability. This thesis compares results of different soil models in the finite element program PLAXIS 2D and the spring supported beam program GeoSuite Excavation (GS) to measured behavior of the SPW during construction of the building pit. Layers of silty clay and quick clay are modeled in PLAXIS with the constitutive models: Hardening Soil (HS), NGI-ADP and Mohr Coulomb (MC). In GS, the clay layers are modeled using the Total Stress Automatic option. Using different models to calculate the same problem raises the question; Which of the models are the most accurate when compared to measured behavior?

A study was performed to gather necessary information about the project and on theory about the different models in each software. The soil parameters were tuned to a strength profile based on CPTu and triaxial tests from the area. A parametric study was performed primarily to examine the effects of LCC and roughness.

NGI-ADP gives the best fit to the measured displacements. When tuning models to a strength profile it easily goes at the expense of stiffness, especially for the HS model. HS is capable to model the long-term effect after consolidation, but may have difficulties in reproducing both short term and long term conditions using one parameter set. Comparing simulated and measured anchor forces was challenging since the load cells are placed at some distance from the chosen cross section. Still, all models seem to give an acceptable fit to the measured anchor forces, except for MC. The model gives too large displacements and the user should be careful when using this model on a multi-anchored wall as the anchor forces might not be representative. Inserting an unloading/reloading stiffness in MC by changing material parameters between phases, gives better results. In NGI-ADP, stiffness and strength relates through a stiffness ratio  $G/s_u$  which seems to contribute in making the model fit better to measured behavior. Among the models used, the NGI-ADP is the one where changes in the input roughness number has the lowest influence on the results. Including LCC in the modeling seems to increase the accuracy of the results for most models.

It is difficult to find the balance between increasing the strength and maintaining the desired stiffness in GS. The installation of anchors will push the wall back towards the soil and active and passive zones in the profile may change during the phases. In GS, the roughness parameter used must be given a direction before calculating the project, and cannot be changed during the calculations. Nevertheless, modeling in GS produces surprisingly good results compared to the measured values, where partly including LCC in the model were most accurate.

Obtaining realistic anchor forces when calculating by hand is challenging for this project. With several simplifications, too low forces were obtained from hand calculations, as pre-stressing of anchors and stiffness of the wall are not included. The use of numerical models is an advantage when calculating a multi-anchored SPW in sloping terrain.

**Keywords:**

1. Modeling of excavation, PLAXIS 2D and GS
2. Multi-anchored SPW in sloping terrain
3. Roughness and lime cement columns
4. NGI-ADP, MC, HS

  
(sign.)

**MASTER DEGREE THESIS**

Spring 2018

for

Students Bernhard Naglestad and Michal Sperre

**The Kværnerdammen F1 project – A comparison of constitutive models in PLAXIS and GeoSuite Excavation to in-situ measurements****BACKGROUND**

Multiconsult is the geotechnical consultant for the Kværnerdammen F1 project in Oslo involving an excavation for a seven-story building at the foot of a slope. The slope contains layers of clay, partly quick. A permanent, anchored sheet pile wall (SPW) is installed to bedrock and lime cement columns (LCC) are used to ensure the stability of the slope. Two rows of anchors are installed to bedrock at different levels while the SPW itself is bolted to bedrock. The project combines a slope stability problem with an earth pressure problem. Appropriate modeling of the system and the soil response is crucial for predicting deformations and assessing the proper stability measures. Complex problems of this type are often analysed by the Finite Element method (FE), and PLAXIS is one special tailored FE program for geotechnical design. GeoSuite Excavation (GS) is a spring supported beam type software for retaining walls developed in Norway and Sweden with a goal to make the calculations as fast, easy and user-friendly as possible. Application of this program is also of interest for Kværnerdammen F1.

**TASK**

The task is to simulate the anchored wall by PLAXIS and GS using various constitutive models and to compare results from the simulations to measured behaviour of the wall during construction.

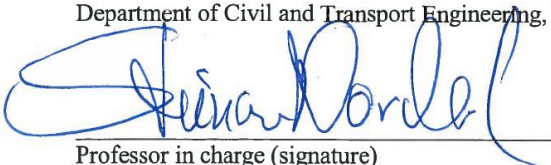
The aim of this thesis is to compare the measured anchor forces and deformations at Kværnerdammen F1 to the results from GS Total Stress Automatic model and simulations with three constitutive models in PLAXIS 2D: Hardening soil, NGI-ADP and Mohr Coulomb. This involves defining a representative cross section, a soil profile and selecting material parameters to fit a strength profile and tuning various parameters to see which model is most appropriate.

Multiconsult suggests that additional focus is put on a parametric study regarding roughness and the effect of modeling the lime cement columns in front of the SPW. This raises the questions:

- Which of the models are best compared to measured data?
- How does modeling of LCC in front of the SPW affect the results?

**Professor in charge:**

Prof. Steinar Nordal  
Department of Civil and Transport Engineering, NTNU



Professor in charge (signature)



---

# Summary

The project Kværnerdammen F1 in Oslo comprises a seven-story building at the toe of a slope, partly consisting of quick clay. Multiconsult is the geotechnical consultant on the project and designed a multi-anchored sheet pile wall (SPW) bolted to bedrock, securing the building pit. Lime cement columns (LCC) was used in front of the SPW to increase stability. This thesis compares results of different soil models in the finite element program PLAXIS 2D and the spring supported beam program GeoSuite Excavation (GS) to measured behavior of the SPW during construction of the building pit. Layers of silty clay and quick clay are modeled in PLAXIS with the constitutive models: Hardening Soil (HS), NGI-ADP and Mohr Coulomb (MC). In GS the clay layers are modeled using the Total Stress Automatic option. Using different models to calculate the same problem raises the question; Which of the models are the most accurate when compared to measured behavior?

A study was performed to gather necessary information about the project and on theory about the different models in each software. The soil parameters were tuned to a strength profile based on CPTu and triaxial tests from the area. A parametric study was performed primarily to examine the effects of LCC and roughness.

NGI-ADP gives the best fit to the measured displacements. When tuning models to a strength profile it easily goes at the expense of stiffness, especially for the HS model. HS is capable to model the long-term effect after consolidation, but may have difficulties in reproducing both short term and long term conditions using one parameter set. Comparing simulated and measured anchor forces was challenging since the load cells were placed at some distance from the chosen cross section. Still, all models seem to give an acceptable fit to the measured anchor forces, except for MC. The model gives too large displacements and the user should be careful when using this model on a multi-anchored wall as the anchor forces might not be representative. Inserting an unloading/reloading stiffness in MC by changing material parameters between phases, gives better results. In NGI-ADP, stiffness and strength relates through a stiffness ratio  $G/s_u$  which seems to contribute in making the model fit better to measured behavior. Among the models used, the NGI-ADP is the one where changes in the input roughness number has the lowest influence on the results. Including LCC in the modeling seems to increase the accuracy of the results for most models.

It is difficult to find the balance between increasing the strength and maintaining the desired stiffness in GS. The installation of anchors will push the wall back towards the soil and active and passive zones in the profile may change during the phases. In GS, the roughness parameter used must be given a direction before calculating the project, and cannot be changed during the calculations. Nevertheless, modeling in GS produces surprisingly good results compared to the measured values, where including LCC with partial effect in the model were most accurate.

---

Obtaining realistic anchor forces when calculating by hand is challenging for this project. With several simplifications, too low forces were obtained from hand calculations, as prestressing of anchors and stiffness of the wall are not included. The use of numerical models is an advantage when calculating a multi-anchored SPW in sloping terrain.

---

# Sammendrag

Prosjektet Kværnerdammen F1 i Oslo består av en syv-etasjers bygning ved enden av en skråning, delvis bestående av kvikkleire. Multiconsult er ansatt som RIG på prosjektet og designet en flerforankret spuntvegg boltet til berggrunn for å sikre byggegroppen. Kalksementstabilisering (LCC) ble brukt foran spunt for å øke stabiliteten. Denne oppgaven sammenligner resultater fra ulike jordmodeller i elementprogrammet PLAXIS 2D og det fjærstøttede bjelkeelementprogrammet GeoSuite Excavation (GS) mot målt oppførsel av spuntveggen. Lag av siltig leire og kvikkleire er modellert i PLAXIS med modellene: Hardening Soil (HS), NGI-ADP og Mohr Coulomb (MC). I GS modelleres leiragene ved hjelp av Total Stress Automatic. Å bruke ulike modeller for å simulere det samme utgravningsproblemet fører til spørsmålet; Hvilken modell er mest nøyaktig sammenlignet med målt oppførsel?

En teoretisk studie ble utført for å samle nødvendig informasjon om prosjektet og teori om de ulike modellene i hvert program. Jordparameterne ble tilpasset et styrkeprofil basert på CPTu og triaksialtester fra området. En parametrisk studie ble utført for å undersøke den simulerte effekten av LCC og ruhet.

NGI-ADP gir best resultat til de målte forskyvningene. Når modeller tilpasses et styrkeprofil går det på bekostning av stivhet, spesielt for HS-modellen. HS er i stand til å modellere den langsiktige oppførselen etter konsolidering, men kan ha problemer med å produsere både kortsiktige og langsiktige realistiske forhold ved å bruke ett parametersett. Sammenligning av simulerte og målte ankerkrefter er utfordrende ettersom lastcellene er plassert et annet sted langs spuntlinjen enn på det valgte tverrsnittet. Likevel viser alle modeller akseptable verdier til målte ankerkrefter, bortsett fra MC. Modellen gir for store forskyvninger, og brukeren bør være forsiktig når den brukes på en flerforankret spuntvegg, ettersom ankerkreftene kan være unøyaktige. Innsetting av en avlastning/rebelastnings stivhet i MC, ved å endre materialparametere mellom faser, gir bedre resultater. I NGI-ADP er stivhet og styrke relatert gjennom et stivhetsforhold  $G/s_u$  som virker å bidra til at modellen passer bedre til målt oppførsel. Blant modellene gir NGI-ADP minst variasjon i resultater når ruheten endres. Inkludering av LCC i modelleringen synes å øke nøyaktigheten av resultatene for de fleste modeller brukt i denne oppgaven.

Det er vanskelig å finne balansen mellom å opprettholde ønsket stivhet og samtidig øke styrken i GS. Installasjon av ankre skyver veggen tilbake mot skråningen slik at aktiv og passiv sone i profilet kan endres i løpet av fasene. I GS må ruhetsparameteren bli definert i en retning før prosjektet kan beregnes, og kan ikke endres under forskjellige faser. Likevel gir modellering i GS overraskende gode resultater opp mot de målte verdiene, hvor modellert LCC med delvis effekt var mest nøyaktig.

Å oppnå realistiske ankerkrefter ved håndkalkulasjon er utfordrende for dette prosjektet. Med flere forenklinger ble det oppnådd for lave krefter, da forspenning av ankre og stivhet

---

av veggen ikke er inkludert. Bruken av numeriske modeller er en fordel ved beregning av en flerforankret spuntvegg i hellende terreng.

---

# Preface

This paper is developed during the spring semester 2018 as a part of the Geotechnology master's degree programme at NTNU. It is written for, and in collaboration with, the Department of Civil and Environmental Engineering.

We would like to thank our supervisor Steinar Nordal for extensive guidance, support and insight throughout this process. Also a huge thanks to our external supervisors Anders Ulvestad and Corneliu Athanasiu at Multiconsult for giving us the opportunity to write about their project and for inviting us to helpful workshops in Oslo. Without their guidance and wisdom during the semester, this thesis would not have been feasible.

We also want to thank Gustav Grimstad, Mirjam Knutsen, Johannes Mydland and Martin Dons for technical help, tips and information.

Trondheim, June 2018

Bernhard Naglestad  
Michal Sperre

---

# Table of Contents

<b>Summary</b>	<b>i</b>
<b>Sammendrag</b>	<b>iii</b>
<b>Preface</b>	<b>v</b>
<b>Table of Contents</b>	<b>viii</b>
<b>List of Tables</b>	<b>x</b>
<b>List of Figures</b>	<b>xiii</b>
<b>List of Appendices</b>	<b>xiv</b>
<b>List of Notations</b>	<b>xv</b>
<b>1 Introduction</b>	<b>1</b>
<b>2 Method</b>	<b>3</b>
<b>3 Literature review</b>	<b>5</b>
3.1 Similiar studies . . . . .	5
3.2 Theory . . . . .	6
3.2.1 PLAXIS . . . . .	6
3.2.2 GeoSuite Excavation . . . . .	18
3.2.3 Hand calculation . . . . .	24
<b>4 Project Kværnerdammen F1</b>	<b>25</b>
4.1 Site information . . . . .	25
4.2 Profile X-X' . . . . .	31
4.3 Input parameters . . . . .	34
4.3.1 Intro . . . . .	34
4.3.2 PLAXIS . . . . .	35
4.3.3 GeoSuite Excavation . . . . .	49
4.4 Simple hand calculation . . . . .	55
4.5 Measurement data . . . . .	56

---

<b>5</b>	<b>Results and discussion</b>	<b>59</b>
5.1	Initial model . . . . .	59
5.1.1	Displacement and structural forces . . . . .	60
5.1.2	Bending moment . . . . .	65
5.1.3	FoS and failure planes . . . . .	66
5.2	Parametric study in PLAXIS . . . . .	71
5.2.1	Stiffness . . . . .	71
5.2.2	$E_{ur}$ in MC . . . . .	74
5.2.3	$R_{inter} = 0.4$ . . . . .	77
5.2.4	$S_u250$ . . . . .	79
5.2.5	$S_u100$ . . . . .	82
5.3	Parametric study in GS . . . . .	85
5.3.1	$r = 0.4$ . . . . .	85
5.3.2	$S_u250$ . . . . .	87
5.3.3	$S_u100$ . . . . .	89
5.4	Simple hand calculation . . . . .	91
5.5	Main Discussion . . . . .	93
<b>6</b>	<b>Conclusion</b>	<b>99</b>
	<b>Bibliography</b>	<b>101</b>



# List of Tables

4.1	Magnitude of loads (MulticonsultASA, 2017a). . . . .	34
4.2	Parameters for the anchors and the rock bolt. . . . .	35
4.3	Parameters of the SPW. . . . .	35
4.4	Input parameters for MC-materials in PLAXIS. . . . .	35
4.5	Input parameters for linear elastic materials in PLAXIS. . . . .	36
4.6	Material type of structural components used in PLAXIS. . . . .	36
4.7	Input parameters for NGI-ADP materials. . . . .	40
4.8	Boreholes with corresponding triaxial tests split into locations. . . . .	40
4.9	Input parameters for HS(B) materials. . . . .	43
4.10	Input parameters for silty clay materials in HS(A). . . . .	45
4.11	Input parameters for quick clay materials in HS(A). . . . .	45
4.12	Input parameters for MC materials. . . . .	46
4.13	Soil parameters at different depths for hand calculations. . . . .	56
4.14	Measured anchor forces in kN. . . . .	58
5.1	Difference in calculated and measured anchor forces, normalized on the latter, given in % for top row of anchors. . . . .	63
5.2	Difference in calculated and measured anchor forces, normalized on the latter given, in % for bottom row of anchors. . . . .	63
5.3	Difference in calculated and measured anchor forces, normalized on the latter, given in % for the top row of anchors . . . . .	78
5.4	Difference in calculated and measured anchor forces, normalized on the latter, given in % for the bottom row of anchors. . . . .	79
5.5	Difference in calculated and measured anchor forces, normalized on the latter, given in % for the top row of anchors. . . . .	81
5.6	Difference in calculated and measured anchor forces, normalized on the latter, given in % for the bottom row of anchors. . . . .	82
5.7	Difference in calculated and measured anchor forces, normalized on the latter, given in % for the top row of anchors. . . . .	84
5.8	Difference in calculated and measured anchor forces, normalized on the latter, given in % for the top row of anchors. . . . .	85
5.9	Calculated anchor forces in different phases in GS for $r = 0.4$ , compared to measured anchor force. Deviance is normalized on measured values. . .	87
5.10	Calculated anchor forces in different phases in GS for $S_u250$ , compared to measured anchor force. Deviance is normalized on measured values. . .	89

---

5.11	Calculated anchor forces in different phases in GS for $S_u$ 100, compared to measured anchor force. . . . .	90
5.12	Values calculated and used in simple hand calculations. . . . .	91
5.13	Calculated earth forces in each area. . . . .	92
5.14	Axial anchor forces for top and bottom row of anchors. . . . .	92
5.15	Absolute average top anchor row in % . . . . .	96
5.16	Absolute average bottom anchor row in % . . . . .	96
5.17	Absolute average for both row of anchors in % . . . . .	97

# List of Figures

3.1	a) Soil profile after applied load. b) Soil response after applied load (Nordal, 2017d).	7
3.2	Six and fifteen noded element (Nordal, 2017b).	7
3.3	Illustration of the MC failure criterion in 3d (Nordal, 2017c).	9
3.4	Varying shear strength along a failure plane in NGI-ADP (Thakur et al., 2014).	10
3.5	Stress paths in NGI-ADP (Brinkgreve et al., 2017a).	11
3.6	Hardening soil yield surface with all stiffnesses included (Johansson and Sandeman, 2014).	13
3.7	a) Interfaces in a 6-noded soil element. b) Interfaces in a 15-noded soil element (Brinkgreve et al., 2017b).	14
3.8	a) Interface boundaries displayed in PLAXIS model setup. b) Interfaces displayed in the mesh window.	15
3.9	Stress paths for different undrained settings from MC in PLAXIS (Johansson and Sandeman, 2014).	17
3.10	Elements in the SPW in GS (Vianova Geosuite, 2009).	19
3.11	Typical earth pressure – displacement relationship for a soil spring in GS (Vianova Geosuite, 2009).	19
3.12	Soil shear stress along the SPW (Vianova Geosuite AB 2009).	21
4.1	Map with placement of Kværnerdammen F1 (MulticonsultASA, 2017e). North is up.	26
4.2	Map of bedrock elevation at Kværnerdammen F1 (MulticonsultASA, 2017b).	27
4.3	Sketch of pattern for installation of LCC (MulticonsultASA, 2017c).	28
4.4	Sketch of initial phase (MulticonsultASA, 2017b).	29
4.5	Sketch of phase 1 (MulticonsultASA, 2017b).	29
4.6	Sketch of phase 2 (MulticonsultASA, 2017b).	30
4.7	Sketch of phase 3 (MulticonsultASA, 2017b).	30
4.8	Sketch of phase 4 (MulticonsultASA, 2017b).	31
4.9	Sketch of phase 5 (MulticonsultASA, 2017b).	31
4.10	Sketch of stratification in profile X-X'.	32
4.11	Layering of soils and bedrock in profile X-X'.	32
4.12	Shear strength interpretation from borehole12 by Multiconsult based on NGI's earlier research (MulticonsultASA, 2017a).	33
4.13	Strength profile ( $S_u^A$ ) for profile X-X'.	34

---

4.14	Interpretation of active triaxial tests (CAU <sub>a</sub> ) against SoilTest done in PLAXIS - 0-4 % strain (MulticonsultASA, 2017a). . . . .	37
4.15	Interpretation of passive triaxial tests (CAU <sub>p</sub> ) against SoilTest done in PLAXIS - 0-4 % strain (MulticonsultASA, 2017a). . . . .	38
4.16	Soil clusters for NGI-ADP in PLAXIS. . . . .	39
4.17	BH17 (QC1=HS1), fitting of soil test to actual triaxial test results, $\tau$ - $\epsilon_1$ . . . . .	41
4.18	BH17 (QC1=HS1), fitting of soil test to actual triaxial test results - Stress path . . . . .	42
4.19	Soil clusters for HS(B) in PLAXIS with location placement. . . . .	43
4.20	Soil clusters for HS(A) in PLAXIS with location placement. . . . .	44
4.21	BH17 (QC1=HS1), triaxial test fitted to curve and adjusted with new parameters, $\tau$ - $\epsilon_1$ . . . . .	44
4.22	Strength profiles in initial phase taken from PLAXIS output for: a) NGI-ADP, b) HS(B) and MC, c) HS(A). . . . .	47
4.23	Calculation phases in PLAXIS. . . . .	48
4.24	Soil profile used in GS. . . . .	50
4.25	Defining additional loads in GS. . . . .	51
4.26	Additional stress on the SPW, from the omitted triangle of weight created by the slope, calculated by GeoSuite Settlement. . . . .	51
4.27	Input window for additional vertical stress in GS. . . . .	52
4.28	Input parameters in GS. . . . .	53
4.29	Calculation phases in GS. . . . .	53
4.30	Values used for the sheet pile input in GS. . . . .	54
4.31	Anchor window showing input for the top row of anchors in GS. . . . .	55
4.32	Placement of inclinometers along the SPW (MulticonsultASA, 2017d). . . . .	56
4.33	Measured horizontal displacement of the SPW in all phases. . . . .	57
5.1	Horizontal displacement of the SPW in PLAXIS with initial parameters. . . . .	60
5.2	Horizontal displacement of the SPW in GS with initial parameters. . . . .	61
5.3	Calculated anchor forces from the initial analysis compared to measured anchor forces. . . . .	62
5.4	Combined calculated rock bolt forces from PLAXIS and GS with initial parameters. . . . .	64
5.5	Bending moment of the SPW in PLAXIS with initial parameters. . . . .	65
5.6	Bending moment of the SPW in GS with initial parameters. . . . .	66
5.7	FoS for different models in PLAXIS with initial parameters. . . . .	67
5.8	Failure surface visualized by incremental shear, in initial phase. . . . .	68
5.9	Failure surface visualized by incremental shear, in excavation +18.5 phase. . . . .	69
5.10	Failure surface visualized by incremental shear, in excavation +18 phase. . . . .	70
5.11	Failure surface visualized by incremental shear, in permanent phase after consolidation. . . . .	71
5.12	Stiffness of soil behind the SPW from PLAXIS. . . . .	72
5.13	Difference in shear strength for OCR = 1.2 and OCR = 1.3 with equal input parameters. . . . .	73
5.14	Illustration of different strain ranges with associated shear stiffness (Liktlersuang et al., 2013). . . . .	74

---

---

5.15	Horizontal displacement and bending moment of the SPW for phases excavating to elevation +21 and +18 using MC( $E_{ur}$ ). . . . .	75
5.16	Combined calculated anchor forces for both MC models compared to measured data. . . . .	76
5.17	Horizontal displacement of the SPW in PLAXIS with $R_{inter} = 0.4$ compared to measured data. . . . .	77
5.18	Calculated anchor forces from the $R_{inter} = 0.4$ analysis compared to measured anchor forces. . . . .	78
5.19	Horizontal displacement of the SPW in PLAXIS with $S_u250$ parameters compared to measured data. . . . .	80
5.20	Calculated anchor forces from the $S_u250$ analysis compared to measured anchor forces. . . . .	81
5.21	Horizontal displacement of the SPW in PLAXIS with $S_u100$ parameters compared to measured data. . . . .	83
5.22	Calculated anchor forces from the $S_u100$ analysis compared to measured anchor forces. . . . .	84
5.23	Horizontal displacement of the SPW in GS with $r = 0.4$ parameters compared to measured data. . . . .	86
5.24	Silty clay and quick clay parameters illustrating the deviating stiffness in GS. . . . .	87
5.25	Horizontal displacement of the SPW in GS with $s_u250$ parameters compared to measured data. . . . .	88
5.26	Horizontal displacement of the SPW in GS with $S_u100$ parameters compared to measured data. . . . .	90
5.27	Earth pressure diagram from hand calculations. . . . .	92
5.28	Horizontal displacement of the SPW when excavating to elevation +21, comparing all parameter sets from PLAXIS with measured data. . . . .	94
5.29	Horizontal displacement of the SPW when excavating to elevation +18 and after consolidation, comparing all parameter sets from PLAXIS with measured data. . . . .	95
5.30	Horizontal displacement of the SPW, when excavating to elevation +21 and +18, comparing all parameter sets from GS to measured data. . . . .	97

---

## List of Appendices

- Appendix A Collection of site information and initial material models
- Appendix B PLAXIS initial model with  $R_{inter} = 0.1$  results
- Appendix C GS initial model with  $r = 0$  results
- Appendix D PLAXIS MC model with  $E_{ur}$  results
- Appendix E PLAXIS with  $R_{inter} = 0.4$  results
- Appendix F PLAXIS modeled with full effect of LCC results
- Appendix G PLAXIS modeled with partial effect of LCC results
- Appendix H GS modeled with  $r = 0.4$  results
- Appendix I GS modeled with full effect of LCC results
- Appendix J GS modeled with partial effect of LCC results
- Appendix K Hand calculation results

---

# List of Notations

## Roman letters

$a$	=	Attraction	[kPa]
$c$	=	Cohesion	[kPa]
$c'$	=	Apparent cohesion	[kPa]
$c_{inter}$	=	Shear strength within interface	[kPa]
$c_{soil}$	=	Soil shear strength	[kPa]
$c_u$	=	Undrained shear strength	[kPa]
$c_{ref}$	=	Reference undrained shear strength	[kPa]
$D_A$	=	Net active total stress difference	[kPa]
$D_P$	=	Net passive total stress difference	[kPa]
$E$	=	Young's modulus	[kPa]
$EA$	=	Axial stiffness	[kN/m]
$EI$	=	Flexural rigidity	[kNm <sup>2</sup> /m]
$E_{oed}$	=	Oedometer modulus	[kPa]
$E_u$	=	Undrained Young's modulus	[kPa]
$E_{ur}$	=	Unload reload stiffness	[kPa]
$E'$	=	Effective Young's modulus	[kPa]
$E'_{50}$	=	Effective secant stiffness	[kPa]
$E'_{oed}$	=	Effective Oedometer stiffness	[kPa]
$E'^{ref}_{50}$	=	Effective secant stiffness at reference pressure	[kPa]
$E'^{ref}_{oed}$	=	Effective Oedometer stiffness at reference pressure	[kPa]
$E'^{ref}_{ur}$	=	Effective unload reload stiffness at reference pressure	[kPa]
$E_{u,initial}$	=	Initial undrained stiffness	[kPa]
$E_{u,new}$	=	New undrained stiffness	[kPa]

---

$F_{max,tens}$	=	Maximum tension force	[kN]
$F_{max,comp}$	=	Maximum compression force	[kN]
$f_i$	=	Yield function	[kPa]
$f_\omega$	=	Stress field rotation parameter	[-]
$G$	=	Shear modulus	[kPa]
$G_{50}$	=	Shear modulus at 50 % of undrained shear strength	[kPa]
$G_u$	=	Undrained shear modulus	[kPa]
$G_{ur}$	=	Unload reload shear modulus	[kPa]
$I_p$	=	Plasticity index	[%]
$K_0$	=	Earth pressure coefficient at rest	[-]
$K'_0$	=	Effective earth pressure coefficient at rest	[-]
$K'^{nc}_0$	=	$K'_0$ for normally consolidated condition	[-]
$K_A$	=	Active earth pressure coefficient	[-]
$K_P$	=	Passive earth pressure coefficient	[-]
$K_y$	=	Tangent spring stiffness	[kPa/m]
$K_y^i$	=	Initial spring stiffness	[kPa/m]
$L_{spacing}$	=	Center spacing	[m]
$\bar{K}_y$	=	Secant spring stiffness	[kPa/m]
$k$	=	Permeability	[m/day]
$M$	=	Stress dependent Oedometer modulus	[kPa]
$m$	=	Power of stress level dependency of stiffness	[-]
$P$	=	Anchor force	[kPa]
$P_H$	=	Horizontal anchor force	[kPa]
$p$	=	Mean stress	[kPa]
$p_a$	=	Active earth pressure	[kPa]
$p_p$	=	Passive earth pressure	[kPa]
$p_v$	=	Vertical earth pressure	[kPa]
$p_v^a$	=	Active vertical earth pressure	[kPa]
$p_v^p$	=	Passive vertical earth pressure	[kPa]
$p_{ref}$	=	Reference pressure	[kPa]

---



---

$q'$	=	Line load	[kPa]
$q$	=	Deviator stress	[kPa]
$R_f$	=	Scaling parameter	[-]
$R_{inter}$	=	Strength reduction factor	[-]
$r$	=	Roughness ratio	[-]
$r_\kappa$	=	Hardening parameter	[-]
$S_u$	=	Undrained shear strength	[kPa]
$S_u^A$	=	Active undrained shear strength	[kPa]
$S_{u,inc}$	=	Increase of undrained shear strength	[kPa/m]
$S_{u,inc}^A$	=	Increase of active undrained shear strength	[kPa/m]
$S_{u,ref}^A$	=	Reference active undrained shear strength	[kPa]
$S_u^{C,TX}$	=	Triaxial compressive undrained shear strength	[kPa]
$S_u^{DSS}$	=	Direct simple undrained shear strength	[kPa]
$S_u^P$	=	Passive undrained shear strength	[kPa]
$S_{u,initial}$	=	Initial undrained shear strength	[kPa]
$S_{u,new}$	=	New undrained shear strength	[kPa]
$S_{u,recon}$	=	Reconsolidated undrained shear strength	[kPa]
$t_i$	=	Virtual interface thickness	[-]
$v$	=	displacement	[m]
$v_i$	=	Vertical inclination	[-]
$v_f$	=	Failure displacement	[m]
$x_{ref}$	=	Horizontal reference	[m]
$y$	=	Depth	[m]
$y_{ref}$	=	Reference depth	[m]
$z$	=	Depth	[m]

---

## Greek letters

$\alpha$	=	inclination of anchor	[°]
$\alpha_A$	=	Angle between critical plane and major principal stress plane	[°]
$\alpha_P$	=	Angle between critical plane and minor principal stress plane	[°]
$\gamma$	=	Weight of soil	[kN/m <sup>3</sup> ]
$\gamma^p$	=	Plastic shear strain	[-]
$\gamma_f^c$	=	Shear strain failure in triaxial compression	[%]
$\gamma_f^{DSS}$	=	Shear strain failure in direct simple shear	[%]
$\gamma_f^E$	=	Shear strain failure in triaxial extension	[%]
$\gamma_f^p$	=	Plastic shear strain failure	[-]
$\gamma_m$	=	Material coefficient	[-]
$\epsilon$	=	Strain	[-]
$\epsilon_1$	=	Major principal strain	[-]
$\epsilon_3$	=	Minor principal strain	[-]
$\epsilon_y$	=	Vertical strain	[-]
$\delta$	=	Displacement	[m]
$\kappa$	=	Earth pressure coefficient	[-]
$\nu$	=	Poisson's ratio	[-]
$\nu_u$	=	Undrained Poisson's ratio	[-]
$\nu'$	=	Effective Poisson's ratio	[-]
$\nu'_{ur}$	=	Effective Poisson's ratio for unload reload	[-]
$\rho$	=	Mobilized friction angle	[°]
$\sigma$	=	Stress	[kPa]
$\sigma_1$	=	Major principal stress	[kPa]
$\sigma_3$	=	Minor principal stress	[kPa]
$\sigma_f$	=	Failure stress	[kPa]
$\sigma_h$	=	Horizontal stress	[kPa]
$\sigma_v$	=	Vertical stress	[kPa]
$\sigma_y$	=	Vertical stress	[kPa]

---

$\sigma_{yi}$	=	Initial vertical earth pressure	[kPa]
$\tau$	=	Shear stress	[kPa]
$\tau_0$	=	Initial shear stress	[kPa]
$\tau_{max}$	=	Maximum shear stress	[kPa]
$\phi$	=	Friction angle	[°]
$\phi_{inter}$	=	Friction angle of interface	[°]
$\phi_{soil}$	=	Friction angle of soil	[°]
$\phi'_{cv}$	=	Critical state friction angle	[°]
$\psi$	=	Dilatancy angle	[°]

## Abbreviations

BH	=	Borehole
CAUa	=	Consolidated anisotropic undrained active shear test
CAUp	=	Consolidated anisotropic undrained passive shear test
CDSS	=	Cyclic direct simple shear test
CIUa	=	Consolidated isotropic undrained active shear test
CPTu	=	Cone penetration test
CRS	=	Constant rate of strain
DSS	=	Direct simple shear test
ESS	=	Effective Stress Simple
FE	=	Finite element
FEM	=	Finite element method
FoS	=	Factor of Safety
GS	=	GeoSuite Excavation
GW	=	Groundwater
HS	=	Hardening soil
HS(A)	=	Hardening soil with undrained(A)
HS(A)nc	=	Hardening soil with undrained(A) and no contraction

---

HS(B)	=	Hardening soil with undrained(B)
INC	=	Inclinometer
HSSs	=	Hardening Soil Small strain
LCC	=	Lime cement columns
LG	=	Løvlien Georåd
MC	=	Mohr Coulomb
MC( $E_{ur}$ )	=	Mohr Coulomb with unloading/reloading stiffness
MC'	=	Multiconsult
NC	=	Normally consolidated
NGI	=	Norwegian Geotechnical Institute
NVE	=	The Norwegian Water Resources and Energy Directorate
NGI-ADP	=	NGI - Active Direct Passive
OC	=	Over-consolidated
OCR	=	Over-consolidation ratio
QC	=	Quick clay
RB	=	Rambøll
SC	=	Silty clay
SPW	=	Sheet Pile Wall
TSA	=	Total Stress Automatic

# Chapter 1

## Introduction

Multiconsult is hired as geotechnical consultants at the Kværnerdammen F1 project which comprises the construction of a seven-story building with basement at the toe of an inclined slope. Quick clay is registered at the site and, to secure the building pit during and after excavation, a permanent sheet pile wall (SPW) is installed to the east of the building. Lime cement columns (LCC) are used to ensure the stability during installation of the SPW. Two rows of anchors are installed and connected to bedrock at different levels, while the SPW itself is bolted to bedrock. Appropriate modeling of the system and the soil response is crucial for predicting deformations and assessing the proper stability measures. Over the years, several computer modeling software has been developed, with PLAXIS being the most prominent. GeoSuite Excavation (GS) is a software developed in Norway and Sweden with a goal to make the calculations as fast, easy and user-friendly as possible.

### **Aim**

The aim of this thesis is to compare the measured anchor forces and deformations at Kværnerdammen F1 to the results from the Total Stress Automatic (TSA) model in GS and three constitutive models in PLAXIS 2D; Hardening soil (HS), NGI-ADP and Mohr-Coulomb (MC). This involves defining a representative cross section and soil profile, selecting material parameters to fit a strength profile and tuning various parameters to see which model is most appropriate. Additional focus is to be put on a parametric study regarding roughness and the effect of modeling LCC in front of the SPW. This raises the questions; Which of the models are the most accurate compared to measured data and how does modeling of LCC in front of the SPW affect the results?

### **Reading guide**

- *Chapter 2 - Method*

This chapter describes how the thesis has been conducted concerning extraction of relevant literature along with critique of the sources. It also briefly mentions how the modeling process was accomplished along with shortcomings of the thesis.

- *Chapter 3 - Literature review*  
This chapter is a literature review which starts with a collection of similar studies. The majority of the chapter is dedicated to an in-depth review of the relevant theoretical background found in literature.
- *Chapter 4 - Start up*  
This chapter describes the project including the soil situation, the excavation process and the structural components used. Also, there is an in-depth explanation on how the modeling was conducted along with the initial parameters used in each model.
- *Chapter 5 - Results and discussion*  
As this is conducted as a trial and error thesis it is natural to present results mixed with critical discussion. The initial results are presented first, followed by parametric studies, and the chapter ends with a main discussion.
- *Chapter 6 - Conclusion*  
The thesis is summed up with the main points discussed in a conclusion, followed by suggestions for future works regarding the subject.

## Method

A desk study was performed to gather necessary information and knowledge about different conventional models in each software and about the project. Master and doctoral theses, science papers and professional presentations were gathered searching through databases, libraries and lecture notes. The project specific reports, drawings and sketches were supplied by Multiconsult. The sources of information were obtained from:

- Internal project reports, documents and drawings from Multiconsult ASA.
- Supporting literature and lecture notes in the courses TBA4116 – Geotechnical Engineering, Advanced Course and TBA4105 – Geotechnics, Design methods, available for students enrolled in the courses at NTNU.
- Scientific papers, presentations, advanced course material and master theses obtained from supervisors mentioned in the preface.
- NTNU libraries.
- Web search through Google Scholar databases, [scholar.google.com](http://scholar.google.com)
- Web search through Oria databases, [www.oria.no](http://www.oria.no)
- Web search through Scopus databases, [www.scopus.com](http://www.scopus.com)

Some of the findings were insufficient, as some sources were restricted by a pay wall to obtain full texts of documents. For the literature review, the theory manuals of each program, combined with lecture notes and supporting literature from geotechnical courses at NTNU, were found to be the most relevant sources. For the project specific details, the documents gathered and prepared by Multiconsult were the greatest source of information.

Initially the soil parameters were tuned to a strength profile using SoilTest. Modeling this way will force stiffness parameters to deviate at the expense of strength. Discussions with supervisors mentioned in the preface were of great value in this area, which was continuous throughout the whole process. Changes were made to the initial set of parameters

to see impacts of certain effects. Therefore, modeling is done by trial and error and it is natural to present results paired with critical discussion.

As this thesis is part of a Master degree program it has time restrictions. The parametric study conducted is relatively superficial as one could spend years focusing on only one of the discussed topics. Also, supplementary field and lab tests could have been done to fill out the lacking data.



## Literature review

The main source of information for this thesis is obtained from Multiconsult. The authors have been given access to all available information such as reports, laboratory data, maps (contour and rock, drill pattern, conducted site investigations) and internal drawings revolving the Kværnerdammen F1 project. Additionally, information from a nearby site, Enebakkveien 69 and 71, is collected as the soil situation is assumed to be similar. These reports are conducted by several different contractors:

- Løvlies georåd (LG) conducted the site investigations (Georåd, 2008)
- Rambøll (RB) conducted supplementary site investigations (Rambøll, 2009)
- NGI mapped quick clay and assessed the stability (NGI, 2009)

### 3.1 Similiar studies

A study by Johansson and Sandeman (2014) compares different methods for back calculating a multi-anchored SPW in soft clay. Parametric studies are performed to best fit the in-situ measurements, focusing on anchor forces and deformation of the SPW. The analysis used Total Stress Automatic (TSA) in GeoSuite Excavation, simple hand calculations and three different PLAXIS 2D models; MC, HS and HSSs. The study concluded that the HS model gave the best result with the data available. MC is preferred when no triaxial data is available and empirical correlations in the HSSs model increased the level of uncertainty regarding the results.

In Surarak et al. (2012), experimental data on Bangkok clays are analysed to determine strength and stiffness parameters for the HS model. Triaxial and oedometer tests, drained and undrained, are simulated in PLAXIS and fitted to the data set. The study concluded that when using the HS model, the drained moduli is needed in the PLAXIS analysis of undrained materials. The reasoning behind this was that the assumption of adding bulk modulus of water to convert to the undrained modulus from the drained modulus, may not

be appropriate.

In Kempfert et al. (2006) it is stated under "reviews of FE-analysis of excavations" (p. 169) that an analysis of a 16.8 m deep excavation done by 14 individuals showed vastly discrepancies among the results. The main reason was the identification of input parameters, particularly differences in the stiffness of the soil. The study concluded that standardizing the finite element (FE) analysis of excavation is needed.

In Kullingsjø (2009), back analysis of deep excavations in soft clay were performed to predict ground deformations and interpret stress change development against a retaining wall system. The isotropic linear elastic MC model, the total stress based strength anisotropy NGI-ADP model, and the bounding surface effective stress MIT-S1 model, were used and compared with in-situ measurements. The study concluded that detailed FE-modeling is not sufficient alone. In order to construct an acceptable and reliable construction, close collaboration between the contractor and the geotechnical consultant, as well as monitoring and continuous follow up, is highly necessary.

In PLAXIS bulletin number 4 by Nurmohamed et al. (1997) a 15 m deep excavation with a 25 m long bored-pile wall is analyzed with both HS and MC. The displacements, moment and heave of the excavation floor from the different models were compared. The study concluded that HS yields much smaller displacements, and that the MC-analysis is far from realistic. The Young's modulus was then increased in MC (4 times  $E_{50}$ ) to obtain  $E_{ur}$  values which gave a good fit with HS when comparing the heave and displacements. The bending moments still differed between the models, and the study concluded that it seems impossible to match MC-results with HS-results when one wants to fit both stresses and deformations. The HS-results were realistic, while bending moments with a MC analysis was impossible to obtain.

## 3.2 Theory

### 3.2.1 PLAXIS

Soil models are used to simulate soil behavior in PLAXIS, a FEM-program for geotechnical applications (Brinkgreve et al., 2017a). FEM based tools do not separate the deformation calculation from the stress calculations, as done in conventional geotechnics, they are integrated in one (Nordal, 2017d). In conventional geotechnics, they must be calculated separately as it is not included in the limit equilibrium solutions. In FEM based tools a load is incrementally applied from zero to its design value, and deformations will gradually appear as the load is increasing. Failure occurs when the deformations become "unlimited" at an adequately high applied load, resulting in no further load increase (fig. 3.1).

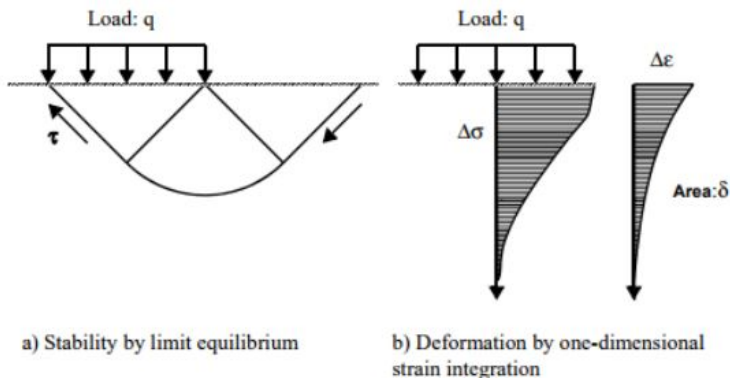


**Figure 3.1:** a) Soil profile after applied load. b) Soil response after applied load (Nordal, 2017d).

The soil volume is divided into elements in FEM, and an approximate description of the behavior is developed for each element (Nordal, 2017d). The elements are joined by a process of numerical and mathematical integration such that the behavior of each element adds up to the behavior of the whole volume of the soil. The finite elements are triangular or square shapes, with or without curved boundaries, which may deform. The deformations are defined by the deformations of nodal points in each element. A set of 6 or 15 nodes are used in PLAXIS (fig. 3.2), where 15 nodes are recommended for 2D and is set by default (Nordal, 2017b).

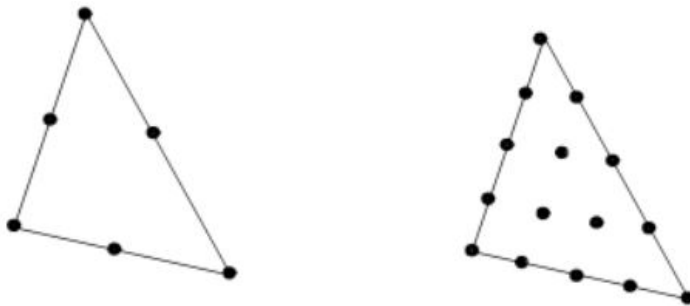


**Figure 3.2:** Six and fifteen noded element (Nordal, 2017b).

The user describes boundary and initial conditions, material parameters, geometry, loads and sequence of loading in a “pre-processor” in a modern FEM program (Nordal, 2017d). The preprocessor will split the soil volume into elements, also called discretization. Information is delivered further to the “finite element engine”, where calculations are performed. The computed results are transferred to the “post-processor”, which displays and presents the results. The finite element engine follows the operations below, from Nordal (2017b):

1. *Element modeling.* Equations for each element are made in an element stiffness

matrix. Numerical integration forms the element stiffness matrix.

2. *Global modeling.* An integration from element level to global level. One large equation system is made from all element stiffness matrixes to form a global stiffness matrix. An incremental load vector is then found.
3. *Equation solving.* The global equation system is solved for the incremental load. Displacement increment is then given.
4. *Stress evaluation.* The strain increments are found from the displacement increments in every element. The stress increments are then found and calculated in each element.
5. *Testing for numerical accuracy.* If the calculations provide unbalanced forces, the load increment is adjusted or more iterations are added. If results are converging, the program proceeds to the next step. If not, the forces are too unbalanced and steps 1-5 are recalculated.
6. *Updating of results.* Adding increments of stress and deformation to create total stresses and total deformations.
7. *Calculation of new load increment.* By repeating steps 1-6, response of new load increment is attained. These increments are added repeatedly until failure occurs, or wanted load is reached.

### **Mohr Coulomb**

When subjected to changes of strain or stress, soils have a non-linear behavior (Brinkgreve et al., 2017a). The stiffness of the soil depends on different conditions such as the strain level, the stress level and the stress path. MC is a linear elastic perfectly-plastic model that includes five input parameters (Brinkgreve et al., 2017a):

- $E$  Young's modulus.
- $\nu$  Poisson's ratio.
- $\phi$  Friction angle.
- $c$  Cohesion.
- $\psi$  Dilatancy angle.

MC is recommended as a first analysis of the problem, as it represents a “first order” approximation of rock or soil behavior (Brinkgreve et al., 2017a). A constant average stiffness is estimated for each layer, which makes the computations relatively fast to run. This way, a first estimate of deformations is obtained (Jalali et al., 2012). A linear elastic perfectly-plastic model assumes a perfectly-plastic behavior when a material is yielding (Johansson and Sandeman, 2014). Hooke's law of isotropic elasticity is a basis for the linear elastic part of the MC model, while the MC failure criterion is a basis for the perfectly-plastic part. The latter is formulated in a “non-associated plasticity framework” (Brinkgreve et al., 2017a). Elasto-plasticity uses Hooke's law to relate the strain rates, which are divided into an elastic and a plastic part, and the stress rates. Irreversible strains

develop in plasticity. A yield function ( $f$ ) of strain and stress is introduced to check if plasticity occurs. Plastic yielding occurs when  $f = 0$ , which can be presented as a surface in a space of principal stresses. Six yield functions ( $f_i$ ) create the full MC yield condition, and setting all yield functions together equal to 0, a fixed hexagonal cone is created (fig. 3.3). These yield surfaces are not affected by plastic straining, only defined by model parameters. Strains are reversible, which means the behavior is elastic.

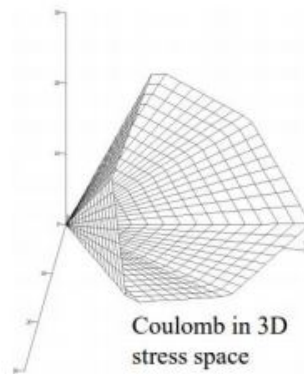


**Figure 3.3:** Illustration of the MC failure criterion in 3d (Nordal, 2017c).

MC can increase strength with depth, but does not include strain dependency, stress-dependency nor stress-path dependency of stiffness or anisotropic stiffness (Brinkgreve et al., 2017a). This means that MC includes, in general, few features that are shown in real soil behavior.

### NGI-ADP

Unlike MC, the NGI-ADP model is an anisotropic undrained shear strength model (Brinkgreve et al., 2017a). Due to factors such as complex geological stress history, particle orientation and induced undrained stress path, the behavior of soft clays is generally anisotropic. The principal stress direction, and therefore the strength, will vary along failure planes (Grimstad et al., 2012). This anisotropy is incorporated in the NGI-ADP model in the form of different shear strengths along various failure surfaces (fig. 3.4) in addition to the corresponding failure strains.

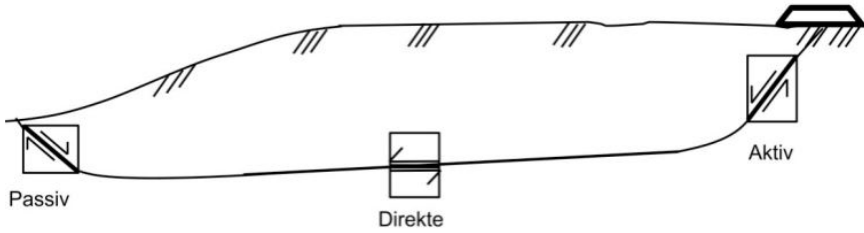


**Figure 3.4:** Varying shear strength along a failure plane in NGI-ADP (Thakur et al., 2014).

The input parameters as listed in Brinkgreve et al. (2017a) are:

- $G_{ur}/S_u^A$  Ratio unloading/reloading shear modulus over active undrained shear strength.
- $\gamma_f^c$  Shear strain failure in triaxial compression.
- $\gamma_f^E$  Shear strain failure in triaxial extension.
- $\gamma_f^{DSS}$  Shear strain failure in direct simple shear.
- $S_{u,ref}^A$  Reference active undrained shear strength.
- $S_u^{C,TX}/S_u^A$  Ratio triaxial compressive undrained shear strength over active undrained shear strength.
- $y_{ref}$  Reference depth.
- $S_{u,inc}^A$  Ratio of passive undrained shear strength over active undrained shear strength.
- $S_u^P/S_u^A$  Power for stress level dependency of stiffness.
- $\tau_0/S_u^A$  Initial mobilization.
- $S_u^{DSS}/S_u^A$  Ratio of direct simple undrained shear strength over active undrained shear strength.
- $\nu'$  Poisson's ratio.

The active shear strength is therefore defined by set reference values in combination with optional linear increase (Grimstad et al., 2012):

$$S_u^A = S_{u,ref}^A + (y_{ref} - y)S_{u,inc}^A \quad (3.1)$$

The anisotropic shear strengths are incorporated by different ratios of passive and direct shear strength over active shear strength, which are defined in plane strain conditions (Brinkgreve et al., 2017a). The parameter  $S_u^{C,TX}/S_u^A$  is a ratio linking the plane strain to triaxial conditions. In PLAXIS this ratio is predefined and cannot be changed man-

ually. It is set to 0.99, which gives nearly similar strengths in plane strain and triaxial conditions. A shear modulus is introduced in the model as the unloading/reloading shear modulus over active shear strength ( $G_{ur}/S_u^A$ ). This is a constant ratio, which means that if the shear strength increases with depth, the shear stiffness will increase with a similar increment (Brinkgreve et al., 2017a).

As the NGI-ADP model uses different failure shear strains, a hardening function must be introduced to account for stress path variance (Grimstad et al., 2012):

$$r_{\kappa} = 2 \frac{\sqrt{\gamma^P/\gamma_f^P}}{1 + \gamma^P/\gamma_f^P} \quad (3.2)$$

This function creates a hardening yield curve defined by an elliptical interpolation function between failure strain in passive/active stress states and direct simple shear state as illustrated in figure 3.5 (Brinkgreve et al., 2017a).

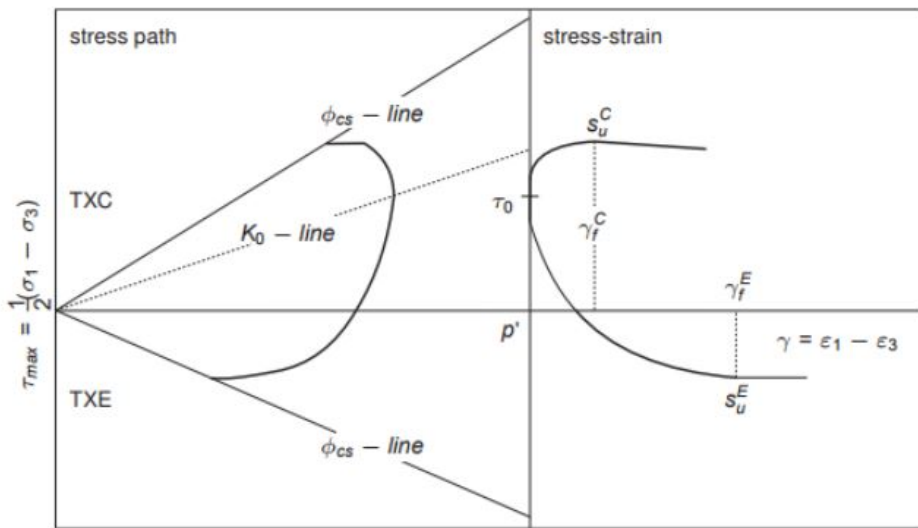


**Figure 3.5:** Stress paths in NGI-ADP (Brinkgreve et al., 2017a).

In NGI-ADP, the anisotropy assumes that the greatest principal stress is initially vertical, hence the anisotropy follows the vertical (Isachsen, 2012). To determine the optimal set of input parameters to make a good fit with real tested soil behavior, trial and error testing of different input parameters is necessary (Ukritchon and Boonyatee, 2015).

### Hardening Soil

The HS model is a constitutive double-stiffness model for elasticity, combined with isotropic strain hardening (Schanz et al., 1999). This model changes the stiffness modulus, depend-

ing on the stress state in the soil (Johansson and Sandeman, 2014). The Cam-Clay model is the most dominant existing double-stiffness model, which describes the non-linear stress-strain behavior of soils (Schanz et al., 1999). HS exceeds the existing double-stiffness model, the Duncan-Chang model (Hyperbolic model), by overcoming the restrictions of collapse load computations in the plastic range, and the ability to frequently distinguish between loading and unloading. This is done by replacing the theory of elasticity with the theory of plasticity, as well as including soil dilatancy and introducing a yield cap. Compared to MC (elastic perfectly-plastic), the yield surfaces of HS expands caused by plastic straining. Therefore it is not fixed in principal stress space. Compression hardening and shear hardening are two different main types of hardening included in HS. To model irreversible strains caused by primary compression in isotropic loading and oedometer loading, compression hardening is used. To model irreversible strain caused by primary deviatoric loading, shear hardening is used. The parameters used in HS are (Brinkgreve et al., 2017a):

- $\phi'_{cv}$  Critical state friction angle.
- $\psi$  Angle of dilatancy.
- $c'$  Apparant cohesion.
- $v'_{ur}$  Effective Poisson ratio for unloading-reloading.
- $E'_{oed}{}^{ref}$  Effective oedometer stiffness.
- $E'_{50}{}^{ref}$  Effective secant stiffness.
- $E'_{ur}{}^{ref}$  Effective unload-reload stiffness.
- $m$  Power for stress level dependency of stiffness.
- $p_{ref}$  Reference pressure.
- $K_0$  Coefficient of lateral earth pressure.

In real soils, the stiffness changes due to different stress levels (Brinkgreve et al., 2017a). HS accounts for this stress level dependency by using the different stiffnesses:

$$E'_{50} = E_{50}{}^{ref} \left( \frac{c' \cos\phi - \sigma'_3 \sin\phi}{c' \cos\phi + p^{ref} \sin\phi} \right)^m \quad (3.3)$$

$$E'_{ur} = E_{ur}{}^{ref} \left( \frac{c' \cos\phi - \sigma'_3 \sin\phi}{c' \cos\phi + p^{ref} \sin\phi} \right)^m \quad (3.4)$$

$$E'_{oed} = E_{oed}{}^{ref} \left( \frac{c' \cos\phi - \frac{\sigma'_3}{K_0^{nc}} \sin\phi}{c' \cos\phi + p^{ref} \sin\phi} \right)^m \quad (3.5)$$

Here, the  $K_0^{nc}$  is an independent input parameter and not a function of Poisson's ratio as in MC (Brinkgreve et al., 2017a). Instead the correlation;  $K_0^{nc} = 1 - \sin\phi$  is used,



however it is possible to manually change this value.  $E'_{50}$  and  $E'_{ur}$  are evaluated from triaxial tests. For one-dimensional compression, there is no fixed relationship between the drained triaxial stiffness  $E'_{50}$  and the oedometer stiffness  $E'_{oed}$ . The power for stress level dependency of stiffness,  $m$ , which accounts for the amount of stress dependency, is set to 1 for soft soils (Johansson and Sandeman, 2014). The volumetric yield surface, or the yield cap surface, is formed as an ellipse with the formula (Brinkgreve et al., 2017a):

$$f_c = \frac{\tilde{q}^2}{M^2} + (p')^2 - p_p^2 \quad (3.6)$$

$M$  relates to  $K_0^{nc}$  and is an auxiliary model parameter (Brinkgreve et al., 2017a).  $p_p$  is the length of the yield surface on the x-axis and is determined by OCR, while the intersection with the q-axis is based on  $K_0^{nc}$  (Johansson and Sandeman, 2014). The yield cap surface is introduced to make it possible for  $E'_{oed}{}^{ref}$  and  $E'_{50}{}^{ref}$  to be input as independent parameters, by closing the elastic region for compressive stress paths (Brinkgreve et al., 2017a). Different moduli apply for the different zones that the stress states are in (fig. 3.6).

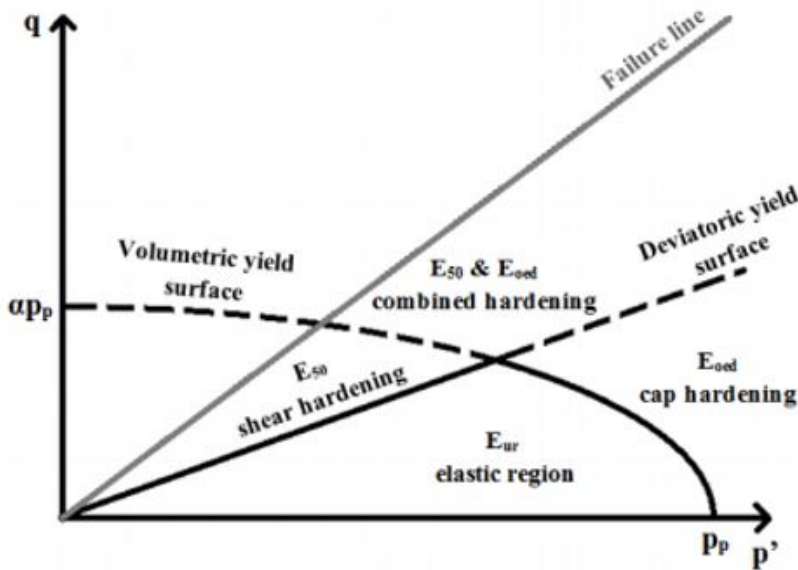


**Figure 3.6:** Hardening soil yield surface with all stiffnesses included (Johansson and Sandeman, 2014).

The shear moduli ( $G$ ) cannot be defined directly in this model. The conversion between  $E$  and  $G$ , can be used to obtain the unloading/reloading stiffness  $E_{ur}$  with the equation:

$$E_{ur} = 2 * (1 + \nu_{ur}) * G_{ur} \quad (3.7)$$

where  $G_{ur}$  is an elastic unloading/reloading shear modulus.  $E_{ur}$  and  $v_{ur}$  can be inserted directly into the program model.

### Interfaces and roughness

To model proper soil-structure interaction, interfaces are used on geogrids and plates in PLAXIS (Brinkgreve et al., 2017b). Interfaces are joint elements and are manually applied along structure-elements or between soil volumes. They simulate the contact between a structure-element and the surrounding soil, which is a thin zone (Jalali et al., 2012). Interfaces are created by interface elements (Brinkgreve et al., 2017b). A pair of 5 nodes defines the interface elements when generating the soil of 15-node elements, while a pair of 3 nodes defines the interface elements when generating the soil of 6-node elements (fig. 3.7).

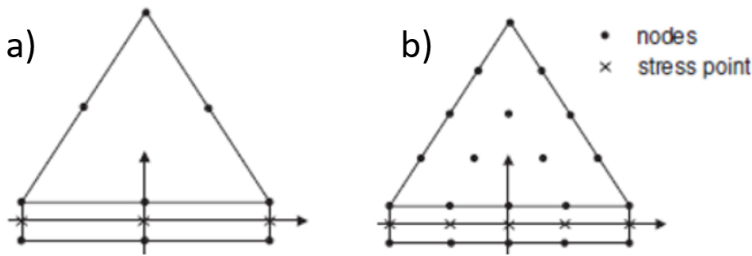


**Figure 3.7:** a) Interfaces in a 6-noded soil element. b) Interfaces in a 15-noded soil element (Brinkgreve et al., 2017b).

Newton-Cotes integration creates the stiffness matrix for the interface elements (Brinkgreve et al., 2017b). Five stress points lie between the pairs of 5-node interface element for a 15-node soil element, while three stress points lie between the pairs of 3-node interface element for a 6-node soil element. The interfaces can be extended beyond structures and corners.

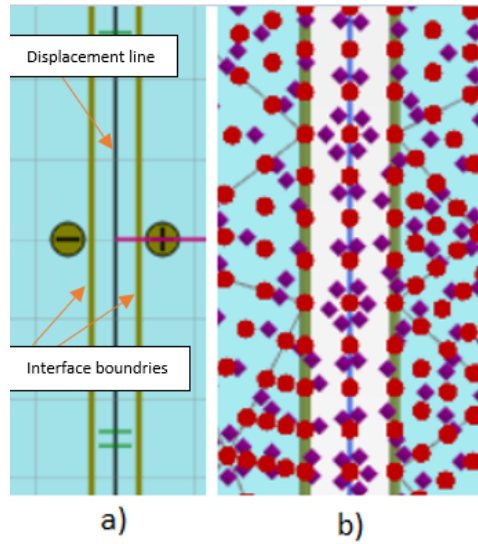


**Figure 3.8:** a) Interface boundaries displayed in PLAXIS model setup. b) Interfaces displayed in the mesh window.

As shown in figure 3.8, a gap between the structure and the surrounding soil is created by the interfaces. It is important to know that the nodes in the interfaces have the same values as the nodes in the structure element, so that the gapping is only present to illustrate the interfaces. The coordinates of the node pairs are equal which means that the interface element has no thickness.

An interface tab sheet is found in the soil window which allows the user to input parameters to describe the soil behavior next to structure elements (Brinkgreve et al., 2017b).  $R_{inter}$  is the strength reduction factor, a roughness ratio, and is the main interface parameter found in this tab sheet in the different models. The interface strength properties are connected to the strength properties of a soil layer by the following equations:

$$c_{inter} = R_{inter} * c_{soil} \quad (3.8)$$

$$\tan(\phi_{inter}) = R_{inter} * \tan(\phi_{soil}) \quad (3.9)$$

$R_{inter}$  can be set rigid, manual or manual with residual strength (Brinkgreve et al., 2017b). The rigid option locks  $R_{inter} = 1$ , which means the interface does not have a reduced strength with respect to the strength in the surrounding soil. Where interfaces are extended beyond structure elements, the  $R_{inter}$  should not have any other value than rigid, as this does not describe the soil-structure interaction. The manual option makes it possible to insert the value of  $R_{inter}$  manually. In reality the soil-structure interaction is not rigid, where the interface is more flexible and weaker than the surrounding soil, and should therefore have a value less than 1 (Johansson and Sandeman, 2014). Installing structures in

the soil, such as a SPW, will usually disturb the soil and cause imperfect adhesion between the two. A value of  $2/3$  for  $R_{inter}$  is assumable when no details are given (Brinkgreve et al., 2017b). A value greater than 1 is possible, but rarely used.

### **SoilTest**

SoilTest is a program within PLAXIS that is, amongst other things, used to evaluate laboratory and field tests (Johansson and Sandeman, 2014). A material is created in PLAXIS which SoilTest uses in combination with the constitutive model to simulate different tests in the material. The basic soil tests simulated are based on a single point algorithm which does not need the creation of a finite element model (Brinkgreve et al., 2017b). The soil test gives the opportunity to simulate different tests; triaxial, oedometer, CRS, DSS, CDSS and general soil test. In this thesis, triaxial and general active and passive tests are simulated to obtain stiffness and strength parameters for different soil models. Undrained isotropic and anisotropic tests were performed by simulating a 10 percent axial strain to see the soil behavior and find the parameters that fit the real test curves done by Multiconsult.

### **Meshing and strength reduction analysis**

In areas where large deformation gradients or large stress concentrations are expected, a finer finite element mesh is desirable (Brinkgreve et al., 2017b). These gradients and concentrations often occur in corners or edges in the geometry model or at structural objects. By default, a coarseness factor of the element mesh is set to 1.0 for geometry entities and 0.25 for loads and structural objects. This can be altered by the user. Acceptable values of the coarseness factor lies between 0.03125 and 8.0.

Running a strength reduction analysis in PLAXIS gives the factor of safety (FoS). All interfaces and soil clusters are taken into account by default. By using enhanced safety analysis, specific soil structures or clusters can be excluded from the strength reduction procedure. This option can be used when some parts of the cluster go into failure with a lower FoS that are not relevant to the failure mechanism in question or to avoid unrealistic failure mechanisms.

### **Drainage type**

Most models in PLAXIS have different drainage types that must be decided (Brinkgreve et al., 2017b). MC can choose between a drained analysis and an undrained analysis from three different undrained options; (A), (B) or (C). NGI-ADP is mainly an undrained shear strength model, but a drained analysis can be carried out. For undrained analysis, only Undrained(B) and Undrained(C) are possible. HS is mainly an effective based model, but an undrained analysis can be carried out with Undrained(A) and Undrained(B). No excess pore pressures are generated using the drained behavior option, which is the case for dry soils or soils with high permeability. Undrained(A) is an undrained analysis with effective strength and effective stiffness parameters. This option gives a prediction of pore pressures and can be followed up by a consolidation analysis. The undrained shear strength ( $S_u$ ) is not an input parameter, but a consequence of the model. Therefore, it is important to

control and compare the shear strength in PLAXIS output with the desired strength profile.

The use of Undrained(A) can overestimate  $c_u$  (Johansson and Sandeman, 2014). It is calculated by being increased until the stress path reaches the failure line. This way the stress path is different from reality as illustrated in figure 3.9. The Undrained(B) option uses effective stiffness and  $S_u$  as input parameters, and gives a prediction of pore pressures (Brinkgreve et al., 2017b). The  $S_u$  is not updated when followed by a consolidation analysis, and therefore should be used with care. In the Undrained(B) setting, the overestimation does not occur as the undrained strength is an input parameter, as long as the undrained parameters are used (Johansson and Sandeman, 2014). Still, this stress path may also differ from the real stress path. Both deviations from the real stress paths come from the assumption of the linear elastic perfectly-plastic behavior in MC. HS includes a cap that forces the stress paths to bend towards the failure line, but still undergoes the same mechanism for overestimation.

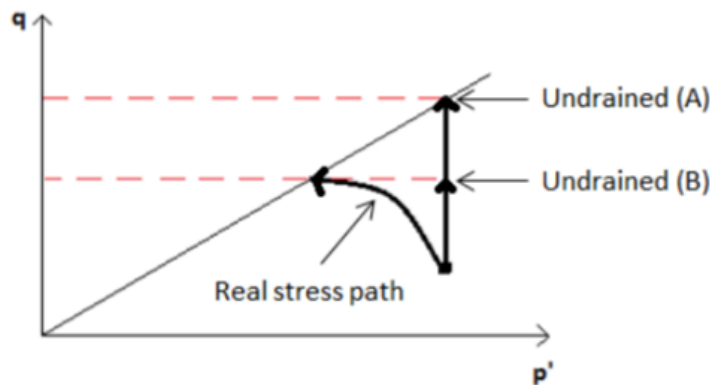


**Figure 3.9:** Stress paths for different undrained settings from MC in PLAXIS (Johansson and Sandeman, 2014).

To get direct control of the undrained shear strength in Undrained(A), the friction angle ( $\phi$ ) may be set to zero and cohesion ( $c$ ) set to  $c_u$  ( $S_u$ ) for undrained materials (Brinkgreve et al., 2017b). By doing this, the model will not include the change of shear strength with consolidation. The Undrained(C) option states all parameters as undrained, like the undrained Young's modulus ( $E_u$ ) and an undrained Poisson's ratio ( $\nu_u$ ) close to 0.5. A value of 0.495 is set by default, as an exact value of 0.5 will lead to singularity in the stiffness matrix. Only MC and NGI-ADP have the possibility to choose the Undrained(C) option. No distinction is generated between the pore pressures and the effective stresses in this option, which gives all effective stress outputs to be the same as the total stress outputs. Hence, there are no pore pressures and the  $K_0$  value that generates initial stresses is related to the total stresses. As the Undrained(C) option does not give a prediction of pore pressures, the model cannot be used to calculate consolidation phases. The Undrained(C) option is chosen for both the MC and NGI-ADP in this thesis, while both Undrained(A) and Undrained(B) options are calculated for HS.

### 3.2.2 GeoSuite Excavation

A team of professional geotechnicians from universities, research organizations and consultant agencies in Norway and Sweden, were assembled in 2002 to develop the program package Geosuite (Lacasse et al., 2016). This thesis is focusing on a part of that package; GeoSuite Excavation.

*"GeoSuite Excavation is a simple FEM-program analyzing a beam supported by non-elastic springs."*, from Vianova Geosuite (2009, pp. 6).

GS is used to calculate displacements and forces in diaphragm walls or sheet piles (Vianova Geosuite, 2009). The earth pressure distribution is determined on both sides of the wall, where excavation, loads, prestressed anchors, struts or other effects may cause reactions in the wall. The program makes it possible to specify several effects as spring stiffness, displacements and load distributions. The construction sequence can be divided into phases, which may be analyzed one by one or continuously within the program. By evaluating the results from the different phases, each phase can be reanalyzed to find the most economical and safe solution to a problem.

#### Basic theory

In GS the sheet pile wall is divided into unit length elements (Vianova Geosuite, 2009). They are approximated to be vertical linear elastic beam elements. The surrounding soil support is represented by continuous non-linear springs, with the spring stiffness linearly varying between the nodes (fig. 3.10). By modeling the SPW in this way, vertical load changes and deformations are not considered. A stiffness matrix is generated for the entire system by establishing a stiffness equation for each element (Vianova Geosuite, 2009). The relationship between resulting displacements and applied loads are given by the stiffness equations and can be used for calculating earth pressure values and cross-sectional forces. When the earth pressures get close to passive or active limit, the stiffness reduces as the spring stiffness down the wall is assumed to be load dependent. The load increments must be divided into load steps as the springs are non-linear. Each load step requires new calculated soil stiffness for the equations, and thereby the "prediction correction principle" is applied. Average soil stiffness and earth pressure are predicted for the next load increment in this method. For each increment, the program uses the tangential stiffness for the middle of the load step. Cross-sectional forces, displacements and soil reactions are accumulated for the different load increments, while the actual soil reaction is continuously controlled contrary to limiting pressures.

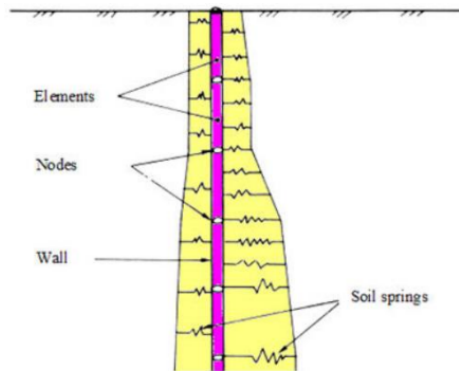


**Figure 3.10:** Elements in the SPW in GS (Vianova Geosuite, 2009).

For each node, the characteristics of the soil-springs are produced on both sides of the SPW (Vianova Geosuite, 2009). All nodes use the same principles for generating displacement and limiting earth pressures relationships. Fundamental soil-spring parameters are displayed in figure 3.11.

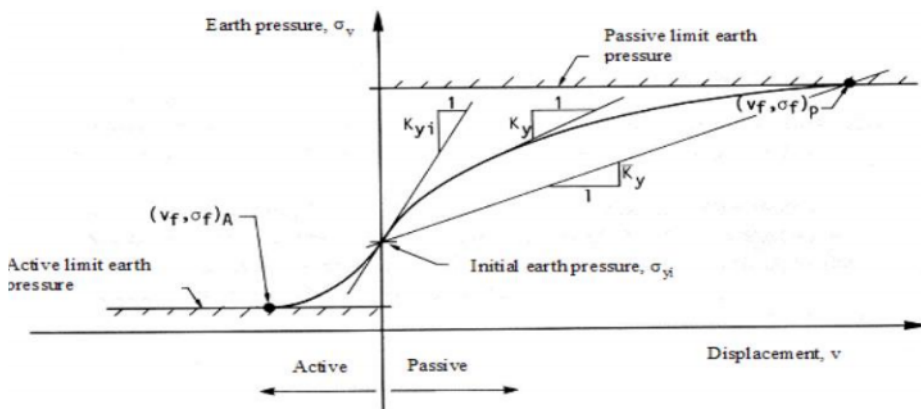


**Figure 3.11:** Typical earth pressure – displacement relationship for a soil spring in GS (Vianova Geosuite, 2009).

As the earth pressure approaches passive or active limit, the spring stiffness decreases (Vianova Geosuite, 2009). To generate the curve shown in figure 3.11 the failure displacement point  $(v_f, \sigma_f)$  and an initial stiffness  $(K_{yi})$  are used. A hyperbola represents the behavior of the spring stiffness as the curve shows. This gives the equation for earth pressure:

$$\sigma_y = \sigma_{yi} \pm \frac{v}{\frac{1}{K_{yi}} + \frac{v * R_f}{\sigma_f - \sigma_{yi}}} \quad (3.10)$$

The failure stress ( $\sigma_f$ ) is calculated using different soil models.  $R_f$  is a scaling parameter and was set to 0.8 in the 2009 version of the program for all models (Vianova Geosuite, 2009). Before this version, it was calculated by the equation:

$$R_f = 1 - \frac{\bar{K}_y}{K_{yi}} \quad (3.11)$$

Where  $\bar{K}_y$  is the secant that intersects the limit pressure and the hyperbola at initial pressure:

$$\bar{K}_y = \frac{\sigma_f - \sigma_{yi}}{v_f} \quad (3.12)$$

Equation 3.11 makes sure the failure displacement point ( $v_f, \sigma_f$ ) is on the curve (Vianova Geosuite, 2009). The initial stiffness ( $K_{yi}$ ) is given from derivation of equation 3.10 for  $v$  equal to zero. The tangent spring stiffness for the passive case is shown in equation 3.13. For active soil condition, similar expressions can be derived.

$$K_y = \frac{d\sigma_y}{dv} = K_{yi} \left[ 1 - \frac{(\sigma_y - \sigma_{yi}) * R_f}{\sigma_f - \sigma_{yi}} \right]^2 \quad (3.13)$$

The soil will often have a stiffer response when a change in load direction appears (Vianova Geosuite, 2009). When the soil pressure moves towards an isotropic stress state caused by a displacement direction, the program defines this as unloading, and initial spring stiffness is used. This usually results in displacement hysteresis.

### **Roughness**

The roughness ( $r$ ) is applied as the soil mass tends to move vertically relative to the SPW (Vianova Geosuite, 2009).  $r$  is a measure of the friction that occurs caused by relative vertical movement, and should not be mistaken as a measurement of maximum skin friction.  $r = 0$  is a correct choice if there is no relative vertical movement. When the SPW rests on impenetrable soil layers or rock,  $r = 0$  is considered a conservative value, and is usually chosen as the vertical movement downwards is rejected.  $r = 0$  is in most cases a non-conservative option when the SPW tip is in soft soil. The roughness number's magnitude and direction needs to be specified by the user, as there is no calculation of vertical displacements. In automatic soil models, the roughness number is used to calculate limit earth pressure values. This generates information about the resulting vertical equilibrium situation. It is assumed that the soil moves in the same vertical direction along the entire wall, hence the wall friction is unidirectional along both sides of the wall. It may not be like this in reality because of different effects, i.e. anchor force. The program requires the user to specify the shear stress direction, either uplift or down-drag. This information is used to define a negative or positive roughness value for passive and active earth pressure. If the soil tends to lift the SPW upwards, the program defines the roughness number as positive, even if it is an active or passive condition. For a wall fixed in the vertical direction, the shear stress will normally be downwards on the back side and upwards on the front side (fig. 3.12).



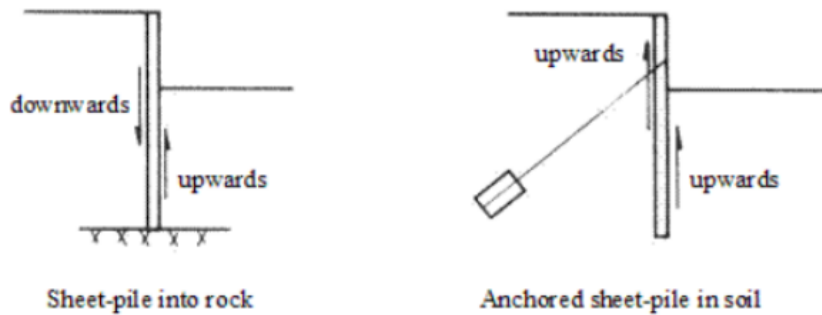


**Figure 3.12:** Soil shear stress along the SPW (Vianova Geosuite AB 2009).

### Soil models

GS Excavation has five soil models available for calculating soil stiffness and limiting earth pressures (Vianova Geosuite, 2009). Two of the models are based on total stresses that are appropriate for soft material with low permeability (clays). The different soil models with corresponding parameters from Vianova Geosuite (2009):

- ESA – Effective Stress Automatic:
  - $a$  Attraction.
  - $\phi$  Friction angle.
  - $M$  Stress dependent Oedometer modulus.
- ESM – Effective Stress Manual:
  - $K_A$  Active earth pressure coefficient.
  - $K_P$  Passive earth pressure coefficient.
  - $K_{yi}$  Initial spring stiffness.
- ESS – Effective Stress Automatic:
  - $c$  Cohesion.
  - $\phi$  Friction angle.
  - $E$  Young's modulus.
- TSA – Total Stress Automatic:
  - $c_u$  Undrained shear strength.
  - $G$  Shear modulus.
- TSM – Total Stress Manual:
  - $D_A$  Net active total stress difference.
  - $D_P$  Net passive total stress difference.
  - $K_{yi}$  Initial spring stiffness.

In this thesis only the ESS and TSA models are used.

### ESS

In this model the condition of equilibrium on the Rankine stress fields gives the basis for calculations of active and passive earth-pressure limits, and are calculated by the equation (Vianova Geosuite, 2009):

$$p_A^p = K_p^A * (p_v' + \frac{c}{\tan \phi}) - \frac{c}{\tan \phi} \quad (3.14)$$

When defining the roughness downwards ( $r < 0$ ), the program will use the following equations for active earth pressure ( $r < 0$ ):

$$\tan(\rho) = \frac{\phi}{\gamma_m} \quad (3.15)$$

where  $\gamma_m$  is a material coefficient defined by the user.

$$\alpha_A = 45 - \frac{\rho}{2} \quad (3.16)$$

$$f = \frac{1}{|r|}(1 - \sqrt{1 - r^2}) \quad (3.17)$$

$$\tan \omega_A = f * \tan \alpha_A \quad (3.18)$$

$$N = \tan^2(45 + \frac{\rho}{2}) \quad (3.19)$$

$$N_\theta = e^{2\omega_A * \tan \phi} \quad (3.20)$$

$$N_\omega = \frac{1 - \sin \rho * \cos 2\omega_A}{\cos^2 \rho} \quad (3.21)$$

$$K_A = \frac{2N_\omega}{N_\theta(N + 1)} \quad (3.22)$$

When defining the roughness upwards, the program will use the following equations for passive earth pressure ( $r > 0$ ):

$$\alpha_P = 45 + \frac{\rho}{2} \quad (3.23)$$

$$f = \frac{1}{|r|}(1 - \sqrt{1 - r^2}) \quad (3.24)$$

$$\tan \omega_P = f * \tan \alpha_P \quad (3.25)$$

$$N = \tan^2(\alpha_P) \quad (3.26)$$

$$N_\theta = e^{2\omega_P * \tan \phi} \quad (3.27)$$

$$N_\omega = \frac{1 + \sin \rho * \cos 2\omega_P}{\cos^2 \rho} \quad (3.28)$$

$$K_P = \frac{2N}{N+1} * N_\theta * N_\omega \quad (3.29)$$

Uplift and active earth pressure ( $r > 0$ ), and down-drag and passive earth-pressure ( $r < 0$ ), (commonly used sign definition gives negative roughness number to both situations) give:

$$K_A^p = \frac{1}{[\sqrt{1 + \tan^2(\rho)} \pm \tan(\rho) * \sqrt{1 - |r|}]^2} \quad (3.30)$$

where the + and – signs refer to active and passive earth-pressures respectively. The unloading/reloading and initial spring stiffness, at both sides of the wall is defined by (Vianova Geosuite, 2009):

$$K_{yi} = 1 * E, \quad (3.31)$$

When soil failure is reached, the secant stiffness ( $K_y$ ) is set to 20 % of the initial stiffness through  $R_f = 0.8$ .

### TSA

This model is also based on the Rankine stress fields for calculations of active and passive earth pressure limits, and are calculated by the following equations:

$$p_A^p = p_v \pm \kappa * \frac{c_u}{\gamma_m} \quad (3.32)$$

$\kappa$  is a parameter defined by the roughness ratio ( $r$ ) of the SPW. With  $r < 0$  and an active earth pressure (down-drag), it is given by the following equations:

$$\kappa = 2 * \omega + \cos 2\omega + 1 \quad (3.33)$$

$$\omega = \frac{1}{2} * \sin^{-1} |r| \quad (3.34)$$

$\kappa$  is given by the same equations for  $r > 0$  and a passive earth pressure (uplift) (Vianova Geosuite, 2009). For  $r > 0$  and an active earth pressure (uplift), and for  $r < 0$  and a passive earth pressure (down-drag),  $\kappa$  is defined by:

$$\kappa = 2\sqrt{1 - |r|} \quad (3.35)$$

For an active earth pressure,  $r = 0$  and uplift, the parameter  $\kappa = 2$  (Johansson and Sandeman, 2014). For a passive earth pressure,  $r = 0$  and uplift, the parameter  $\kappa = 1$ . Influence from any local weak layer is not considered, which in reality, may cause the development of a failure surface (Vianova Geosuite, 2009). To include such an effect, the undrained shear strength ( $S_u$ ) must be adjusted manually to get the desired earth pressure along the wall. The initial spring stiffness is assumed to be  $K_{yi} = 4 * G$  on both sides of the SPW.

### 3.2.3 Hand calculation

One should always perform hand calculations to get an indication of what is to be expected. Both drained and undrained analysis is necessary in this thesis as the profile is complex. The drained analysis will rely on equation 3.14 and 3.30, while the undrained will rely on the following equations (Janbu et al., 2016):

$$p_a^p = p_v \pm \kappa S_u \quad (3.36)$$

$$\kappa = 2\left(\omega + \frac{1}{1 + f_\omega^2}\right) \quad (3.37)$$

$$\tan \omega = f_\omega \quad (3.38)$$

$$f_\omega = \frac{1}{r}(1 - \sqrt{1 - r^2}) \quad (3.39)$$

The earth pressure from equation 3.14 and equation 3.36 is integrated along the wall to find earth forces. To simplify, the two anchor forces are assumed equal as the terrain is inclined, given as a possible method from Flaate (1966). The forces are calculated as the active force above excavation level. Also, suction will be ignored. The force obtained will be the horizontal anchor force ( $P_H$ ). When the anchors are inclined, the forces need to be transformed to obtain the actual anchor force ( $P$ ) by the formula (Johansson and Sandeman, 2014):

$$P = \frac{P_H}{\cos(\alpha)} \quad (3.40)$$

Where  $\alpha$  is the angle of the anchors.

# Project Kværnerdammen F1

## 4.1 Site information

The Kværnerdammen F1 project (fig. 4.1) comprises the construction of a seven-story building with basement at the toe of a slope at Kværnerbyen, Oslo (MulticonsultASA, 2017a). Multiconsult is engaged as RIG (consulting engineer geotechnics) regarding the detailed projection of Kværnerdammen. The construction pit is established with a permanent SPW in the slope to the east side of the building. Quick clay is registered where the SPW is installed, hence LCC are used to ensure the stability during the installation of the SPW. The SPW is strengthened to have a lifetime of one hundred years. It is installed with two rows of anchors connected to bedrock at different levels, while the SPW itself is bolted to bedrock.

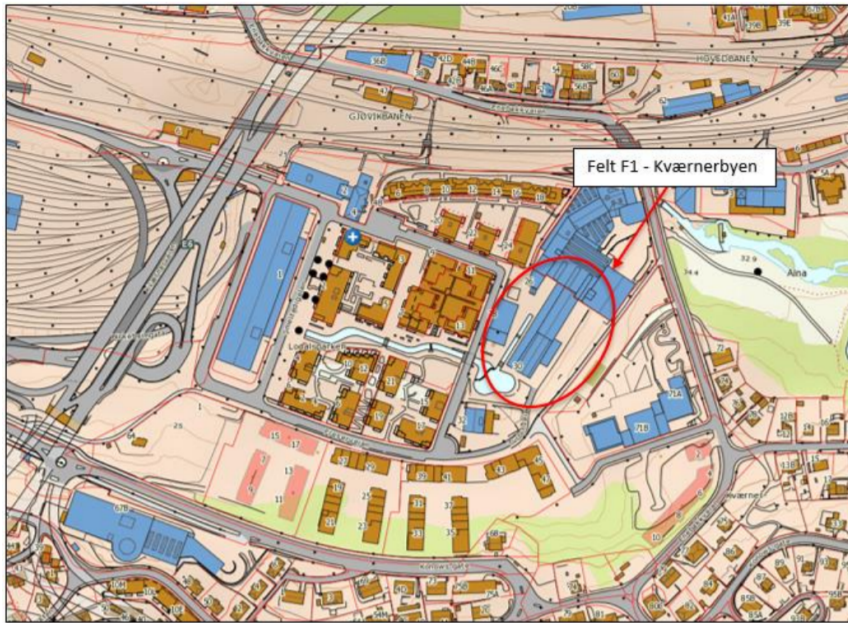


**Figure 4.1:** Map with placement of Kværnerdammen F1 (MulticonsultASA, 2017e). North is up.

### Topography

The main part of the building is on a flat terrain, at the elevation of approximately +18 m at the toe of a sloping terrain (MulticonsultASA, 2017e). The eastern side of the building is cutting in to the slope, which is affected by a pedestrian bikepath (w/c path), a parking garage and a kindergarten further up the slope. The w/c path is placed on an established plateau in the slope at the elevation of +26 m to +27 m.

### Soils

Quaternary geological map indicates that the soils in the area consist of thick marine deposits (MulticonsultASA, 2017e). Ground examinations performed by Multiconsult and former examinations done by NGI and Rambøll (RB), indicate that the masses consist of a relatively hard top layer of fill and dry crust above silty clay and quick clay. Solid masses are registered at several places over bedrock, assumed to be moraine. The dry crust varies between 1 to 4 m in thickness, while the silty clay layer beneath varies between 2 to 5 m. The quick clay detected in the slope has a thickness up to 9 m. The closest zone of quick clay is just east to the planning area, and has a medium degree of danger obtained from NVE interactive database, which is also obtained in Vernang et al. (2011). There is no evidence of quick clay beneath the footprint of the building, but the ending and extent of the quick clay is unsure. Piezometers show that the groundwater table is about 2 to 4 m beneath the current terrain.

## Bedrock

By looking at figure 4.2, the depth to assumed bedrock is increasing up the slope. At the bottom of the slope, the depth is about 3 to 6 m. The SPW is bolted to the bedrock, but as the depth varies there may be openings in between.

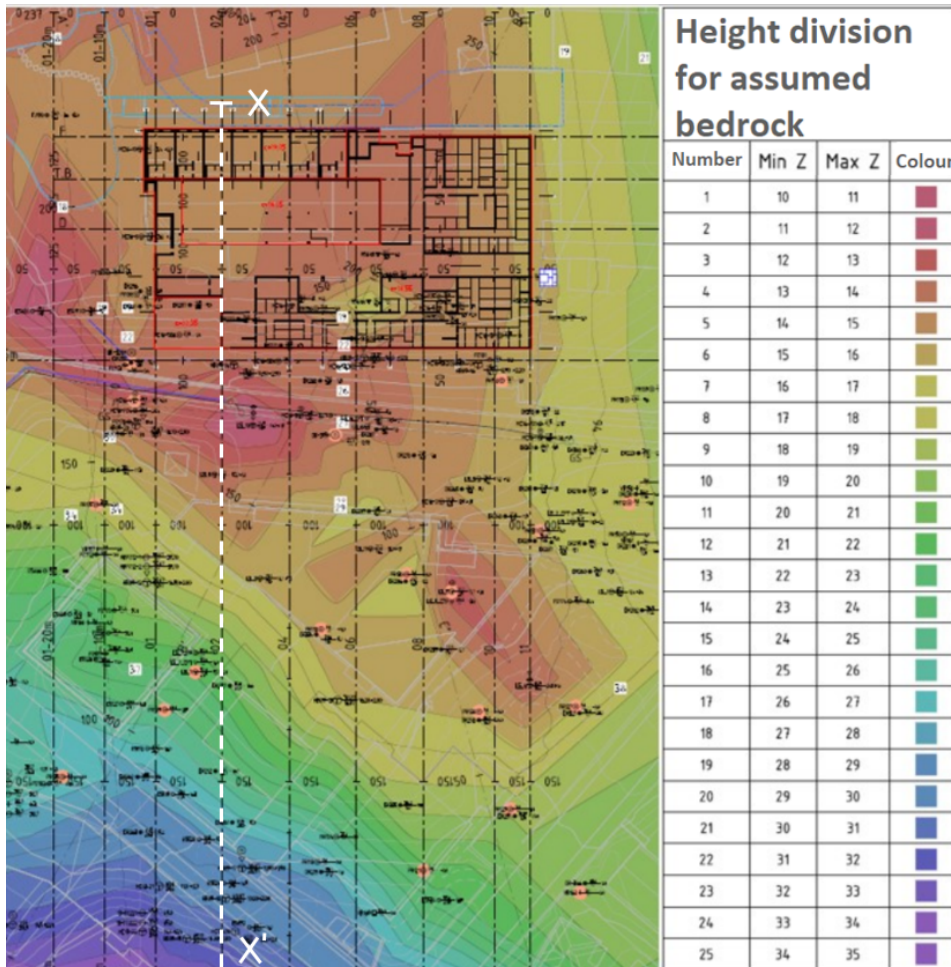


Figure 4.2: Map of bedrock elevation at Kværnerdammen F1 (MulticonsultASA, 2017b).

## Lime cement columns

After quick clay was detected in the slope it was decided to stabilize using lime cement. The reinforcement is placed on the pit side (between the SPW and the building) after the SPW is installed. The piles are inserted as ribs in a grid pattern as close to the SPW as possible, illustrated in figure 4.3. This figure deviates a bit from reality as there are no LCC behind the SPW. There is not 100 % contact between the lime cement piles and the SPW,

and the lime cemented area is not fully influenced by the reinforcement, as seen by the gaps. Tests of the LCC at 5 m and 10 m below terrain 14 days and 28 days after installation, show an average strength of 225 kPa and 260 kPa respectively (MulticonsultASA, 2017e). Note that these tests are taken from the lime cement piles, and not the surrounding soil.

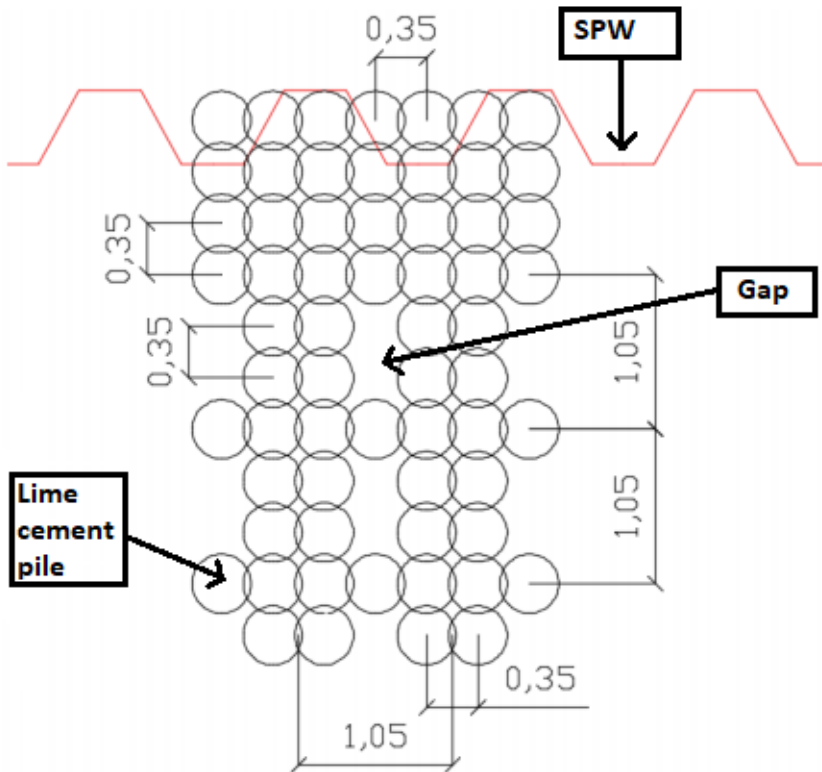


Figure 4.3: Sketch of pattern for installation of LCC (MulticonsultASA, 2017c).

### Excavation process

The excavation process is divided into several steps, called phases, and consists of both anchoring and excavation. Note that these phases are not numbered in the same way in the simulation programs. The excavation process is taken from MulticonsultASA (2017b).

- **Initial phase:** Before starting the excavation, a fill is placed at the foot of the slope to work as a counterweight, as well as a working plateau for machines that install the SPW and LCC to stabilize the area (fig. 4.4). The SPW is then installed with footing bolted into bedrock before LCC is installed.



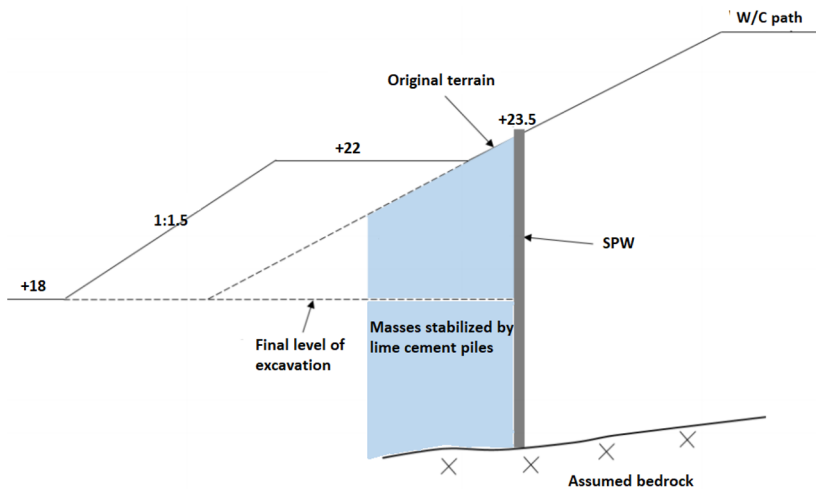


Figure 4.4: Sketch of initial phase (MulticonsultASA, 2017b).

- Phase 1:** The first excavation phase is to elevation +21, locally creating a plateau of 1 m width and shortening the counter fill by 0.5 m to elevation +21.5 m (fig. 4.5). The maximum allowed sloping between the SPW and the plateau is 1:1.

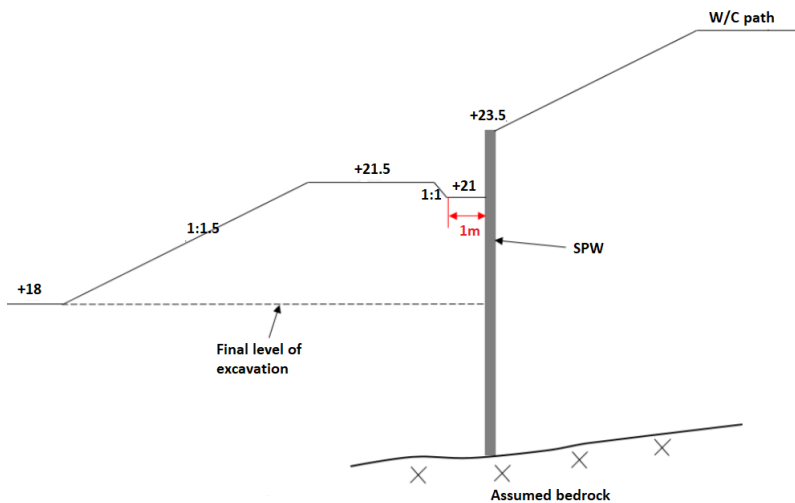
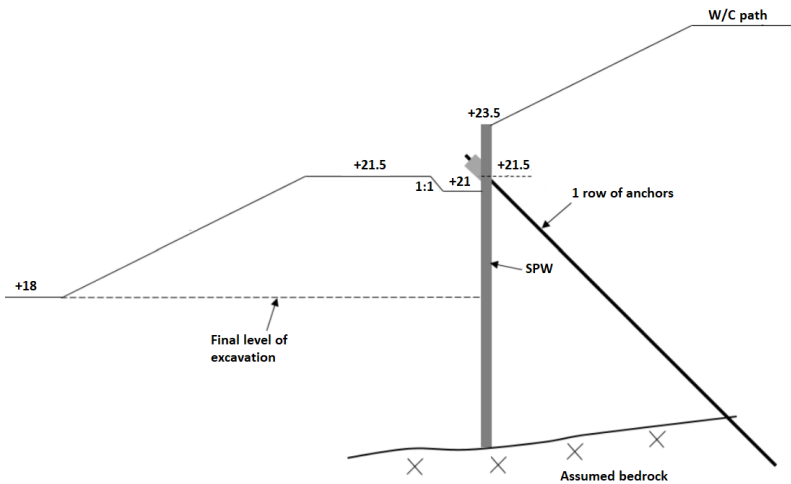


Figure 4.5: Sketch of phase 1 (MulticonsultASA, 2017b).

- Phase 2:** The top row of anchors is established at elevation +21.5 with a 45-degree angle to bedrock (fig. 4.6). The center spacing is 2.8 m. The anchors are prestressed and tested.



**Figure 4.6:** Sketch of phase 2 (MulticonsultASA, 2017b).

- Phase 3:** After the top row of anchors is installed, excavation is done sectional along the SPW line. The excavation is done to elevation +18.5 m, locally creating a plateau of 1 m width and shortening the counter fill to +19.5 m (fig. 4.7). The maximum allowed sloping between the SPW and working plateau is 1:1.

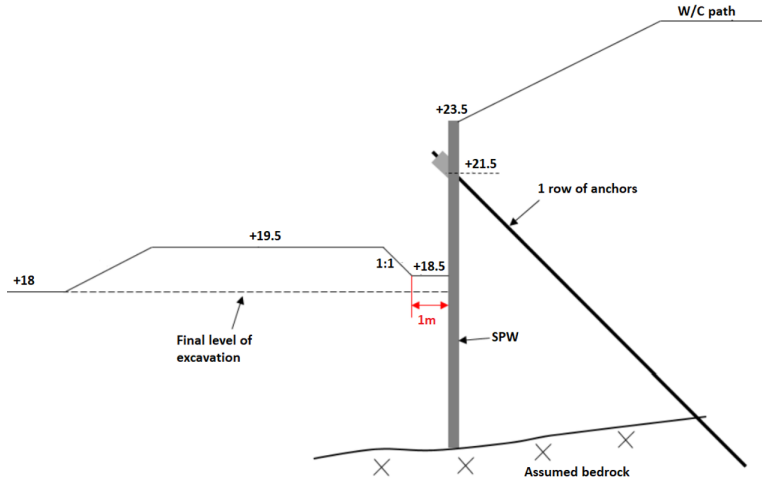


**Figure 4.7:** Sketch of phase 3 (MulticonsultASA, 2017b).

- Phase 4:** The bottom row of anchors is established at elevation +19 m with a 45-degree angle to bedrock (fig. 4.8). The center spacing is 2.8 m. The anchors are prestressed and tested.

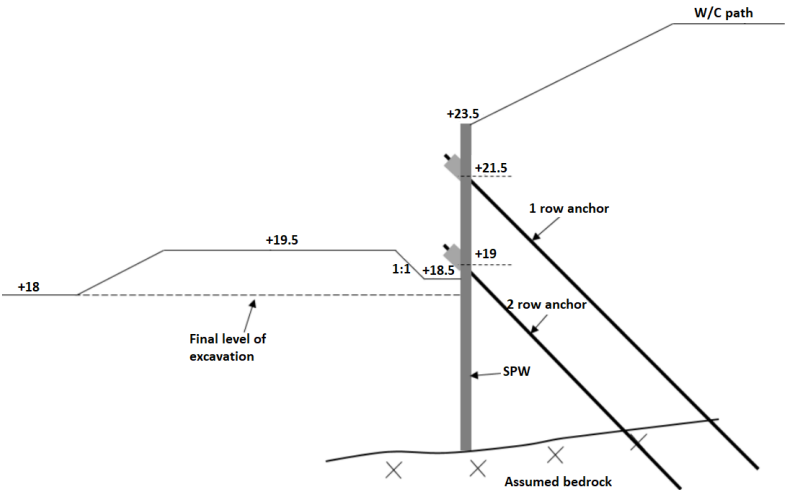


Figure 4.8: Sketch of phase 4 (MulticonsultASA, 2017b).

- **Phase 5:** After the bottom row of anchors is installed, excavation is done to the final level at elevation +18 m (fig. 4.9).

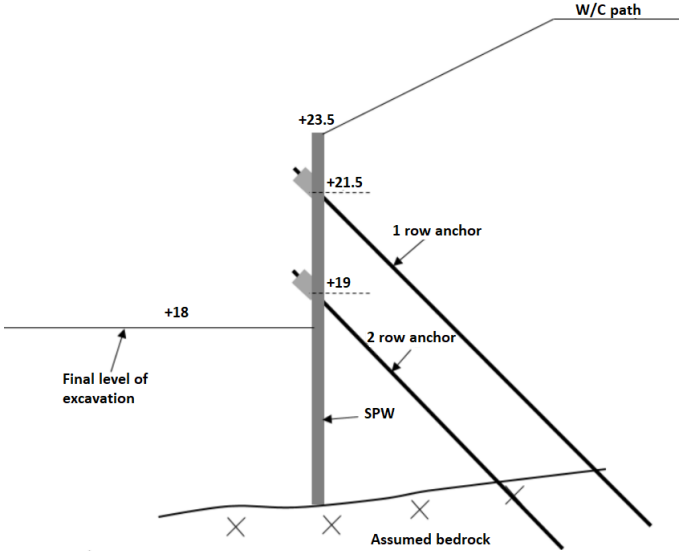


Figure 4.9: Sketch of phase 5 (MulticonsultASA, 2017b).

## 4.2 Profile X-X'

The profile marked on the map in figure 4.2 and appendix A.1 is chosen as the cross section for calculations of the SPW. Looking at the bedrock elevation map (fig. 4.2) and

topographical maps combined with Multiconsult's internal drawings, the cross section is formed to represent a typical profile along the SPW line. Profile X-X' is chosen based on several reasons; Nearly maximum depth to bedrock along the SPW-line is at this area (10.5 m), both the parking garage and kindergarten are directly in contact with the profile line, and moraine material is registered over bedrock. Also, the profile is orthogonal on the SPW close to an inclinometer which, in theory, should give accurate displacement results.

### Stratification

Different boreholes located close to profile X-X' are projected on to the profile line (fig. 4.10). These boreholes are taken from several tests done by Multiconsult (MulticonsultASA, 2017e), NGI (NGI, 2009), Rambøll (Rambøll, 2009) and Løvlien Georåd (Georåd, 2008) in the local area. The different soil materials are observed in some of the different boreholes and are used in combination with different profiles to decide the magnitude and thickness of each layer.

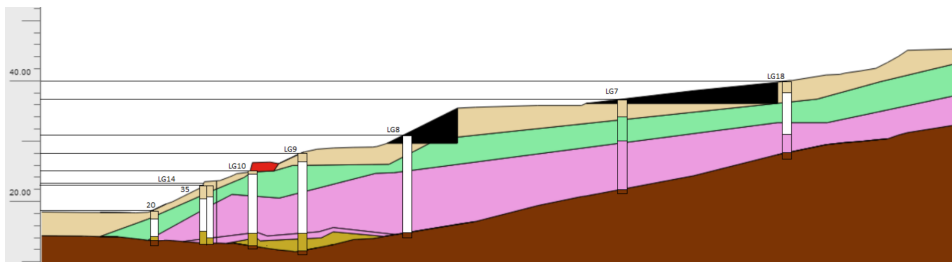


**Figure 4.10:** Sketch of stratification in profile X-X'.

The thickness of the quick clay is partially uncertain up the slope, hence an assessment of generalized and assumed conservative layering has been made for the entire slope behind the placement of the SPW. The profile with boreholes included are shown in figure 4.11.

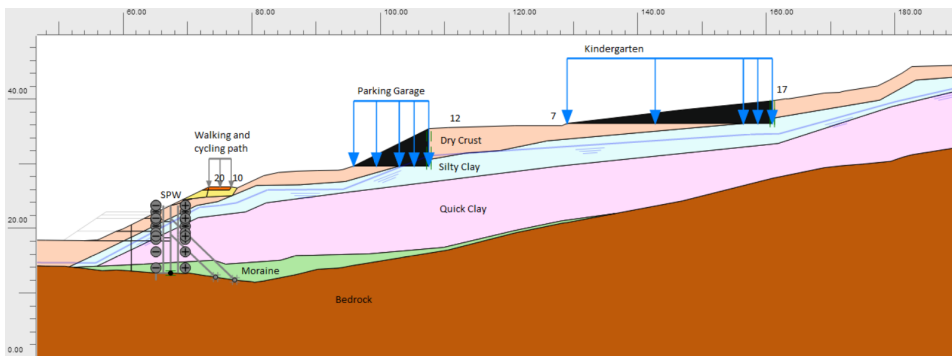


**Figure 4.11:** Layering of soils and bedrock in profile X-X'.

### Strength profile

A study of boreholes and tests throughout the whole area are done to see the change in undrained strength ( $S_u$ ) with depth. Boreholes close to profile X-X' are primarily studied along several interpretations done by MulticonsultASA (2017e) and NGI (2009). Boreholes 6, 7, 10, 12, 17 and 20 from NGI (2009) are chosen. These boreholes are included in NGI's stability analysis of profile A-A' (NGI, 2009), a profile located close to profile X-X' (app. A.1). The interpretations of undrained strength with depth includes values based on CPTu, cone tests and triaxial tests (fig. 4.12).

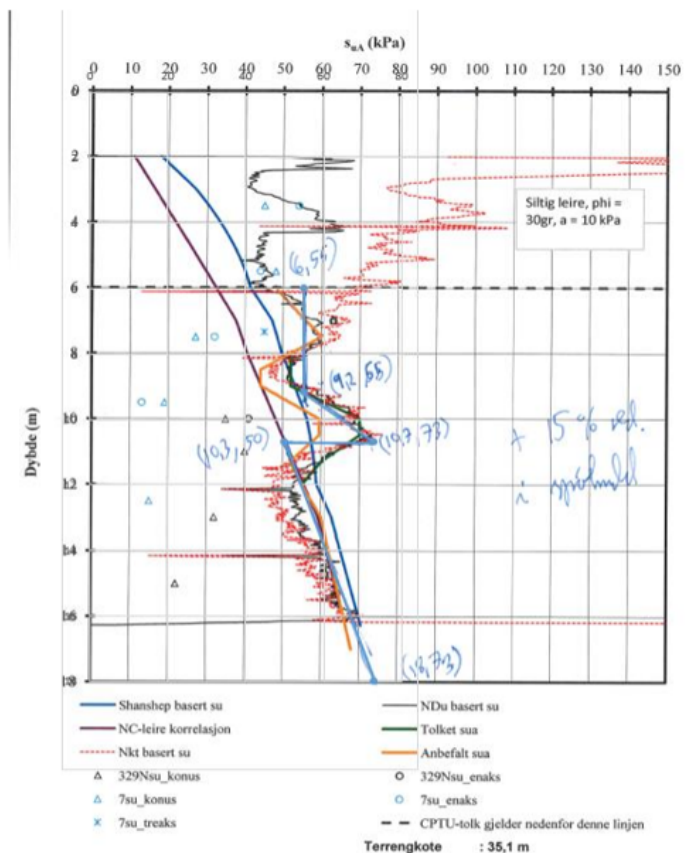


**Figure 4.12:** Shear strength interpretation from borehole 12 by Multiconsult based on NGI's earlier research (MulticonsultASA, 2017a).

The interpretations of undrained shear strength from the different boreholes are projected to profile X-X' as shown in figure 4.13. Note that figure 4.13 is added in appendix A.2 for better visibility of details. All interpretations of undrained shear strength are added in appendices A.3 - A.7.

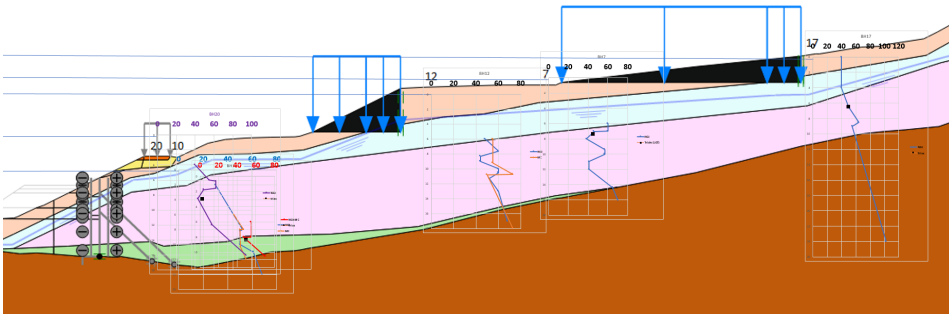


**Figure 4.13:** Strength profile ( $S_u^A$ ) for profile X-X'.

The black squares in the interpretation lines (fig. 4.13) are triaxial tests taken close to the same boreholes as the different CPTu tests. As this is slope involving excavation in a project with strict displacement demands, it's important that the different materials correspond to the strength profile.

## 4.3 Input parameters

### 4.3.1 Intro

To create the input parameters for the different soil models in PLAXIS and GS, laboratory tests done by MC' (MulticonsultASA, 2017e), NGI (NGI, 2009), RB (Rambøll, 2009) and LG (Georåd, 2008) are studied. SoilTest is used to create input parameters for different soil models by comparing results with real test results. Different models are then tuned to fit the strength profile. The loads of the existing structures are added as vertical loads in the models with values shown in table 4.1.

**Table 4.1:** Magnitude of loads (MulticonsultASA, 2017a).

Type of load	Magnitude	Unit
Kindergarten	30	kN
Parking garage	30	kN
w/c path	13	kN

The values for the structural components are presented in table 4.2 and 4.3 given by MulticonsultASA (2017a). The prestressing of anchors is described to be 1500 kN for both rows of anchors in MulticonsultASA (2017f). These values are changed in the simulation programs as measured values obtained from load cells show a different magnitude of prestressing (section 4.5).

**Table 4.2:** Parameters for the anchors and the rock bolt.

Component	Upper anchor	Lower anchor	Bolt	Unit
EA	$5.9 \times 10^5$	$5.9 \times 10^5$	$6 \times 10^5$	kN
$L_{spacing}$	2.8	2.8	1.4	m
$ F_{max,tens} $	2375	2375	499	kN
$ F_{max,comp} $	1.0	1.0	499	kN
Pre-stress	1775	1390	-	kN

**Table 4.3:** Parameters of the SPW.

Component	AZ38-700	Unit
EA	$4.83 \times 10^6$	kN/m
EI	$199 \times 10^3$	$kNm^2/m$
w	1.808	kN/m/m
$\nu$	0.2	-

### 4.3.2 PLAXIS

Different constitutive models are inserted in the clay layers while the dry crust, moraine and fills stay the same throughout the changing of models. The parameters for the dry crust, moraine and different fills are obtained from MulticonsultASA (2017a) combined with Multiconsult's own PLAXIS model of the problem (tab. 4.4). Hence, only the silty clay and quick clay are tested with the constitutive models: NGI-ADP, HS and MC.

**Table 4.4:** Input parameters for MC-materials in PLAXIS.

	Stone fill	Fill	Counter fill	Dry Crust	Moraine	Unit
Model	MC	MC	MC	MC	MC	-
Drainage	Drained	Drained	Drained	Drained	Drained	-
$\gamma$	19	19	19	19.5	19	$kn/m^3$
$E'$	10830	10830	10830	10000	20800	kPa
$E'_{oed}^{ref}$	14580	14580	14580	13460	28000	kPa
$c_{ref}$	0.1	4	5	3.5	0.1	kPa
$\phi$	45	31	45	30	38	°
$\psi$	0	0	0	0	0	°
$R_{inter}$	N/A	N/A	N/A	0.5	0.5	-

The stone fill and fill defines the top layers of the w/c path. The bedrock and rigid materials (tab. 4.5) consist of parameters taken from the same data source as table 4.4. The existing buildings are modeled as vertical loads cutting horizontally into the slope, with weightless linear elastic material filling out the cut-out terrain (see appendix A.8).

**Table 4.5:** Input parameters for linear elastic materials in PLAXIS.

	<b>Bedrock</b>	<b>Rigid (buildings)</b>	<b>Unit</b>
Model	Linear elastic	Linear elastic	-
Drainage	Drained	Drained	-
$\gamma$	19.5	0	$kn/m^3$
$E'$	1300000	200000	kPa
$E_{ged}^{ref}$	1750000	269200	kPa
$E_{inc}$	0	9360	kPa/m
$y_{ref}$	0	41.16	m
$R_{inter}$	N/A	N/A	-

The structural components in PLAXIS are added as elastoplastic materials for all soil models (tab. 4.6).

**Table 4.6:** Material type of structural components used in PLAXIS.

<b>Component</b>	<b>Set type</b>	<b>Material type</b>
Anchor n1 +22	Anchors	Elastoplastic
Anchor n2 +19	Anchors	Elastoplastic
Bolt	Anchors	Elastoplastic
SPW	Plate	Elastoplastic

The different soil models are tuned to have approximately the same FoS in the initial state, before any excavation or installation of the SPW. This way the different soil models should represent approximately the same strength in the terrain. The FoS in the terrain is decided to be given by NGI-ADP, as this is an anisotropic model. As mentioned in section 3.2.1 the behavior of soft clays is generally anisotropic and NGI-ADP incorporates active, passive and direct shear strengths. As the case at hand comprises loading/unloading of soil material, the different undrained shear strengths are of importance. HS and MC use an average shear strength, and the models are fitted to a strength profile of  $S_u^{DSS}$  instead of  $S_u^A$ . As this results in a lower FoS for HS and MC in the initial state, before installing the SPW, the  $S_u^{DSS}$  is increased throughout the whole profile to approximately give the same FoS as NGI-ADP.

### NGI-ADP

In Multiconsult's analysis, NGI-ADP parameters were mainly obtained by tuning SoilTest to triaxial tests (fig. 4.14 and 4.15). In this thesis, parameters in all models are tuned primarily using the same triaxials. Two CAUa tests by MC' (MC'1 and MC'4) and three CAUa/CAUp tests by RB (RB5, RB6 and RB17). The location of boreholes from which the samples are taken are shown in appendices A.1 and A.9. The undrained(C) option is chosen for this model.



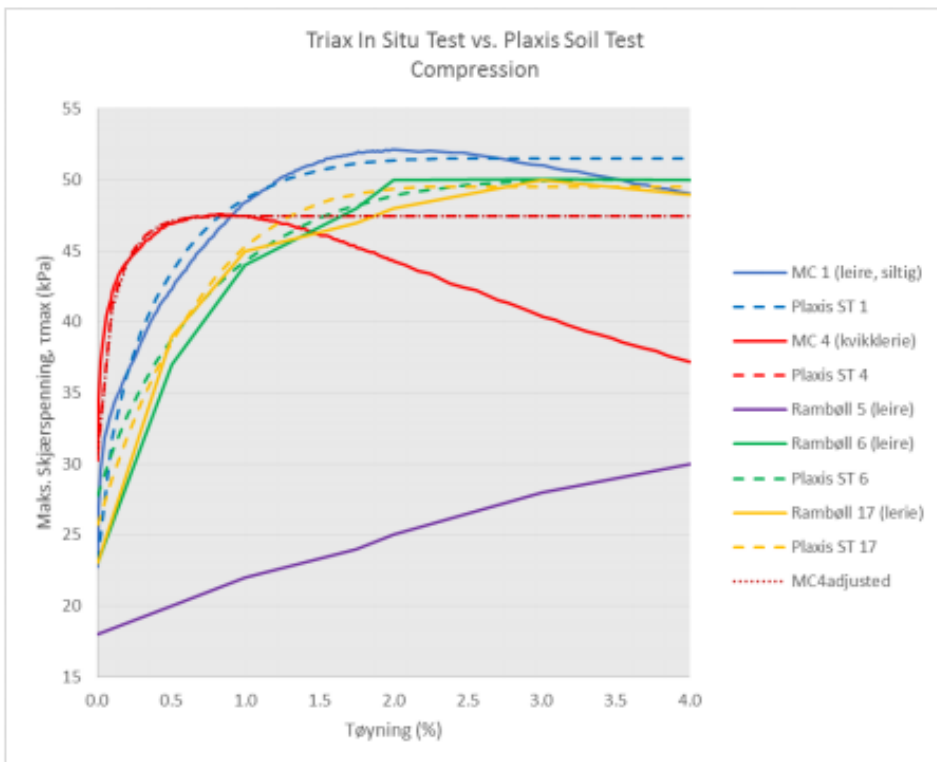


**Figure 4.14:** Interpretation of active triaxial tests (CAUa) against SoilTest done in PLAXIS - 0-4 % strain (MulticonsultASA, 2017a).

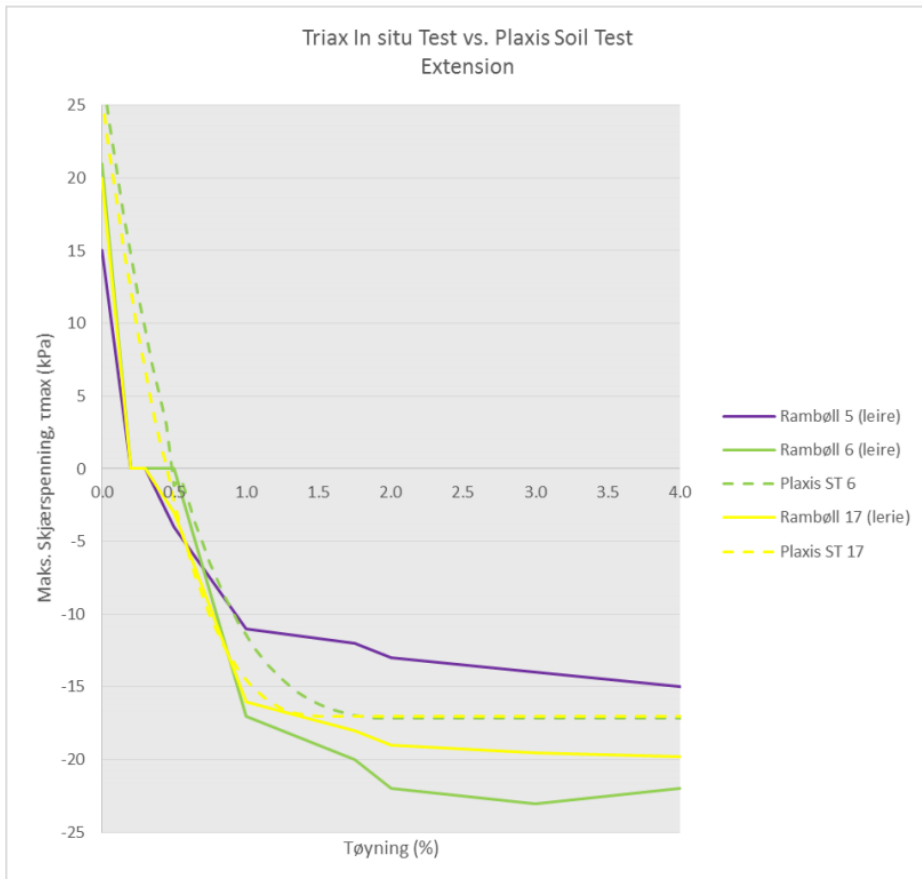


**Figure 4.15:** Interpretation of passive triaxial tests (CAUp) against SoilTest done in PLAXIS - 0-4 % strain (MulticonsultASA, 2017a).

The anisotropic shear strength relations are calculated according to the recommendation from Thakur et al. (2014) for clays with a plasticity index of 15 %. The triaxial tests done by RB are defined as poor to good quality based on the volum of expelled water during consolidation of the tests (MulticonsultASA, 2017a). Multiconsult's MC'1 (silty clay) is defined as good quality, also based on water expulsion, in combination with an analysis of the stress path in the shear phase. This test is mainly used to interpret the parameters for the silty clay. Multiconsult's MC'4 (quick clay) is defined as poor quality, hence a conservative interpretation of the quick clay parameters are based on an approximation between the tests on quick clay (MC'4) and silty clay (MC'1).

As the undrained shear strength show different values with depth at different locations (fig. 4.13), profile X-X' in PLAXIS is split into several clusters to best fit the strength profile. PLAXIS does not interpolate between different strength profiles and layers throughout the cross section, but increases the  $S_u$  horizontally with depth. A vertical inclination ( $vi$ ) is

inserted in the different soil materials, giving the opportunity to create fewer clusters and more accurate correspondence to the strength profile. The  $vi$  tilts the strength profile, and is thus not increasing horizontally with depth. This is not a basic function that can be changed in the soil windows in PLAXIS, but by entering a code in the command window:

`sps (materialname) 'verticalinc' (valueofinclination - dx/dy)`

The  $vi$  tilts around  $x_{ref} = 0$ , and is not a value that can be changed. As the profile X-X' in PLAXIS is not centered around  $x_{ref} = 0$ , the  $y_{ref}$  in the soil models does not represent the height from the horizontal line  $x = 0$ . Hence,  $y_{ref}$  are values chosen to make the PLAXIS model fit the strength profile. A total of 1 silty clay cluster, as the silty clay mainly shows a constant  $S_u$  with depth, and 6 quick clay clusters are made for NGI-ADP (fig. 4.16).

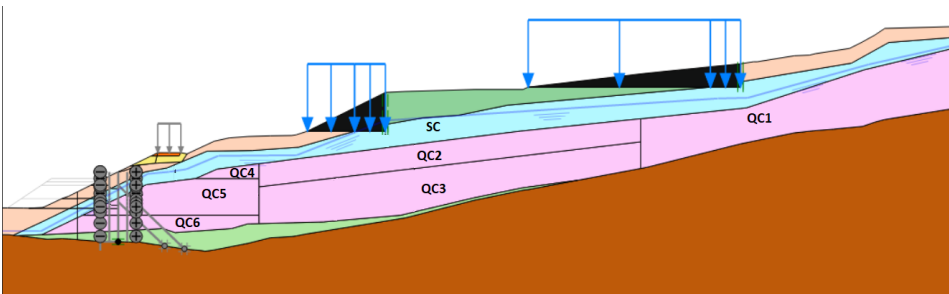


**Figure 4.16:** Soil clusters for NGI-ADP in PLAXIS.

A presentation of the strength profile in PLAXIS from the initial state before excavating are presented in figure 4.22 together with the other constitutive models. The input parameters for NGI-ADP materials are added in table 4.7.

**Table 4.7:** Input parameters for NGI-ADP materials.

	SC	QC1	QC2	QC3	QC4	QC5	QC6	Unit
$\gamma$	19	19	19	19	19	19	19	kN/m <sup>3</sup>
$G_{ur}/S_{uA}$	250	750	750	750	750	750	750	-
$\gamma_f^C$	3.5	1.1	1.1	1.1	1.1	1.1	1.1	%
$\gamma_f^E$	4.5	3	3	3	3	3	3	%
$\gamma_f^{DSS}$	4	2	2	2	2	2	2	%
$S_{u,ref}^A$	55	40	52	48	48	43	50	kPa
$y_{ref}^*$	0	6	0	10	0	14	10	m
$vi$	0	0.17	0	0.12	0	0.1	0.1	-
$S_{u,inc}^A$	0	3	0	3	0	2.3	2.3	kPa/m
$S_u^P/S_u^A$	0.35	0.35	0.35	0.35	0.35	0.35	0.35	-
$\tau_0/S_u^A$	0.45	0.45	0.45	0.45	0.45	0.45	0.45	-
$S_u^{DSS}/S_u^A$	0.63	0.63	0.63	0.63	0.63	0.63	0.63	-
$\nu$	0.495	0.495	0.495	0.495	0.495	0.495	0.495	-
$R_{inter}$	0.5	0.1	0.1	0.1	0.1	0.1	0.1	-

## HS

To create the input parameters for HS, a study of the OCR is performed. In NGI (2009) a study of historical terrain level and today's terrain level shows a change in OCR with depth from 1.37 in the top of the clay layer, to 1.1 in the bottom throughout profile A-A'. This profile is the closest to the profile used in this thesis; profile X-X'. A value of 1.2 is set in the model as a representative value of the clay materials.

**Table 4.8:** Boreholes with corresponding triaxial tests split into locations.

Borehole	Triaxial test	Location
BH17	RB17	1
BH7	LG7	2
BH12	LG7	2
BH20	MC'4	3
BH10	MC'4	3
BH6	RB6	3

As mentioned in section 4.2 the black squares in figure 4.13 show triaxial tests taken close to the same boreholes as CPTu's taken along the strength profile (tab. 4.8). The tests in table 4.8 are used to create HS model materials for silty clay and quick clay at the different locations by using SoilTest. Triaxial CAUa and CAUp tests are primarily used as a basis for the curve fitting in SoilTest, as the case at hand comprises unloading of soil material. Note that LG7 from Georåd (2008) is added in the fitting of the clay materials in HS, which contains a triaxial CIUa test (app. A.10). Oedometer tests are neglected in the fitting of soil material parameters, as fitting to both triaxial and oedometer test results is hard in

practice. The SPW is placed at the end of the slope which indicates that the zone of active undrained shear strength is greater than the zone of the passive undrained shear strength for the failure surface. Hence, active triaxial test results are chosen as the basis for fitting when the fitting of both tests simultaneously are unobtainable. The stiffness parameters  $E_{50}^{ref}$ ,  $E_{oed}^{ref}$ , and  $E_{ur}^{ref}$  are changed in SoilTest to fit the triaxial curves, together with cohesion ( $c$ ), frictional angle ( $\phi$ ) and dilatancy angle ( $\psi$ ). As provided by Surarak et al. (2012) the drained moduli should be used when analyzing undrained materials in HS, hence the undrained(A) option is chosen (with effective stiffnesses) to fit the parameters with undrained tests (see section 3.1). No drained tests are taken. The earth coefficient at rest ( $K_0$ ) is set to 0.59 in SoilTest for all materials as shown in the triaxial tests done by Multiconsult for both quick clay and silty clay. The power  $m$  is set to unity as this is a usual value for soft clays (Nordal, 2017a). Figure 4.17 and 4.18 shows the triaxial curve fitting of the HS clay material in the top of the slope (QC1).

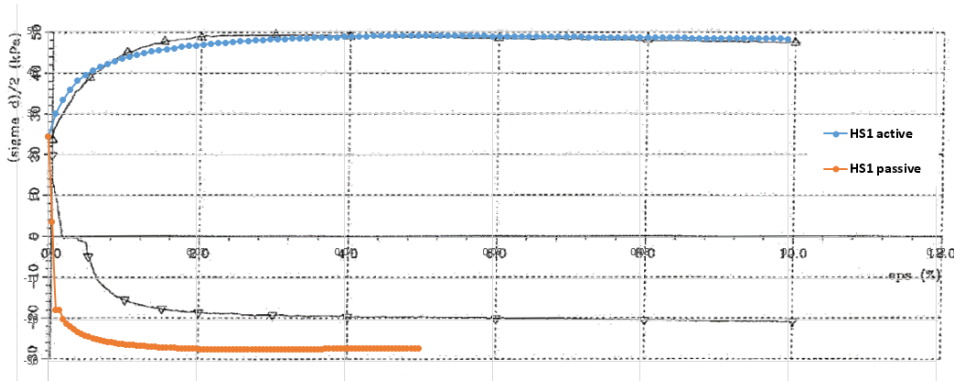


**Figure 4.17:** BH17 (QC1=HS1), fitting of soil test to actual triaxial test results,  $\tau$ - $\epsilon_1$

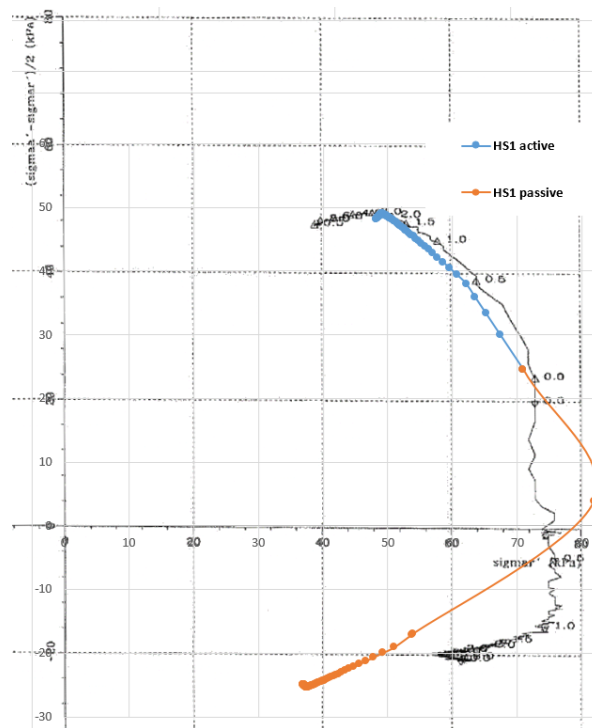


**Figure 4.18:** BH17 (QC1=HS1), fitting of soil test to actual triaxial test results - Stress path

Mainly, the soil materials at location 1 are tuned to triaxial test RB17 (fig. 4.19), the soil materials at location 2 are tuned to triaxial test LG7 and the soil materials at location 3 are tuned to MC'4 (see table 4.8). The silty clay are tuned to triaxial test MC'1, see appendices A.10-A.13 for curve fitting of all clay materials. The stiffness parameters for the HS materials remains unchanged when changing to HS undrained(B), but the undrained shear strength ( $S_u$ ) is changed in the different clusters to fit the strength profile. Changing the model to undrained(B) causes the materials to deviate from their tested stress path as undrained shear strength is inserted. As HS(B) uses an average undrained shear strength,  $S_u^{DSS}$  is inserted ( $0.63 * S_u^A$ ). That means dividing the whole strength profile (fig. 4.13) by a factor to create  $S_u^{DSS}$ . To obtain the same FoS as NGI-ADP in the initial phase,  $S_u^{DSS}$  in the HS(B) materials are increased by 24 % after trial and error. This seems reasonable since the active shear strength zone is much greater as discussed earlier in this section.  $v_i$  and  $y_{ref}$  are added in this model, with the same values as in NGI-ADP (tab. 4.9).

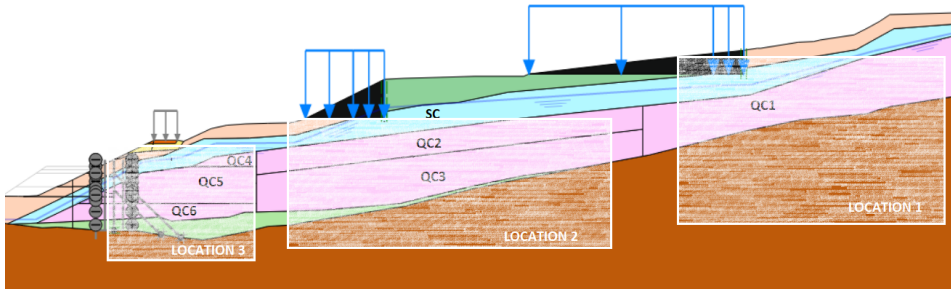


**Figure 4.19:** Soil clusters for HS(B) in PLAXIS with location placement.

**Table 4.9:** Input parameters for HS(B) materials.

	SC	QC1	QC2	QC3	QC4	QC5	QC6	Unit
$\gamma$	19	19	19	19	19	19	19	kN/m <sup>3</sup>
$E_{50}^{ref}$	22000	18000	25000	25000	35000	35000	35000	kPa
$E_{oed}^{ref}$	19000	20000	25000	25000	25000	25000	25000	kPa
$E_{ur}^{ref}$	50000	60000	60000	60000	10E+4	10E+4	10E+4	kPa
$m$	1	1	1	1	1	1	1	-
$S_u^{ref}$	42.79	31.12	40.46	37.35	37.35	33.46	38.9	kPa
$\nu'_{ur}$	0.2	0.2	0.2	0.2	0.2	0.2	0.2	-
$S_{u,inc}$	0	2.33	0	2.33	0	1.79	1.79	kPa/m
$y_{ref}^*$	0	6	0	10	0	14	10	m
$\nu_i$	0	0.17	0	0.12	0	0.1	0.1	-
$OCR$	1.2	1.2	1.2	1.2	1.2	1.2	1.2	-
$K_0$	0.59	0.59	0.59	0.59	0.59	0.59	0.59	-
$R_{inter}$	0.5	0.1	0.1	0.1	0.1	0.1	0.1	-

To fit the HS undrained(A) model to the strength profile,  $\tau_{max}$ -output are inspected in PLAXIS.  $\tau_{max}$  shows the strength profile for HS(A), which is controlled in PLAXIS. By trial and error, the friction angle ( $\phi$ ) and cohesion ( $c$ ) are mainly reduced in this process, as the triaxial curve-fitting alone gives an overestimation throughout the profile. To create a proper strength profile for this model, more clusters are added as illustrated in figure 4.20.

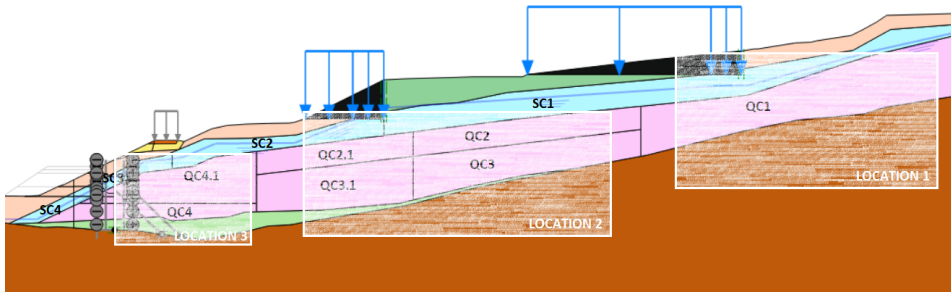


**Figure 4.20:** Soil clusters for HS(A) in PLAXIS with location placement.

The silty clay layer are split into 4 clusters to obtain a constant value along the profile. For the quick clay layer, two more clusters are added in location 2 while one cluster is removed at the top of location 3, giving a total of seven clusters in the quick clay. No  $v_i$  is inserted in the clusters of HS(A) as no undrained shear strength is used. The new parameters still slightly overestimate the strength profile, but is decided to be a good fit. A presentation of the strength profile in PLAXIS from the initial state before excavating are gathered in figure 4.22 together with the other constitutive models. The fitting to the strength profile causes the soil materials to deviate from their coherent triaxial tests. Figure 4.21 shows how a CAUa test from BH17 deviates from its original path with the new parameters inserted to fit the strength profile. The rest of the boreholes are added in appendices A.10-A.13.

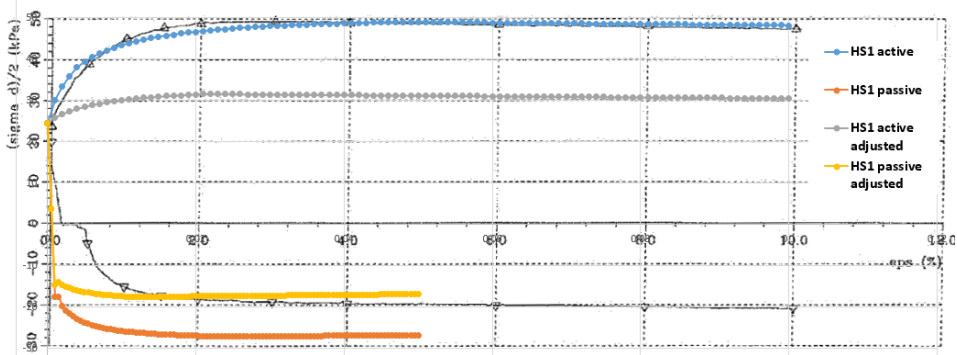


**Figure 4.21:** BH17 (QC1=HS1), triaxial test fitted to curve and adjusted with new parameters,  $\tau$ - $\epsilon_1$

HS(A) is used to control the forces occurring in anchors and rock bolt, and the failure mechanism in a permanent situation. A consolidation phase is run with a following strength reduction analysis. The input parameters for HS(A) materials are added in table 4.10 and 4.11. The permeability ( $k$ ) is based on lab-testing done by MulticonsultASA (2017g).



**Table 4.10:** Input parameters for silty clay materials in HS(A).

	SC1	SC2	SC3	SC4	Unit
$\gamma$	19	19	19	19	kN/m <sup>3</sup>
$E_{50}^{ref}$	22000	22000	22000	22000	kPa
$E_{oed}^{ref}$	19000	15000	19000	19000	kPa
$E_{ur}^{ref}$	50000	50000	50000	50000	kPa
$m$	1	1	1	1	-
$c_{ref}$	4.2	6	6	4.2	kPa
$\phi$	23	34	32	28	°
$\psi$	-0.8	-0.8	-0.8	-0.8	°
$\nu_{ur}$	0.2	0.2	0.2	0.2	-
$K_0^{nc}$	0.61	0.44	0.47	0.53	-
$y_{ref}^*$	0	0	0	0	m
$OCR$	1.2	1.2	1.2	1.2	-
$k$	1.8E-4	1.8E-4	1.8E-4	1.8E-4	m/day
$K_0$	N/A	N/A	N/A	N/A	-
$R_{inter}$	0.5	0.5	0.5	0.5	-

**Table 4.11:** Input parameters for quick clay materials in HS(A).

	QC1	QC2	QC2.1	QC3	QC3.1	QC4	QC4.1	Unit
$\gamma$	19	19	19	19	19	19	19	kN/m <sup>3</sup>
$E_{50}^{ref}$	18000	25000	25000	25000	25000	35000	35000	kPa
$E_{oed}^{ref}$	19250	19250	19250	23170	19250	25000	25000	kPa
$E_{ur}^{ref}$	60000	60000	60000	60000	60000	10E+4	10E+4	kPa
$m$	1	1	1	1	1	1	1	-
$c_{ref}$	0.01	2	5	0.01	1	0.01	0.01	kPa
$\phi$	19	19	26	16	19	21	28	°
$\psi$	-0.05	-0.3	-0.3	-0.3	-0.3	-0.52	-0.52	°
$\nu_{ur}$	0.2	0.2	0.2	0.2	0.2	0.2	0.2	-
$K_0^{nc}$	0.67	0.67	0.56	0.72	0.67	0.64	0.53	-
$y_{ref}^*$	0	0	0	0	0	0	0	m
$OCR$	1.2	1.2	1.2	1.2	1.2	1.2	1.2	-
$k$	1.8E-4	1.8E-4	1.8E-4	1.8E-4	1.8E-4	1.8E-4	1.8E-4	m/day
$K_0$	N/A	N/A	N/A	N/A	N/A	N/A	N/A	-
$R_{inter}$	0.1	0.1	0.1	0.1	0.1	0.1	0.1	-

## MC

The creation of MC undrained(C) is based on parameters presented by MC' (Multiconsult-ASA, 2017a) in addition to triaxial active tests MC'1 for silty clay and MC'4 for quick clay, see appendices A.14 and A.15 for curve-fitting. This model is used as a simplifica-

tion of the problem, with parameters adjusted to triaxial tests taken from boreholes close to the SPW (Location 3). The undrained shear strength inserted in the different clusters are the same as the  $S_u$  inserted in HS(B), that means a  $S_u^{DSS} * 24 \%$ . The same  $v_i$ ,  $y_{ref}$  and clusters of HS(B) are also used in this model (tab. 4.12).

**Table 4.12:** Input parameters for MC materials.

	SC	QC1	QC2	QC3	QC4	QC5	QC6	Unit
$\gamma$	19	19	19	19	19	19	19	kN/m <sup>3</sup>
$E_u$	7176	3987	3987	3987	3987	3987	3987	kPa
$G$	2400	1333	1333	1333	1333	1333	1333	kPa
$\nu'_u$	0.495	0.495	0.495	0.495	0.495	0.495	0.495	-
$S_u^{ref}$	42.79	31.12	40.46	37.35	37.35	33.46	38.9	kPa
$S_{u,inc}$	0	2.33	0	2.33	0	1.79	1.79	kPa/m
$E_{u,inc}$	0	209.3	0	209.3	0	209.3	209.3	kPa/m
$y_{ref}^*$	0	6	0	10	0	14	10	m
$v_i$	0	0.17	0	0.12	0	0.1	0.1	-
$K_0$	1	1	1	1	1	1	1	-
$R_{inter}$	0.5	0.1	0.1	0.1	0.1	0.1	0.1	-

The strength profile of the different constitutive models in the initial state before excavating are shown in figure 4.22. Please note that HS(A) shows  $\tau_{max}$  including all materials, while MC and NGI-ADP shows current cohesion which is why the moraine is "active" in the former. The strength profile of HS(B) is equal to MC.

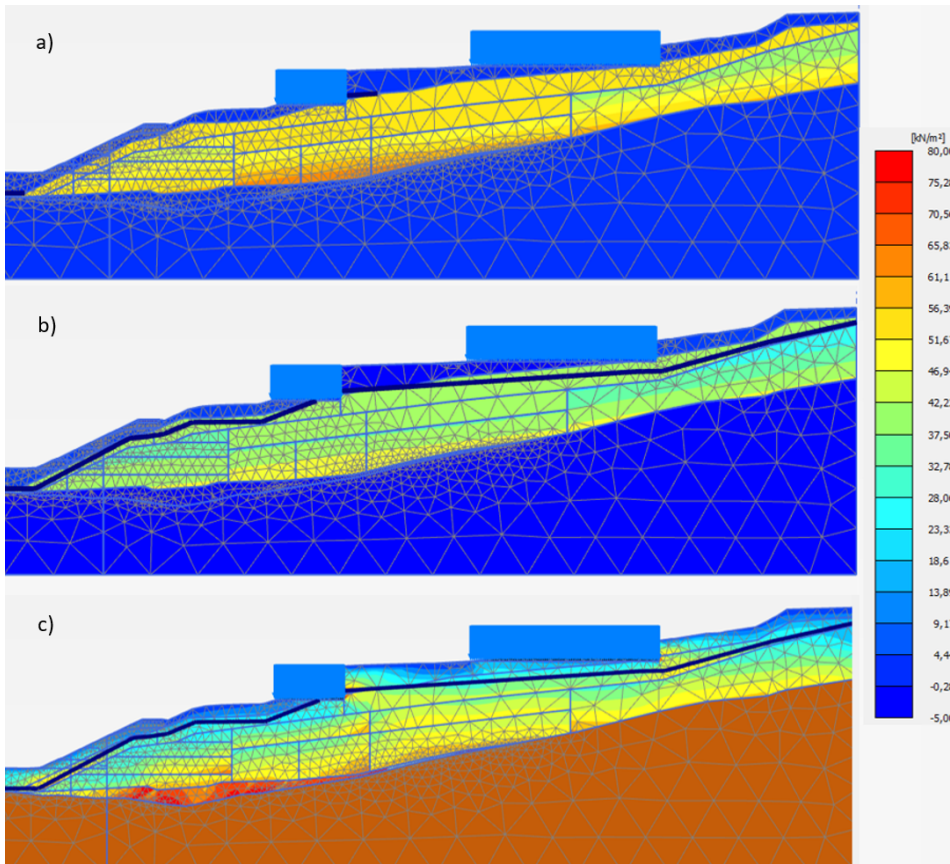


**Figure 4.22:** Strength profiles in initial phase taken from PLAXIS output for: a) NGI-ADP, b) HS(B) and MC, c) HS(A).

### Roughness

The roughness against the SPW is modeled by changing  $R_{inter}$  in the soil material windows as explained in section 3.2.1. The interfaces are affected by the adjacent soil materials. The roughness is set to 0.5 in the dry crust, silty clay and in the moraine obtained from MulticonsultASA (2017a). A simplistic consideration of the roughness against the SPW is done for the quick clay materials. During installation of the SPW a thin zone of fully stirred quick clay along the SPW may appear. The thin zone of stirred clay is assumed to be reconsolidated before starting the excavation in front of the SPW. For normally consolidated clay, the strength is assumed to be (MulticonsultASA, 2017a):

$$S_{u,recon} = 0.2 * p_0' \quad (4.1)$$

Compared to the original strength ( $S_u^A$ ), the reconsolidated strength has a magnitude of 0.1-0.5 ( $S_{u,recon}/S_u^A$ ) of the original strength (MulticonsultASA, 2017a). LCC is not

included directly in the initial model. As the LCC may force the thin zone along the SPW to be stirred once again, the new reconsolidated strength  $S_{u,recon,2}$  may be even lower. The roughness of 0.1 on both sides of the SPW is therefore chosen as a conservative value.

## Mesh

The mesh is set to fine in all the models calculated by PLAXIS with a default coarseness factor of 1. A coarseness factor of 0.25 is set around the SPW, from below the counter fill to below the parking garage to increase the accuracy around the structure. Structures and loads are given a coarseness factor of 0.25 by default.

## Phases in PLAXIS

The phases in PLAXIS are set up by several steps, and has more phases than presented in section 4.1 (fig. 4.23).

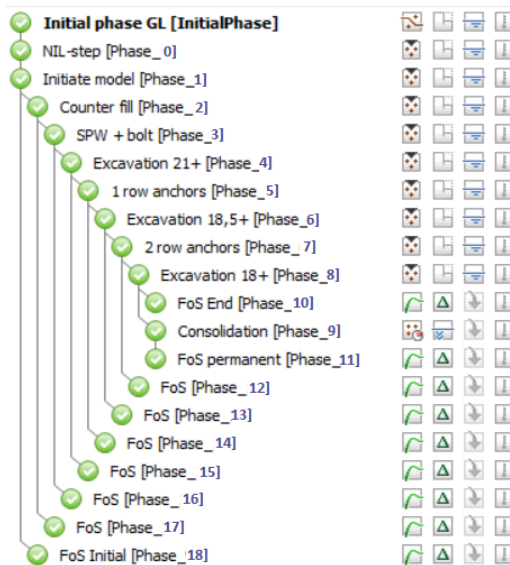


Figure 4.23: Calculation phases in PLAXIS.

- **Initial phase:** The initial phase is set to gravity loading with MC materials.
- **NIL-step:** A plastic calculated NIL-step. No additional loading is applied in this step, and is added to solve "large out-of-balance" forces and restore equilibrium (Brinkgreve et al., 2017b). This is done to prevent the different loads (parking garage and kindergarten) from influencing the model which will deviate from reality as these are "old loads".
- **Phase 1:** Initiating the material models used (i.e. NGI-ADP) for the silty clay and the quick clay.

- **Phase 2:** The counter fill is applied.
- **Phase 3:** The SPW with interfaces, the rock bolt and the w/c path load are enabled.
- **Phase 4:** Excavation to elevation +21.
- **Phase 5:** Installing top row of anchors with prestress.
- **Phase 6:** Excavation to elevation +18.5.
- **Phase 7:** Installing bottom row of anchors with prestress.
- **Phase 8:** Final excavation to elevation +18.
- **Phase 9:** Consolidation step is done to check the long term effects of the SPW when using HS(A) through phases 1 to 9. The consolidation phase is run to a minimum excess pore pressure of 1 kPa.

Phase 1 to 8 are done with plastic calculation with pore pressure calculation from phreatic level. A safety calculation, strength reduction procedure, is added for phase 1 to 9 to check the safety against failure during the different steps.

### **4.3.3 GeoSuite Excavation**

GS is a 1-dimensional model, and does therefore not allow oblique layers. Hence, the triangle of weight "created" by the slope on the active side is not taken into account. Please note that the profile in GS in figure 4.24 is flipped compared to PLAXIS. This is taken into account when presenting results as the graphs from GS will be corrected.

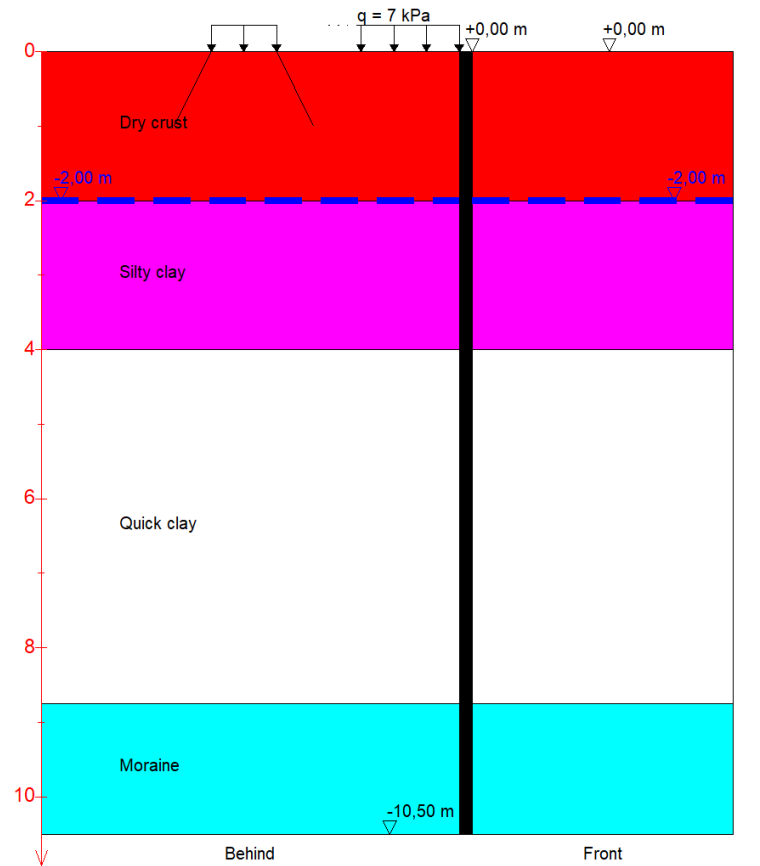


**Figure 4.24:** Soil profile used in GS.

The w/c-path load is added as a continuous load starting from the SPW (fig. 4.25). The value is reduced from  $13 \text{ kN/m}^2$  to  $7 \text{ kN/m}^2$  due to this. The sloping terrain is incorporated by the "Additional vertical stress behind the wall" option. To calculate this impact, another program from the GS package was used; GeoSuite Settlement. In this program, loads are defined at a distance from a given point and the additional stress on the wall in that point is calculated using finite boussinesq. All loads are defined as strip loads 1 m apart and calculated with  $\gamma = 20 \text{ kN/m}^3$  multiplied by the vertical distance to the top of the SPW (app. A.16). As each load is placed further from the wall, the impact diminishes. At 25 m horizontal distance the impact is 0.4 kPa (app. A.17) which is considered neglectable.

---

Water	
Initial ground water depth:	<input type="text" value="2,00"/> m
Load	
Terrain load, behind, q:	<input type="text" value="7,00"/> kPa
Additional vertical stress behind wall	
Exists: Yes	<input type="button" value="Add/View"/>

**Figure 4.25:** Defining additional loads in GS.

The output from GS Stability shows an almost linear increase with depth (fig. 4.26) maxing out at around 17 kPa. Using this, the stresses are input in GS as a linear increase with depth from 0 to 20 kPa as shown in figure 4.27.

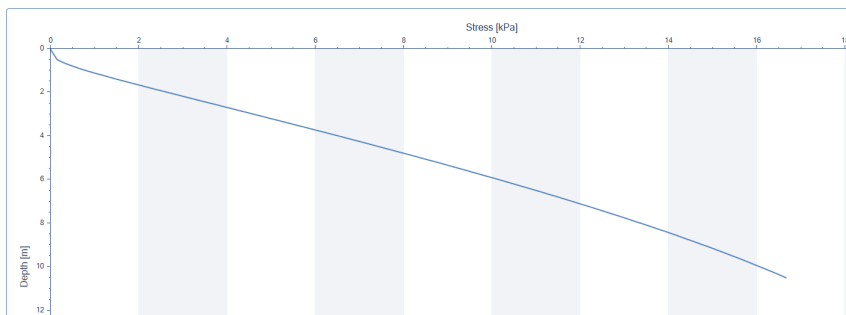


**Figure 4.26:** Additional stress on the SPW, from the omitted triangle of weight created by the slope, calculated by GeoSuite Settlement.

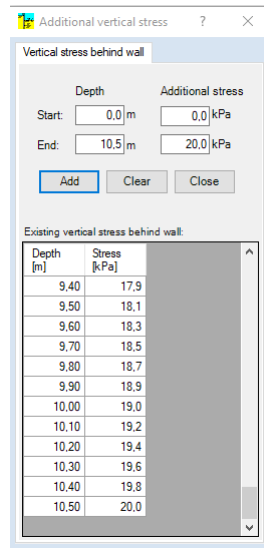


**Figure 4.27:** Input window for additional vertical stress in GS.

In GS there is interpolation between input values. Due to relatively small differences in strength and stiffness values, a single quick clay layer is sufficient for modeling. Since NGI-ADP share similarities with TSA it is natural to link these two closely. The values chosen are averaged from all corresponding layers closest to the SPW. The shear strength on the front side is defined as the passive strength with NGI-ADP ratio  $S_u^P/S_u^A = 0.35$ . When there is a difference in the shear strength on either side in GS, the stiffness will deviate from what is intended. Defining stiffness in the TSA model is done by either inputting  $G$  directly, which will apply on both sides, or by the  $G/c_u$ -ratio:

$$\frac{G}{c_u} \text{ ratio} = \frac{2G}{c_{u_{behind}} + c_{u_{front}}} \quad (4.2)$$

This yields a somewhat different soil situation compared to PLAXIS. As the difference in shear strength on each side grows, so does the mismatch in stiffness. The dry crust and moraine parameters remain the same in all models in PLAXIS and GS except for the  $K_0$  value. Since there exists no direct input of the degree of consolidation in GS, the OCR was incorporated by equation 4.3 (Johansson and Sandeman, 2014). All soil parameters used in the initial analysis is displayed in figure 4.28.

$$K_0 = (1 - \sin\phi') * \sqrt{OCR} = K_0^{nc} * \sqrt{OCR} \quad (4.3)$$



Name	Model	Depth [m]	Soil Weight [kN/m <sup>3</sup> ]	c [kPa]	Phi [deg]	K0_eff [-]	E-modulus [kPa]	
Dry crust	ESS - Effective stress simplified	0.00	19.50	3.50	30.00	0.55	10000.00	NA
		2.00	19.50	3.50	30.00	0.55	10000.00	NA
			Soil Weight [kN/m <sup>3</sup> ]	Cu_behind [kPa]	Cu_front [kPa]	K0_eff [-]	G [kPa]	G/Cu-ratio [-]
Silty clay	TSA - Total stress automatic	2.00	19.00	55.00	19.00	0.65	9250.00	250.00
		4.00	19.00	55.00	19.00	0.65	9250.00	250.00
Quick clay	TSA - Total stress automatic	4.00	19.00	43.00	15.00	0.65	21750.00	750.00
		8.75	19.00	50.00	18.00	0.65	25500.00	750.00
			Soil Weight [kN/m <sup>3</sup> ]	c [kPa]	Phi [deg]	K0_eff [-]	E-modulus [kPa]	
Moraine	ESS - Effective stress simplified	8.75	19.00	0.10	38.00	0.42	20800.00	NA
		10.50	19.00	0.10	38.00	0.42	20800.00	NA

Figure 4.28: Input parameters in GS.

## Phases

The excavation process is done in accordance with section 4.1. However, since GS is not able to simulate trenches, the excavation level will be fully excavated at trench levels. This will remove an extra load on the supportive side which will yield a more conservative result. Also, ground water level on the front side is reduced to the excavated level in each phase, while keeping it constant behind (fig. 4.24). The phases are displayed in figure 4.29.

No	Type
1	Tip condition fixity
2	Excavation/Water pressure
3	Strut/Anchor
4	Excavation/Water pressure
5	Strut/Anchor
6	Excavation/Water pressure

Figure 4.29: Calculation phases in GS.

## Structural components

The SPW is taken directly from the database in GS which gives all the necessary parameters (fig. 4.30). The option of a tip bolt is chosen to simulate the rock bolt. The anchors are defined according to section 4.3.1 and the values are shown in figure 4.31.

Calculation Data   Soil   Sheet pile   Model Data   Calculate

Sheet pile tip  
 Sheet pile tip: To rock with tip bolt

Section from database

Section from database  
 Database: GeoSuite  
 Type: Z sections  
 Section: AZ 38-700  
 View   Edit   Delete

Direct input of variable cross section data

New section   Divide section   Delete section   System width: 1,400 m

Section no	Depth [m]	E-modulus [kN/m <sup>2</sup> ]	Moment of inertia [m <sup>4</sup> ]	Color
▶ 1	0,00	2,100E+008	9,484E-004	
	10,50	2,100E+008	9,484E-004	

Figure 4.30: Values used for the sheet pile input in GS.

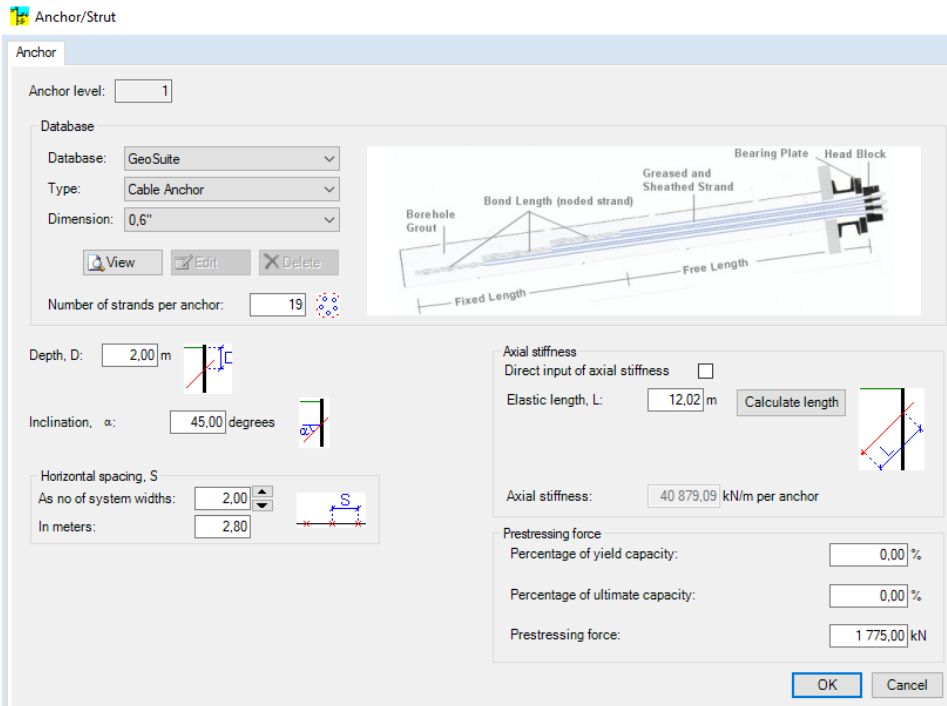


Figure 4.31: Anchor window showing input for the top row of anchors in GS.

### Roughness

Vianova Geosuite (2009) recommends setting the roughness to zero when there is no relative vertical movement between the soil and the SPW. As the SPW is defined as "To rock with tip bolt" the roughness number is set to 0 initially. In phases when installing anchors, the roughness is likely to change, but it is not possible to alter the roughness during the analysis.

## 4.4 Simple hand calculation

In order to give a rough estimation of earth pressures and anchor forces, simple hand calculation is done. The profile used in hand calculations is simplified by a horizontal terrain, with a line load of 100 kPa at the active side to substitute for the sloping terrain and building loads. The moraine is substituted by clay at the bottom and the parameters used are also averaged along the wall, but with the use of direct shear strength. The analysis will be run with  $FoS = 1$  and  $r = 0$  for simplification. The GW table is at the top of the silty clay. The soil parameters are listed in table 4.13 below:

**Table 4.13:** Soil parameters at different depths for hand calculations.

	Depth [m]	$\gamma$ [kN/m <sup>3</sup> ]	$S_u$ [kPa]	$S_u^{inc}$ [kPa]	$\phi$ [°]	$a$ [kPa]
Dry crust:	0	19.5	-	-	30	6.2
	2	19.5	-	-	30	6.2
Silty clay:	2	19	43	0	-	-
	4	19	43	0	-	-
Quick clay	4	19	34	1.8	-	-
	10.5	19	46	1.8	-	-

## 4.5 Measurement data

The strict demands to displacements and deformations of the SPW has led to a great focus on surveillance. During excavation, MC' have used inclinometers to measure displacements, and load cells in each row of anchors to measure anchor loads. The placement of the 3 inclinometers along the SPW is shown in figure 4.32 and the displacement results from all 3 in every phase are shown in figure 4.33. The measurement points are spaced 0.5m apart, represented by crosses, and has straight, interpolated lines in between.

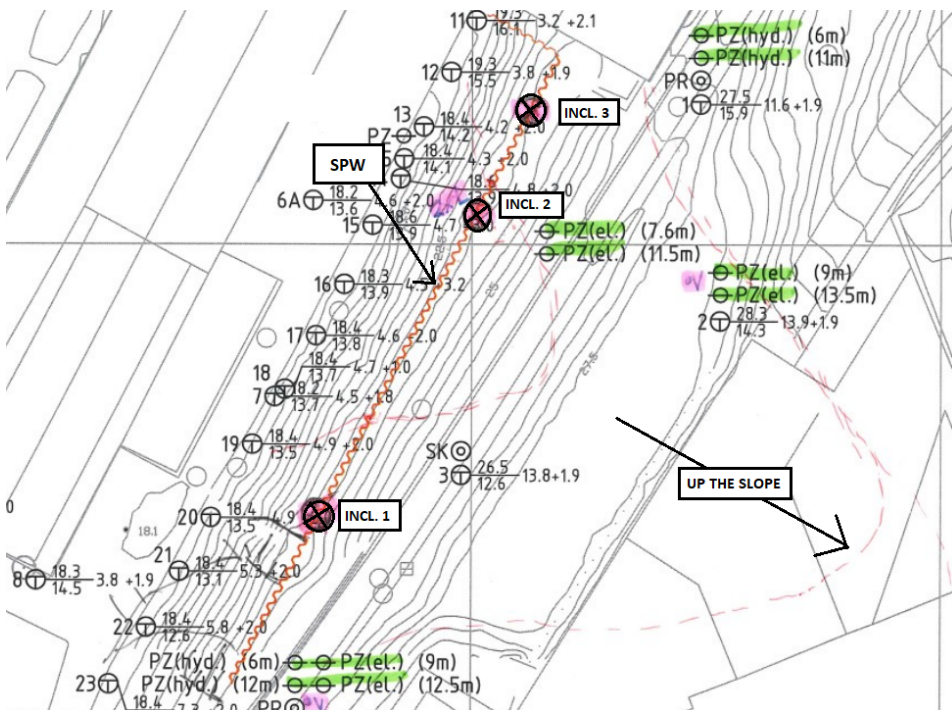


**Figure 4.32:** Placement of inclinometers along the SPW (MulticonsultASA, 2017d).

Profile X-X' is placed almost directly at inclinometer 1. The load cells installed to measure

anchor forces are placed at inclinometer 2, measuring loads in both the top and bottom rows of anchors.

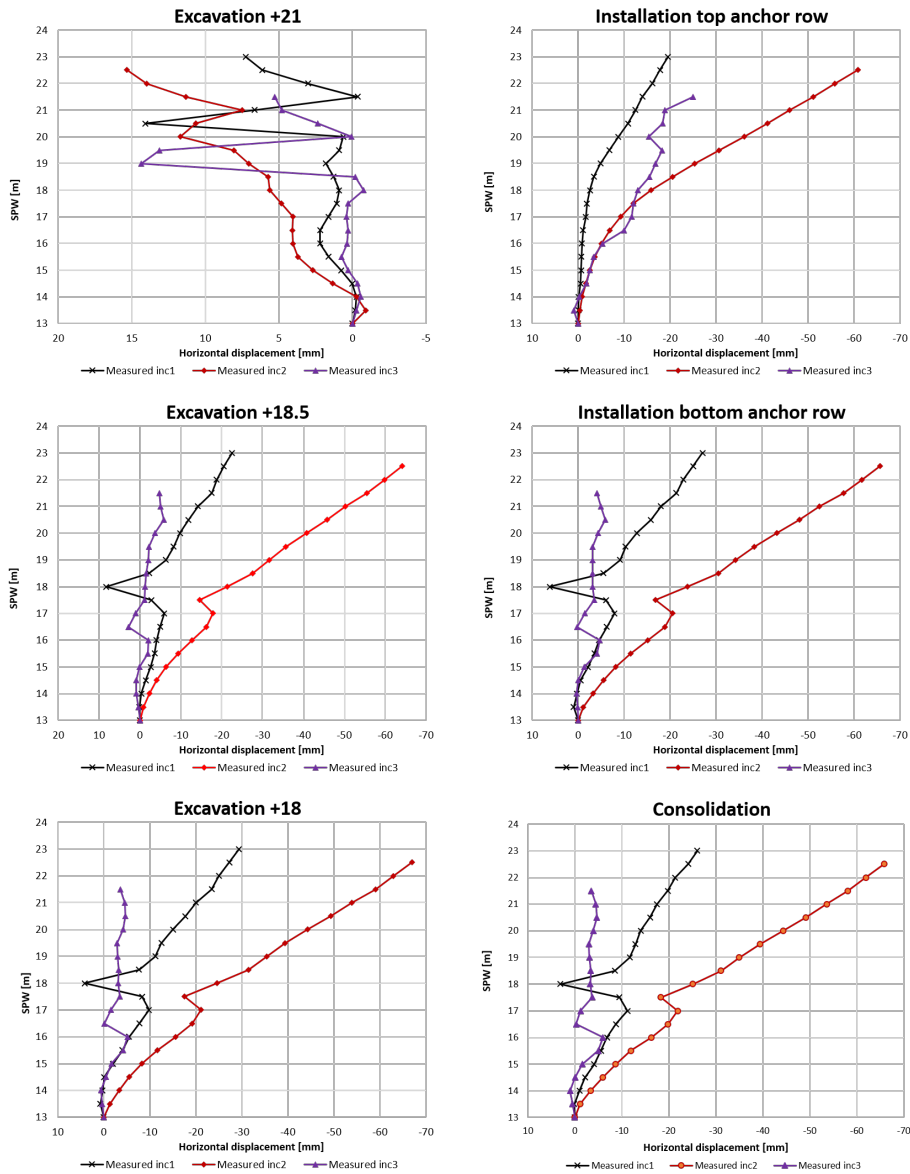


**Figure 4.33:** Measured horizontal displacement of the SPW in all phases.

The separate inclinometers show different values which could be due to several reasons such as a change in layering behind the SPW (fig. 4.33). Looking at figure 4.2 the bedrock is tilting upwards to the north along the SPW. This means that the length of anchors differs

at the separate inclinometers. Shorter length of anchors gives greater displacements into the slope and cause greater anchor forces by the equation  $P = (EA/L) \cdot \delta$ . This is not the case for inclinometer 3 which has the shortest anchors. The reason it shows least displacement may come from the connection to Enebakkveien 69, the building in top of figure 4.32. The inclinometers are controlled with laser measurements taken at the top of the SPW and correspond well (app. A.18). There are no measured data from phase 3 when SPW with rock bolt is installed. In this thesis, inclinometer 1 is used as a benchmark against the different models, as discussed in section 4.2. The measured data has not been adjusted in any way in this thesis. Some irregularities are shown in the plots which in reality might not represent the true movement of the wall, i.e. on elevation level +18. Rotation of the inclinometers or yielding of the welded connection between the inclinometers and the SPW might be the reason for these irregularities. As the load cells which measure anchor forces are located at inclinometer 2, the forces do not directly correspond to the displacements at inclinometer 1. Measured anchor forces are shown in table 4.14.

**Table 4.14:** Measured anchor forces in kN.

	<b>Top row anchors</b>	<b>Exc +18.5</b>	<b>Bottom row anchors</b>	<b>Exc +18</b>	<b>Permanent</b>
Top anchor	1775	1765	1650	1620	1620
Bottom anchor	-	-	1390	1350	1345

## Results and discussion

As this is a trial and error thesis it is natural to present results together with a discussion around the findings. It is summed up in a main discussion at the end. To best visualize the results from PLAXIS and GS, the max and min values on the x-axis is attempted to stay the same throughout the calculation phases. The phases before installation of the top anchor row will have smaller values and hence it is natural to present them in a smaller scale. All results are shown in appendix B.1 to C.3. Some results have been filtered out in this chapter as presenting everything would take up a lot of space.

### 5.1 Initial model

To check the FoS and failure surface in each phase for HS(A), the soils in the model is run with no contraction. When the dilatancy angle ( $\psi$ ) is set to 0, the strength in the material should be reduced to the residual strength obtained by test results. The strength in the models is not reduced as the materials are already deviating from the triaxial tests and show lower values than the residual strengths in general (section 4.3.2). In addition to finding failure surfaces and FoS, the strength reduction analysis are controlled in PLAXIS output to secure that no non-relevant failure mechanisms occur. When running "HS(A) no contraction" (HS(A)nc), a non-relevant shallow failure occurs at the top of the pedestrian path (w/c path). This effect happens after excavation to elevation +21, namely phases 5, 6, 7, 8 and 9 (see fig. 4.23 for phases). The top layer of the w/c path is therefore excluded from the strength reduction procedure in the phases mentioned above, solving this problem. The anchor and rock bolt forces, the displacement and the bending moment are approximately the same for both HS(A) and HS(A)nc. Note that the phase of consolidation is only run with HS(A) and that NGI-ADP is referred to as ADP in graphs and tables.

### 5.1.1 Displacement and structural forces

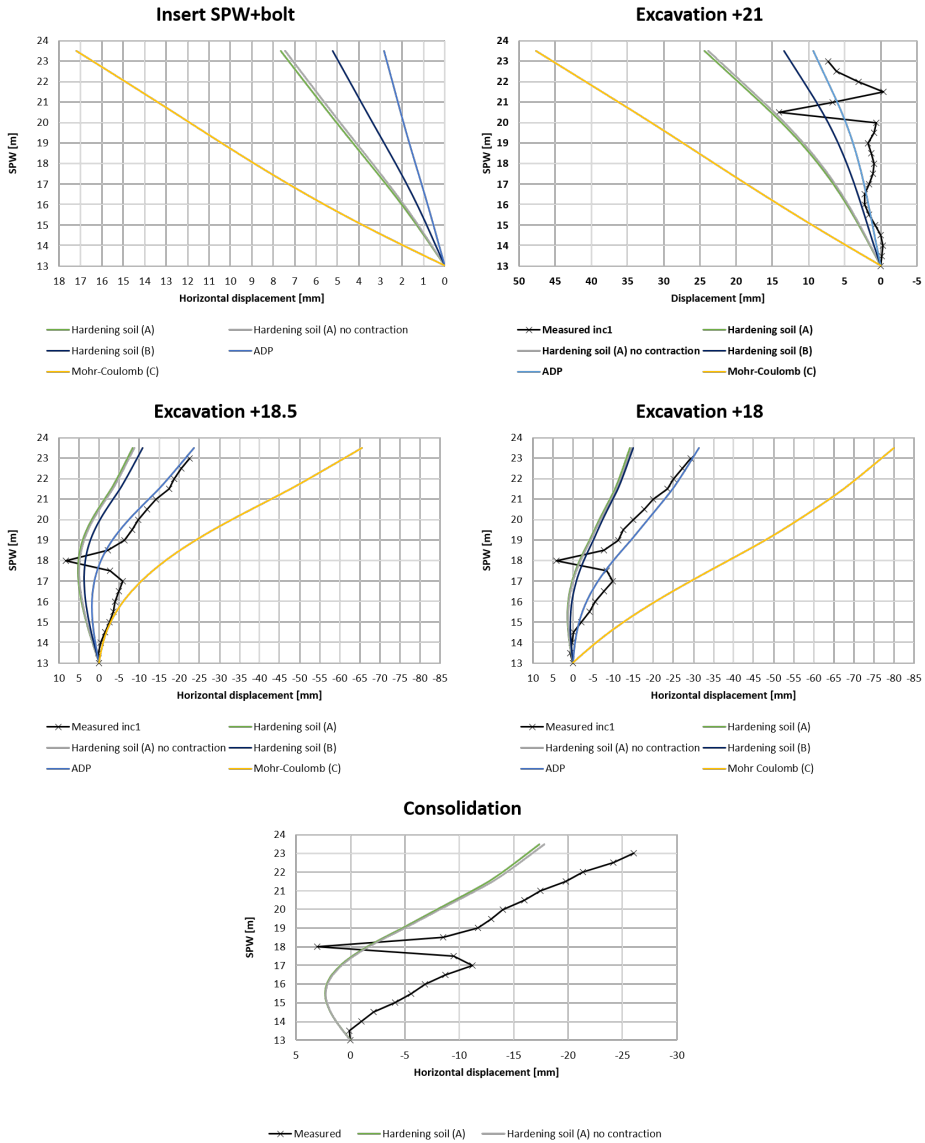
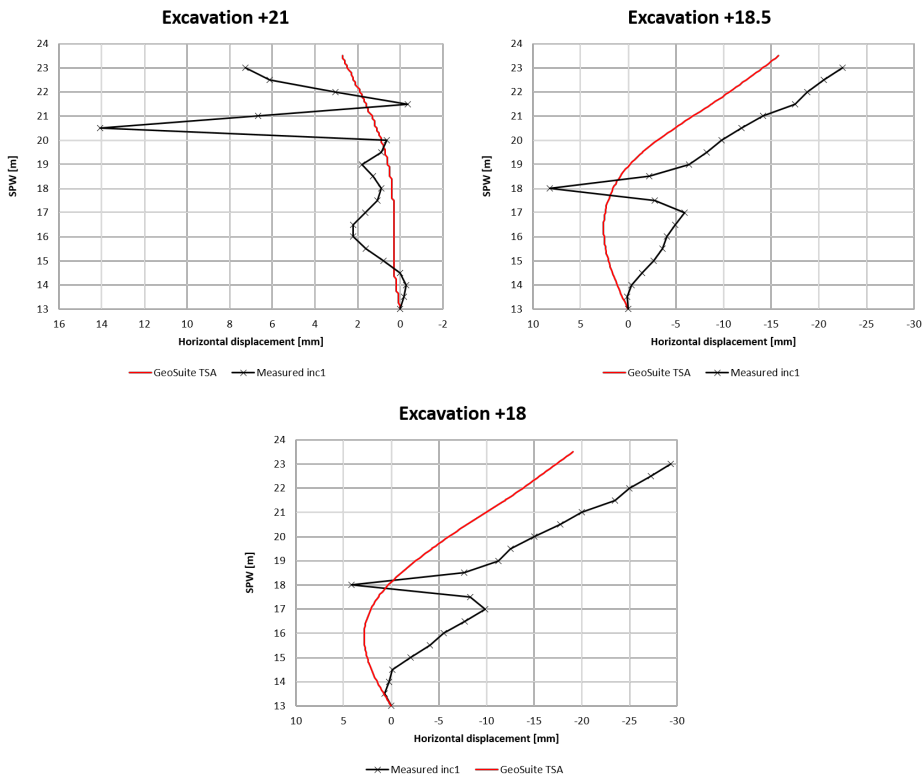


Figure 5.1: Horizontal displacement of the SPW in PLAXIS with initial parameters.





**Figure 5.2:** Horizontal displacement of the SPW in GS with initial parameters.

Examining the displacement results from PLAXIS in figure 5.1, NGI-ADP seems to fit well with the measured displacement of the SPW through all phases, while MC deviates the most. MC clearly overestimates the displacement of the wall. Deciding a representative stiffness ( $E_u$ ) in this model can be difficult as this model only includes one stiffness parameter. Both Nurmohamed et al. (1997) and Johansson and Sandeman (2014) states that the stiffness ( $E_u$ ) should be increased when dealing with excavation problems. When installing the SPW with rock bolts and excavating to elevation +21, HS(A), HS(B) and MC show greater displacement than the measured data, hence a softer response. On the contrary, the GS model in figure 5.2 shows smaller displacement than the measured data, hence a stiffer response. This is clearly observed in the phases with no anchors. For primarily GS, HS(A) and HS(B), the SPW bulges outwards after installation of the top row of anchors from elevation +13 to about elevation +19. After the installation of anchors, the difference in the top vertex ( $\Delta x$ ) seems approximately the same between the models in PLAXIS when excavating further. After installation, the stiffness of the anchors are integrated in the stiffness matrix of the wall. Therefore, the prestress and stiffness of the anchors are mainly controlling the displacement of the SPW. The permanent phase after consolidation, which is calculated by HS(A), seems to give less displacement in the slope than the measured data, missing by approximately 8 mm in the top vertex. Results from

phases when installing the SPW with rock bolt and consolidation is not obtainable in GS.

When inserting the SPW, no displacement of the wall is expected as the terrain should be in equilibrium. However, as shown by the PLAXIS results, some displacement occurs when installing the SPW with rock bolt. The reasoning for this could be that the load from the w/c path is added in this phase, which in reality does not act as a constant load. Also, a thin stirred zone may appear during installation which reduces the relative roughness. This might cause the SPW to move as the wall is installed in sloping terrain.

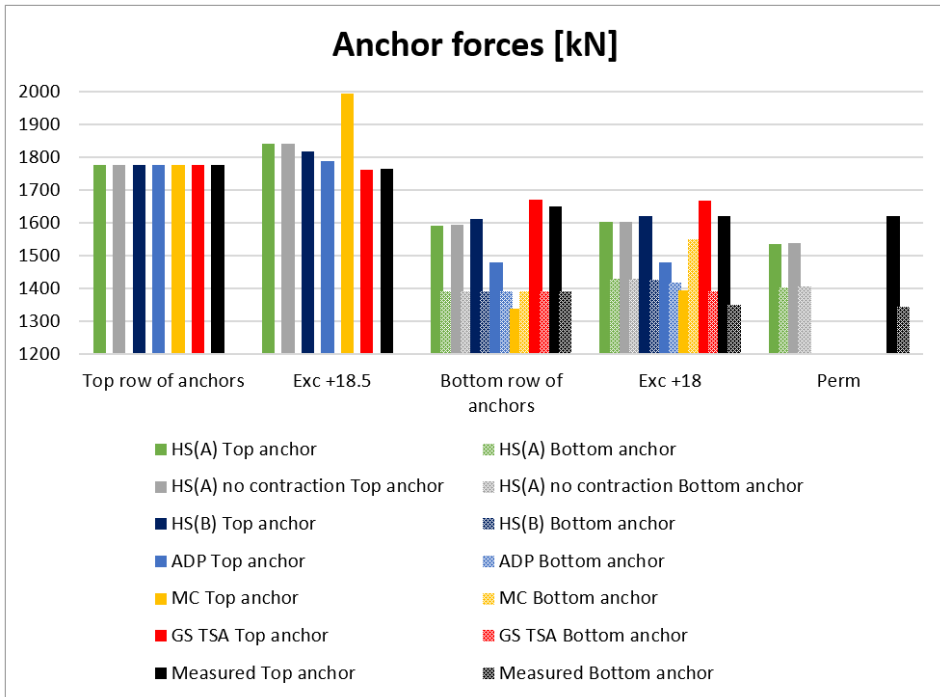


**Figure 5.3:** Calculated anchor forces from the initial analysis compared to measured anchor forces.

Table 5.1 shows the difference between calculated and measured anchor forces for top row of anchors in %, while table 5.2 shows the difference for the bottom row of anchors. A negative value means that the calculated is less than the measured. An absolute average is added which shows the total difference in %. For the top row of anchors, the absolute average includes 4 phases, from installing the top row of anchors to the final excavation to elevation +18. The bottom row of anchors only includes 2 phases, installing the bottom row of anchors and the final excavation to elevation +18. Hence, the permanent phase after consolidation is not included in the absolute average.

**Table 5.1:** Difference in calculated and measured anchor forces, normalized on the latter, given in % for top row of anchors.

	<b>Top anchor</b>	<b>Exc +18.5</b>	<b>Bot. anchor</b>	<b>Exc +18</b>	<b>Perm.</b>	<b>Abs. av.</b>
HS(A)nc	0.0	4.2	-3.5	-1.1	-0.1	2.2
HS(A)	0.0	4.3	-3.5	-1.2	-0.1	2.2
HS(B)	0.0	2.9	-2.3	0.0	-	1.3
ADP	0.0	1.3	-10.4	-8.8	-	5.1
MC	0.0	12.9	-19.0	-14.1	-	11.5
GS TSA	0.0	-0.2	0.9	3.0	-	1.0

**Table 5.2:** Difference in calculated and measured anchor forces, normalized on the latter given, in % for bottom row of anchors.

	<b>Bot. anchor</b>	<b>Exc +18</b>	<b>Perm.</b>	<b>Abs. av.</b>
HS(A)nc	0.0	5.9	4.5	3.0
HS(A)	0.0	5.9	4.4	2.9
HS(B)	0.0	5.6	-	2.8
ADP	0.0	4.9	-	2.4
MC	0.0	14.8	-	7.4
GS TSA	0.0	3.0	-	1.5

Most models fit well with the measured results (fig. 5.3). The only major deviance is MC, which gives an anchor force of 19 % less than the measured data when installing bottom row of anchors (tab. 5.1). It gives the highest anchor force of almost 2000 kN, which is close to the maximum allowed tension force (2375 kN). In addition, MC shows that the bottom row force is greater than the top row which is the opposite of the measured data.

As NGI-ADP gives the best fit to the measured displacement, one might expect that the anchor forces should give the most accurate values. This is not the case and may be because the load cells for measuring anchor force are placed at inclinometer 2 as described in section 4.5. GS seems to give the best fit in total, while HS(B) gives the best fit of the PLAXIS models.

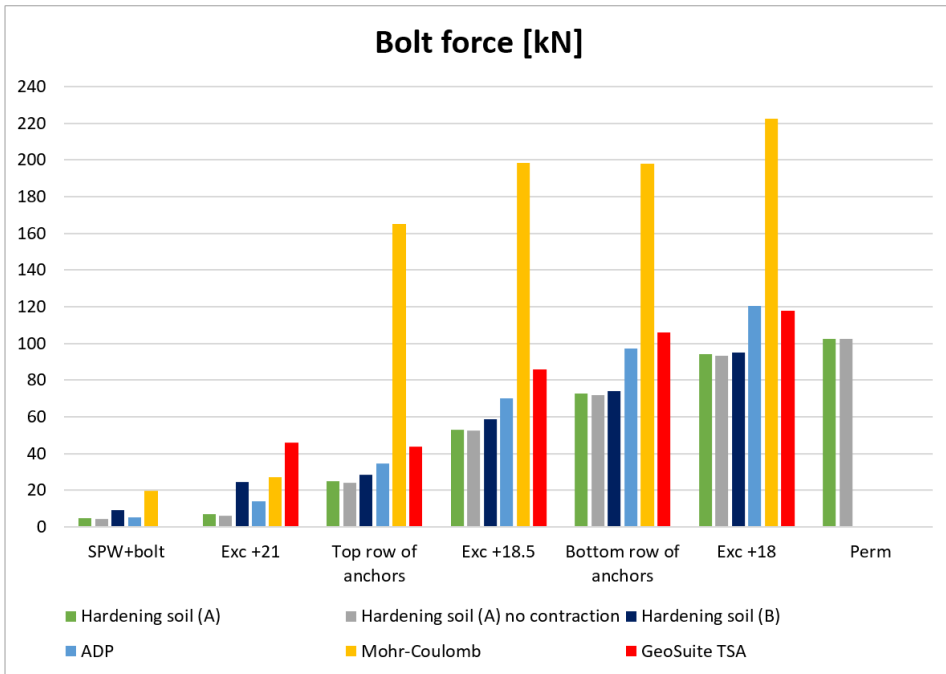


**Figure 5.4:** Combined calculated rock bolt forces from PLAXIS and GS with initial parameters.

All the constitutive models show an increase in rock bolt force during excavation of the slope (fig. 5.4). GS shows the greatest rock bolt force when excavating to elevation +21, but increases with a slower rate during the phases than the PLAXIS models. MC shows approximately double the force when comparing to the other PLAXIS models. Looking at the displacement curves (fig. 5.1), MC deviates the most, indicating that the forces from this model might not be representative. Nevertheless, the maximum value could increase by a factor of 2 and still be within dimension requirements of the rock bolt.

### 5.1.2 Bending moment

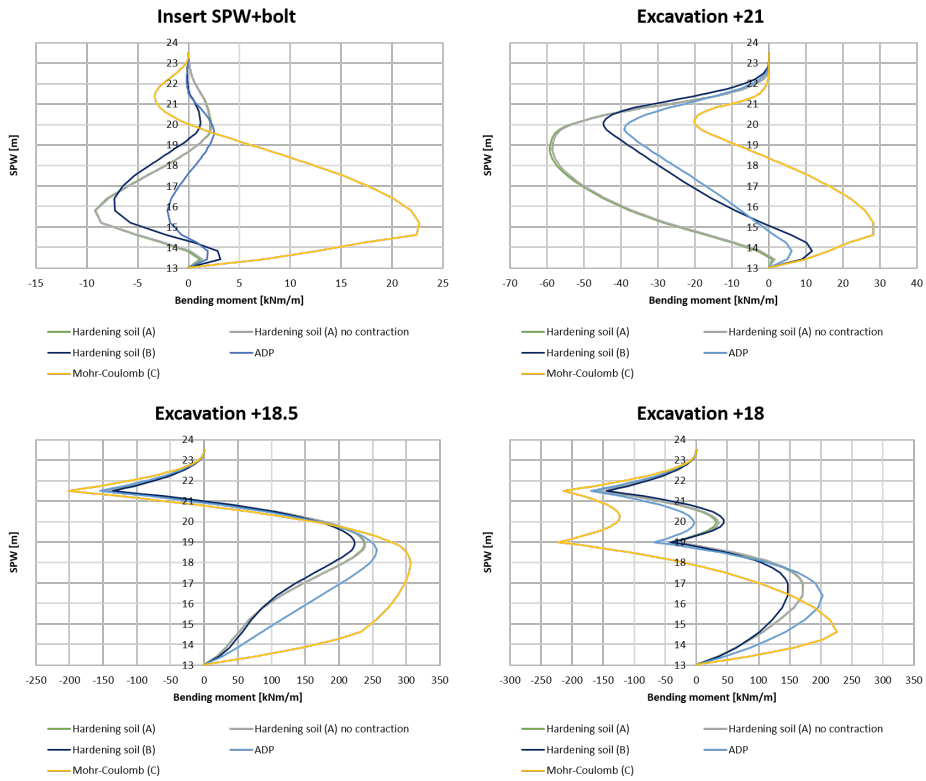
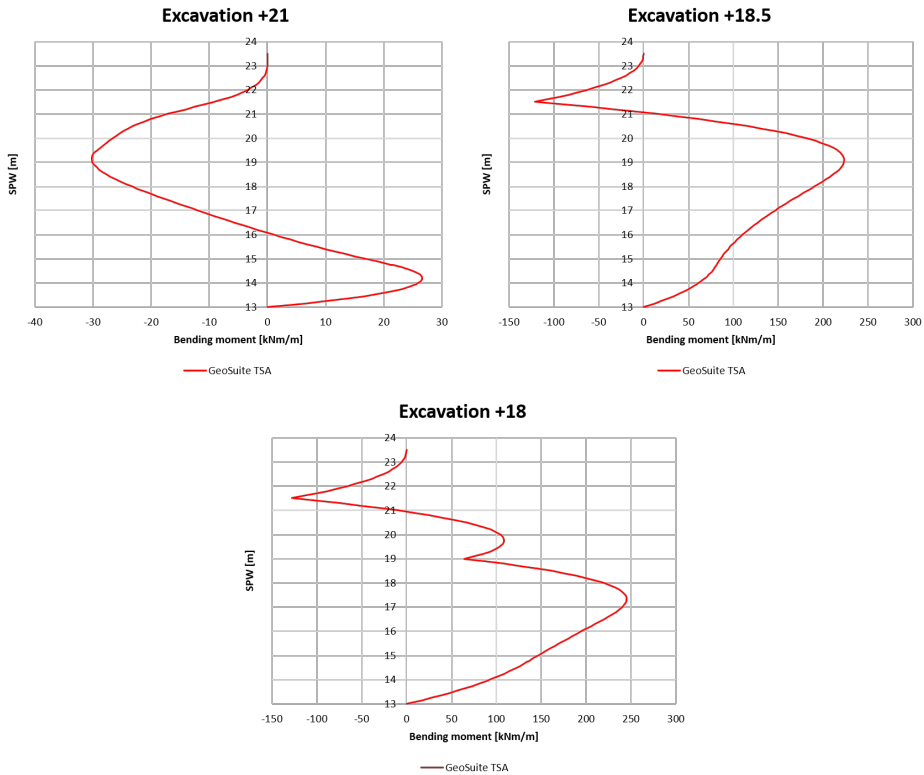


Figure 5.5: Bending moment of the SPW in PLAXIS with initial parameters.



**Figure 5.6:** Bending moment of the SPW in GS with initial parameters.

All models show similar behaviour in moment except MC (fig. 5.5 and 5.6). This is especially shown in the first phase when installing the SPW with rock bolts. Looking at the displacement curves, MC gives the most displacement, and the wall slightly bends in the other direction. The bending moments are similar for all models after the first excavation phase, but MC seems to overestimate the maximum bending moment, which is also seen by Nurmohamed et al. (1997). The bending moments of the first two phases are small compared to the bending moments that occurs when the anchors are installed. When installing the second row of anchors, the bending moments and shear forces differ as MC gives a higher force for the bottom row than the top row of anchors.

### 5.1.3 FoS and failure planes

The values for the FoS in each phase is shown in figure 5.7. In the initial phase a value of 1.3 is given by all the models as described in section 4.3.2. HS(B) and MC shows approximately the same FoS through all phases, which is slightly higher than NGI-ADP. This might come from the use of an average undrained shear strength. NGI-ADP includes strength anisotropy where the direct and passive shear strengths might have a varying impact during the phases. The strength anisotropy in NGI-ADP assumes to follow the

vertical. This could cause the model to give a lower FoS than reality, as the case at hand is in sloping terrain where the anisotropy should be tilted. There is no FoS extracted from GS.

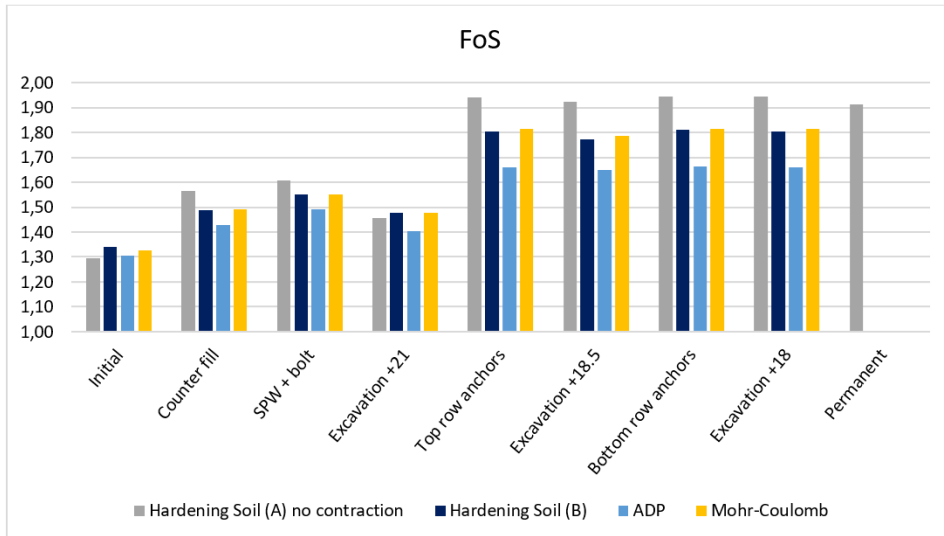


**Figure 5.7:** FoS for different models in PLAXIS with initial parameters.

When the top row of anchors is installed the FoS increases by at least 0.25 in all models, giving all models a FoS greater than 1.6. HS(B) and MC gives a FoS approximately 0.1 greater than NGI-ADP after this phase. HS(A)nc is approximately 0.2 greater than NGI-ADP when the top row of anchors is installed. An increase in FoS is registered in all models when the bottom row of anchors is installed. As seen in figure 4.22, there is a small deviance in the strength profile between HS(A) and HS(B), which affect the output results giving the FoS of HS(A) to be slightly higher.

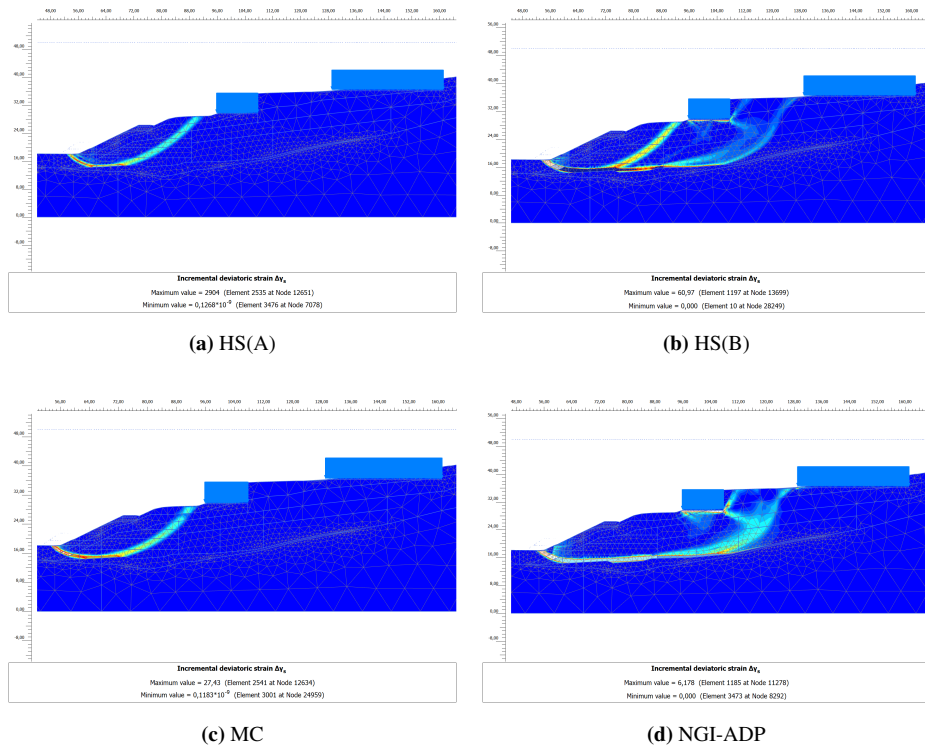


**Figure 5.8:** Failure surface visualized by incremental shear, in initial phase.

The failure planes for the most critical phases are shown in figures 5.8, 5.9 and 5.10. The figures are only for visualization and the numbers and text is not relevant. In the initial phase, HS(A) and MC share the same failure surface, while HS(B) share the failure surfaces of both MC and NGI-ADP. The latter is designed for clays with horizontal surfaces, making the  $S_u^{DSS}$  working in  $0^\circ$  from the horizontal. As NGI-ADP searches for the failure surface obtained by the direct shear strength ( $S_u^{DSS}$ ), the failure surface might be drawn further back in the slope relative to the other models.



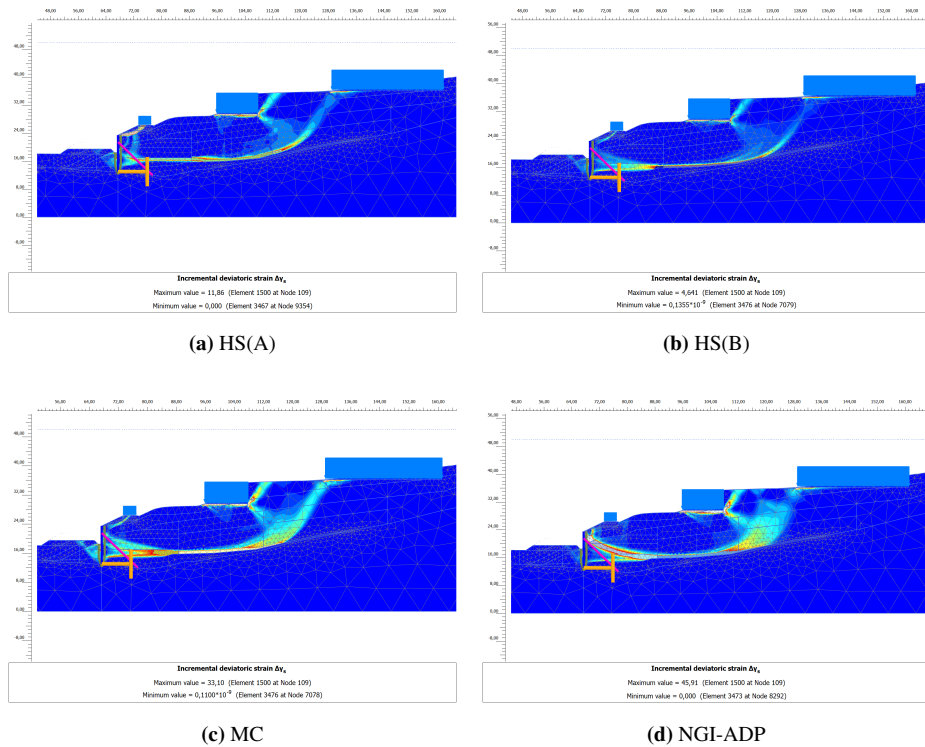


**Figure 5.9:** Failure surface visualized by incremental shear, in excavation +18.5 phase.

In the excavation phase to elevation +18.5 (fig. 5.9), all models primarily seems to share the same failure surface. The failure surfaces of MC and HS(A) seem to cut through the constructed SPW, while the failure surface of NGI-ADP cuts at the top of the SPW.

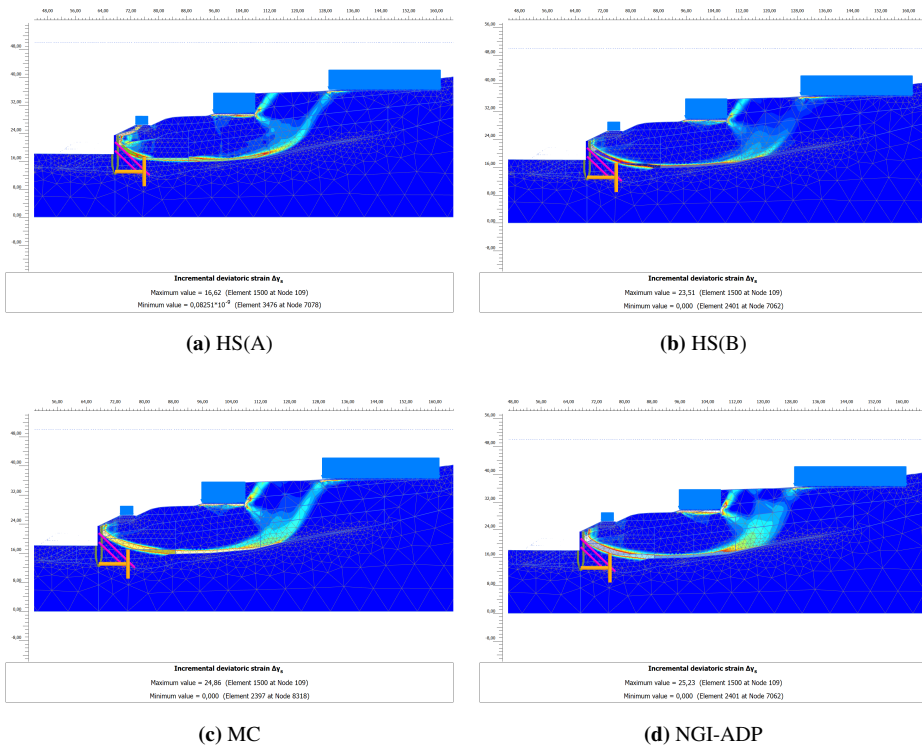


**Figure 5.10:** Failure surface visualized by incremental shear, in excavation +18 phase.

In the final excavation phase all models seem to share the same failure surface. The failure surfaces of all models start at the top of the SPW giving a FoS above 1.6.

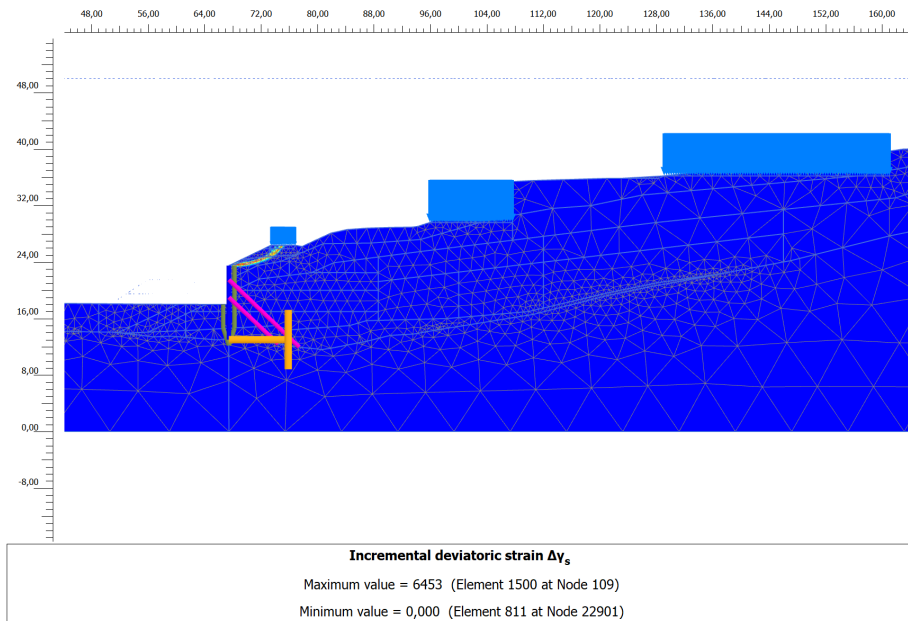


**Figure 5.11:** Failure surface visualized by incremental shear, in permanent phase after consolidation.

The strength reduction analysis run after consolidation gives a failure surface that does not cut through the constructed SPW. Only surface slippage of the w/c path occurs which represents a FoS greater than 1.7 (fig. 5.7). Note that this analysis is only done with HS(A)nc. As this model generally show a FoS greater than the other models by a value of 0.1 - 0.2 in the other phases, FoS = 1.71 in a permanent phase might be a conservative estimate. The calculated FoS for the establishment of the permanent SPW seems satisfying for all phases.

## 5.2 Parametric study in PLAXIS

In this section the initial model will be tweaked in a parametric study. Some scenarios are created to include the LCC in front of the SPW, called  $S_u250$  and  $S_u100$ .  $S_u250$  includes full effect of LCC while  $S_u100$  include partial effect of LCC. Differences in displacement and anchor forces are the main focus in this section, as they are comparable to measured data. Results from all phases are added in appendices D.1-G.5.

### 5.2.1 Stiffness

To see the differences in stiffness,  $E_{ur}$  directly behind the wall is plotted against depth in the clay materials (fig. 5.12).

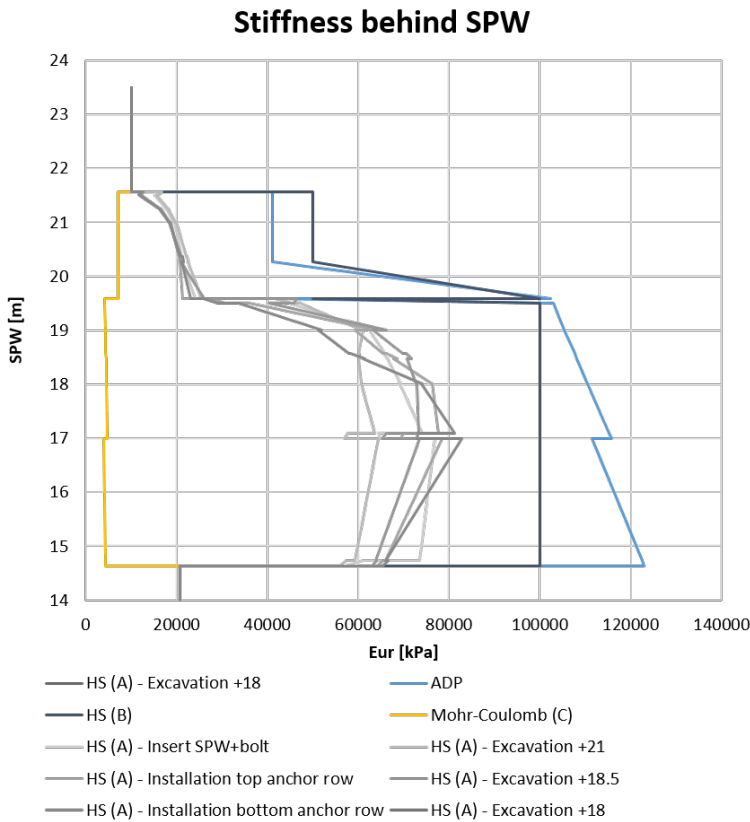


**Figure 5.12:** Stiffness of soil behind the SPW from PLAXIS.

As expected from the displacement results, figure 5.12 shows that NGI-ADP has a higher stiffness compared to the other models. HS(A), whose stiffness is defined by shifting stresses in the soil, varies throughout the excavation process. The stiffnesses of NGI-ADP, MC and HS(B) is constant. The material parameters in this project are primarily fitted to a strength-profile focusing on safety, which has been at the expense of adjustments to stiffness. This mainly applies to the HS materials. HS(A) materials has been tuned to triaxial test, before fitted to the strength profile throughout the model. The HS(B) model has been fitted to triaxial tests in SoilTest with undrained(A), before inserting the different  $S_u$  corresponding to the strength profile. This causes both models to deviate from their realistic stiffness. In addition, no oedometer tests were used to tune the soil materials. As mentioned in section 3.1, Kempfert et al. (2006) stated that discrepancies occurred among the results when 14 individuals calculated the same excavation, mainly originating from differences in stiffness of the soil.

In this thesis, triaxial tests in SoilTest are tuned with  $K_0 = 0.59$  for all clay materials, as this ratio are obtainable from Multiconsult's lab testing. This ratio might not be true for

all tests provided, which could affect the curve-fitting in SoilTest resulting in an unrealistic stiffness. The quality of the laboratory tests was classified from poor to good, which might cause the tests to deviate from real soil behavior.

As an average, an OCR of 1.2 is set for all clay materials when the analysis gave a decreasing OCR from 1.37 in the top to 1.1 in the bottom. A normally consolidated (NC) soil will generally have lower moduli than the same over-consolidated (OC) soil because the NC soil is on the first loading part of the stress strain curve while the OC soil is on the reload part (Briaud, 2001). An increase in OCR will cause the soil to act stiffer. The difference in OCR is tested in PLAXIS SoilTest, which shows a stiffer response for a higher OCR with the same input parameters (fig. 5.13).

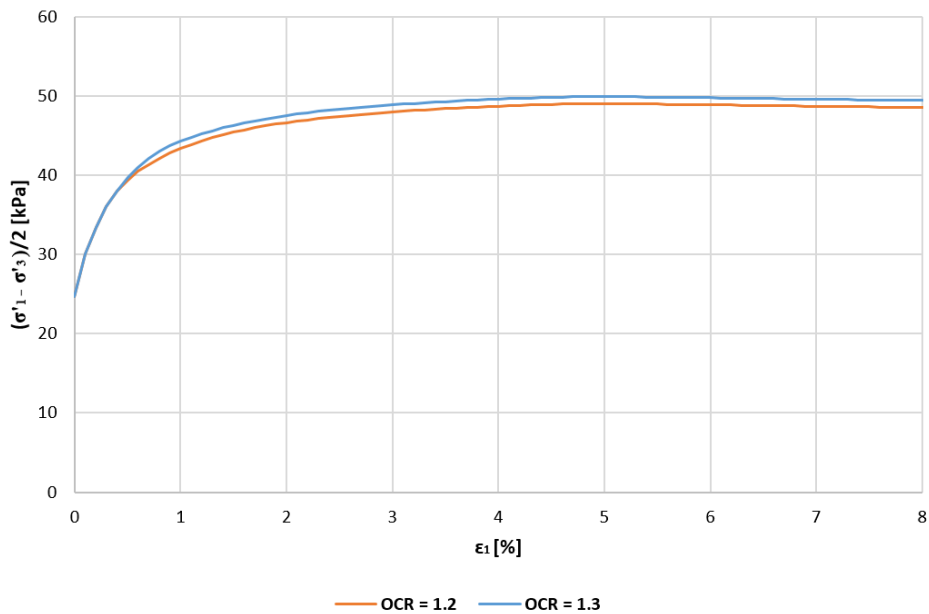


**Figure 5.13:** Difference in shear strength for OCR = 1.2 and OCR = 1.3 with equal input parameters.

An OCR of 1.2 might be a low value, forcing the soil to behave softer. OCR is generally decreasing with depth as shown by the analysis done by NGI, and the use of POP or a decreasing OCR instead of a constant OCR with depth in the HS models, could be a better solution in this project.

There is a possibility that small strains occur at Kværnerdammen which will make the material stiffer as illustrated in figure 5.14.

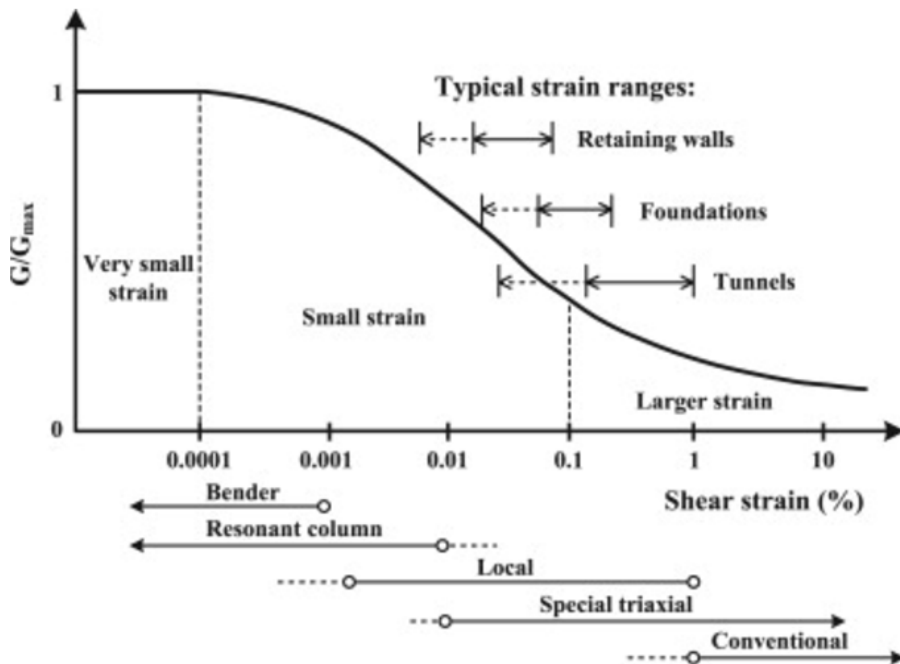


**Figure 5.14:** Illustration of different strain ranges with associated shear stiffness (Likitlersuang et al., 2013).

In Johansson and Sandeman (2014) the Hardening soil small strain model (HSSs), which includes small strains, gave a maximum displacement of the SPW almost half the value of the displacement achieved from HS. This taken into account, the displacement results in this thesis might fit better with a HSSs model analysis. On the other hand, HS gave a better fit to the displacement of the SPW in Johansson and Sandeman (2014), while HSSs gave too low values.

## 5.2.2 $E_{ur}$ in MC

MC overestimates the displacement of the wall and gives unrealistic values compared to the measured data. It includes only one stiffness parameter and therefore assumes that the soil loading stiffness is equal to the soil unloading/reloading stiffness ( $E_{50} = E_{ur}$ ). In reality, soils usually have a much stiffer response during unloading/reloading conditions when compared to loading conditions (Gouw Dr, 2014). The use of  $E_{50}$  seems too conservative. The unloading-reloading stiffness should have a magnitude of 2-5 times greater than the loading stiffness ( $E_{ur} = 2$  to  $5 * E_{50}$ ). This effect is described by Johansson and Sandeman (2014) and Nurmohamed et al. (1997) to give better fit to displacement values.

An unloading/reloading stiffness ( $E_{ur}$ ) should be used where the material is affected by unloading/reloading.  $E_{ur} = 3 * E_{50}$  was inserted in soil materials in different phases (fig. 4.23). In phase 3, 4, 6, 8 and 9 the materials in front of the SPW are experiencing un-

loading caused by excavation, hence an  $E_{ur}$  is inserted in these materials in the mentioned phases. In phase 5 and 7 the materials behind the SPW are experiencing reloading due to the installation of anchors and hence an  $E_{ur}$  is inserted in the materials located close behind the SPW.

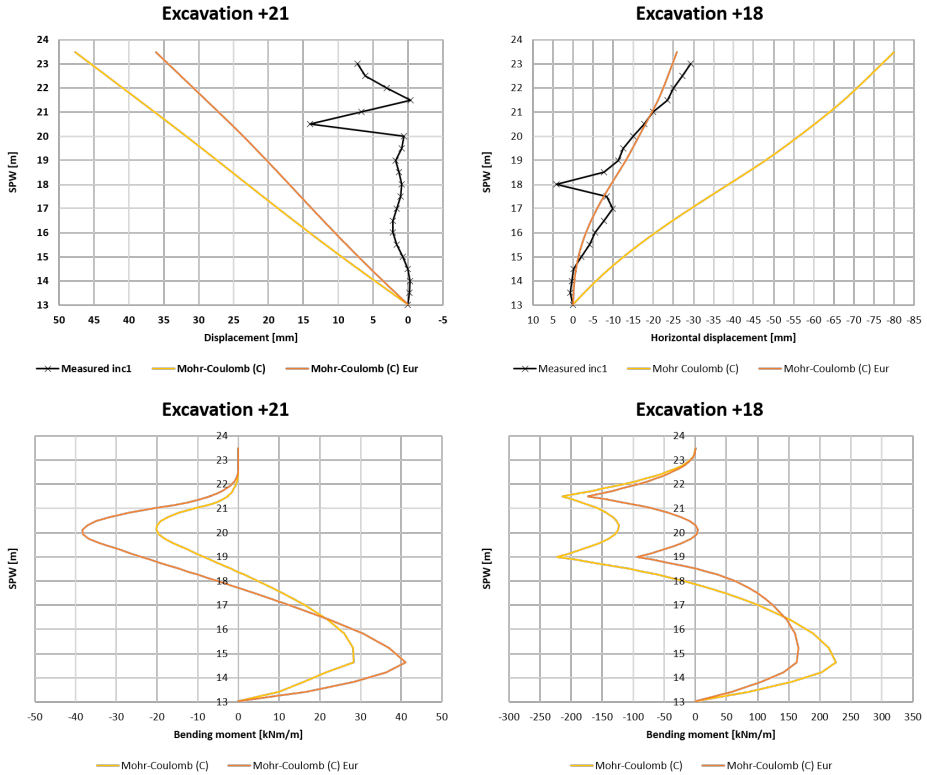


**Figure 5.15:** Horizontal displacement and bending moment of the SPW for phases excavating to elevation +21 and +18 using MC( $E_{ur}$ ).

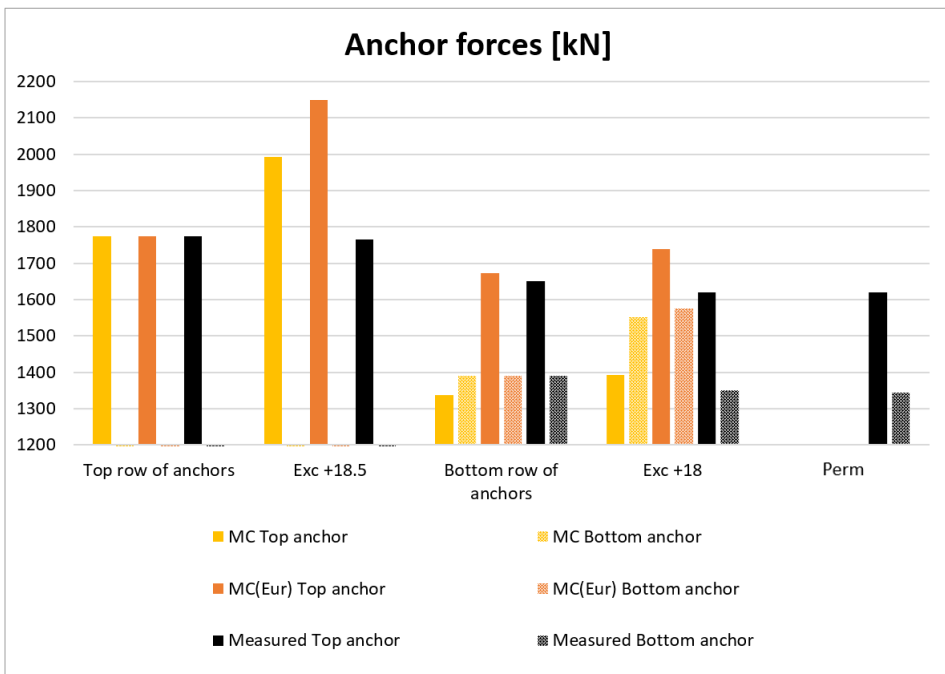


**Figure 5.16:** Combined calculated anchor forces for both MC models compared to measured data.

Inserting  $E_{ur}$  in MC when excavating to elevation +21, reduces the displacement of the SPW which fit better to the measured data when compared to MC without  $E_{ur}$  (fig. 5.15). Still, the displacement seems off by approximately 30 mm in the top vertex. Looking at the excavation phase to elevation +18, the model improves and gives displacements close to the measured data. The top vertex is off by 4 mm. The bending moment seems to slightly increase in magnitude during the first phases, but is corrected after installing the top row of anchors. There is an increase in force of the top anchor when excavating to elevation +18.5 which deviates more from the measured data (fig. 5.16). This value is also getting very close to the dimension of the anchors (2375 kN). On the other hand, the anchor forces are greatest in the top row when the bottom row of anchors is installed, which correlates well with the measured value. This is also seen by the bending moment of the SPW, which is reversed in MC. Overall the increase of stiffness in MC( $E_{ur}$ ) gives more accurate displacement of the SPW and anchor forces, even though they still get overestimated.

The FoS and failure surfaces in this model stay the same as MC without  $E_{ur}$ , as the strength is not changed. This is controlled in PLAXIS output. The rock bolt shows a decrease in force after the top row of anchors is installed compared to the MC model. See appendices D.4 and D.5.

MC( $E_{ur}$ ) is included in the further analyses.



5.2.3  $R_{inter} = 0.4$

In general, the different models in PLAXIS gave too much displacement in the first excavating phase. Increasing the roughness results in greater connection between the soil and the SPW, making the soil absorb greater forces. Therefore, the  $R_{inter}$  in the quick clay materials are changed to 0.4 on both sides, as 0.1 might be too conservative.

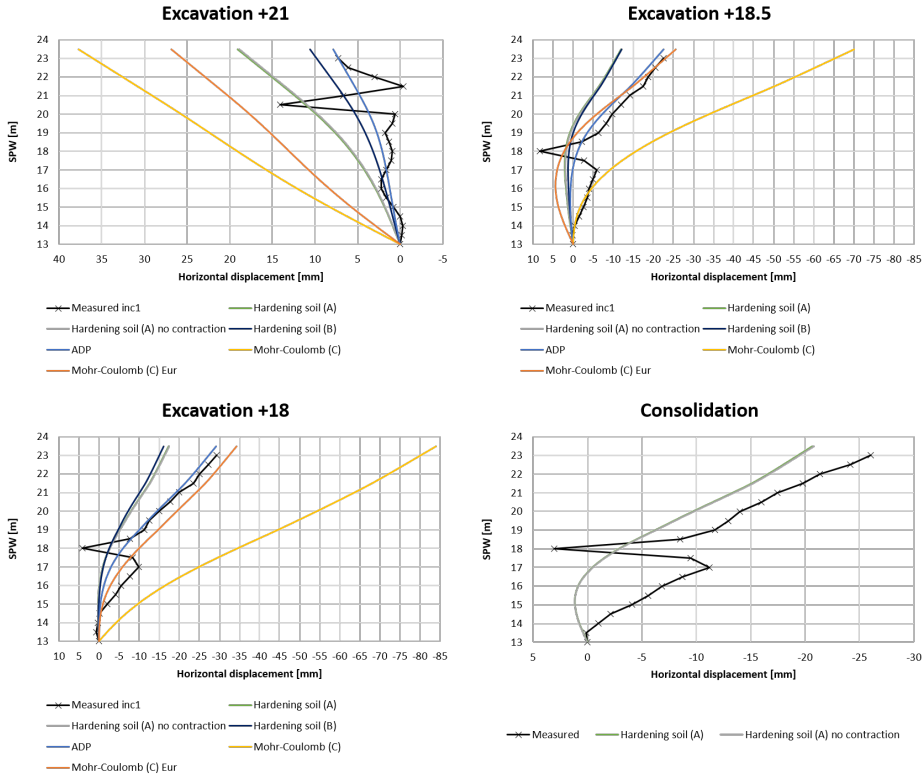


**Figure 5.17:** Horizontal displacement of the SPW in PLAXIS with  $R_{inter} = 0.4$  compared to measured data.

When excavating to +21, all models seems to give a better fit to the measured data in displacement (fig. 5.17). Excavating to elevation +18.5 and elevation +18, the HS models and NGI-ADP increase their accuracy in displacement, while MC and  $MC(E_{ur})$  give a greater displacement than the initial model. Even though NGI-ADP deviates more in the top vertex, the model generally fits better to the measured data. The displacement in the consolidation phase seems to fit better with the measured data compared to the the initial analysis.

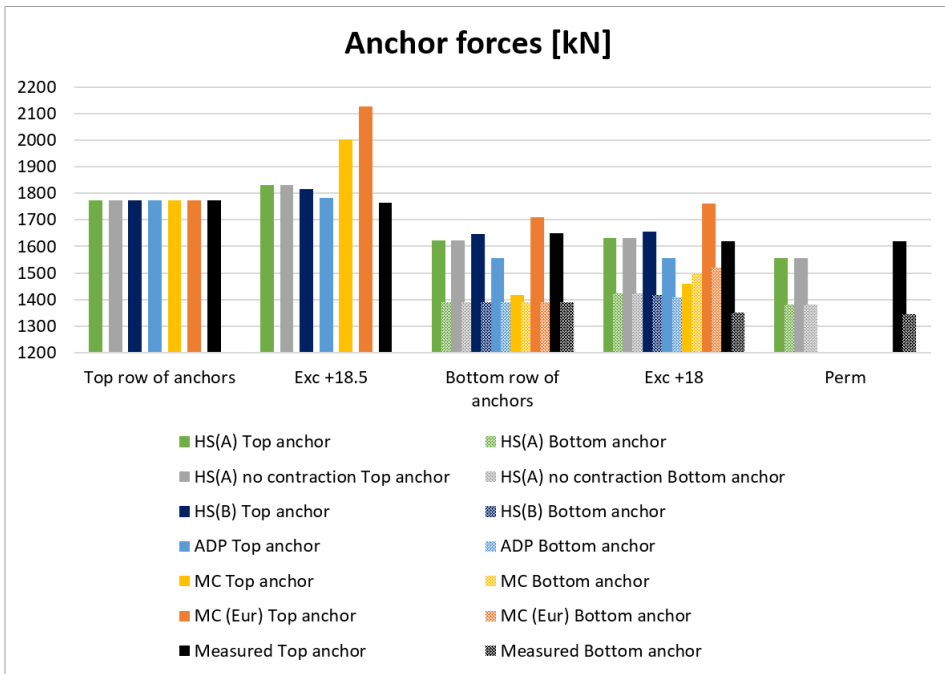


**Figure 5.18:** Calculated anchor forces from the  $R_{inter} = 0.4$  analysis compared to measured anchor forces.

Looking at figure 5.18 and tables 5.3 and 5.4, the anchor forces seem to give a better fit in total to the measured values for all models. The top row of anchors seems to deviate more in the permanent phase after consolidation, while the bottom anchor seems to improve.

**Table 5.3:** Difference in calculated and measured anchor forces, normalized on the latter, given in % for the top row of anchors

	Top anchor	Exc +18.5	Bot. anchor	Exc +18	Perm.	Abs. av.
HS(A)nc	0.0	3.7	-1.7	0.7	-3.9	1.5
HS(A)	0.0	3.7	-1.7	0.7	-3.9	1.5
HS(B)	0.0	2.8	-0.2	2.2	-	1.3
ADP	0.0	1.0	-5.7	-3.9	-	2.7
MC	0.0	13.6	-14.1	-10.0	-	9.4
MC(Eur)	0.0	20.5	3.7	8.8	-	8.2

**Table 5.4:** Difference in calculated and measured anchor forces, normalized on the latter, given in % for the bottom row of anchors.

	<b>Bot. anchor</b>	<b>Exc +18</b>	<b>Perm.</b>	<b>Abs. av.</b>
HS(A)nc	0.0	5.5	2.7	2.7
HS(A)	0.0	5.5	2.6	2.7
HS(B)	0.0	5.0	-	1.3
ADP	0.0	4.3	-	2.1
MC	0.0	10.8	-	5.4
MC(Eur)	0.0	12.7	-	6.3

There is a small change in FoS when  $R_{inter}$  is changed to 0.4 from 0.1, where the largest change, -0.053 for HS(A)nc, occurs during excavating to +21 (app. E.5). This value is so small its considered negligible and may be due to mesh-dependency.

#### 5.2.4 $S_u250$

To model LCC, the  $S_u$  is increased in the clay layers in a 6 m wide area in front of the SPW (fig. 4.4). As the shear strength of the lime cemented area gave values of approximately 250 kPa, the  $S_u^A$  in NGI-ADP is set to this value. The gaps between the columns in the lime cemented area (fig. 4.3) are therefore not accounted for, hence the area in front of the SPW is fully reinforced by the LCC. In MC and HS(B) the undrained shear strength is set to  $0.63 \cdot 250$  kPa. In HS(A),  $\phi$  and  $c'$  are increased so that the strength profile matches the strength profile of HS(B) with modeled lime cement. The stiffnesses are increased by the same ratio as between the initial stiffness and strength  $E_{u,initial}/S_{u,initial} = E_{u,new}/S_{u,new}$ .  $R_{inter}$  is set to 0.25 against the slope and 0.1 against the pit as the front of the SPW may be stirred twice, described in section 4.3.2.

Interface materials are inserted in the interface in front of the SPW, and has the same parameters as the initial material. This forces the strength along the front of the SPW to be reduced in relation to the initial clay material instead of the reinforced lime cemented material with increased strength.

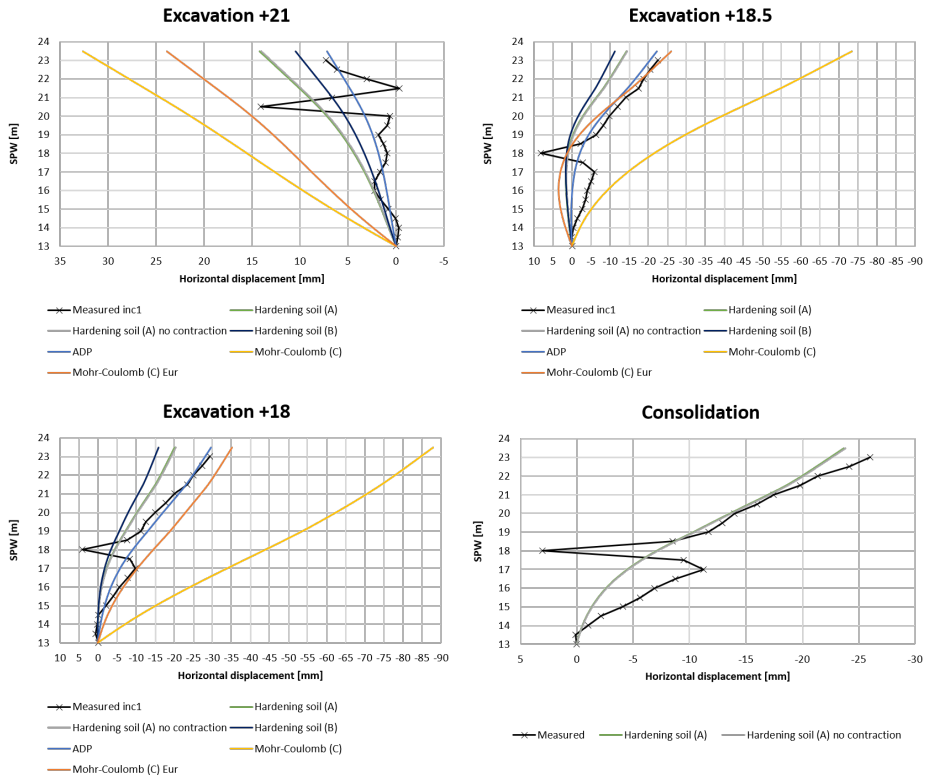


**Figure 5.19:** Horizontal displacement of the SPW in PLAXIS with  $S_u250$  parameters compared to measured data.

When excavating to elevation +21, all models seems to give a better fit to the measured data in displacement when compared to the scenario of  $R_{inter} = 0.4$ . Except for HS(B) (fig. 5.19) which stays approximately the same in all phases. Excavating to elevation +18.5, HS(A) increases its accuracy, while MC and MC( $E_{ur}$ ) gives a greater displacement. When excavating to elevation +18, there is a small change in NGI-ADP, fitting better than the previous analysis. In this phase, both MC, MC( $E_{ur}$ ) and HS(A) gives greater displacement, causing HS(A) to improve while the MC models deviate more from the measured data. The displacement after consolidation seems to give a good fit to the measured displacement, and seems more accurate when compared to the scenario of  $R_{inter} = 0.4$ , and therefore also the initial model. A significant decrease of the bulging is obtained, which seems to correspond well to measured data.

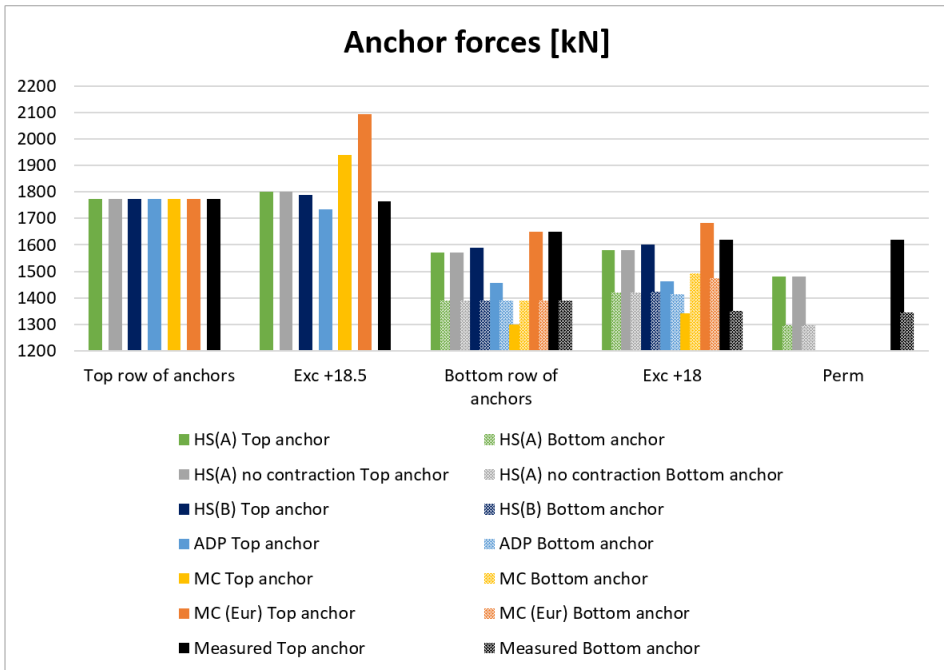


**Figure 5.20:** Calculated anchor forces from the  $S_u250$  analysis compared to measured anchor forces.

The anchor forces seem to give a worse fit in total to the measured values for all models when compared to the scenario of  $R_{inter} = 0.4$ , except for  $MC(E_{ur})$  (fig. 5.20 and tables 5.5 and 5.6). The top row of anchors seems to fit better to the measured force after the phase of consolidation. The bottom anchor seems to be less than the measured values instead of greater, as shown in the scenario of  $R_{inter} = 0.4$ .

**Table 5.5:** Difference in calculated and measured anchor forces, normalized on the latter, given in % for the top row of anchors.

	Top anchor	Exc +18.5	Bot. anchor	Exc +18	Perm.	Abs. av.
HS(A)nc	0.0	2.0	-4.8	-2.4	-0.1	2.3
HS(A)	0.0	2.0	-4.8	-2.5	-0.1	2.3
HS(B)	0.0	1.4	-3.7	-1.2	-	1.6
ADP	0.0	-1.7	-11.8	-9.8	-	5.8
MC	0.0	10.0	-21.2	-17.1	-	12.1
MC(Eur)	0.0	18.7	0.0	4.0	-	5.7

**Table 5.6:** Difference in calculated and measured anchor forces, normalized on the latter, given in % for the bottom row of anchors.

	<b>Bot. anchor</b>	<b>Exc +18</b>	<b>Perm.</b>	<b>Abs. av.</b>
HS(A)nc	0.0	5.3	-3.7	2.6
HS(A)	0.0	5.3	-3.7	2.6
HS(B)	0.0	5.3	-	2.7
ADP	0.0	4.8	-	2.4
MC	0.0	10.6	-	5.3
MC(Eur)	0.0	9.1	-	4.6

There is a small change in FoS when compared to the initial model ( $R_{inter} = 0.1$ ), where the largest change of -0.16 for HS(A)nc occurs during excavating to +21 (app. F.5).

### 5.2.5 $S_u$ 100

To simulate the gaps in the lime cement, the same tuning as in the previous section is done but with  $S_u^A$  set to 100 kPa in the lime cemented area. In MC and HS(B) the undrained shear strength is set to  $0.63 * S_u^A$  kPa. The strength is reduced as the lime cemented area is likely to not be fully reinforced. The displacement results are displayed in figure 5.21.

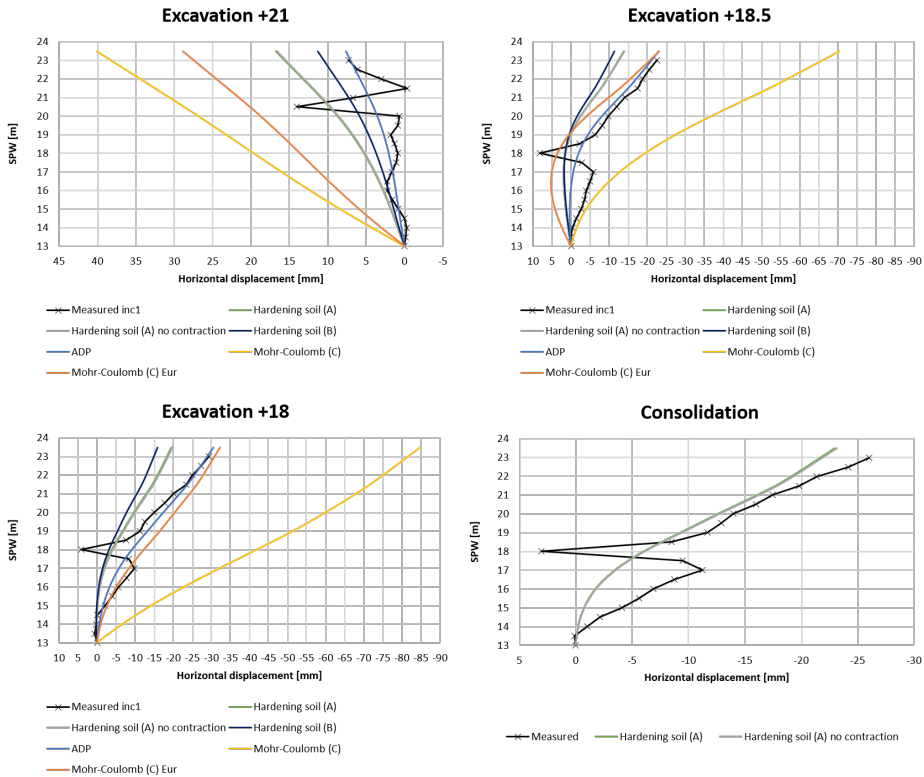


**Figure 5.21:** Horizontal displacement of the SPW in PLAXIS with  $S_u$ 100 parameters compared to measured data.

When excavating to elevation +21, all models seem to give a worse fit to the measured data in displacement when compared to the previous scenario. Excavating to elevation +18.5 and elevation +18, HS(A) and HS(B) stay approximately the same. MC and MC( $E_{ur}$ ) give less displacement into the slope in these phases, which correlates better to the measured data. For MC( $E_{ur}$ ) this is only true when excavating to elevation +18. The bulging of the SPW is greater in MC( $E_{ur}$ ) when compared to the previous scenario. There is a small change in NGI-ADP, primarily resulting in less displacements of the SPW into the slope. The displacement after consolidation seems to give a good fit to the measured data, but is further off-set when compared to the previous scenario. The displacements are still better when compared to the initial model.

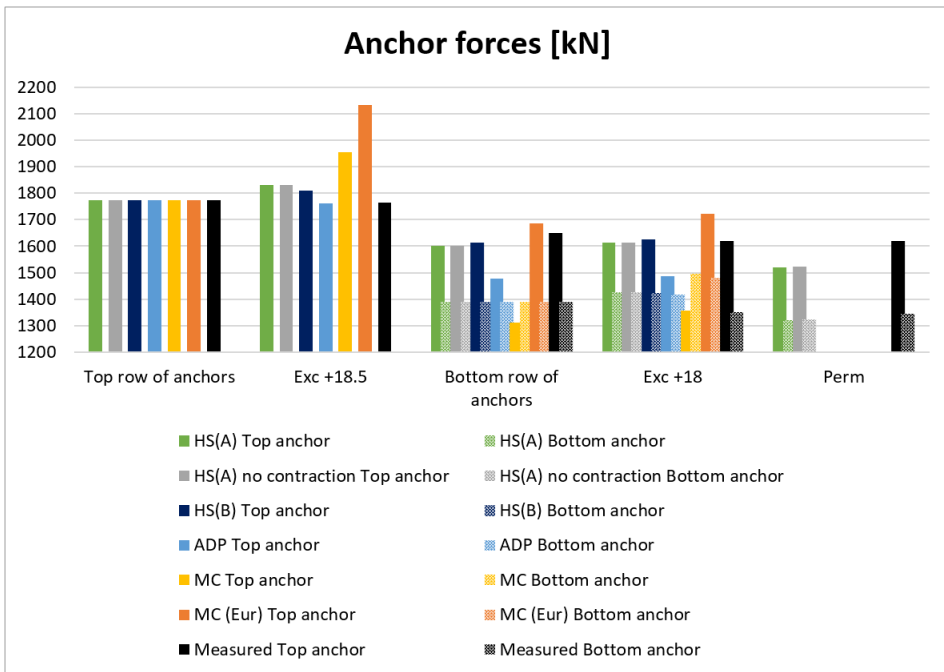


**Figure 5.22:** Calculated anchor forces from the  $S_u/100$  analysis compared to measured anchor forces.

The anchor forces seem to give a better fit in total to the measured values for all models when compared to the previous scenario, except for  $MC(E_{ur})$  (fig. 5.22 and tab. 5.7 and 5.8). The LCC seems less effective at inclinometer 2. The top row of anchors seems to fit less to the measured force in the permanent phase after consolidation, while the bottom anchor seems to give a better fit. The anchor force is less than the measured force instead of greater, as shown in the scenario of  $R_{inter} = 0.4$ .

**Table 5.7:** Difference in calculated and measured anchor forces, normalized on the latter, given in % for the top row of anchors.

	Top anchor	Exc +18.5	Bot. anchor	Exc +18	Perm.	Abs. av.
HS(A)nc	0.0	3.9	-2.8	-0.4	-6.0	1.8
HS(A)	0.0	3.9	-2.9	-0.4	-6.1	1.8
HS(B)	0.0	2.5	-2.2	0.3	-	1.3
ADP	0.0	-0.2	-10.4	-8.3	-	4.7
MC	0.0	10.7	-20.5	-16.4	-	11.9
MC(Eur)	0.0	21.0	2.2	6.4	-	7.4



**Table 5.8:** Difference in calculated and measured anchor forces, normalized on the latter, given in % for the top row of anchors.

	<b>Bot. anchor</b>	<b>Exc +18</b>	<b>Perm.</b>	<b>Abs. av.</b>
HS(A)nc	0.0	5.6	-1.7	2.8
HS(A)	0.0	5.6	-1.8	2.8
HS(B)	0.0	5.5	-	2.7
ADP	0.0	5.0	-	2.5
MC	0.0	10.8	-	5.4
MC(Eur)	0.0	9.6	-	4.8

There is a small change in FoS when compared to the initial model ( $R_{inter} = 0.1$ ), where the largest change of -0.11 for HS(A)nc occurs during excavating to +21 (app. G.5).

## 5.3 Parametric study in GS

The parametric study of GS is not presented with the parametric study of PLAXIS, mainly because the roughness is not equal by definition. Also, in GS it will act on the entire wall, which means changing the roughness in GS will change the roughness for the entire profile. In PLAXIS the roughness, or  $R_{inter}$ , is only changed in the quick clay layer. Changing the roughness in GS and obtaining new results is a fast process. Therefore, not all values tested will be presented. The front roughness has little impact on the overall results and will hence be set to 0 in this thesis. All results from GS are added in appendices H.1-J.3.

### 5.3.1 $r = 0.4$

In GS one decides active and passive sides based on which way the roughness is chosen. In this thesis it is natural to set the side behind the SPW to downwards as the slope is falling into the SPW. This is in contrast to PLAXIS where a strength reduction factor ( $R_{inter}$ ) is used.

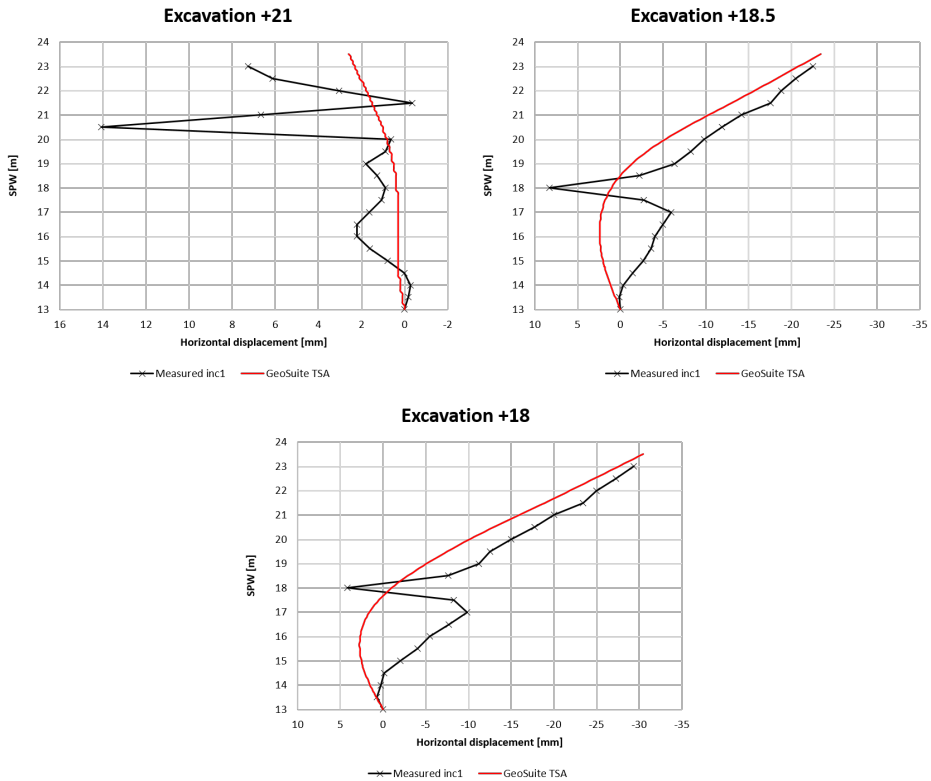


**Figure 5.23:** Horizontal displacement of the SPW in GS with  $r = 0.4$  parameters compared to measured data.

Running  $r = 0.4$  downwards gave the best fit with the measurement data when no LCC are modeled. The displacement is almost identical in the top vertex with a similar deflection pattern throughout (fig. 5.23). This scenario fits better to the measured data when comparing to the initial model ( $r = 0$ ). However, the bulge in the lower vertices is still present. Table 5.9 show anchor forces obtained in top and bottom anchor in GS, as well as difference between calculated and measured forces, normalized on measured values.

**Table 5.9:** Calculated anchor forces in different phases in GS for  $r = 0.4$ , compared to measured anchor force. Deviance is normalized on measured values.

	Top anchors	Exc +18.5	Bot. anchors	Exc +18	Abs. av.
Top anchor Force [kN]	1775	1758	1584	1582	-
Top anchor Deviance [%]	0.0	-0.4	-3.9	-2.3	1.7
Bottom anchor Force [kN]	-	-	1390	1389	-
Bottom anchor Deviance [%]	-	-	0.0	2.9	1.5

Comparing the anchor forces to the initial model, the top row of anchors seems to slightly deviate from the measured data. The bottom row of anchors stays approximately the same and seems unaffected by any changes made.

### 5.3.2 $S_u$ 250

Similarly to PLAXIS, the  $S_u$  is increased in front of the SPW to account for the increase in strength due to full effect of the lime cement. The  $S_u^P$  is set to  $0.35 \cdot 250$  kPa and  $r$  is kept at 0.4 downwards behind the SPW. As mentioned in section 4.3.3, the stiffness will deviate from what is desired. Figure 5.24 shows that the stiffness is about twice as big as the initial stiffness (fig. 4.28) on the behind side. The stiffness could be input directly instead of using  $G/S_u$ , but nonetheless the stiffness will be off on either side.

			Soil Weight [kN/m <sup>3</sup> ]	$C_u$ _behind [kPa]	$C_u$ _front [kPa]	$K_0$ _eff [-]	G [kPa]	G/ $C_u$ -ratio [-]	
Silty clay	TSA - Total stress automatic	▼	2.00	19.00	55.00	87.50	0.65	17812.50	250.00
			4.00	19.00	55.00	87.50	0.65	17812.50	250.00
Quick clay	TSA - Total stress automatic	▼	4.00	19.00	43.00	87.50	0.65	48937.50	750.00
			8.75	19.00	50.00	87.50	0.65	51562.50	750.00

**Figure 5.24:** Silty clay and quick clay parameters illustrating the deviating stiffness in GS.

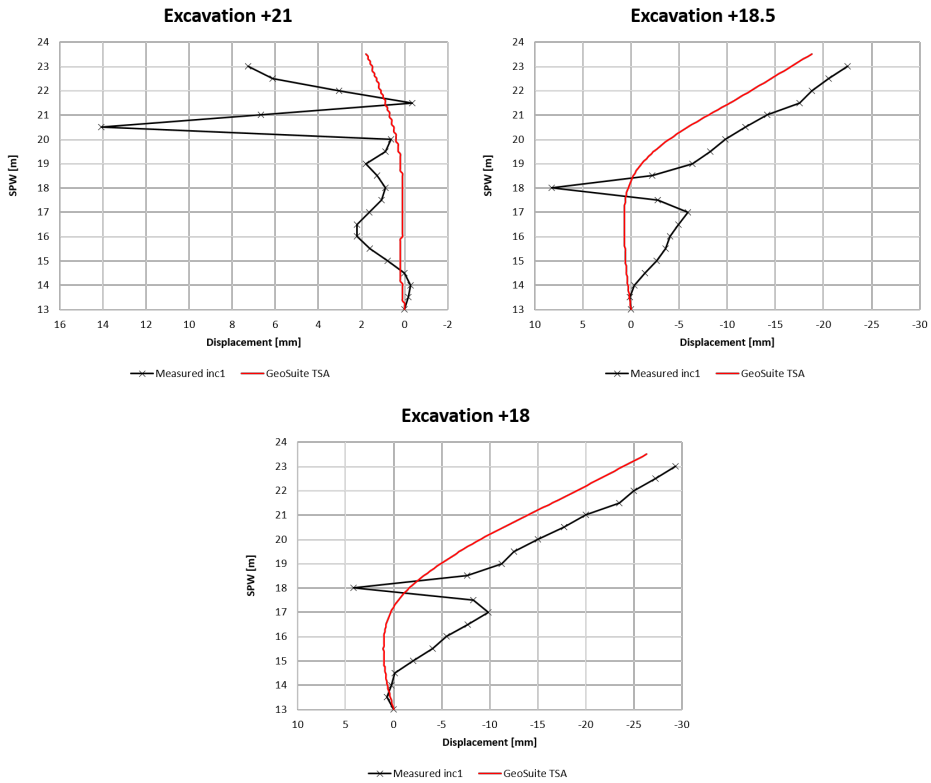


**Figure 5.25:** Horizontal displacement of the SPW in GS with  $s_u$ 250 parameters compared to measured data.

The bulge has been significantly improved with increased shear strength in front of the SPW (fig. 5.25). The displacements seem to correspond worse to the measured data in the top vertex than for the previous scenario ( $r = 0.4$ ).

**Table 5.10:** Calculated anchor forces in different phases in GS for  $S_u250$ , compared to measured anchor force. Deviance is normalized on measured values.

	<b>Top anchors</b>	<b>Exc +18.5</b>	<b>Bot. anchors</b>	<b>Exc +18</b>	<b>Abs. av.</b>
Top anchor Force [kN]	1775	1770	1580	1579	-
Top anchor Deviance [%]	0.0	0.3	-4.2	-2.6	1.6
Bottom anchor Force [kN]	-	-	1390	1389	-
Bottom anchor Deviance [%]	-	-	0.0	2.9	1.5

The force of the top row of anchors seems to fit slightly better to the measured data when compared to the previous scenario (tab. 5.10). The bottom row of anchors stay approximately the same.

### 5.3.3 $S_u100$

Similarly to PLAXIS, the  $S_u$  is increased in front of the SPW to account for the increase in strength due to partial effect of the lime cement. The  $S_u^P$  is set to  $0.35 \cdot 100$  kPa and  $r$  is kept at 0.4 downwards behind the SPW.

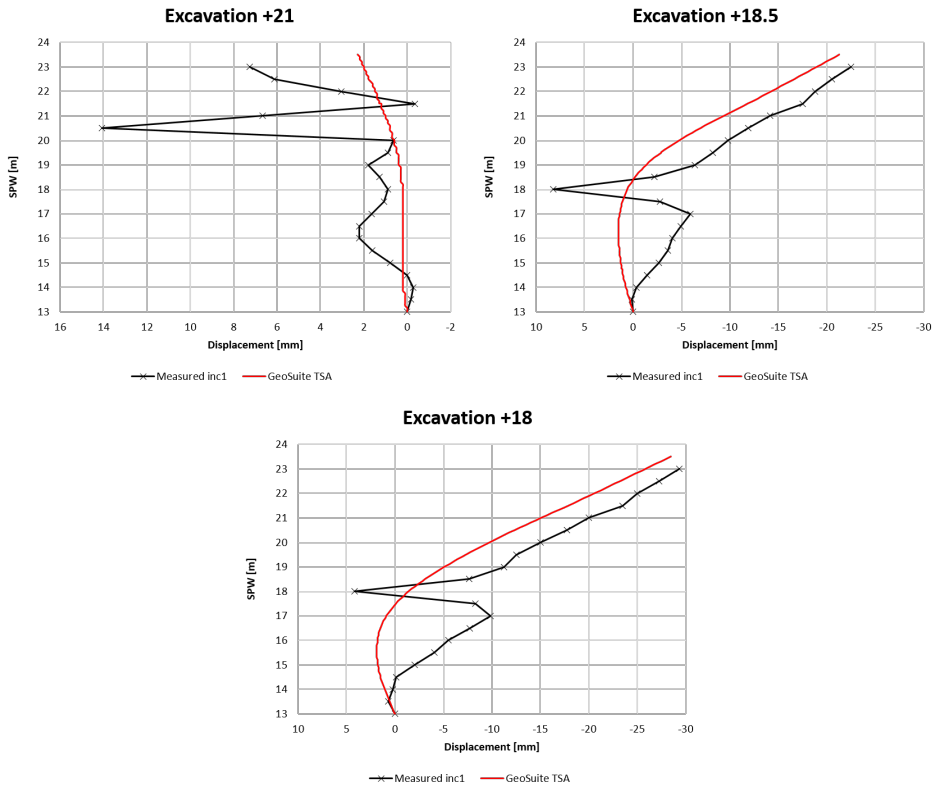


**Figure 5.26:** Horizontal displacement of the SPW in GS with  $S_u$ 100 parameters compared to measured data.

The displacements seems to give a better fit to the measured data than for the previous scenario, and is in total more accurate than for the scenario of  $r = 0.4$ . The bulge is more present when compared to the previous scenario (fig. 5.26).

**Table 5.11:** Calculated anchor forces in different phases in GS for  $S_u$ 100, compared to measured anchor force.

	Top anchors	Exc +18.5	Bot. anchors	Exc +18	Abs. av.
Top anchor Force [kN]	1775	1764	1582	1580	-
Top anchor Deviance [%]	0.0	-0.1	-4.1	-2.5	1.7
Bottom anchor Force [kN]	-	-	1390	1389	-
Bottom anchor Deviance [%]	-	-	0.0	2.9	1.5

The force of the top row of anchors is almost exactly the same as the scenario when using  $r = 0.4$  (tab. 5.11).

## 5.4 Simple hand calculation

As mentioned in section 4.4, a hand calculated analysis is performed. Several simplifications and assumptions are made. As the calculations assume horizontal terrain, a load of  $q' = 100$  kPa is added behind the SPW to add the effect of the slope and building loads. The FoS is set to unity, and the roughness is set to be zero along the entire SPW. The earth pressure coefficients are displayed in table 5.12.

**Table 5.12:** Values calculated and used in simple hand calculations.

FoS	1
$\tan(\rho)$	0.57
$r$	0.00
$K_a$	0.33
$K_p$	3.10
$\omega$	0.00
$f_\omega$	0.00
$\kappa$	2.00

As mentioned in section 3.2.3, only the part above the final excavation level will be considered in the anchor force calculations (fig. 5.27). The rest of the active earth pressure is assumed to be resisted by the passive earth pressure and rock bolt. The earth forces for each area are summed up (tab. 5.13) and divided by two, giving the calculated horizontal anchor force ( $P_H$ ). Earth pressure calculations are found in appendix K.1.

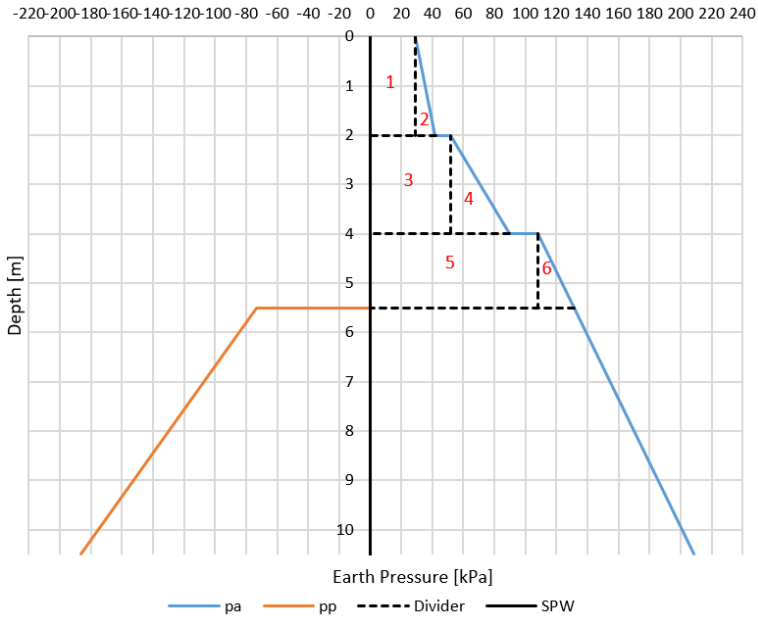


**Figure 5.27:** Earth pressure diagram from hand calculations.

**Table 5.13:** Calculated earth forces in each area.

Area	Horizontal earth force [kN/m]
1	58
2	13
3	104
4	38
5	162
6	17
<b>Sum</b>	<b>392</b>

To obtain the inclined anchor forces, equation 3.40 is used with  $\alpha = 45^\circ$ . This gives both anchor forces to be:

**Table 5.14:** Axial anchor forces for top and bottom row of anchors.

Anchor	Anchor force P [kN/m]
Top	278
Bottom	278

As FoS is set to unity, these anchor forces are needed to reach force equilibrium. This is far of from both the measured data and the forces obtained from PLAXIS and GS. This is due



to the fact that this is a slope stability analysis with a complex structure, hence the hand calculations are conducted with several simplifications. Also, traditional earth pressure calculations need the soil to move to utilize its full strength. In this project the prestress is so high that it pushes the SPW into the slope far from fully mobilized shear strength, and reaches a FoS of 1.71. The stiffness of the wall is also not included in hand calculations. The use of numerical models is an advantage when calculating a multi-anchored SPW in sloping terrain.

## **5.5 Main Discussion**

To see which scenario corresponds best to the measured values, displacement diagrams of the separate models containing different scenarios are presented in figures 5.28 and 5.29. Only the first excavation phase to elevation +21 and the final excavation to elevation +18 are included. HS(A) and HS(A)nc are added in the same plots, as the difference is relatively small. Please note the difference on the x-axis to each plot.

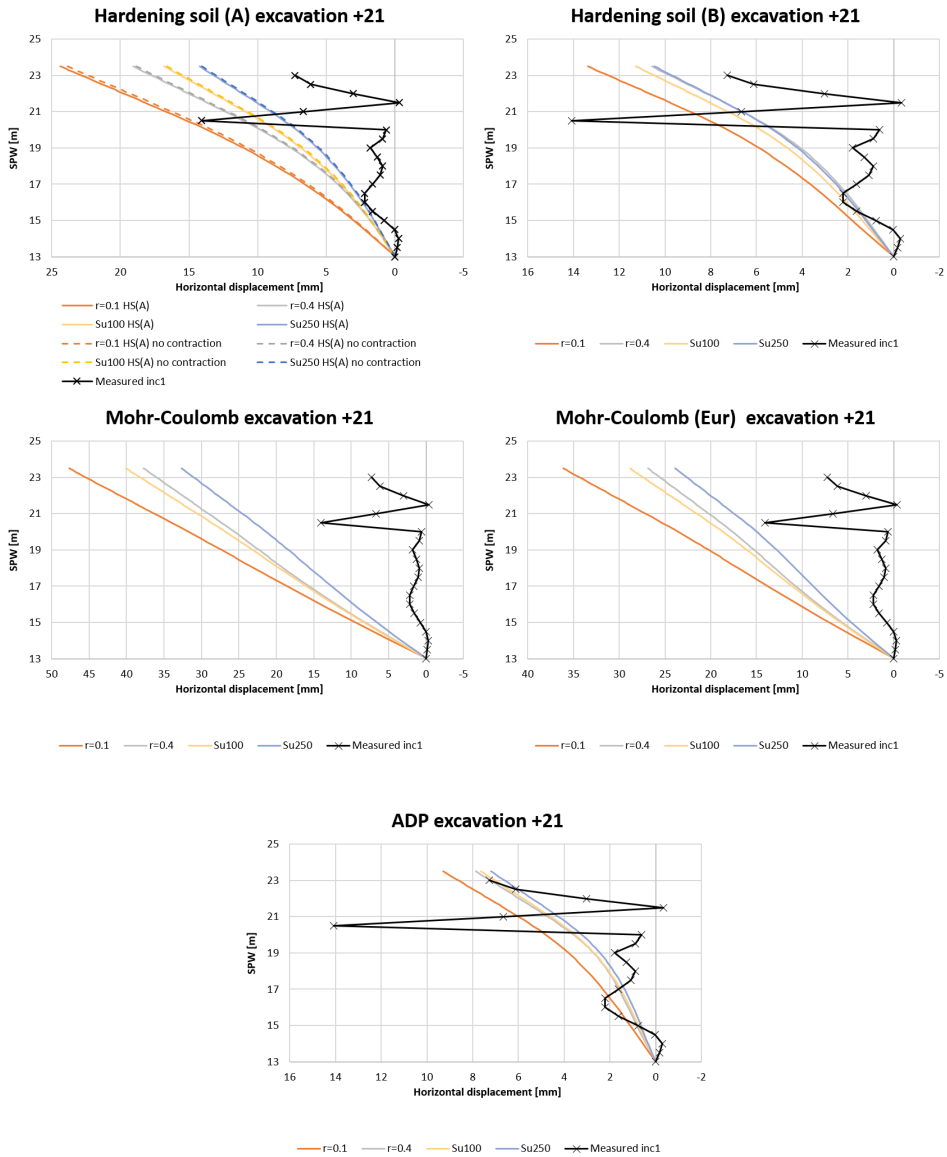


**Figure 5.28:** Horizontal displacement of the SPW when excavating to elevation +21, comparing all parameter sets from PLAXIS with measured data.

Modeling lime cement in front of the SPW with  $S_u^A = 250$  kPa, gives best fit to the measured data in all models when excavating to elevation +21.  $R_{inter} = 0.4$  seems to also give a good fit for HS(B). The corrected stiffness in MC( $E_{ur}$ ) gives more accurate results when compared to MC.

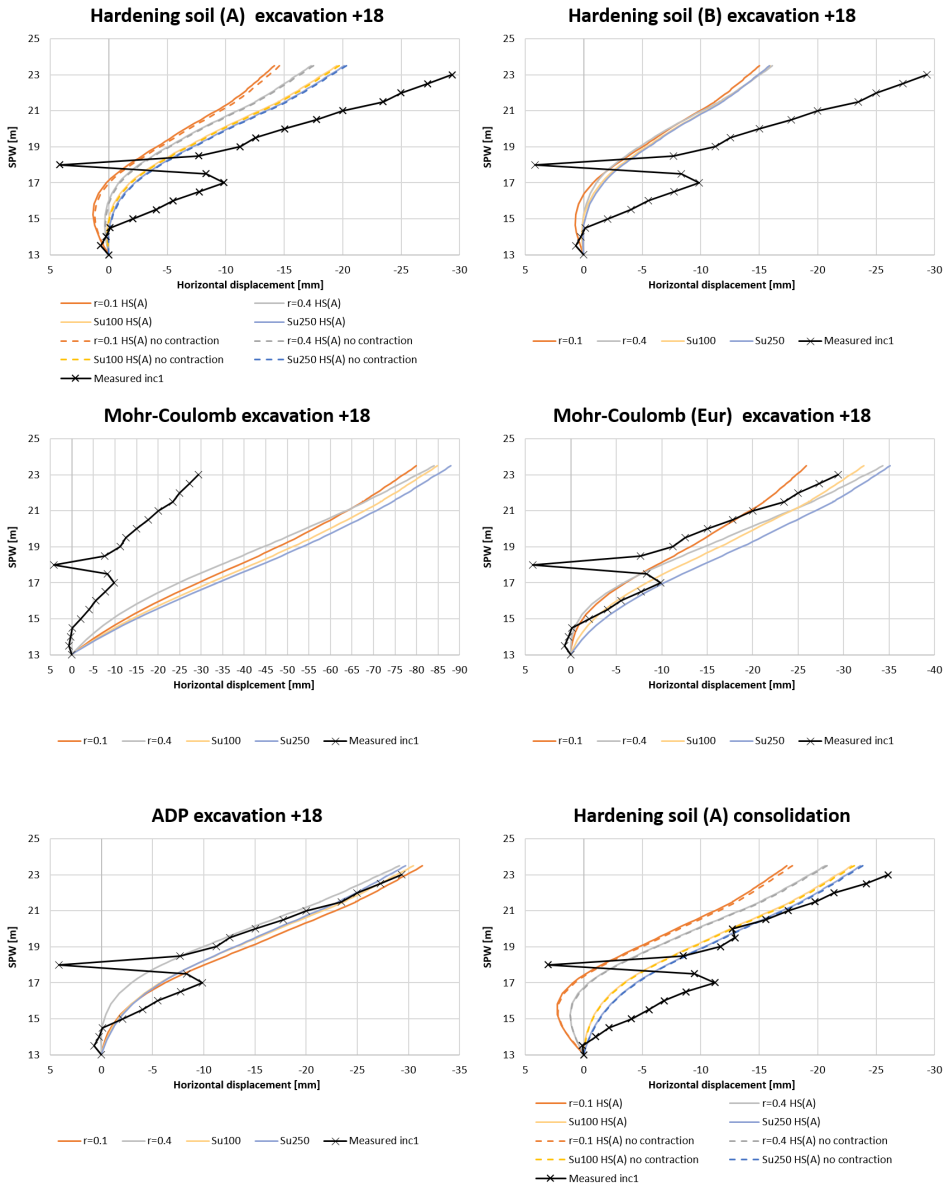


**Figure 5.29:** Horizontal displacement of the SPW when excavating to elevation +18 and after consolidation, comparing all parameter sets from PLAXIS with measured data.

When excavating to elevation +18, the results vary. For HS(A) and HS(B), the scenario of modeling lime cement in front of the SPW with  $S_u^A = 250$  kPa gives the best fit, which is also true for the permanent phase after consolidation. HS(B) gives in general too small displacements in this phase. For MC, both  $R_{inter} = 0.4$  and  $R_{inter} = 0.1$  seem to give the

best fit. For  $MC(E_{ur})$ ,  $R_{inter} = 0.4$  and the scenario of modeling lime cement in front of the SPW with  $S_u^A = 100$  kPa, gives best fit when excavating to elevation +18. It is difficult to decide which scenario that fits best for NGI-ADP as the difference is small, but both  $R_{inter} = 0.4$  and the scenario of modeling lime cement in front of the SPW with  $S_u^A = 100$  kPa fits well overall.

The anchor forces of the different scenarios are added in table 5.15 and 5.16. They show the absolute average of the difference between calculated and measured forces normalized on the latter. For the top row of anchors, the absolute average includes 4 phases, from installing the top row of anchors to the final excavation to elevation +18. For the bottom row of anchors, the absolute average includes 2 phases, installing the bottom row of anchors and the final excavation to elevation +18. Hence, the permanent phase after consolidation is not added in the absolute average. The difference is shown in %.

**Table 5.15:** Absolute average top anchor row in %

	<b>Initial <math>R_{inter} = 0.1</math></b>	<b><math>R_{inter} = 0.4</math></b>	<b><math>S_u 250</math></b>	<b><math>S_u 100</math></b>
HS(A)nc	2.2	1.5	2.3	1.8
HS(A)	2.2	1.5	2.3	1.8
HS(B)	1.3	1.3	1.6	1.3
ADP	5.1	2.7	5.8	4.7
MC	11.5	9.4	12.1	11.9
MC(Eur)	7.6	8.2	5.7	7.4

**Table 5.16:** Absolute average bottom anchor row in %

	<b>Initial <math>R_{inter} = 0.1</math></b>	<b><math>R_{inter} = 0.4</math></b>	<b><math>S_u 250</math></b>	<b><math>S_u 100</math></b>
HS(A)nc	3.0	2.7	2.6	2.8
HS(A)	2.9	2.7	2.6	2.8
HS(B)	2.8	2.5	2.7	2.7
ADP	2.4	2.1	2.4	2.5
MC	7.4	5.4	5.3	5.4
MC(Eur)	8.3	6.3	4.6	4.8

The absolute average of the anchor forces indicates that HS(B) produces the most accurate forces in the top row of anchors. The scenarios with  $R_{inter} = 0.1$ ,  $R_{inter} = 0.4$  and the scenario of modeling LCC in front of the SPW with  $S_u^A = 100$  kPa gives the most accurate anchor forces in total.  $R_{inter} = 0.4$  gives the most accurate anchor forces of all the models, except for  $MC(E_{ur})$  where the scenario of modeling lime cement in front of the SPW with  $S_u^A = 100$  kPa is most accurate. NGI-ADP produces the most accurate forces in the bottom row of anchors when  $R_{inter} = 0.4$  is used. HS(A), MC and  $MC(E_{ur})$  prefers the scenario of modeling lime cement in front of the SPW with  $S_u^A = 250$  kPa, while HS(B) prefers  $R_{inter} = 0.4$ .

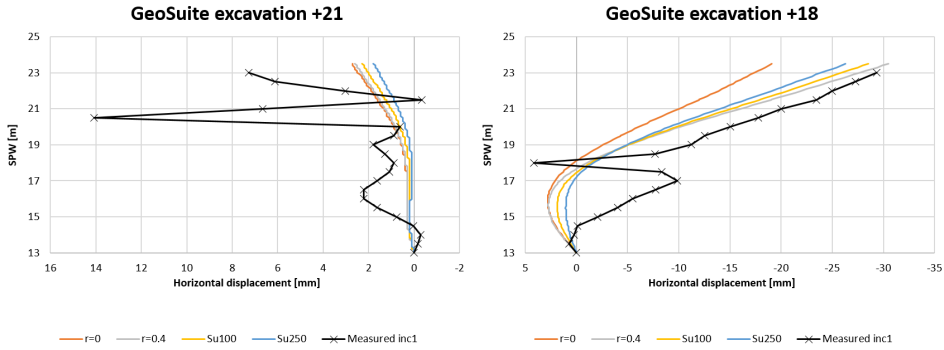


**Figure 5.30:** Horizontal displacement of the SPW, when excavating to elevation +21 and +18, comparing all parameter sets from GS to measured data.

GS produces little difference when excavating to elevation +21 (fig. 5.30). The different scenarios have little impact in this phase, but the initial scenario ( $r = 0$ ) seems to give best fit. When excavating to elevation +18, the scenario of modeling lime cement in front of the SPW with  $S_u^A = 100$  kPa seems preferable in total.

**Table 5.17:** Absolute average for both row of anchors in %

	Initial $r = 0$	$r = 0.4$	$S_u 250$	$S_u 100$
Top anchor	1.0	1.7	1.6	1.7
Bottom anchor	1.5	1.5	1.5	1.5

The absolute average of the anchor forces indicates that  $r = 0$  produces the most accurate forces in both the top row of anchors for GS (tab. 5.17). For the bottom row of anchors, all scenarios produce the same absolute average, meaning small difference between the scenarios.

In total, NGI-ADP gives the best fit to the measured values. The model did not produce the most accurate anchor forces which may come from the load cells being placed at inclinometer 2. The profile X-X' cuts through inclinometer 1, hence this inclinometer is used when comparing displacements. Inclinometer 2 differs in displacement which could be due to different layering behind the SPW and less distance to bedrock. The latter causes the anchors at inclinometer 2 to be shorter, hence giving greater displacements into the slope. This again causes greater anchor forces by the equation  $P = (EA/L) \cdot \delta$ . The LCC seems less effective at inclinometer 2, as the anchor forces correspond better when the undrained shear strength is reduced from 250 kPa to 100 kPa in the soil in front of the SPW. Still, all models seem to give an acceptable fit to the measured anchor forces.

Of all the models used, NGI-ADP gives least variation in results when changing roughness and modeling LCC. There are still some differences at a small scale, and even though

they might be small, such changes could still be critical to a project that only allows for minor displacements. When tuning models to a strength profile it goes at the expense of stiffness, especially for the HS model. NGI-ADP internally corrects this behaviour with the use of a stiffness ratio ( $G/S_u$ ). HS(A) seems capable to model the long-term effect after consolidation, but may have difficulties in reproducing both short term and long term conditions using one parameter set. Including LCC seems to improve the accuracy for all models when compared to measured displacement, except for MC. Usually the MC model is used as a first analysis to a problem, as it overestimates the displacement. The model in total gives too large displacements in this thesis. One should be careful when using this model on a multi-anchored wall, as the anchor forces might not be representative. The increased stiffness in MC( $E_{ur}$ ) gives more accurate results, hence an increased stiffness is preferable to be used in the MC model when the material undergoes unloading/reloading.

It is difficult finding the balance between increasing the strength and maintaining the desired stiffness situation in GS. Especially when LCC, or other effects that cause big deviance between the undrained shear strengths, is involved. As the installation of anchors pushes the wall into the slope, active and passive sides of the SPW may switch during the calculation phases. In GS, the roughness must be given a direction before running the analysis, and cannot be changed during the phases. The modeling in GS produces surprisingly good results compared to the measured values, as the program is simple in contrast to PLAXIS. Increasing the roughness number from 0 to 0.4 downwards and including partially modeled LCC gave the most accurate results. Modeling LCC on one side of a SPW is challenging in GS due to the stiffness mismatch.

Obtaining realistic anchor forces when calculating by hand is challenging in this thesis. The hand calculations are conducted with several simplifications, and do not include prestressing of anchors and stiffness of the wall, hence too low forces were obtained from hand calculations. In this project the prestress is so high that it pushes the SPW into the slope far from fully mobilized shear strength, and reaches a FoS of 1.71. The use of numerical models is an advantage when calculating a multi-anchored SPW in sloping terrain.

## Conclusion

In this thesis, NGI-ADP gave the best fit to the measured displacement of the SPW. It includes anisotropic shear strength behaviour, which often is the case for soft clays. All models are adjusted to a strength profile, at the expense of stiffness. This is especially true for HS which includes several stiffness parameters that does not change relatively to the strength. No oedometer tests were included, as fitting to both triaxial and oedometer test results is hard in practice. The sample quality of the triaxials used were ranging from poor to good quality and using higher quality samples could have given better results. HS seems capable to model the long-term effect after consolidation, but may have difficulties in reproducing both short term and long term conditions using one parameter set. The use of HSSs may be a better option in this thesis as the stiffness of small strains is greater and therefore generates less displacement in the excavation phases.

Modeling of LCC seems to give a good fit to the measured values, reducing bulging of the wall and gives accurate displacement along the SPW. The magnitude of LCC when modeling can be hard to decide. In this thesis, a partially reinforced soil in front of the SPW gave a good fit for NGI-ADP and MC with an unloading/reloading stiffness included. For HS, a fully reinforced soil gave good results. A possible solution to reduce the displacement into the slope could be the use of LCC behind the SPW.

Comparing simulated to measured anchor forces, NGI-ADP did not produce the most accurate results. The reason may come from the load cells being placed at a distance from the chosen cross section, with different layering and depth to bedrock behind the SPW. Still, all models seems to produce acceptable results, except for MC. This model is often chosen as a first analysis to a problem as it's quick to use, with few input parameters. Only one static stiffness is included which does not simulate real non-linear soil behavior when subjected to changes of stress or strain. In this thesis, MC gave too large displacement of the SPW and big difference between simulated and measured anchor forces. When calculating a multi-anchored wall one should be careful using MC as the anchor forces might not be corresponding to the measured values. An increased stiffness is preferable to be

used when the material undergoes unloading/reloading, which increases the accuracy of the model.

The modeling in GS produces surprisingly good results compared to both measured displacement and anchor forces, as the program is simple in contrast to PLAXIS. It is difficult finding the balance between increasing the strength and maintaining the desired stiffness situation in GS, especially when there is a big difference in  $S_u$  on each side of the SPW. Choosing appropriate roughness can be challenging when working with several layers since the roughness is defined on each side of the SPW, not each layer. The modeling in GS produces surprisingly good results compared to the measured values, as the program is simple in contrast to PLAXIS. Including partially modeled LCC gave the most accurate results.

Obtaining realistic anchor forces when calculating by hand is challenging for this project. With several simplifications, too low forces were obtained from hand calculations as prestressing of anchors and stiffness of the wall are not included. The use of numerical models is an advantage when calculating a multi-anchored SPW in sloping terrain.

### **Further work**

To further compare the measured data from Kværnerdammen with computational programs, modeling several profiles along the SPW would be of interest. Especially a profile that cuts through the placement of inclinometer 2 where the load cells measuring anchor forces are placed. Therefore, a calculation with PLAXIS 3D is an option for further work. The use of the HSSs model is recommended for testing, as the small strain stiffness might increase the accuracy. Also, more field and laboratory work would be ideal.



# Bibliography

- Briaud, J. L., 2001. Introduction to soil moduli. *Geotechnical News* 19 (2), 54–58.
- Brinkgreve, R. B. J., Kumerswamy, S., Swolfs, W. M., 2017a. PLAXIS 2D 2017 - Material Models Manual.
- Brinkgreve, R. B. J., Kumerswamy, S., Swolfs, W. M., 2017b. PLAXIS 2D 2017 - Reference Manual.
- Flaate, K. S., 1966. Stresses and movements in connection with braced cuts in sand and clay. Ph.D. thesis.
- Georåd, L., 2008. Geoteknisk rapport 08-135 enebakkveien 71, grunnundersøkelse. Om-sorgsbygg Oslo KF Enebakkveien 71 1.
- Gouw Dr, T.-L., 01 2014. Common mistakes on the application of plaxis 2d in analyzing excavation problems 9, 8291–8311.
- Grimstad, G., Andresen, L., Jostad, H. P., 2012. Ngi-adp: Anisotropic shear strength model for clay. *International Journal for Numerical and Analytical Methods in Geomechanics* 36 (4), 483–497.
- Isachsen, M., 2012. Effekt av anisotropi på udrenert skjærstyrke i naturlige skråninger. Master's thesis, Institutt for bygg, anlegg og transport, NTNU.
- Jalali, M. M., Golmaei, S. H., Jalali, M. R., Borthwick, A., Ahmadi, M. K. Z., Moradi, R., 2012. Using finite element method for pile-soil interface (through plaxis and ansys). Vol. 3. *Academic Journals*, pp. 256–272.
- Janbu, N., Emdal, A., Grande, L., Nordal, S., 2016. Tba5100 theoretical soil mechanics. Geotechnical Division, NTNU, Trondheim.
- Johansson, E., Sandeman, E., 2014. Modelling of a deep excavation in soft clay a comparison of different calculation methods to in-situ measurements. Master's thesis.

- 
- Kempfert, H., Reul, O., Gebreselassie, B., 2006. Excavations and Foundations in Soft Soils. Springer Science & Business Media.  
URL <https://link.springer.com/book/10.1007%2F3-540-32895-5>
- Kullingsjø, A., 2009. Effects of deep excavations in soft clay on the immediate surroundings. Vol. 3. pp. 1923–1930.
- Lacasse, S., Jostad, H. P., L’Heureux, J.-S., Torgersrud, Ø., Sandven, R. B., 2016. Geosuite—a modular system for geotechnical design. In: Proceedings of the 17th Nordic Geotechnical Meeting.
- Likitlersuang, S., Teachavorasinskun, S., Surarak, C., Oh, E., Balasubramaniam, A., 2013. Small strain stiffness and stiffness degradation curve of bangkok clays. Soils and Foundations 53 (4), 498–509.
- MulticonsultASA, 2017a. 128517-1-rig-not-006a-rev01 beregningsnotat plaxis-input. Kværnerdammen, F1 1.
- MulticonsultASA, 2017b. 128517-1-rig-not-008-rev01 etablering av byggegrop. Kværnerdammen, F1 1.
- MulticonsultASA, 2017c. 128517-1-rig-not-009-rev01 grunnforsterkning. Kværnerdammen, F1 1.
- MulticonsultASA, 2017d. 128517-1-rig-not-010-rev001 overvåkning, oppfølging og kontrollplan. Kværnerdammen F1 1.
- MulticonsultASA, 2017e. 128517-1-rig-rap-001-rev03 geoteknisk grunnundersøkelse, datarapport. Kværnerdammen, F1 3.
- MulticonsultASA, 2017f. 128517-1-rig-teg-502-rev01 spuntoppriss mot gang og sykkelvei. Kværnerdammen, F1 1.
- MulticonsultASA, 2017g. 129000-rig-rap-001-rev001 geoteknisk datarapport, enebakkveien 69. Enebakkveien 69 AS 2.
- NGI, 2009. 20091259-00-22-rev03 enebakkveien 71, kvikkleirekartlegging og stabilitetsberegning. Enebakkveien 71 3.
- Nordal, S., 2017a. Determination of soil stiffness parameters clay. Lecture in TBA4116 Geotechnical Engineering - Advanced Course, Geotechnical Division, NTNU, Trondheim.
- Nordal, S., 2017b. On fem in geotechnical engineering. Lecture in TBA4116 Geotechnical Engineering - Advanced Course, Geotechnical Division, NTNU, Trondheim.
- Nordal, S., 2017c. Tba4116 geotechnical engineering ac. Lecture in TBA4116 Geotechnical Engineering - Advanced Course, Geotechnical Division, NTNU, Trondheim.
- Nordal, S., 2017d. Tba4116 geotechnical engineering, advanced course. Geotechnical Division, NTNU, Trondheim.

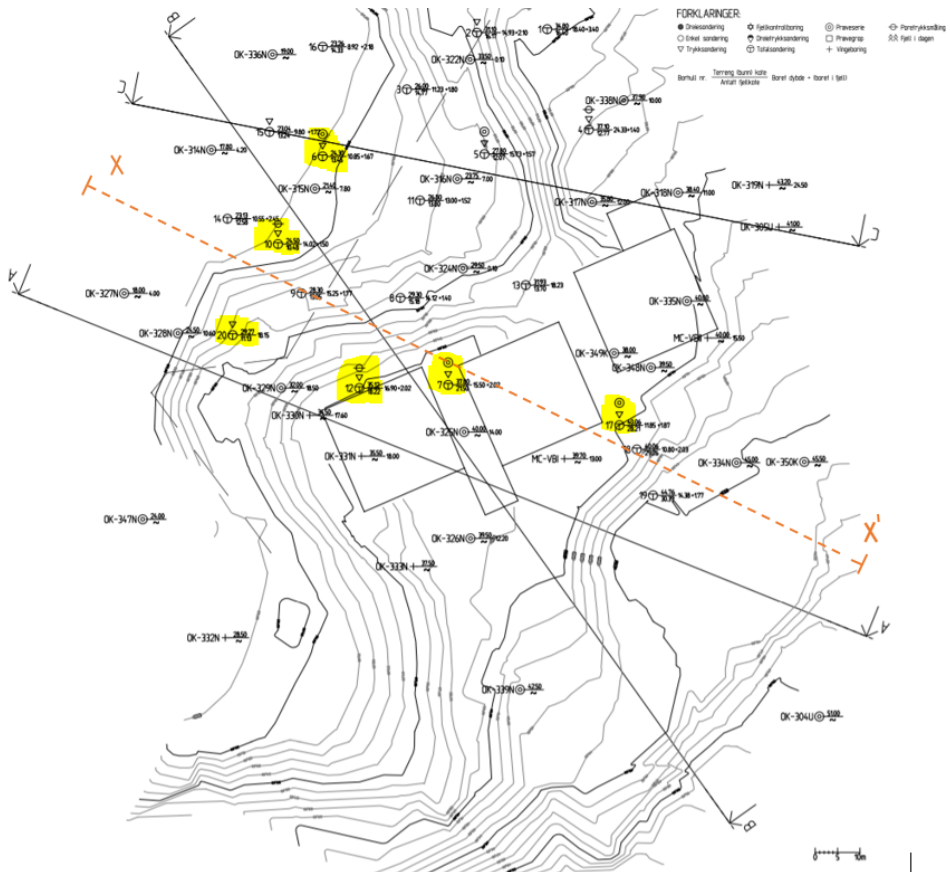
- 
- Nurmohamed, N., Sluimer, E., Brand, P., 1997. Plaxis bulletin nr. 4.  
URL <https://www.plaxis.com/content/uploads/2016/10/Plaxis-Bulletin-04.pdf>
- Rambøll, 2009. 6090146-rev01 supplerende grunnundersøkelser datarapport, enebakkveien 71. Enebakkveien 71 1.
- Schanz, T., Vermeer, P. A., Bonnier, P. G., 1999. The hardening soil model: formulation and verification. *Beyond 2000 in computational geotechnics*, 281–296.
- Surarak, C., Likitlersuang, S., Wanatowski, D., Balasubramaniam, A., Oh, E., Guan, H., 2012. Stiffness and strength parameters for hardening soil model of soft and stiff bangkok clays. *Soils and Foundations* 52 (4), 682 – 697.  
URL <http://www.sciencedirect.com/science/article/pii/S0038080612000790>
- Thakur, V., Oset, F., Viklund, M., Strand, S. A., Gjeskiv, V., Christensen, S., Fauskerud, O. A., 2014. En omforent anbefaling for bruk av anisotropifaktorer i prosjektering i norske leirer. NVE, SV, JERNBANEVERKET (ed.) Naturfareprosjektet Dp 6.
- Ukritchon, B., Boonyatee, T., 2015. Soil parameter optimization of the ngi-adp constitutive model for bangkok soft clay. *Geotechnical Engineering Journal of the SEAGS & AGSSEA* 46 (1), 28–36.
- Vernang, T., Heyerdahl, H., Cepeda, J., Kalsnes, B., 2011. Fare- og risikokartlegging av kvikkleireområder, oslo kommune. Tech. rep.  
URL <http://webfileservice.nve.no/API/PublishedFiles/Download/201600907/1866567>
- Vianova Geosuite, A., 2009. Theory and Reference Manual for GS Supported Excavation calculation engine version 2.



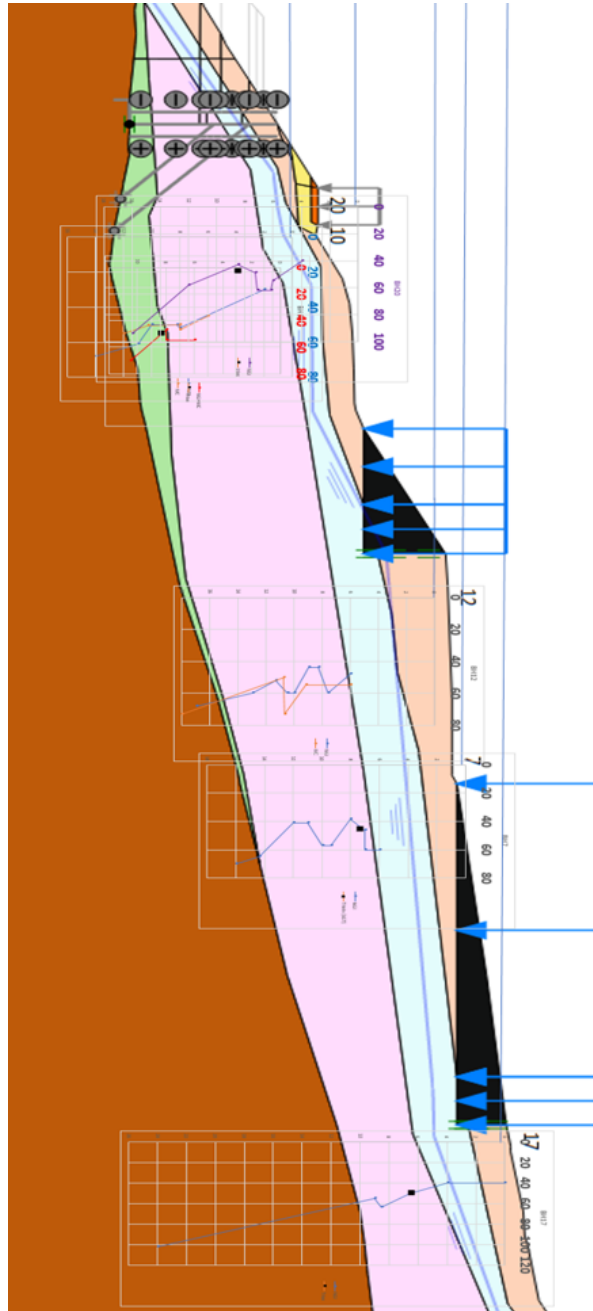
Appendix **A**

Collection of site information and  
initial material models

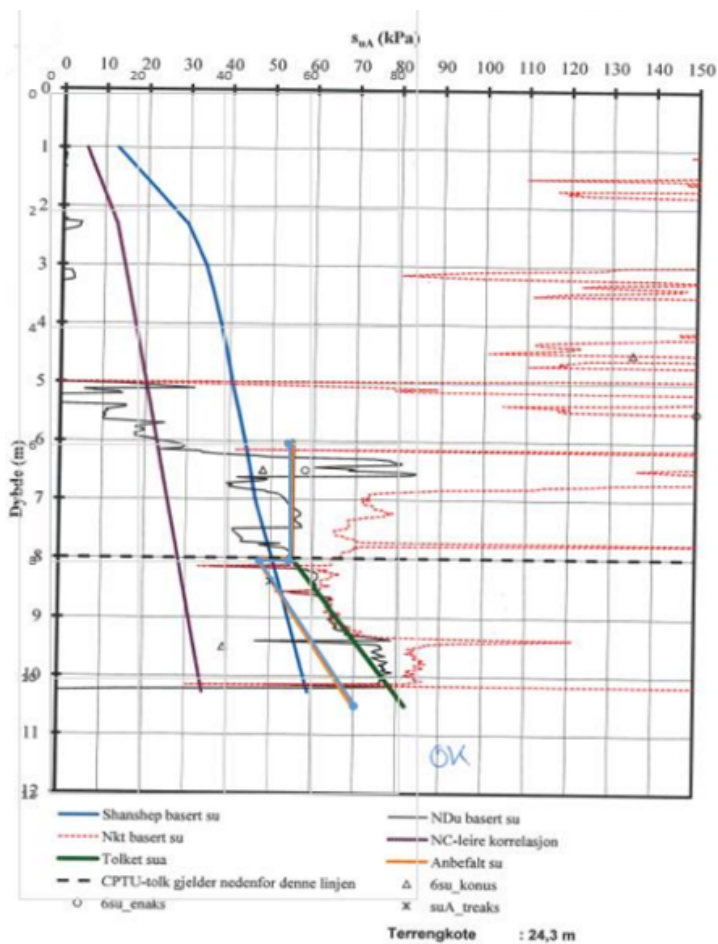
# A.1 Map of terrain to the east of construction site with profiles and boreholes marked in yellow colour (NGI, 2009)



## A.2 Strength profile for profile X-X'

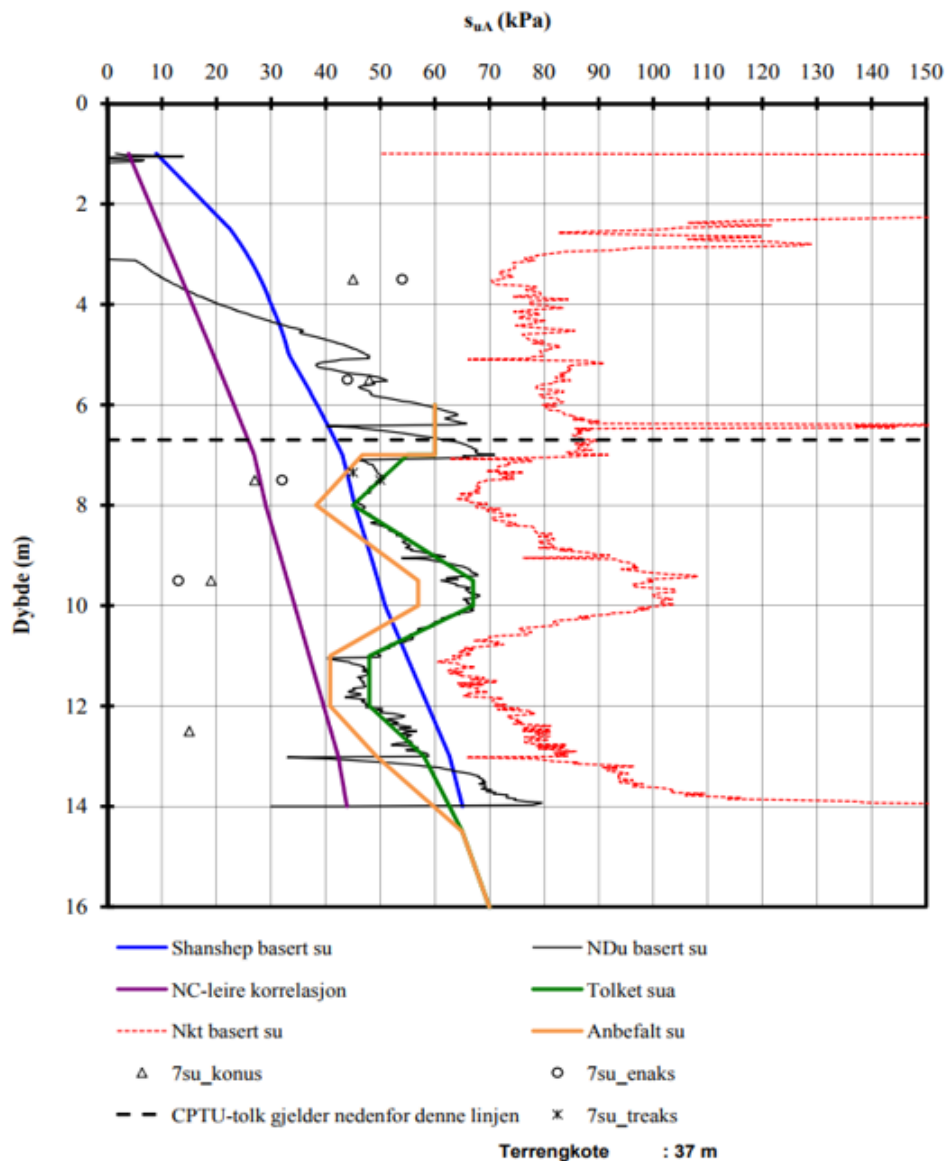


### A.3 Borehole6. CPTu interpretation by Multiconsult based on NGI's earlier analysis (MulticonsultASA, 2017a)

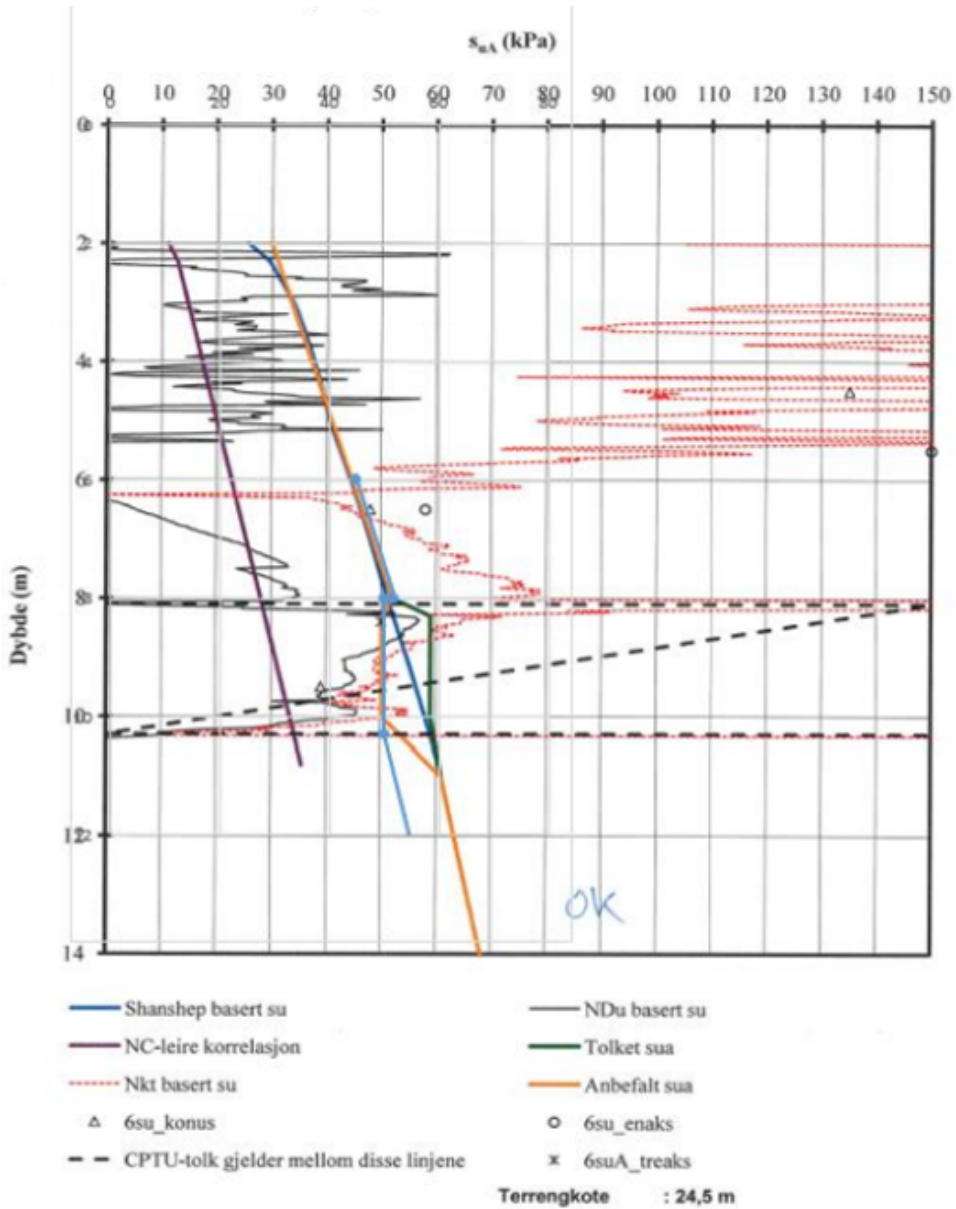




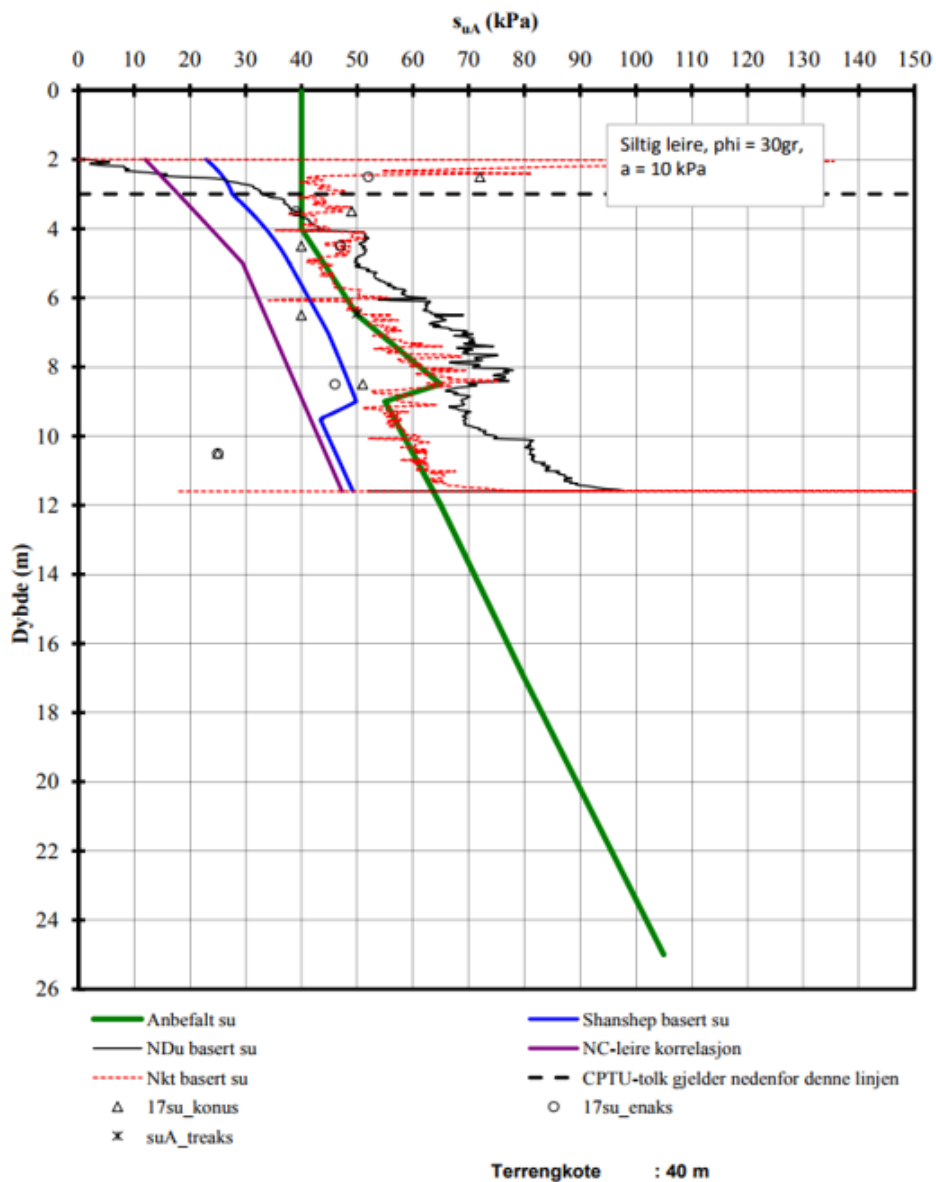
## A.4 Borehole7. CPTu interpretation by NGI (NGI, 2009)



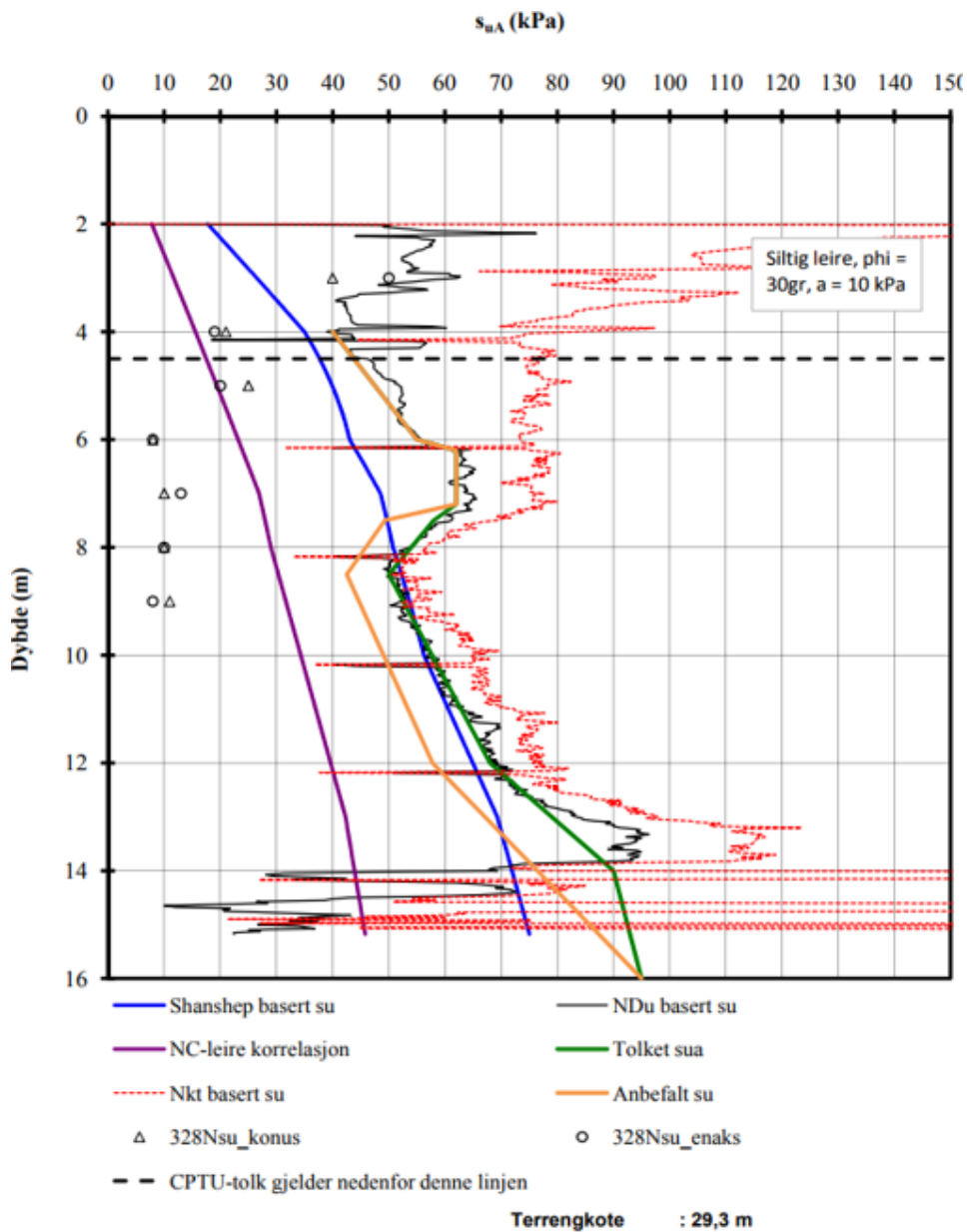
## A.5 Borehole10. CPTu interpretation by Multiconsult based on NGI's earlier analysis (MulticonsultASA, 2017a)



## A.6 Borehole17. CPTu interpretation by NGI (NGI, 2009)

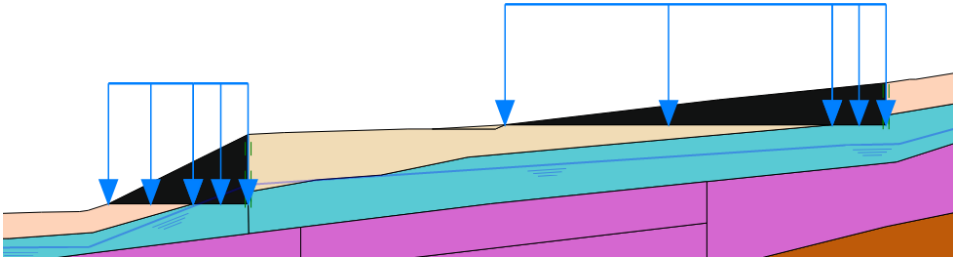


## A.7 Borehole20. CPTu interpretation by NGI (NGI, 2009)

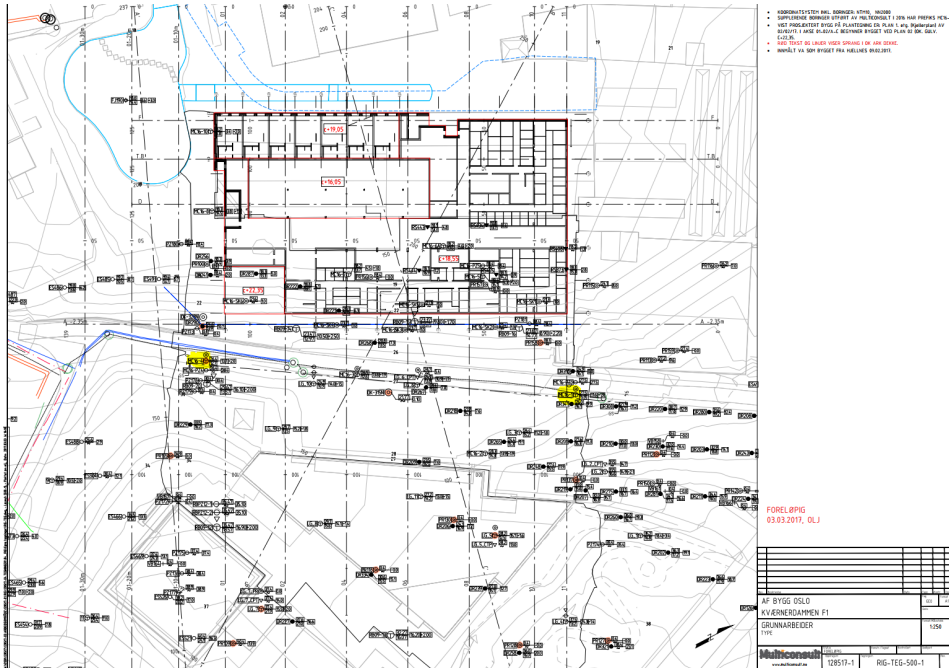


---

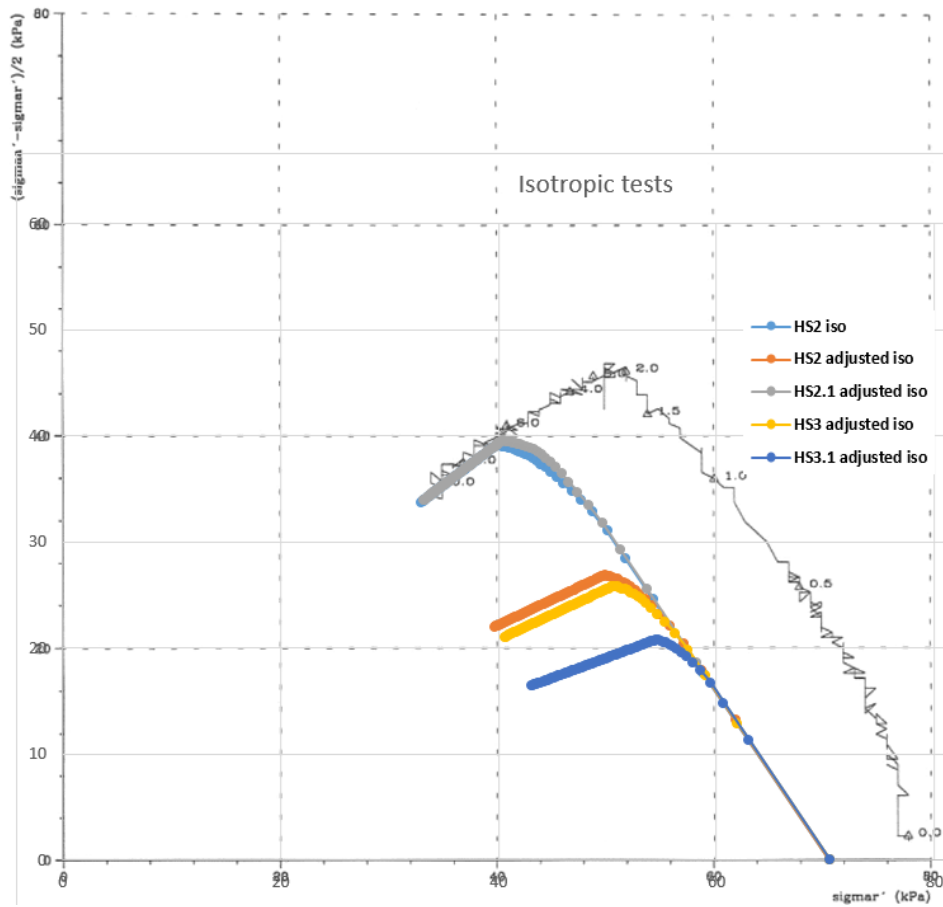
## A.8 Modelling of loads coming from the kindergarten and parking garage in PLAXIS

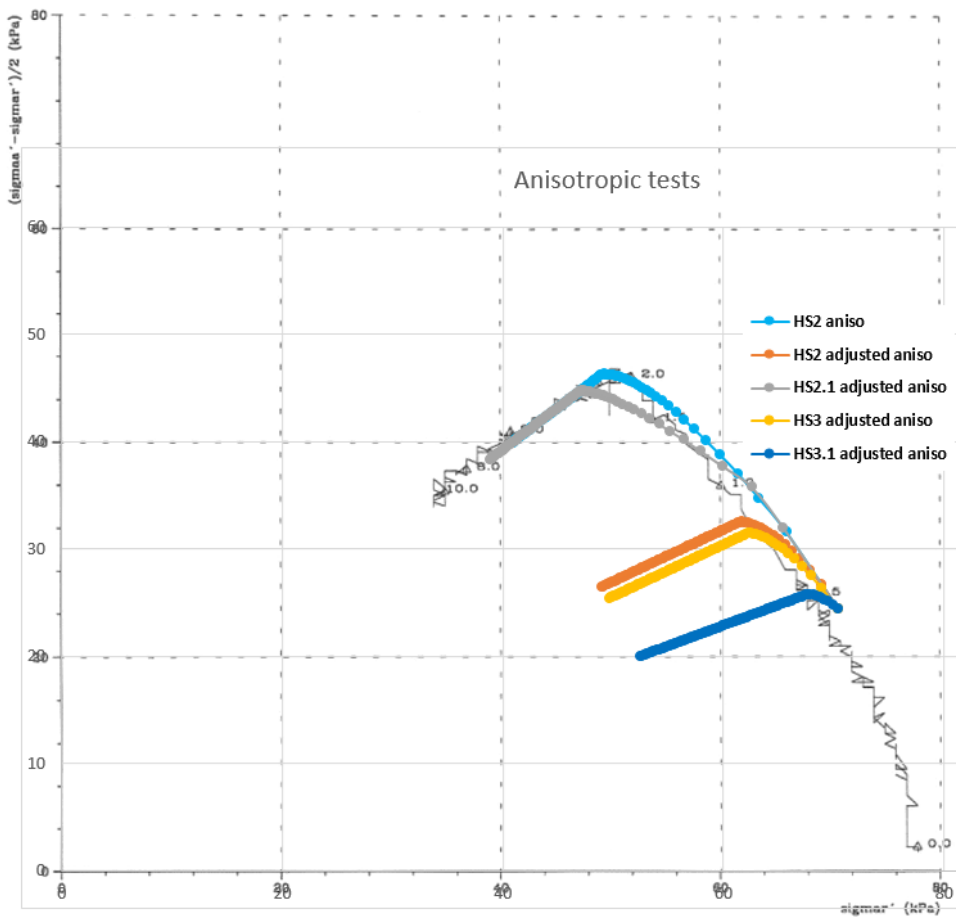


## A.9 Map with location of boreholes MC1(right) and MC4(left) marked with yellow colour (MulticonsultASA, 2017a)



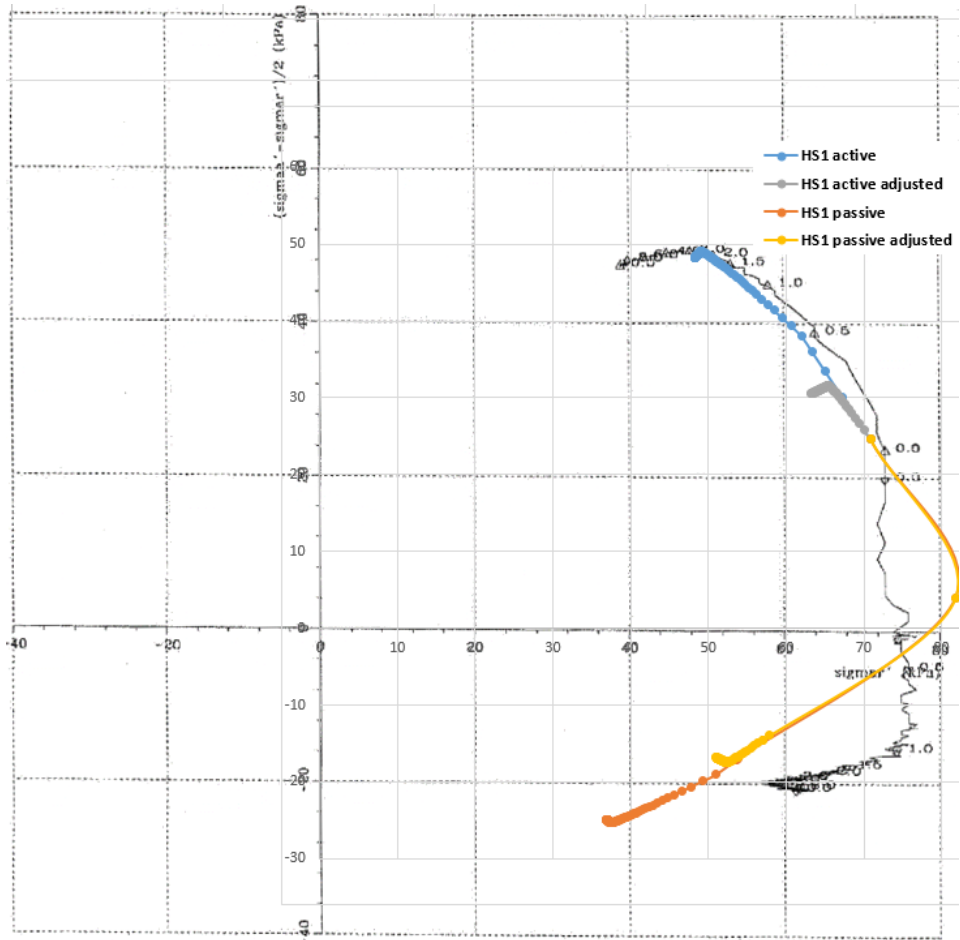
## A.10 BH7, fitting of soil test to actual triaxial isotropic and anisotropic test results, and adjusted with new parameters



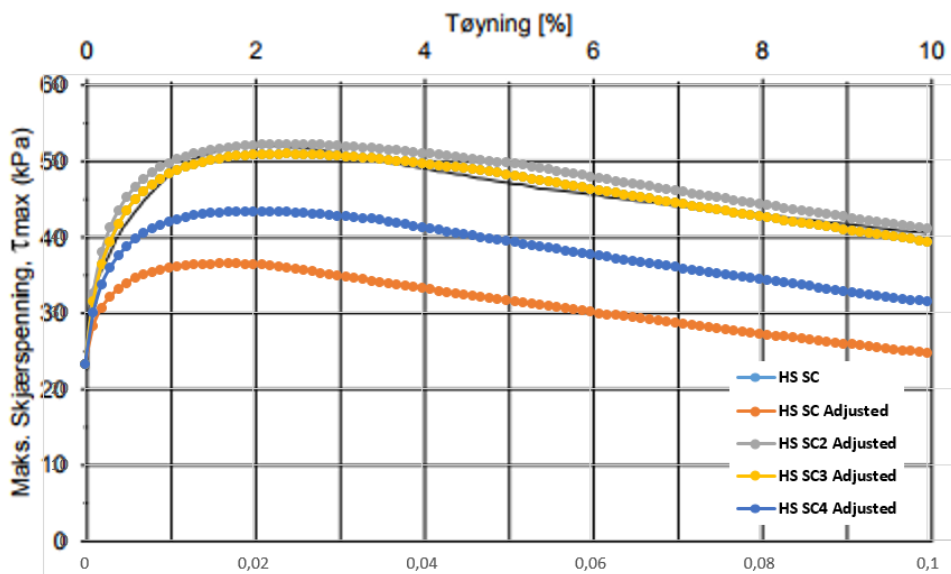


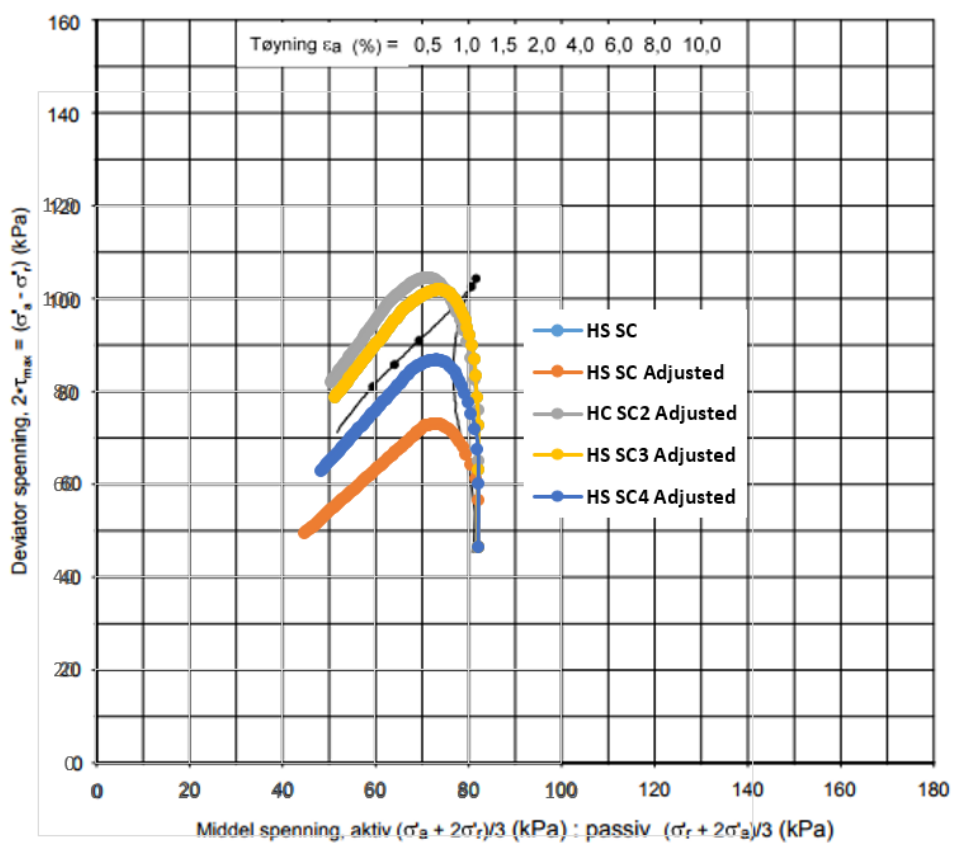


## A.11 BH17, fitting of soil test to actual triaxial anisotropic test results, and adjusted with new parameters - Stress path



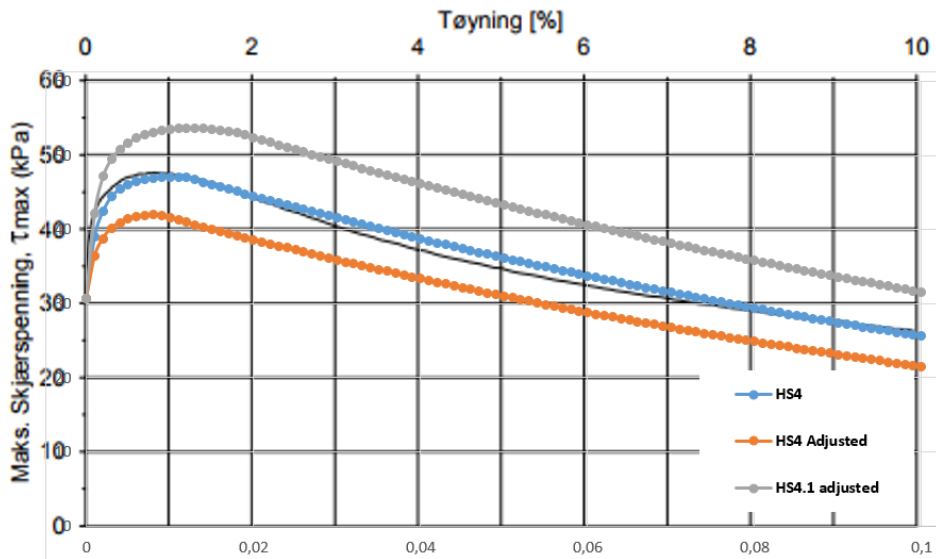
## A.12 Multiconsult' MC'1 , fitting of soil test to actual triaxial anisotropic test results

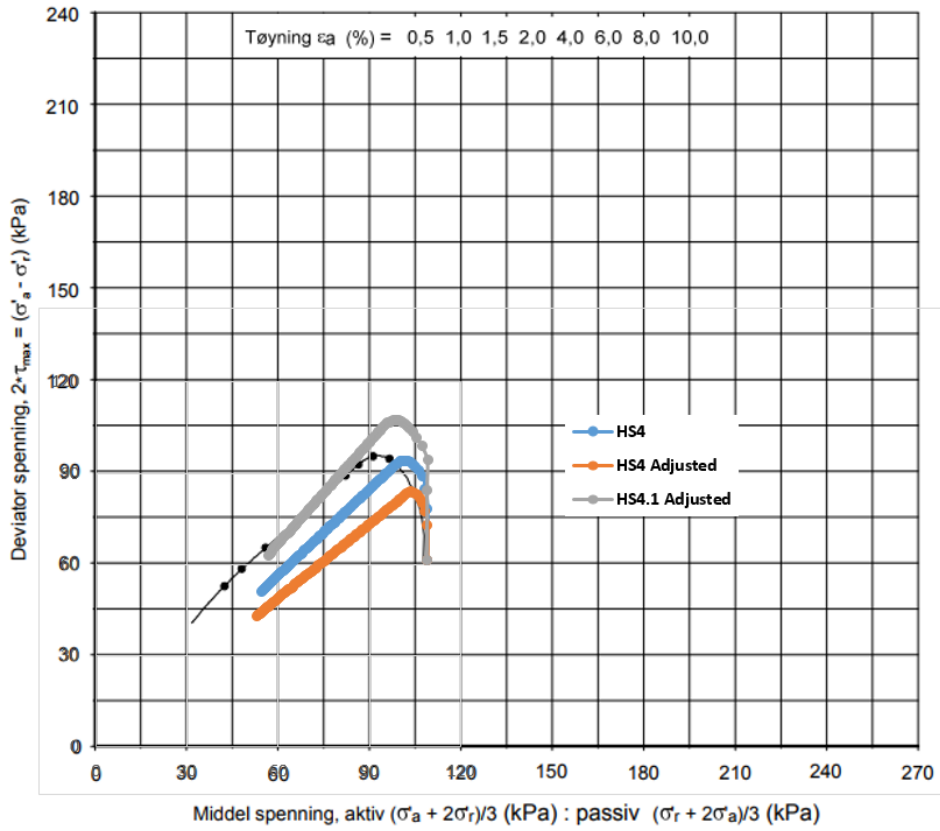




---

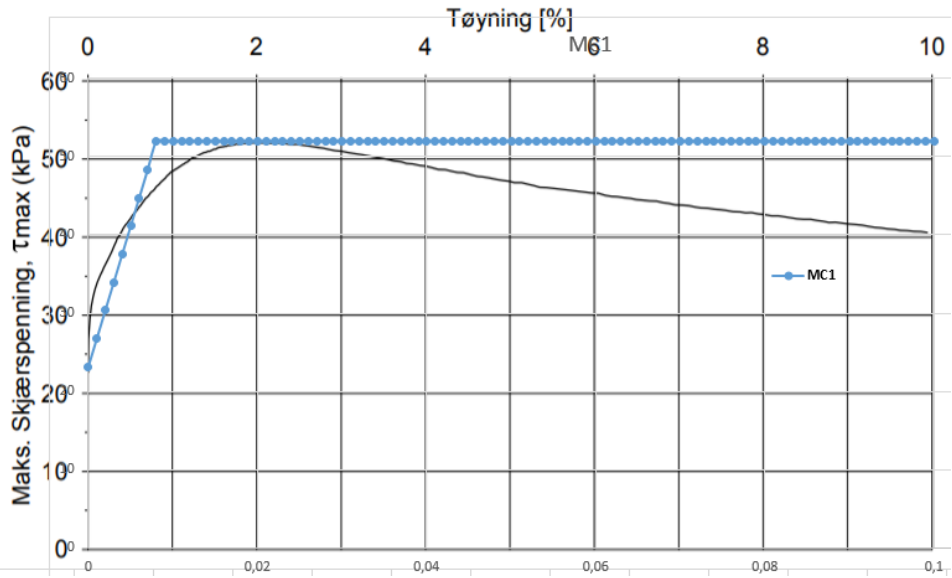
### A.13 Multiconsult MC'4 , fitting of soil test to actual triaxial anisotropic test results





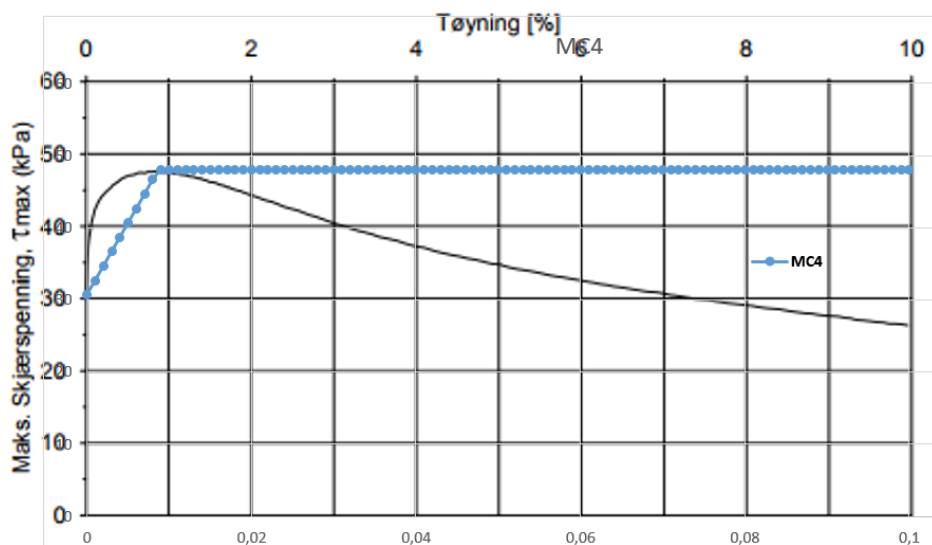
---

## A.14 MC model, fitting of soil test to actual triaxial anisotropic test results for silty clay (MC'1)- Stress path



---

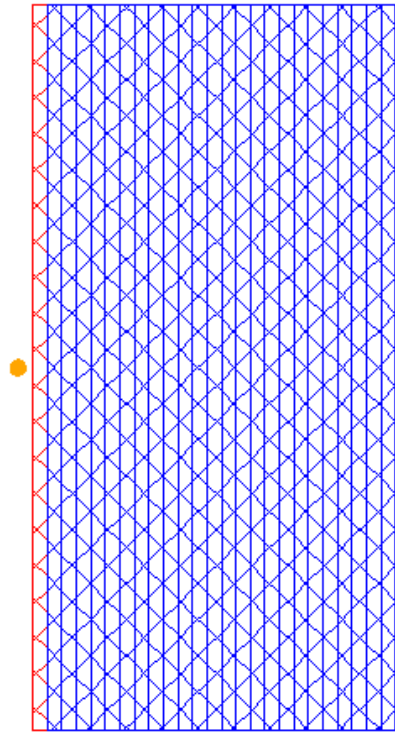
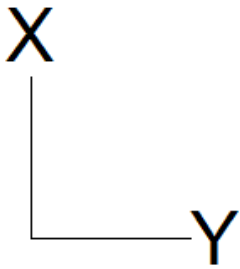
## A.15 MC model, fitting of soil test to actual triaxial anisotropic test results for quick clay (MC'4) - Stress path



## A.16 Load definition and placement for GS settlement

No	Reference depth [m]	Load pressure [kPa]	Stress distribution model	Lower left X [m]	Upper right X [m]	Lower left Y [m]	Upper right Y [m]		Load history
▶ 1	0,00	6,50	Finite Boussinesq	-25,000	25,000	1,000	2,000	NA	+
2	0,00	13,00	Finite Boussinesq	-25,000	25,000	2,000	3,000	NA	+
3	0,00	19,50	Finite Boussinesq	-25,000	25,000	3,000	4,000	NA	+
4	0,00	26,00	Finite Boussinesq	-25,000	25,000	4,000	5,000	NA	+
5	0,00	32,50	Finite Boussinesq	-25,000	25,000	5,000	6,000	NA	+
6	0,00	39,00	Finite Boussinesq	-25,000	25,000	6,000	7,000	NA	+
7	0,00	45,50	Finite Boussinesq	-25,000	25,000	7,000	8,000	NA	+
8	0,00	52,00	Finite Boussinesq	-25,000	25,000	8,000	9,000	NA	+
9	0,00	58,50	Finite Boussinesq	-25,000	25,000	9,000	10,000	NA	+
10	0,00	65,00	Finite Boussinesq	-25,000	25,000	10,000	11,000	NA	+
11	0,00	71,50	Finite Boussinesq	-25,000	25,000	11,000	12,000	NA	+
12	0,00	78,00	Finite Boussinesq	-25,000	25,000	12,000	13,000	NA	+
13	0,00	84,50	Finite Boussinesq	-25,000	25,000	13,000	14,000	NA	+
14	0,00	91,00	Finite Boussinesq	-25,000	25,000	14,000	15,000	NA	+
15	0,00	97,50	Finite Boussinesq	-25,000	25,000	15,000	16,000	NA	+
16	0,00	104,00	Finite Boussinesq	-25,000	25,000	16,000	17,000	NA	+
17	0,00	110,50	Finite Boussinesq	-25,000	25,000	17,000	18,000	NA	+
18	0,00	117,00	Finite Boussinesq	-25,000	25,000	18,000	19,000	NA	+
19	0,00	123,50	Finite Boussinesq	-25,000	25,000	19,000	20,000	NA	+
20	0,00	130,00	Finite Boussinesq	-25,000	25,000	20,000	21,000	NA	+
21	0,00	136,50	Finite Boussinesq	-25,000	25,000	21,000	22,000	NA	+
22	0,00	143,00	Finite Boussinesq	-25,000	25,000	22,000	23,000	NA	+
23	0,00	149,50	Finite Boussinesq	-25,000	25,000	23,000	24,000	NA	+
24	0,00	156,00	Finite Boussinesq	-25,000	25,000	24,000	25,000	NA	+
25	0,00	162,50	Finite Boussinesq	-25,000	25,000	25,000	26,000	NA	+





---

## A.17 Testing impact of distance on the wall in GS Settlement

Loads										
No	Reference depth [m]	Load pressure [kPa]	Stress distribution model	Lower left X [m]	Upper right X [m]	Lower left Y [m]	Upper right Y [m]			Load history
▶ 1	0,00	169,00	Finite Boussinesq	-25,000	25,000	26,000	27,000		NA	+



---

**A.18 Laser measurements of top vertex shown in mm,  
done by Multiconsult**

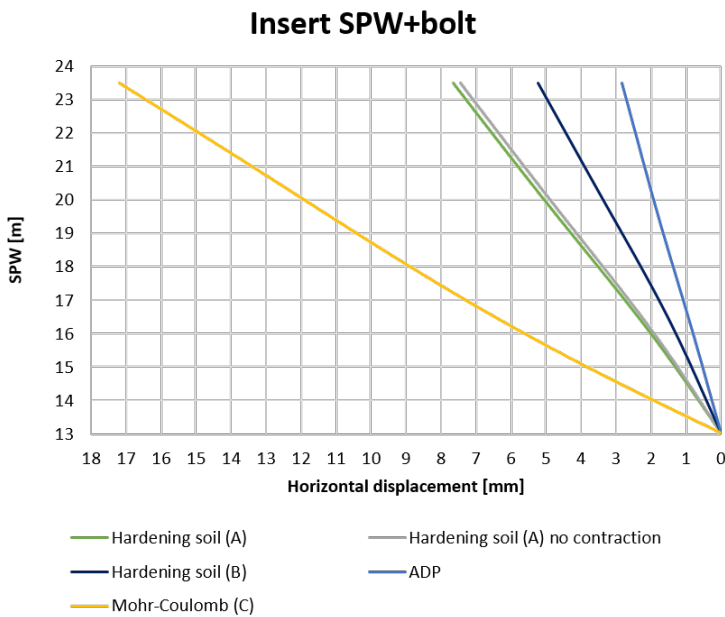
Green = installation top row of anchors	Yellow = excavating to contour +18.5	Red = excavating to contour +18
Inclinometer 3	Inclinometer 2	Inclinometer 1
0	0	0
-19	-58	1.5
-19	-60	1.5
0	-61	1.5
-1.5	-63	1.5
-5	-66	-18.5
-6	-66	-20
-5	-66	-21
-5	-65	-22
-5	-67	-28
-5	-67	-29



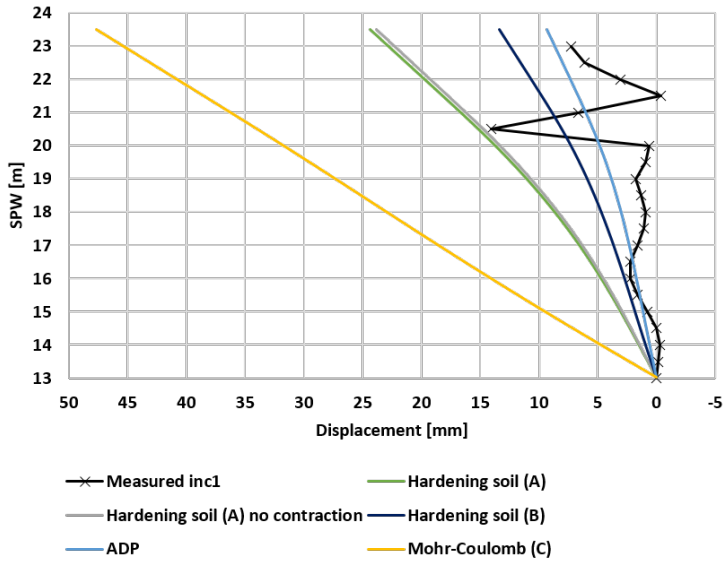
# Appendix B

## PLAXIS initial model with $R_{inter} = 0.1$ results

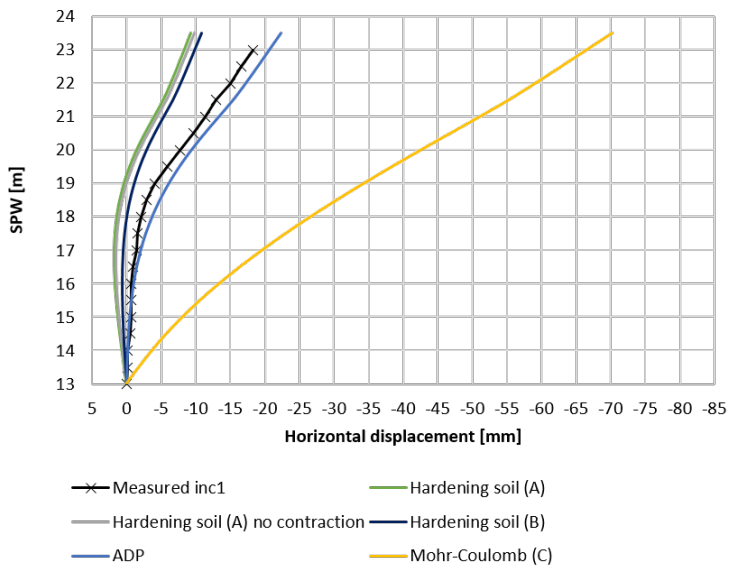
### B.1 Displacement of SPW with $R_{inter} = 0.1$ in PLAXIS



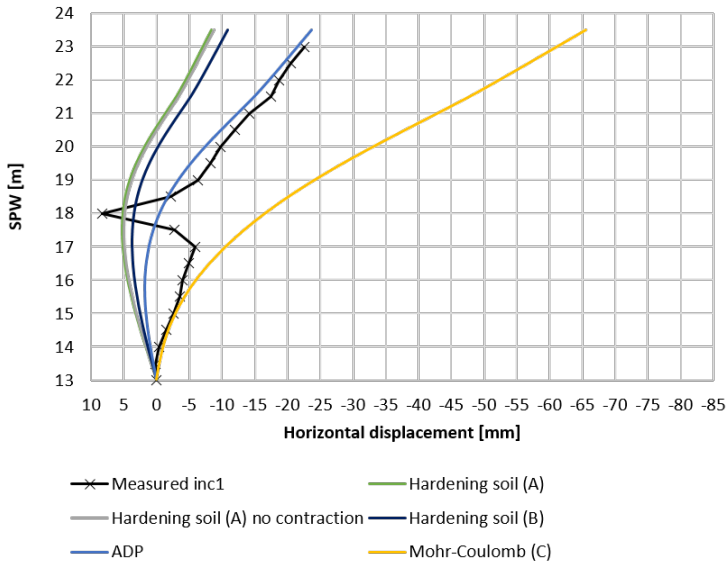
### Excavation +21



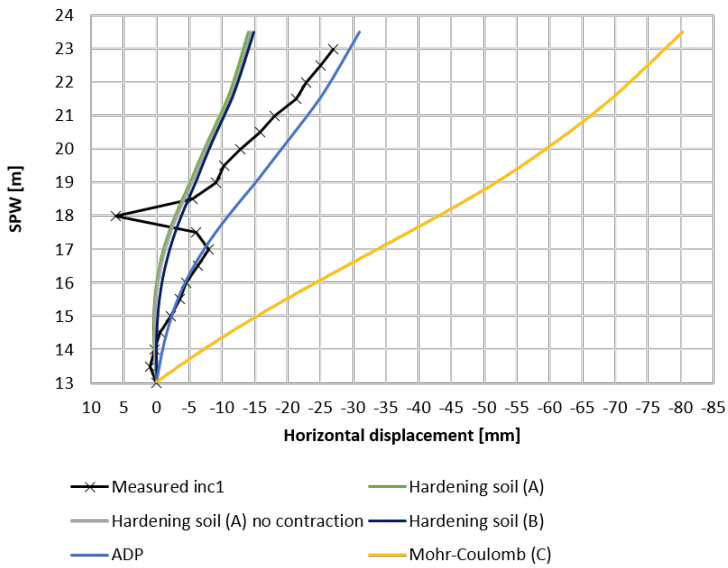
### Installation top anchor row



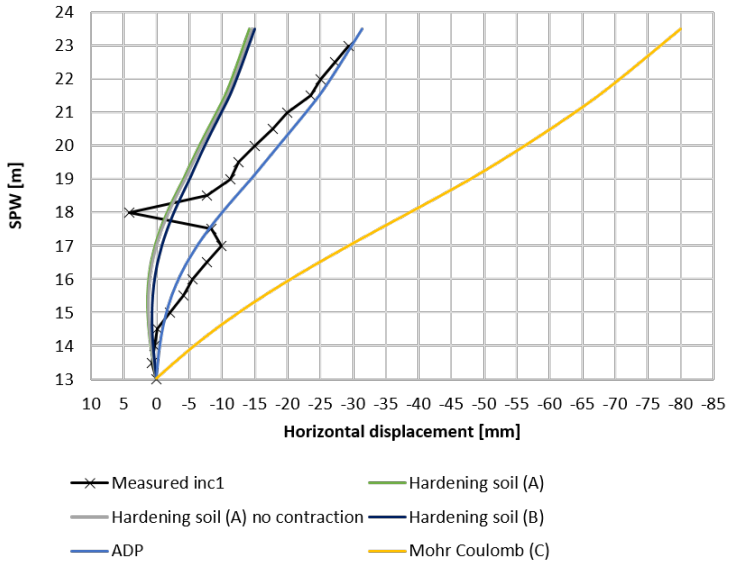
### Excavation +18.5



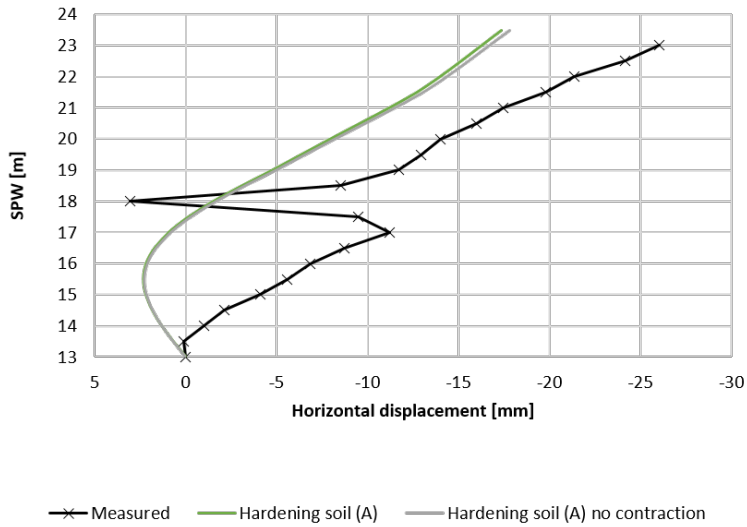
### Installation bottom anchor row



### Excavation +18



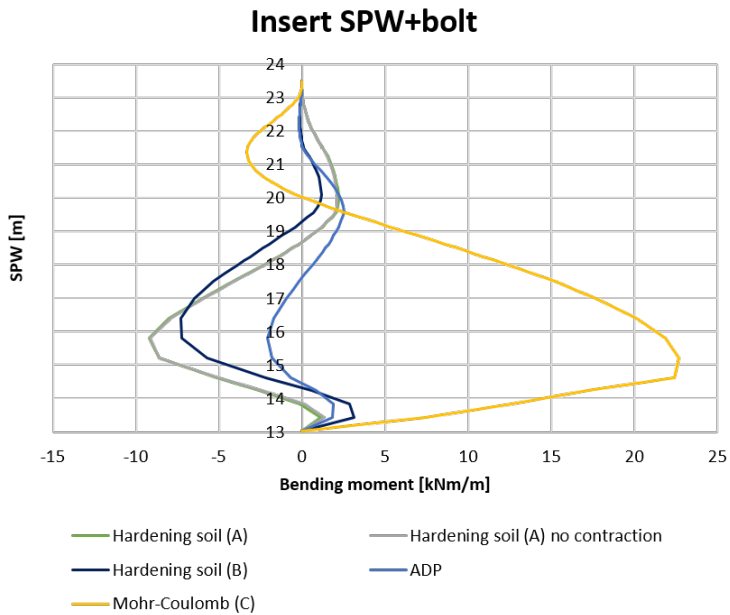
### Consolidation



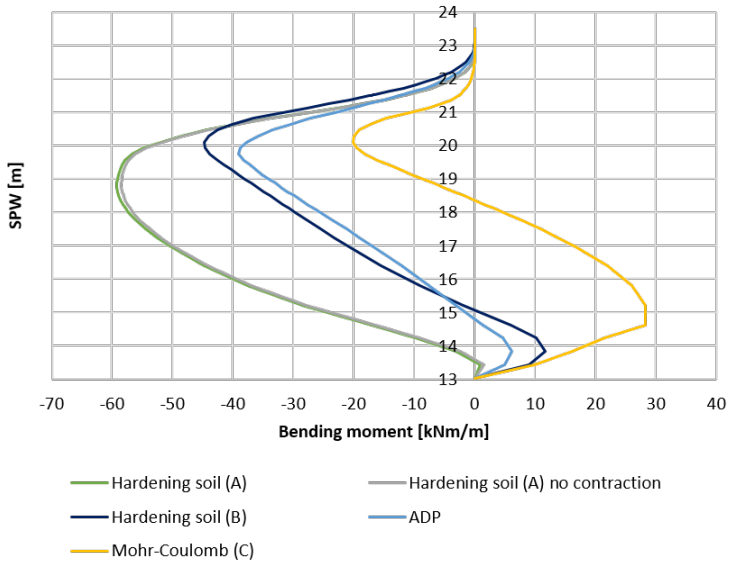


---

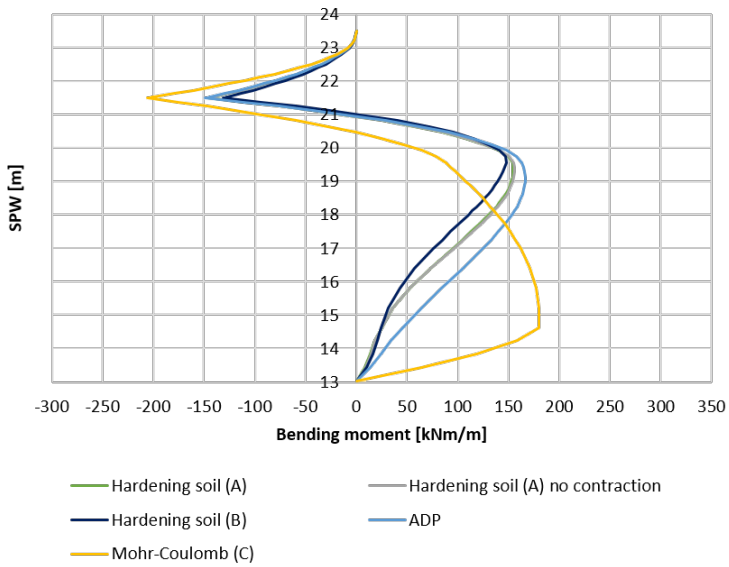
## B.2 Bending moment of SPW with $R_{inter} = 0.1$ in PLAXIS



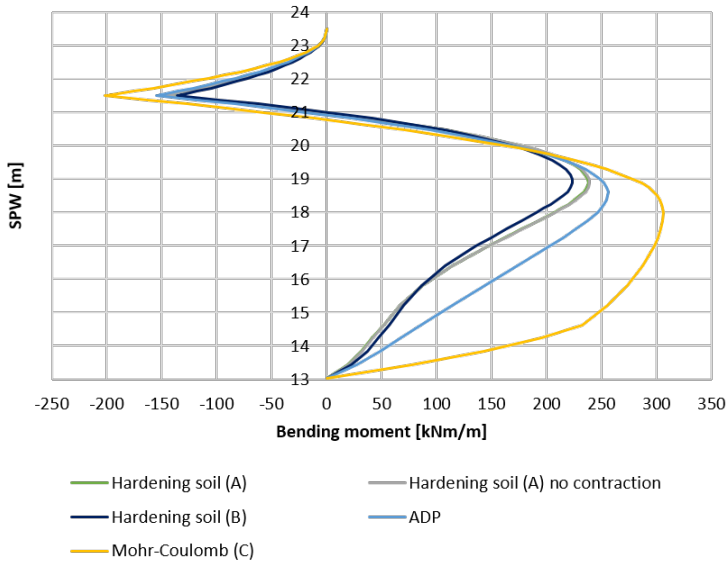
### Excavation +21



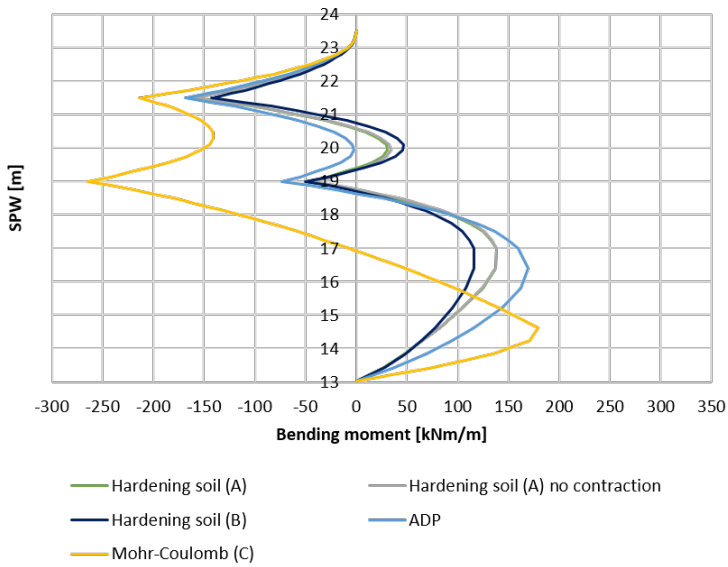
### Installation top anchor row



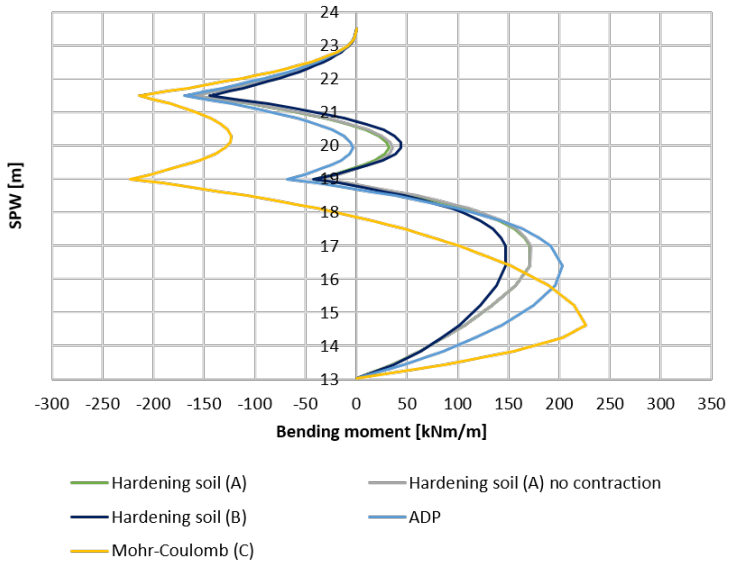
### Excavation +18.5



### Installation bottom anchor row

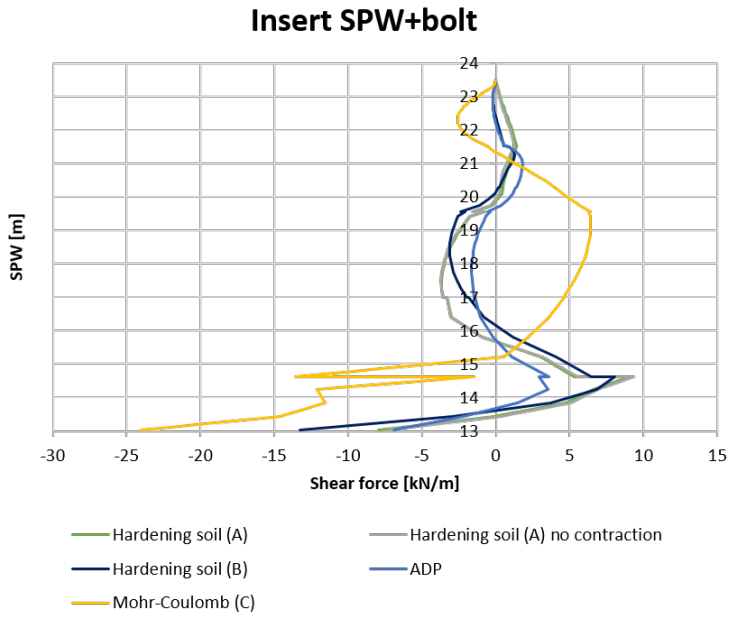


### Excavation +18

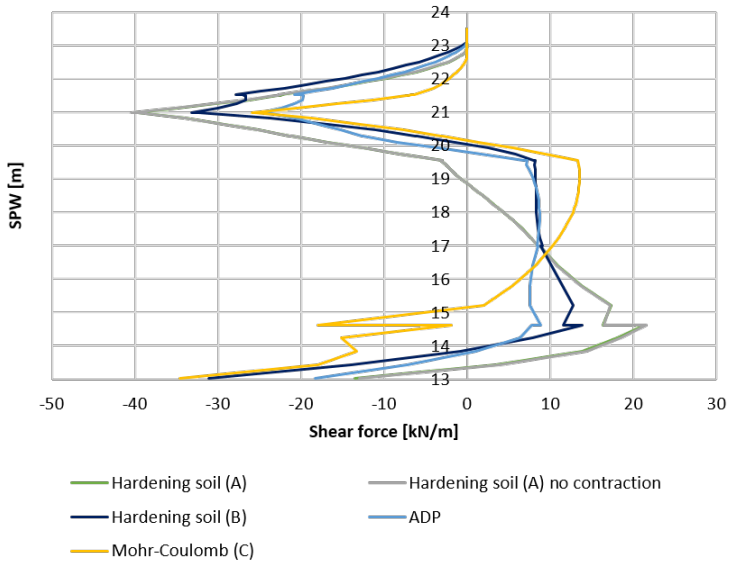


---

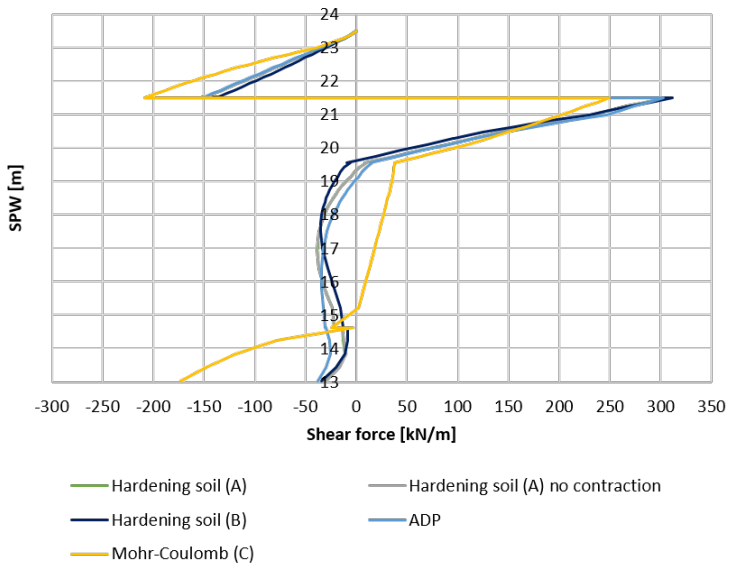
### B.3 Shear force of SPW with $R_{inter} = 0.1$ in PLAXIS



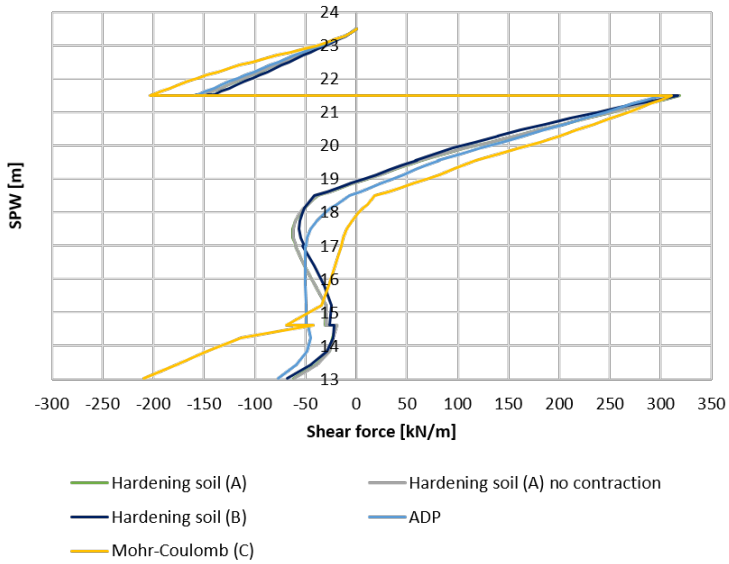
### Excavation +21



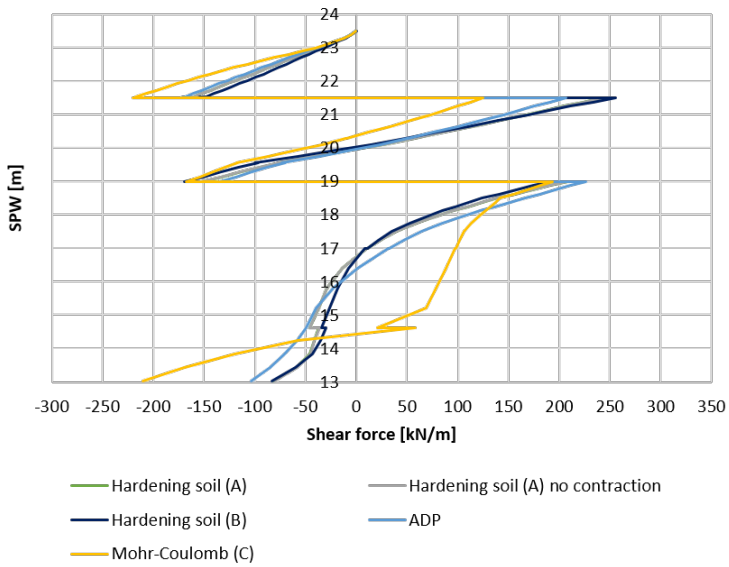
### Installation top anchor row



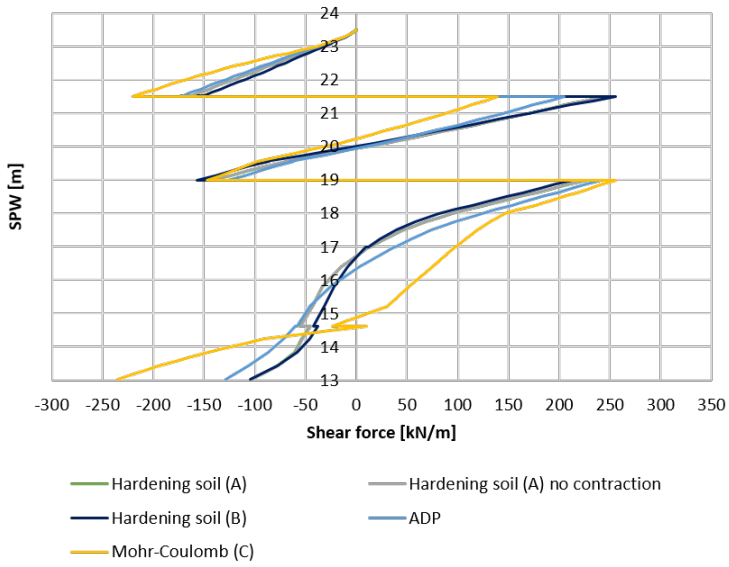
### Excavation +18.5



### Installation bottom anchor row



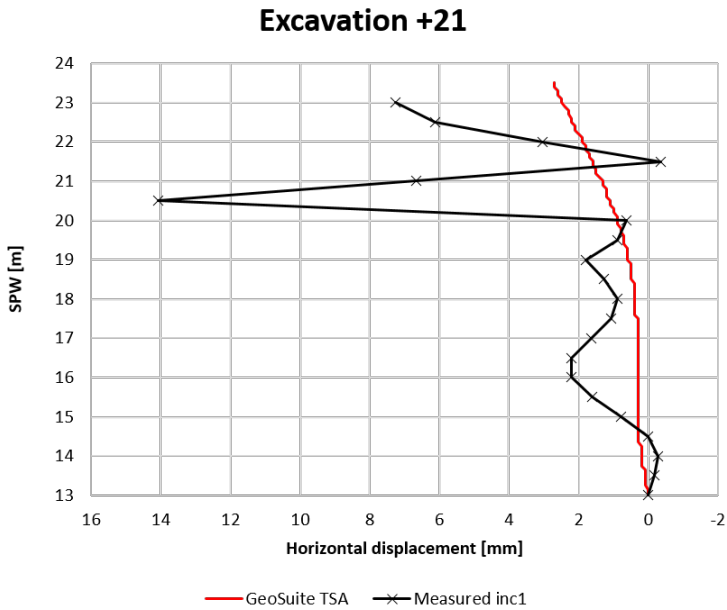
## Excavation +18



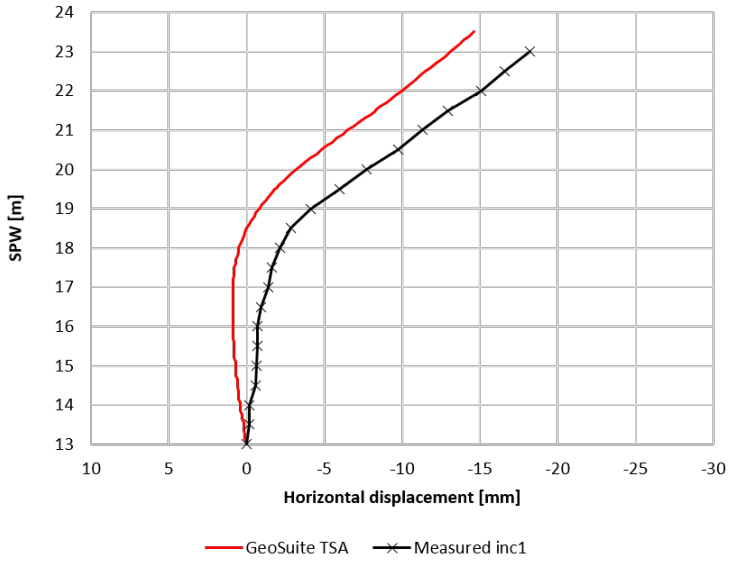


## GS initial model with $r = 0$ results

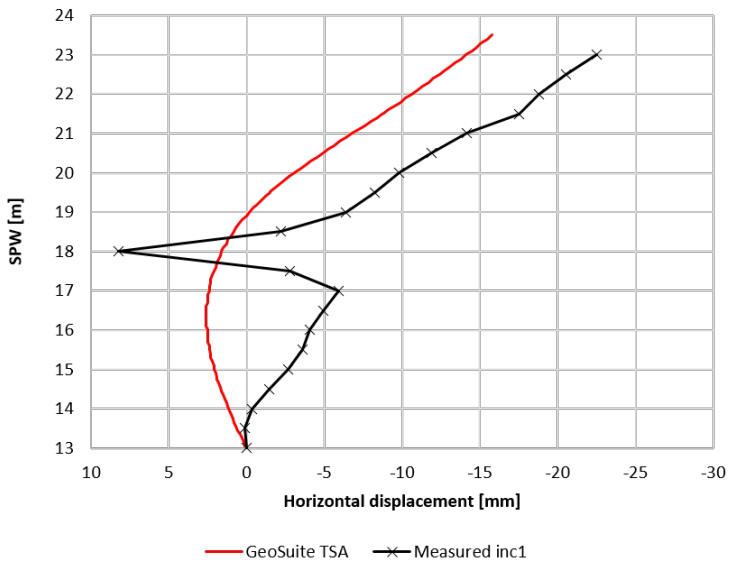
### C.1 Displacement of SPW with $r = 0$ in GS Excavation



### Installation top anchor row

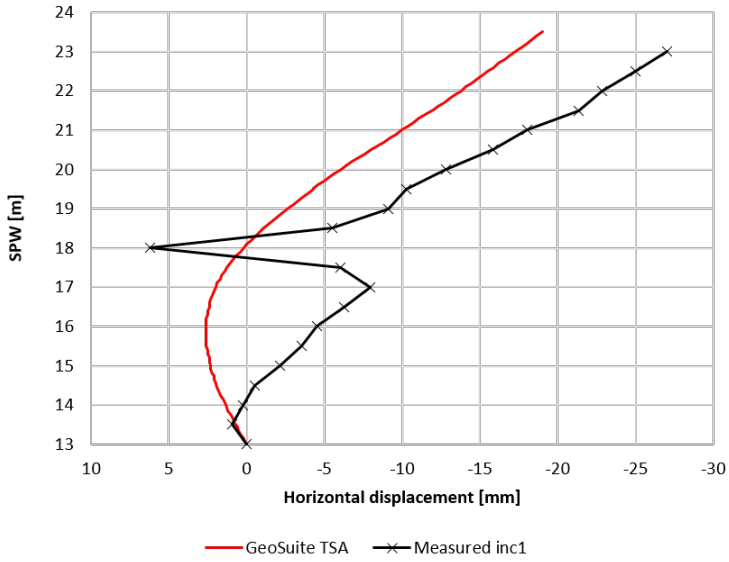


### Excavation +18.5



---

### Installation bottom anchor row

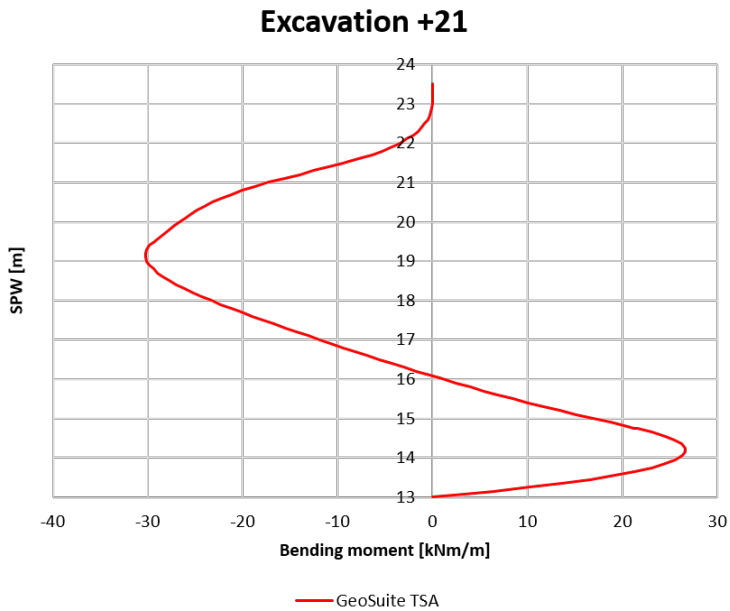


### Excavation +18



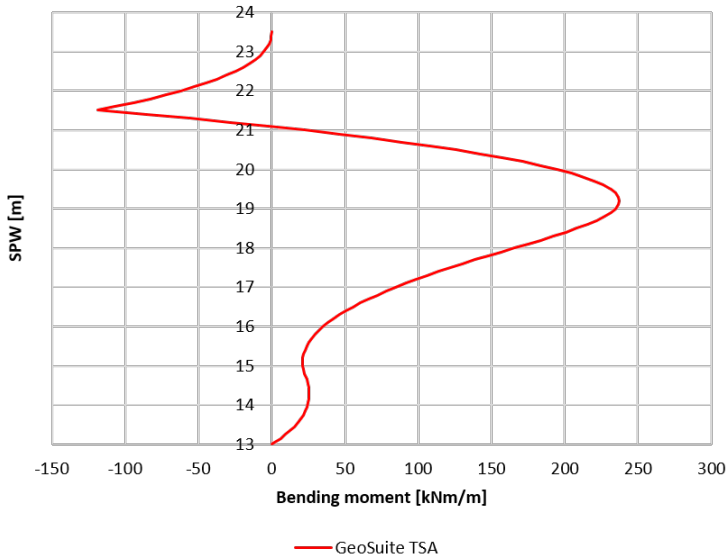
---

## C.2 Bending moment of SPW with $r = 0$ in GS Excavation

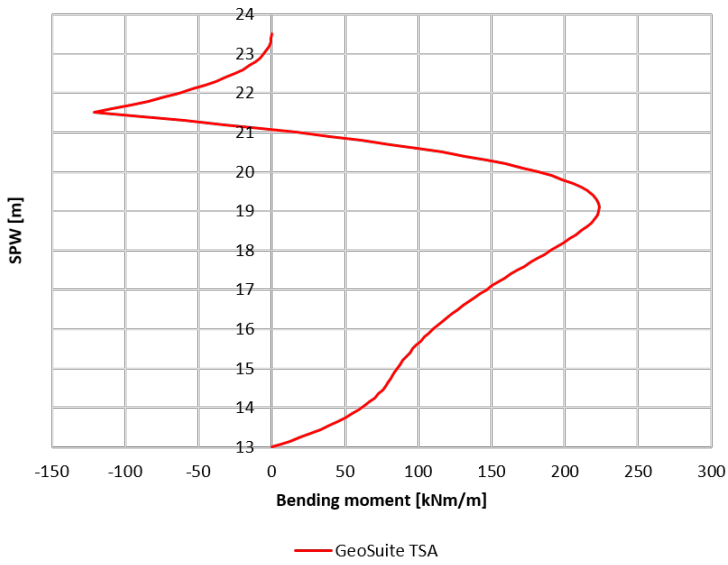


---

### Installation top anchor row

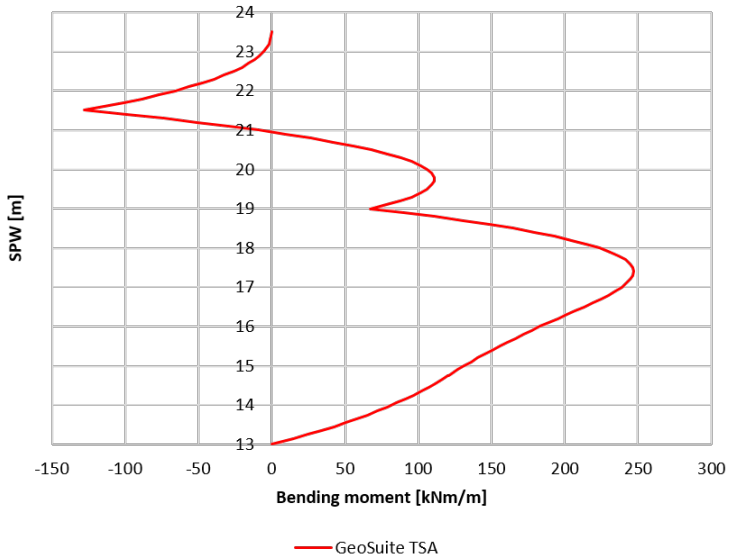


### Excavation +18.5

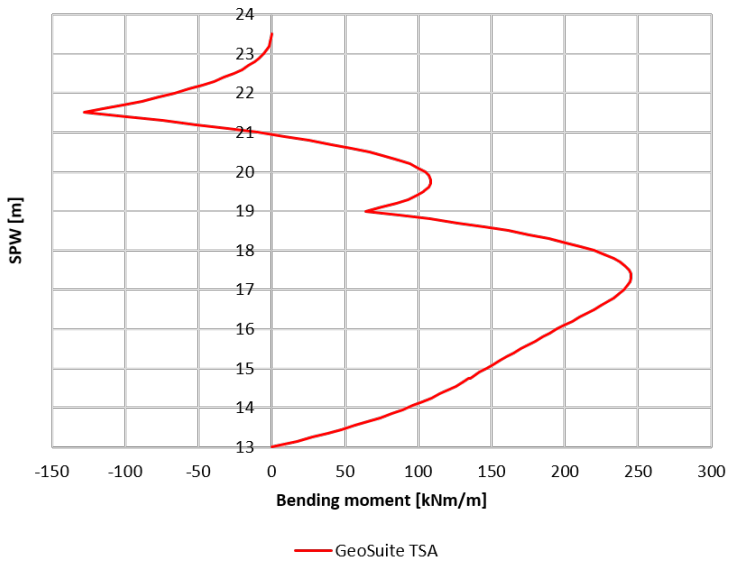


---

### Installation bottom anchor row

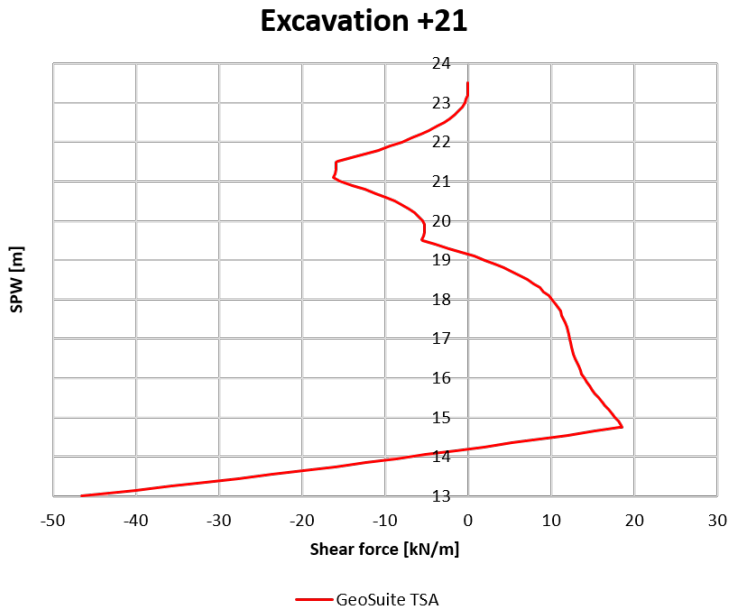


### Excavation +18



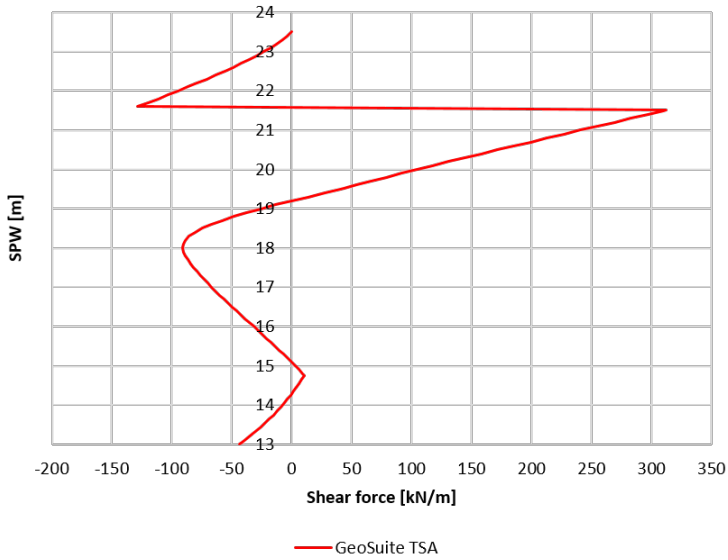
---

### C.3 Shear force of SPW with $r = 0$ in GS Excavation

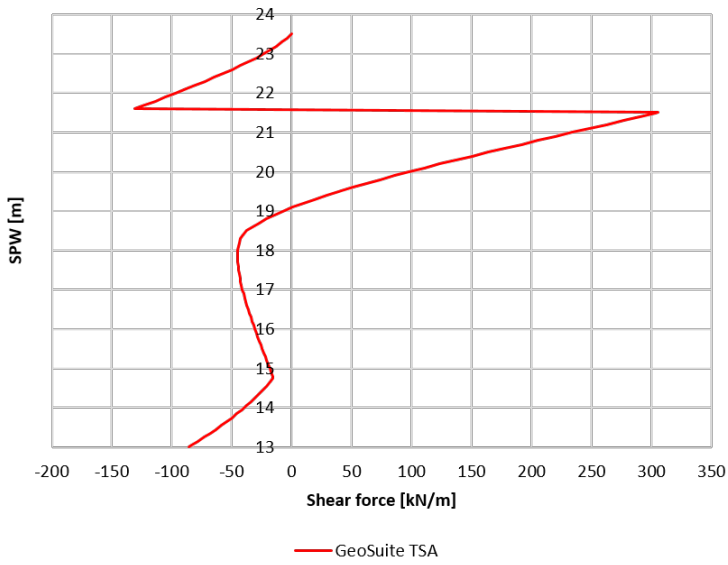


---

### Installation top anchor row



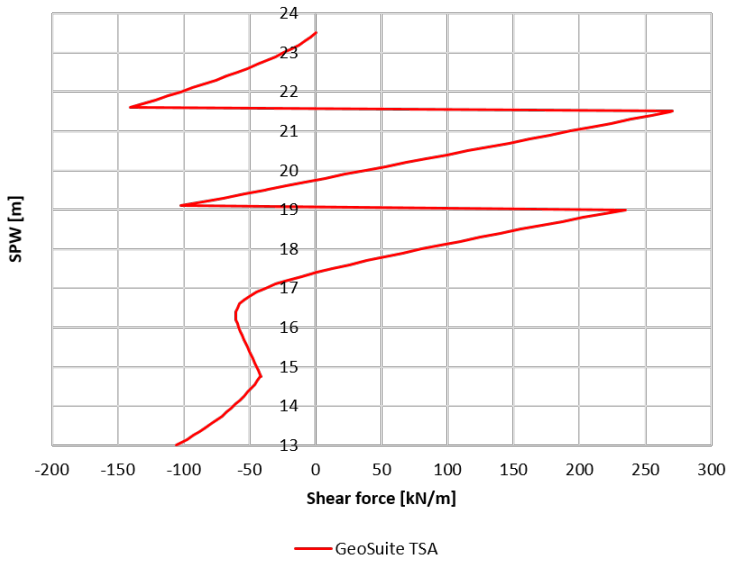
### Excavation +18.5



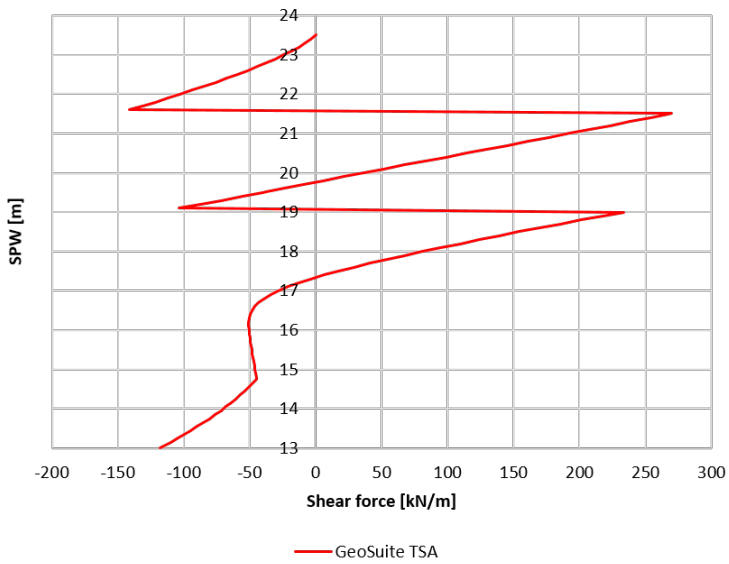


---

### Installation bottom anchor row



### Excavation +18

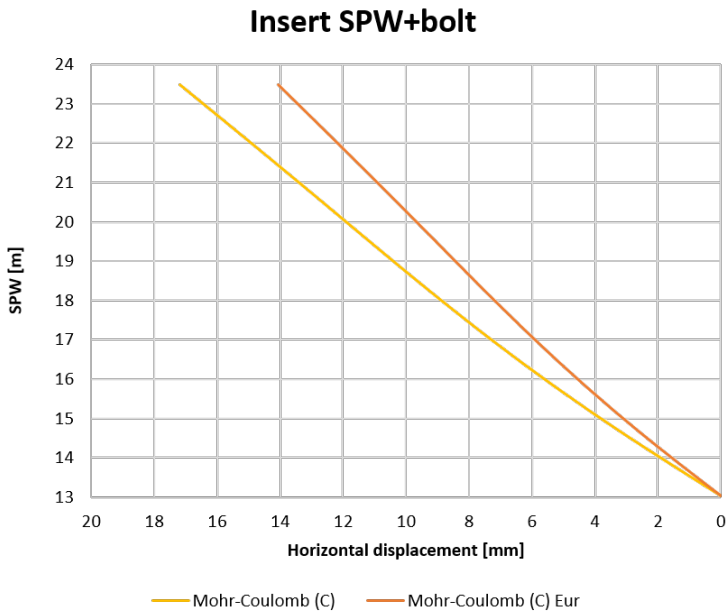


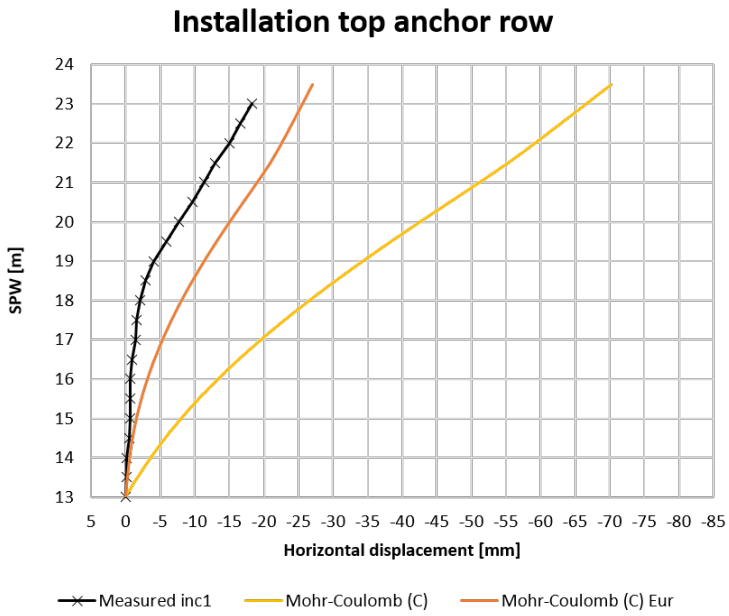
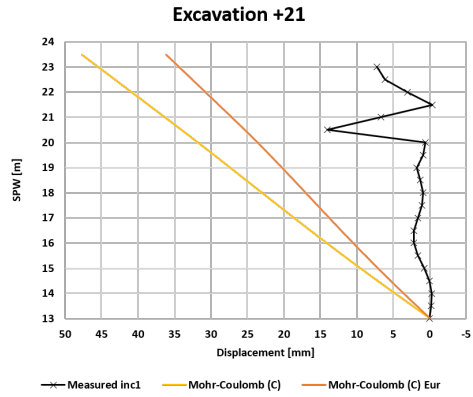


# Appendix D

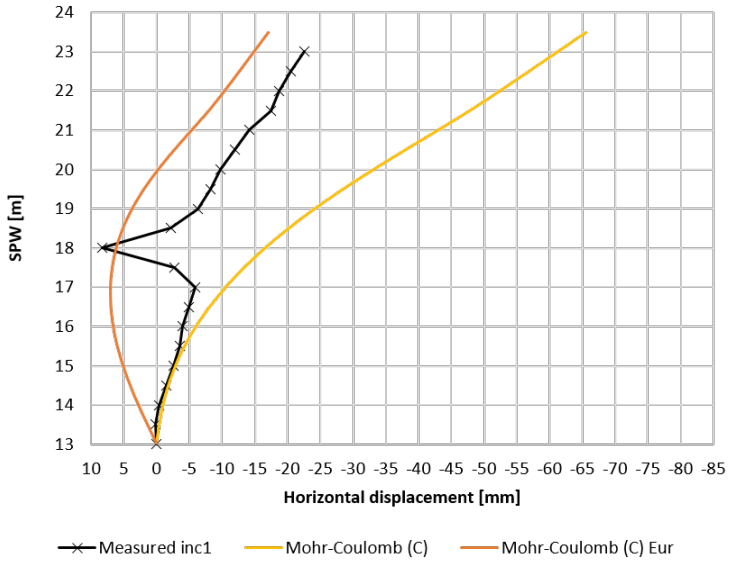
## PLAXIS MC model with $E_{ur}$ results

### D.1 Displacement of SPW with MC( $E_{ur}$ ) in PLAXIS

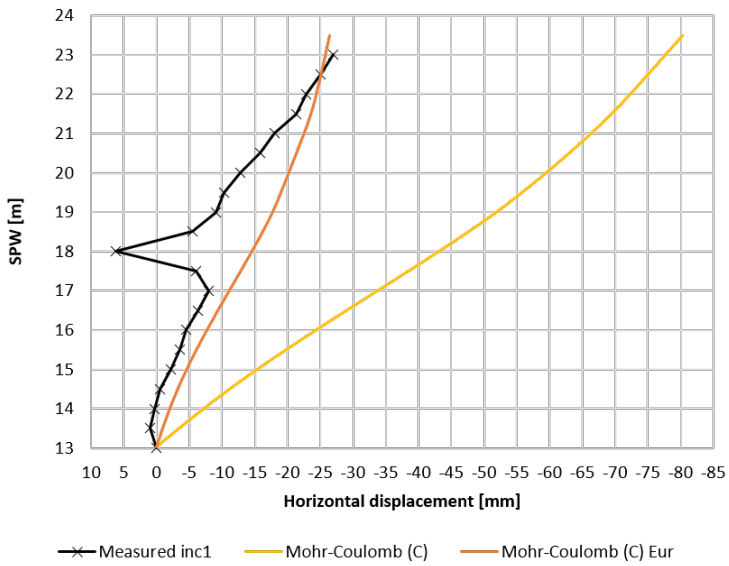




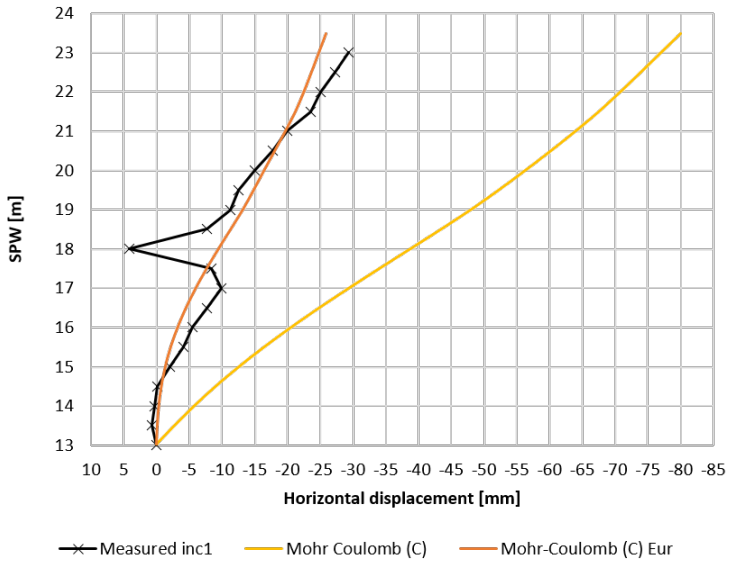
### Excavation +18.5



### Installation bottom anchor row

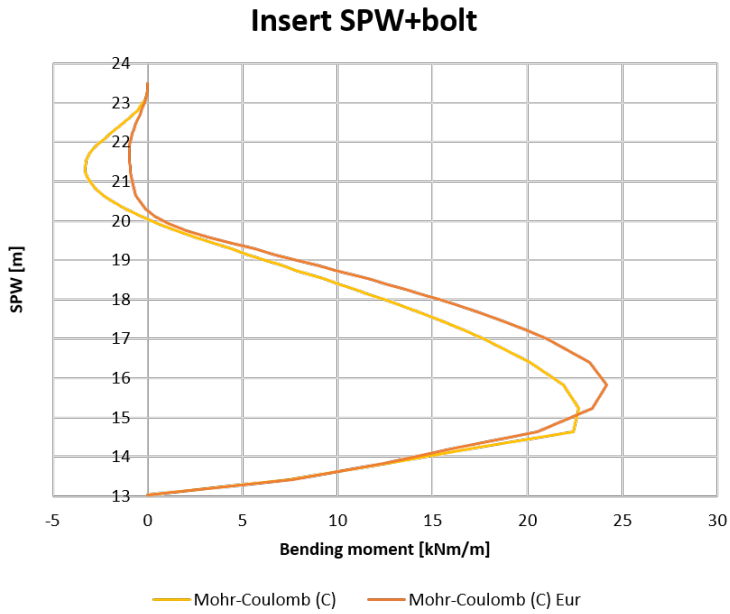


### Excavation +18

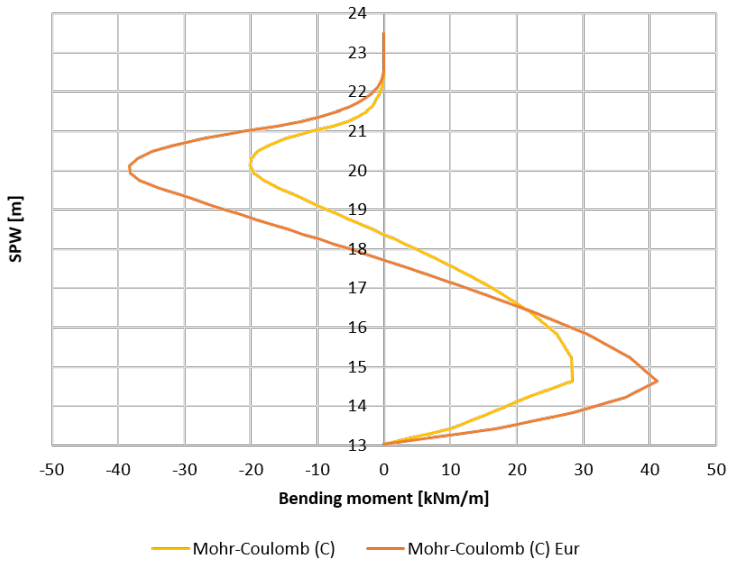


---

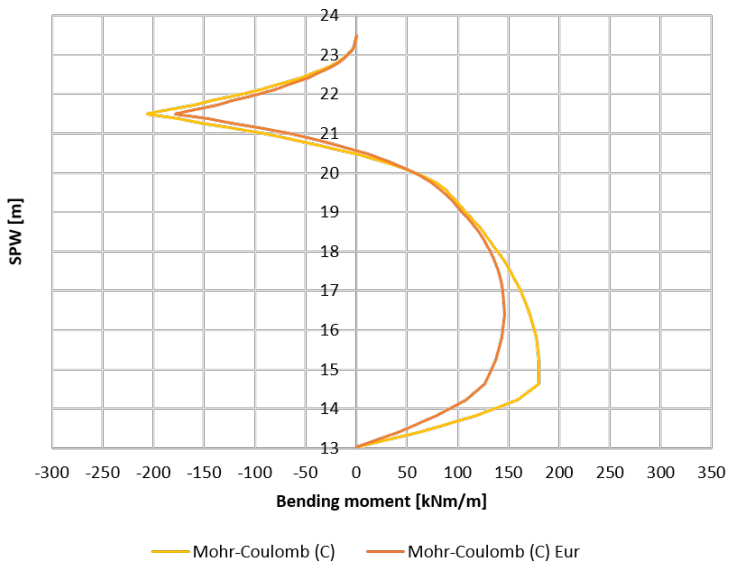
## D.2 Bending moment of SPW with MC( $E_{ur}$ ) in PLAXIS



### Excavation +21

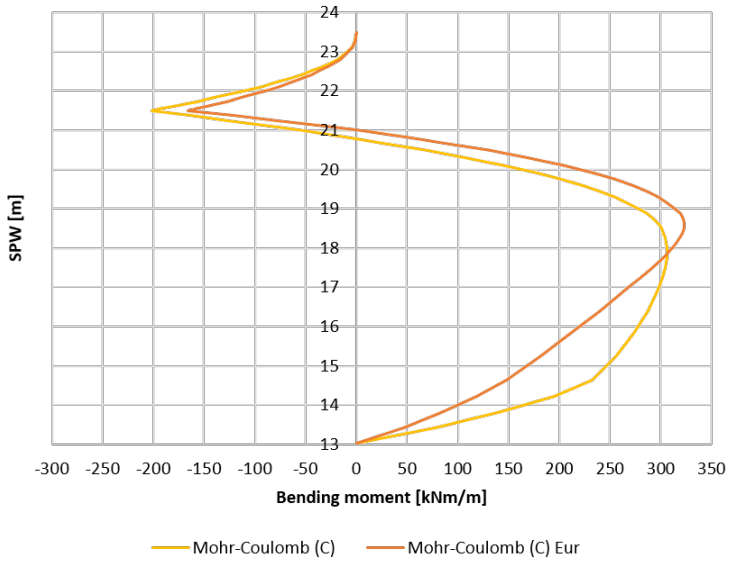


### Installation top anchor row

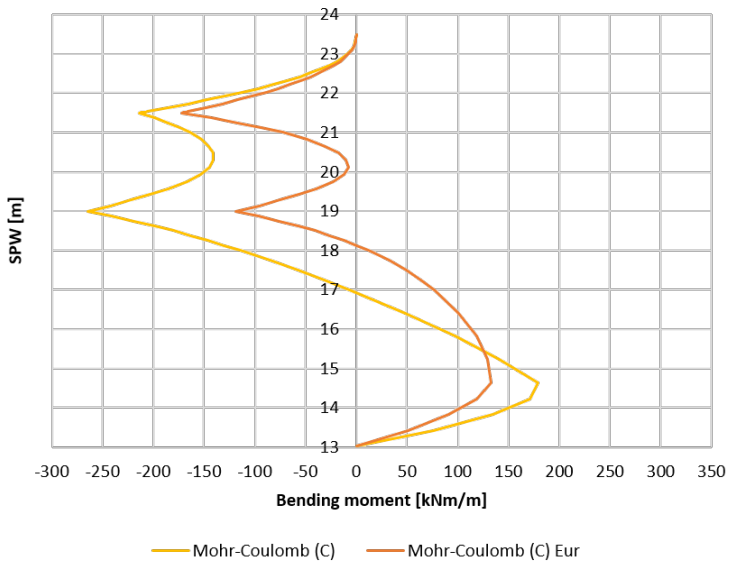




### Excavation +18.5

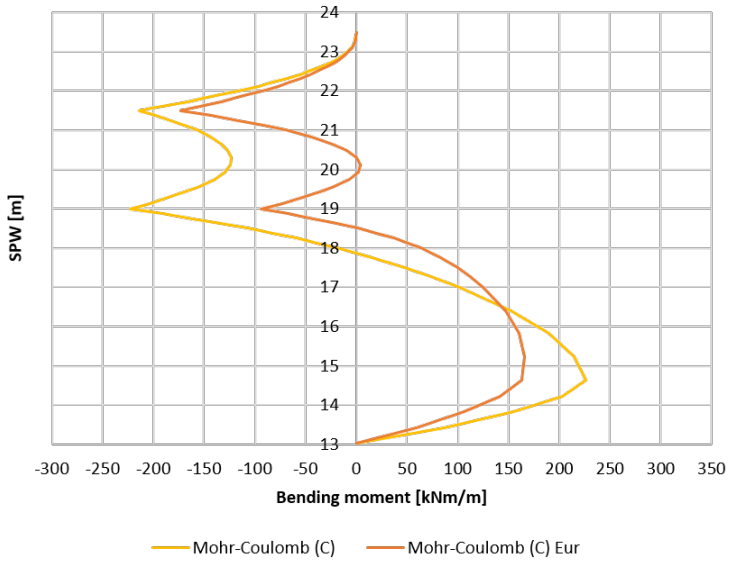


### Installation bottom anchor row



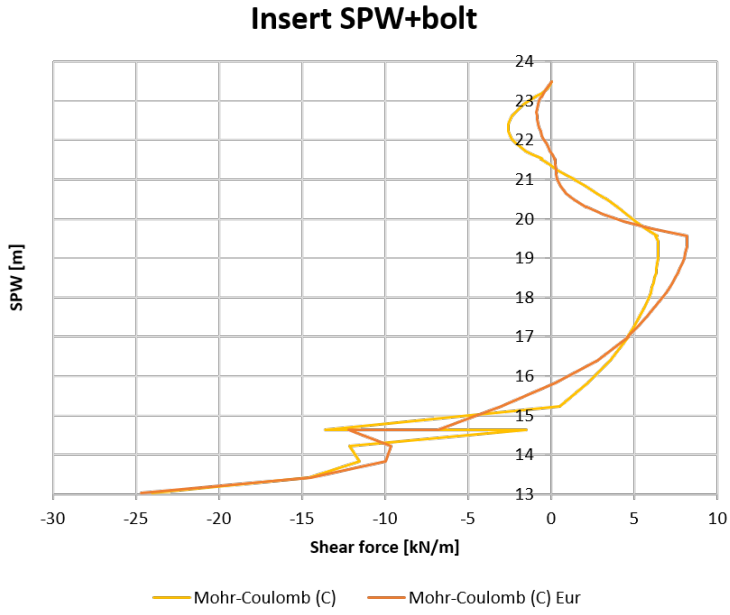
---

### Excavation +18

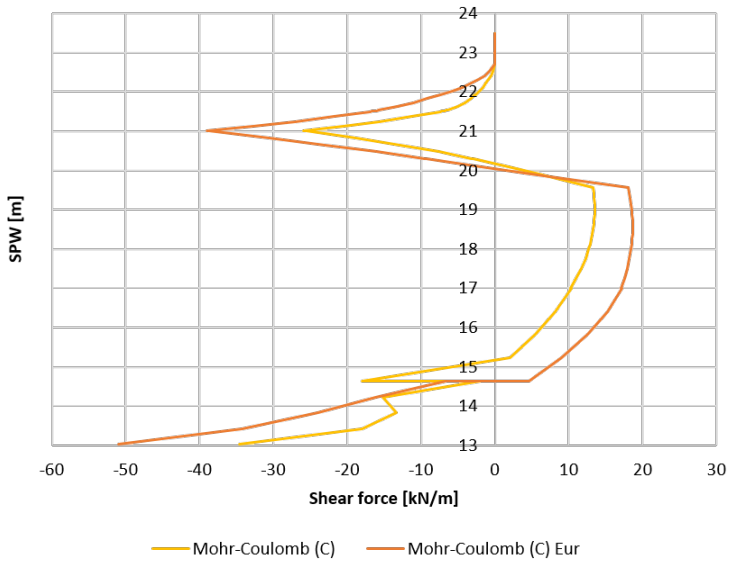


---

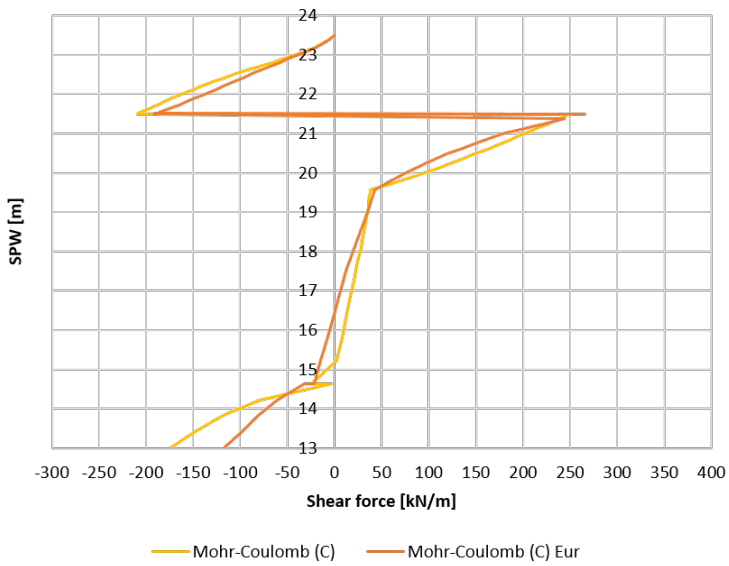
### D.3 Shear force of SPW with MC( $E_{ur}$ ) in PLAXIS



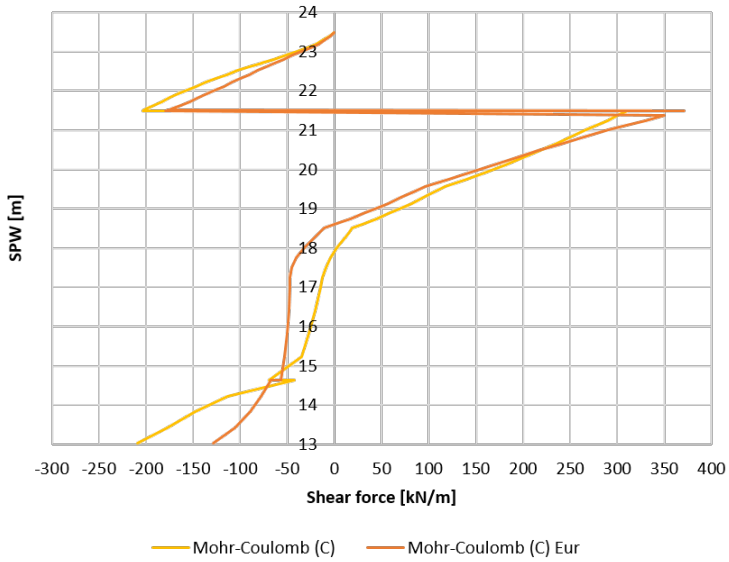
### Excavation +21



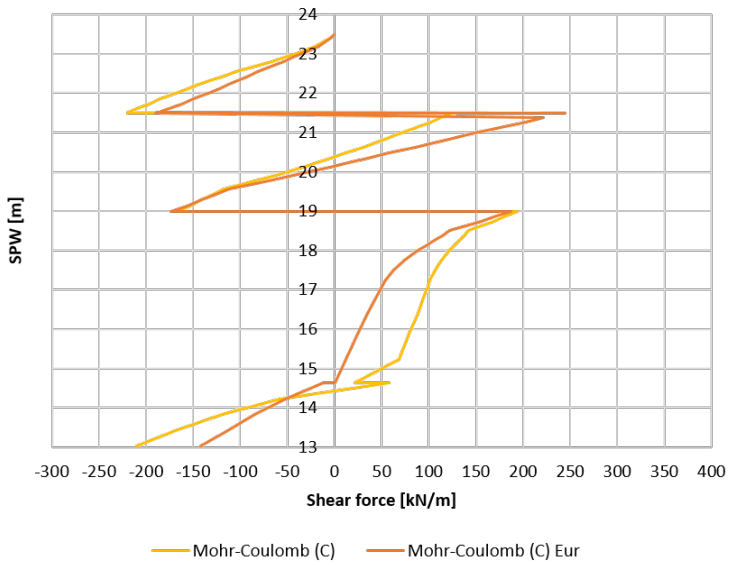
### Installation top anchor row



### Excavation +18.5

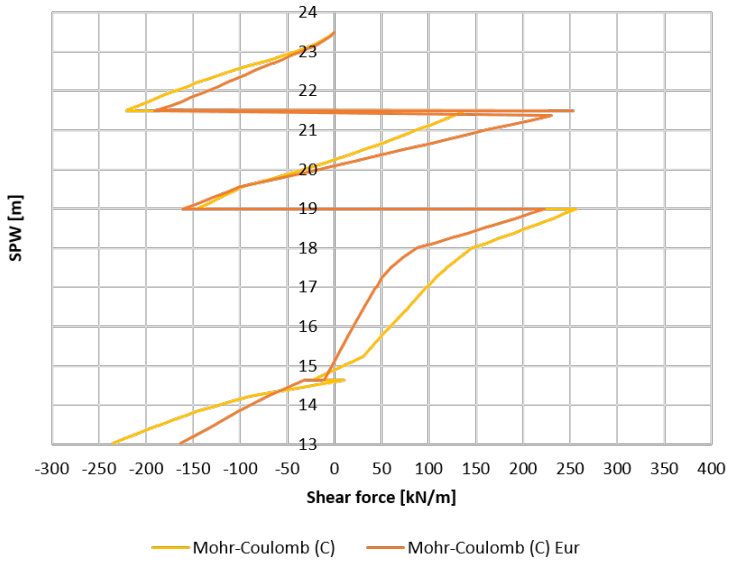


### Installation bottom anchor row

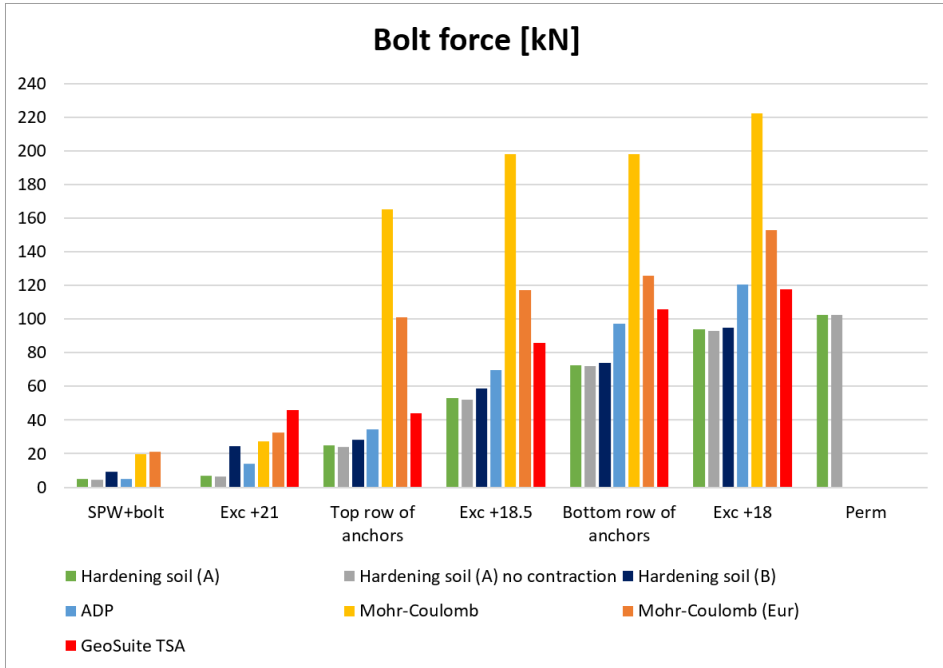


---

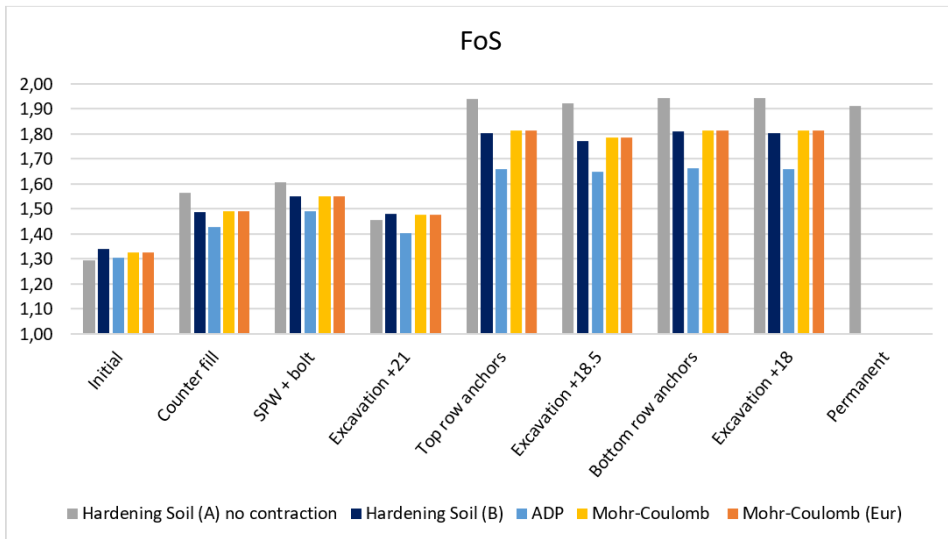
### Excavation +18



## D.4 Bolt force with $MC(E_{ur})$ in PLAXIS



## D.5 FoS in all phases with $MC(E_{ur})$ in PLAXIS

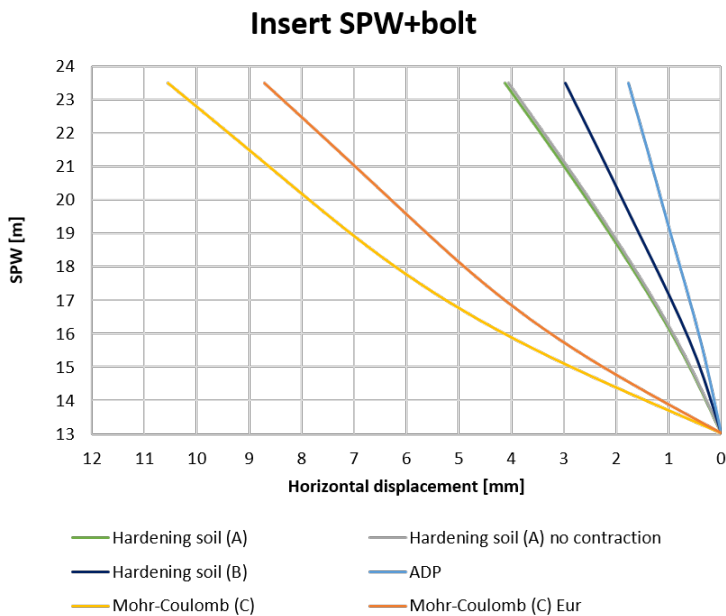




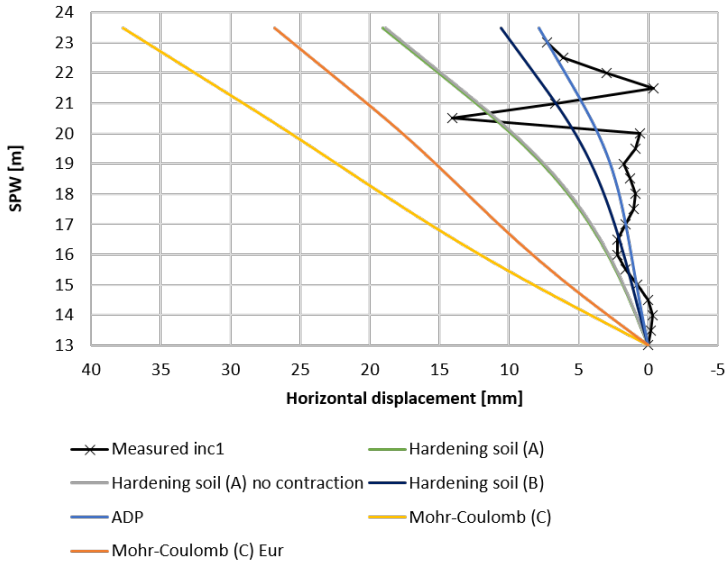
# Appendix E

## PLAXIS with $R_{inter} = 0.4$ results

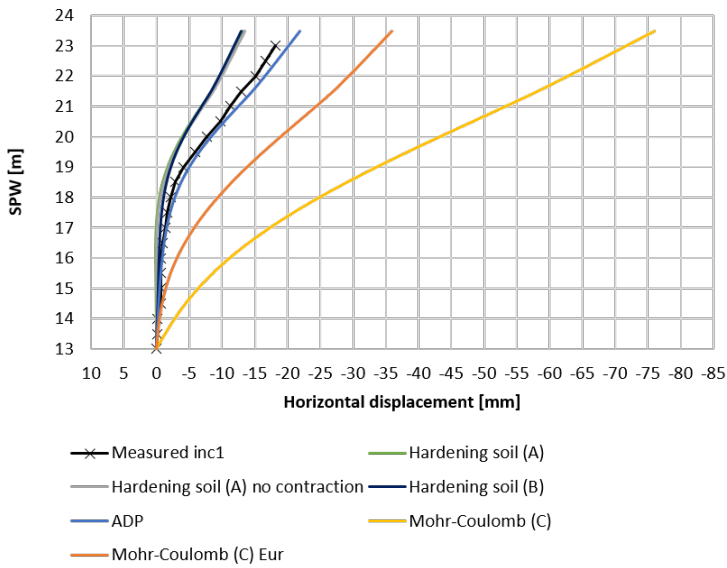
### E.1 Displacement of SPW for $R_{inter} = 0.4$ in PLAXIS



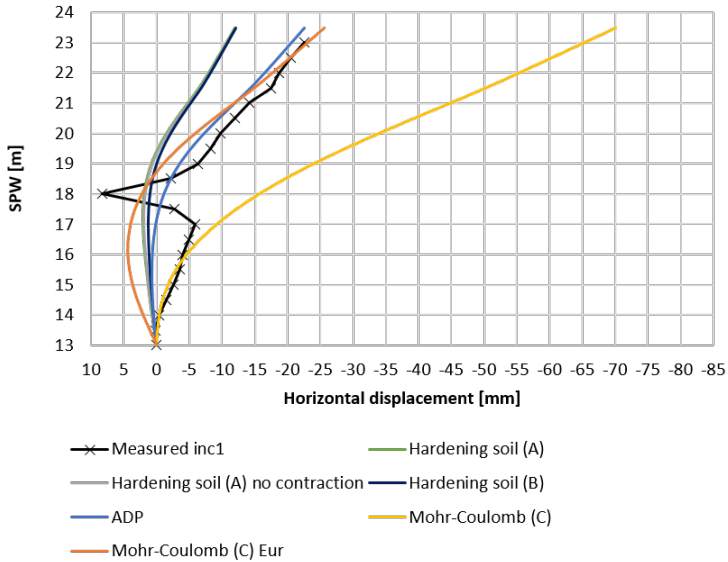
### Excavation +21



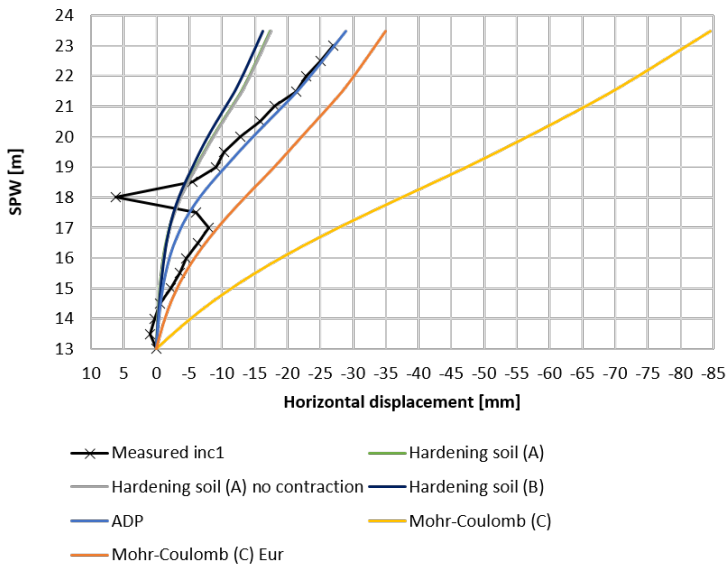
### Installation top anchor row



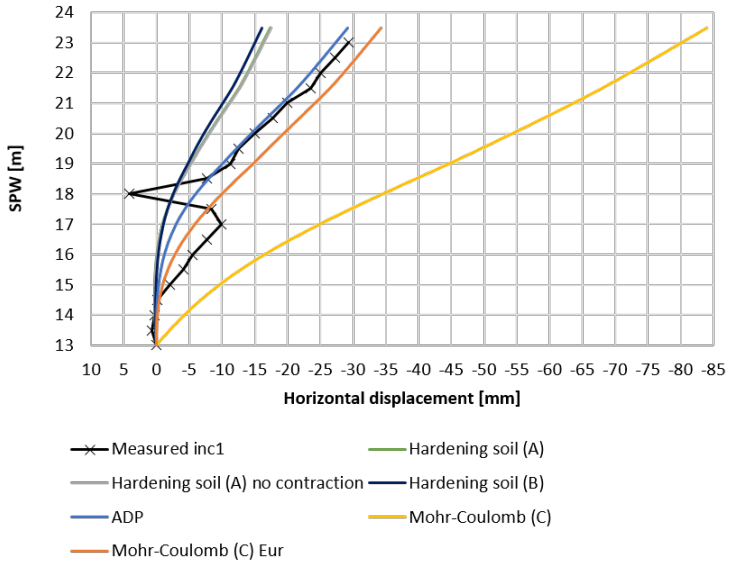
### Excavation +18.5



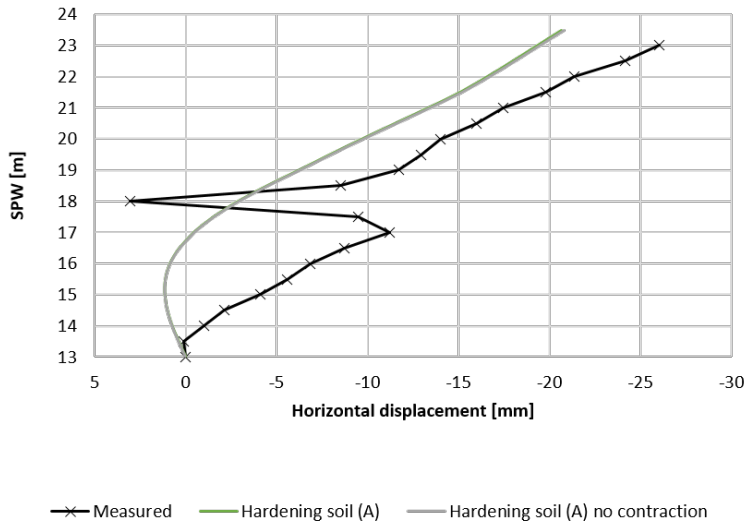
### Installation bottom anchor row



### Excavation +18

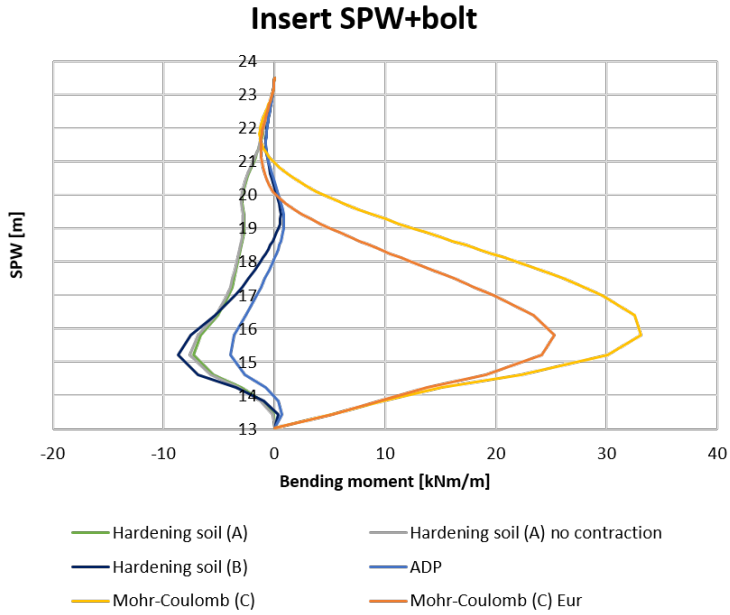


### Consolidation

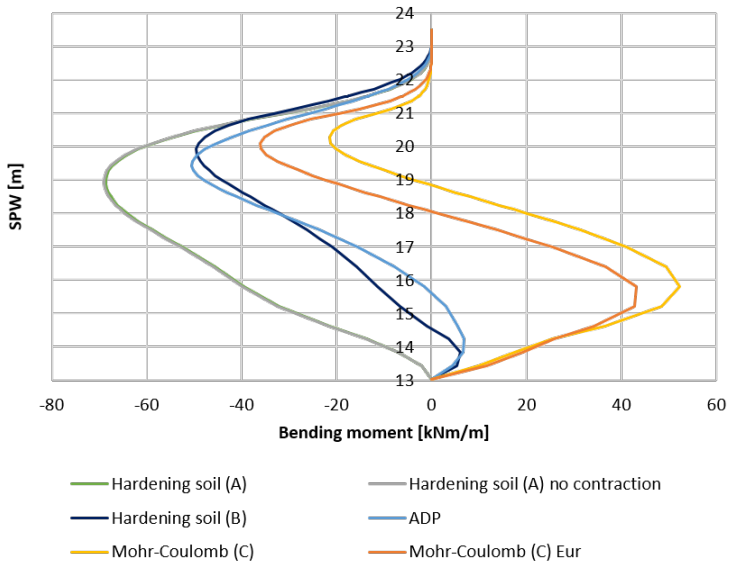


---

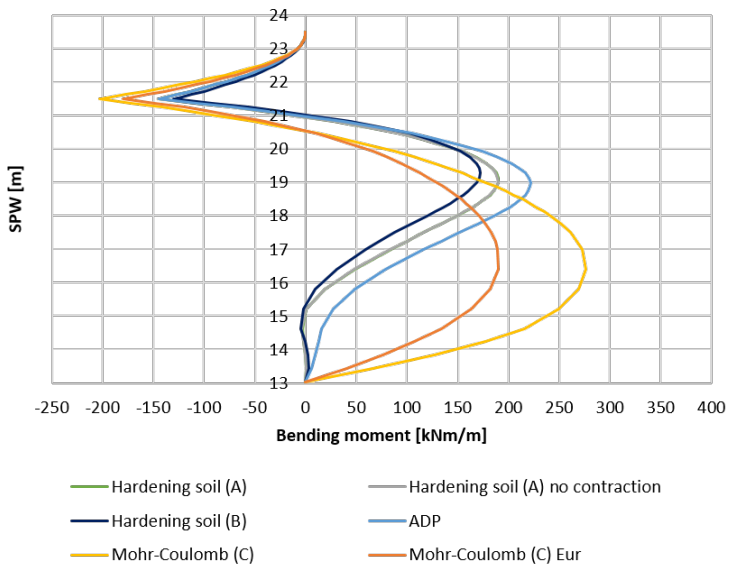
## E.2 Bending moment of SPW for $R_{inter} = 0.4$ in PLAXIS



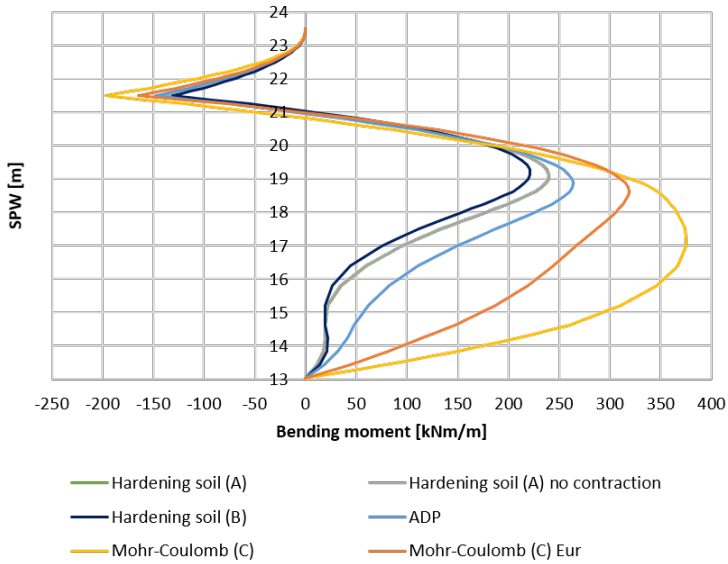
### Excavation +21



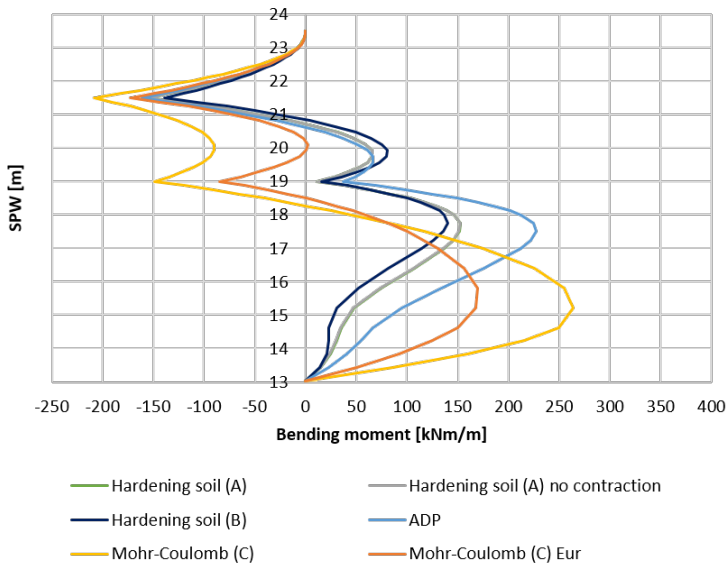
### Installation top anchor row



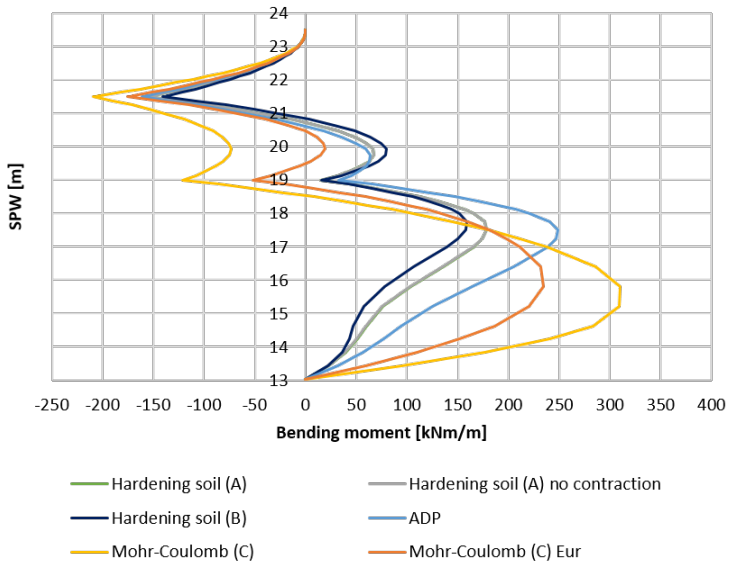
### Excavation +18.5



### Installation bottom anchor row



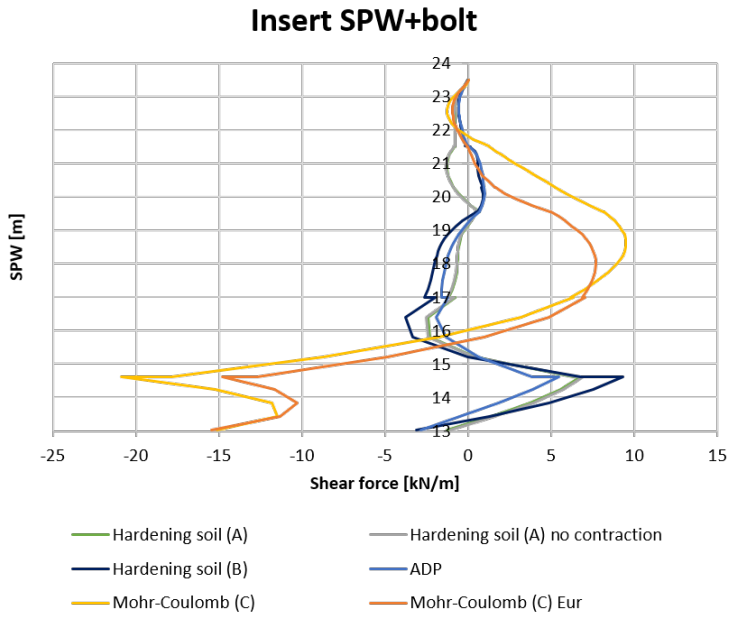
## Excavation +18



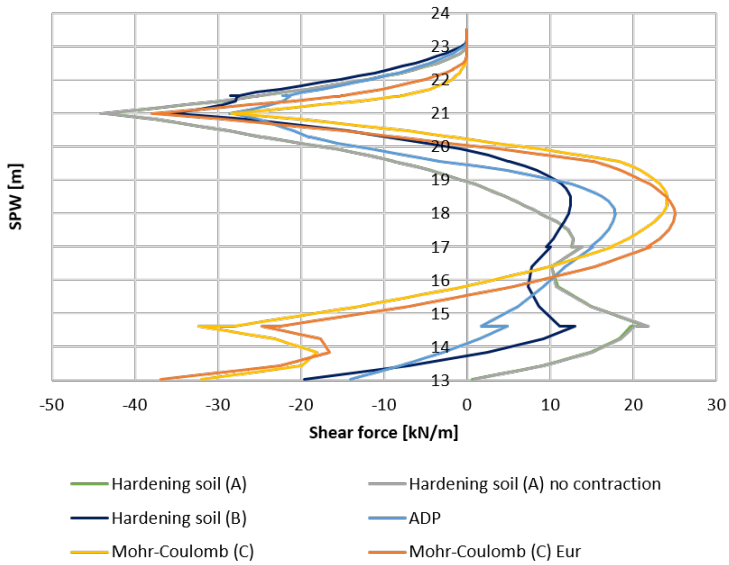


---

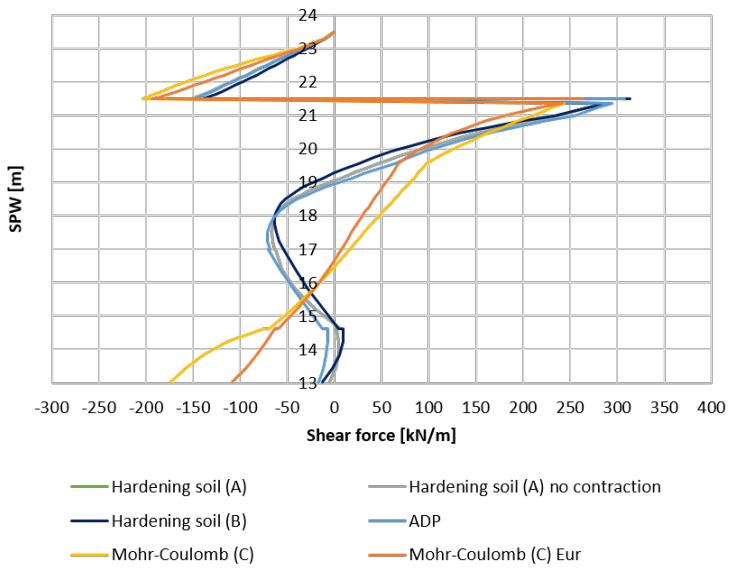
### E.3 Shear force of SPW for $R_{inter} = 0.4$ in PLAXIS



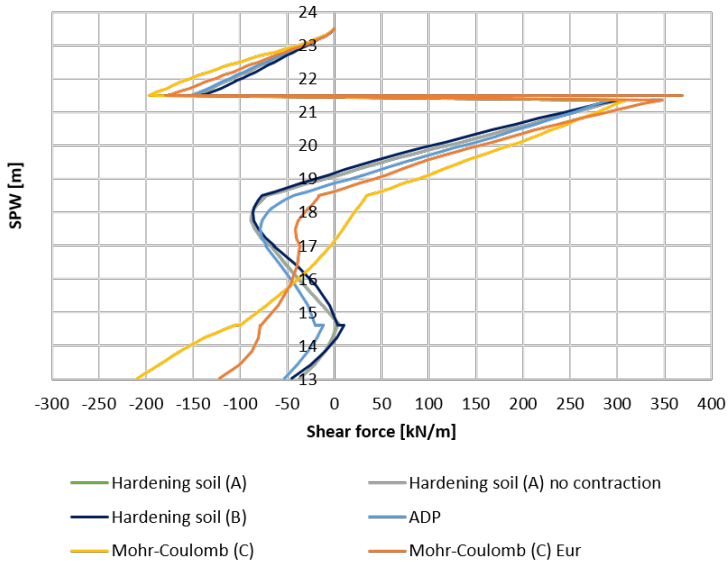
### Excavation +21



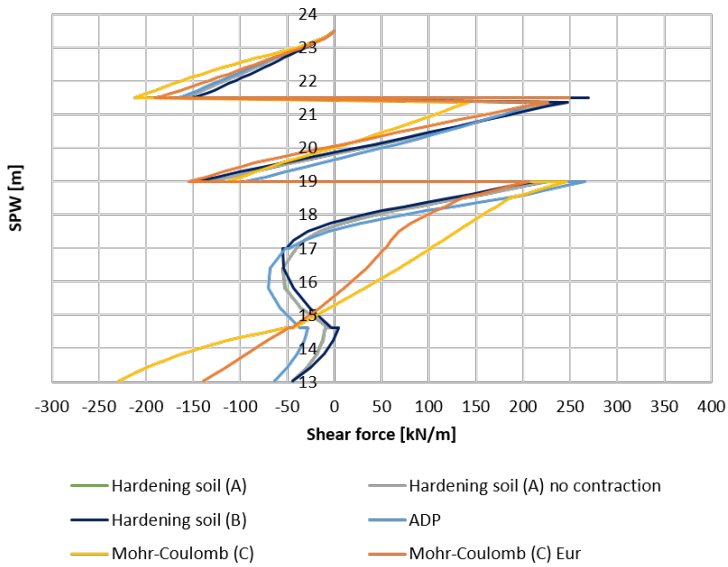
### Installation top anchor row



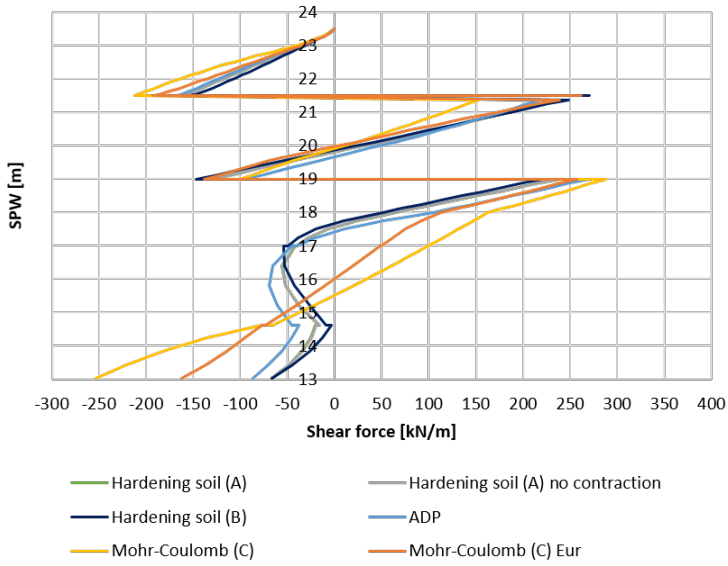
### Excavation +18.5



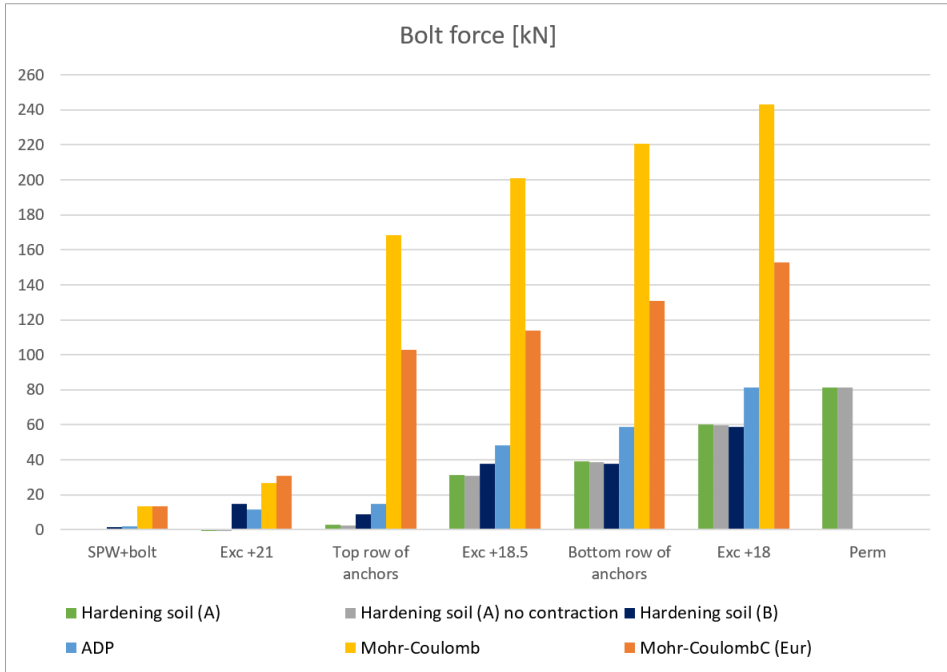
### Installation bottom anchor row



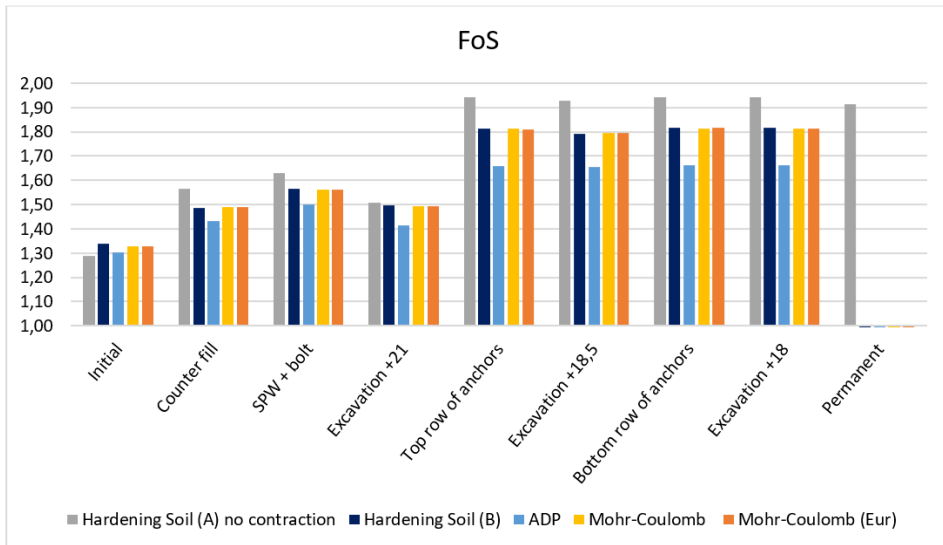
## Excavation +18



## E.4 Bolt force for $R_{inter} = 0.4$ in PLAXIS



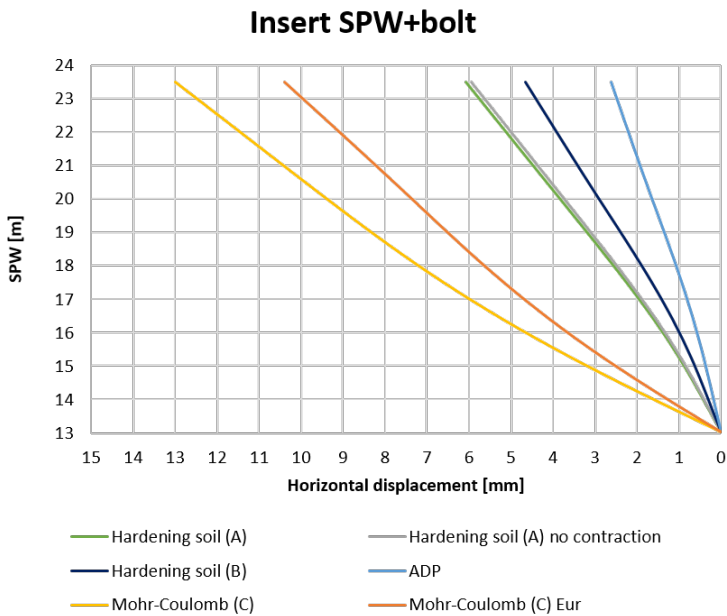
## E.5 FoS in all phases for $R_{inter} = 0.4$ in PLAXIS



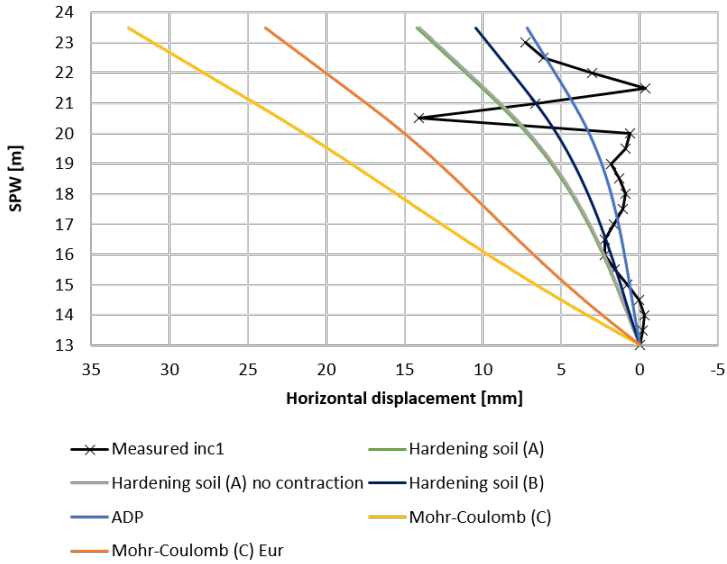
# Appendix F

## PLAXIS modeled with full effect of LCC results

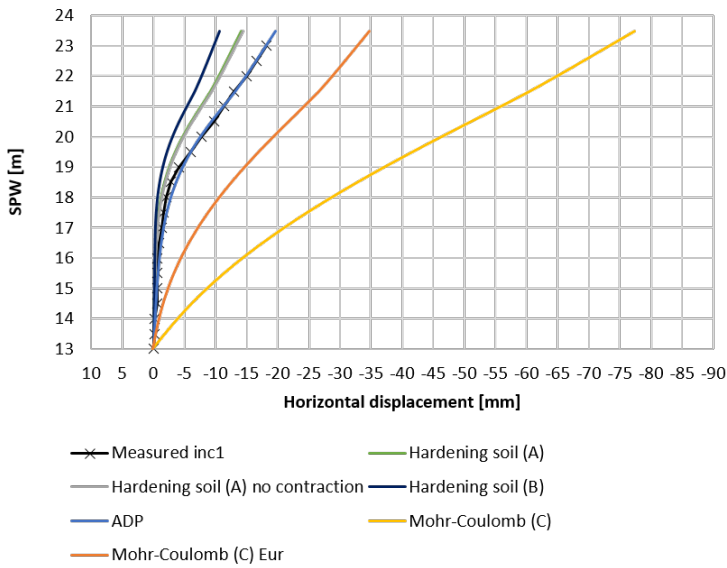
### F.1 Displacement of SPW with full effect of LCC in PLAXIS



### Excavation +21

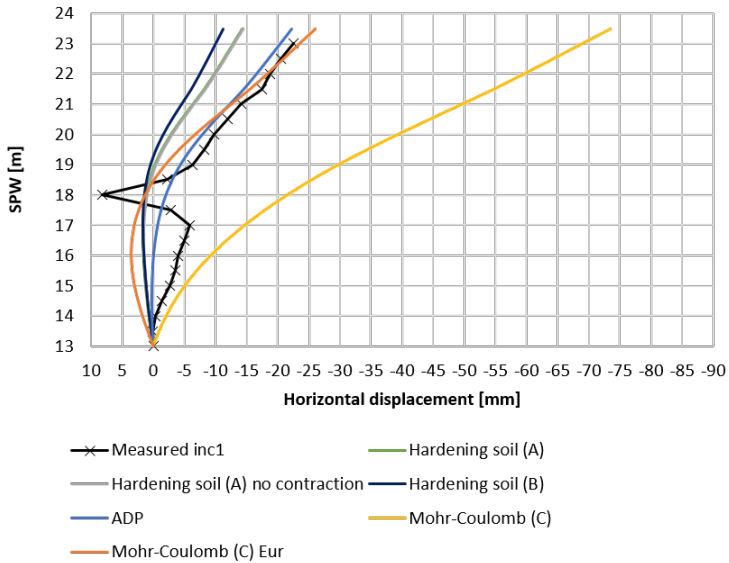


### Installation top anchor row

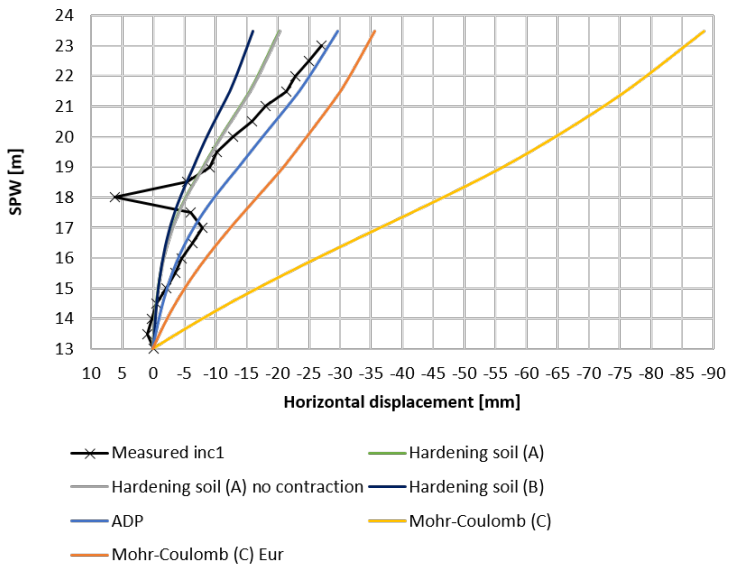




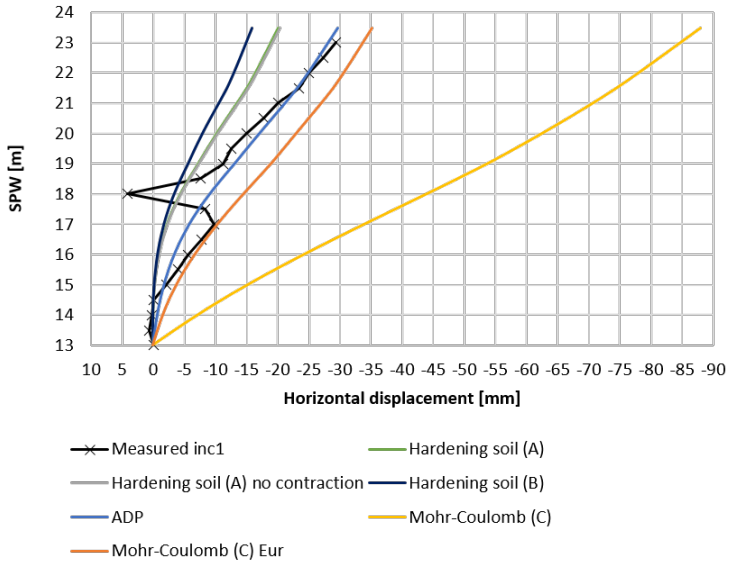
### Excavation +18.5



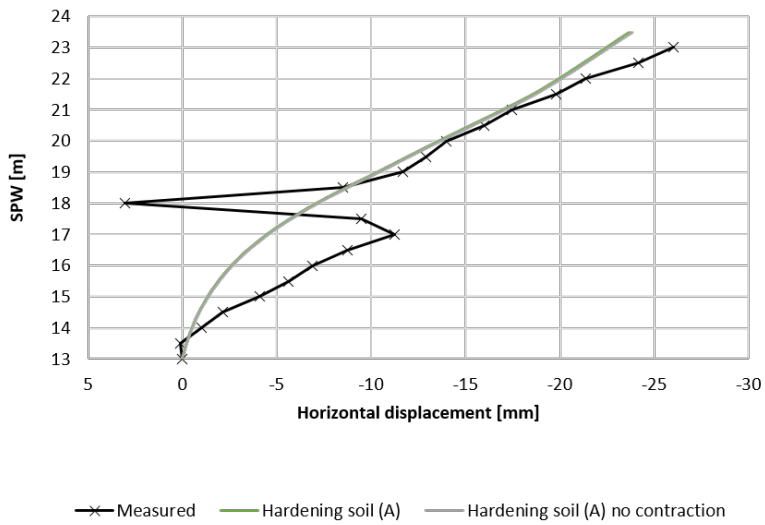
### Installation bottom anchor row



### Excavation +18

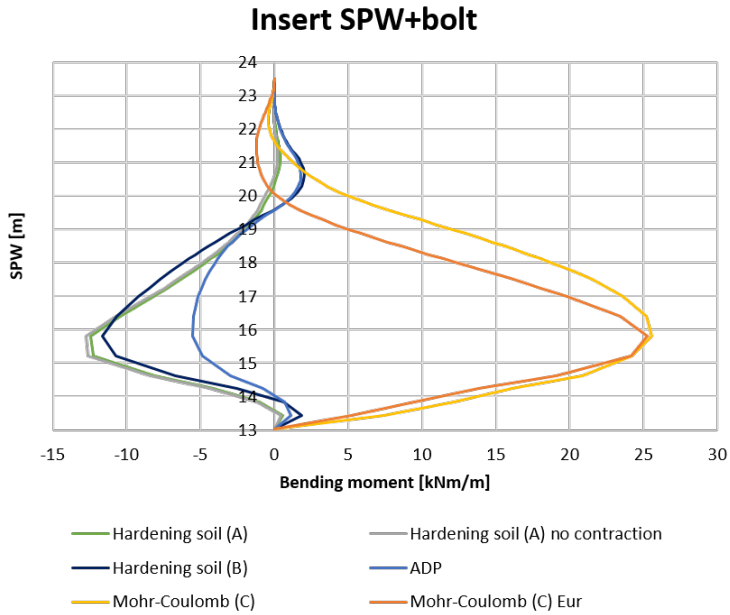


### Consolidation

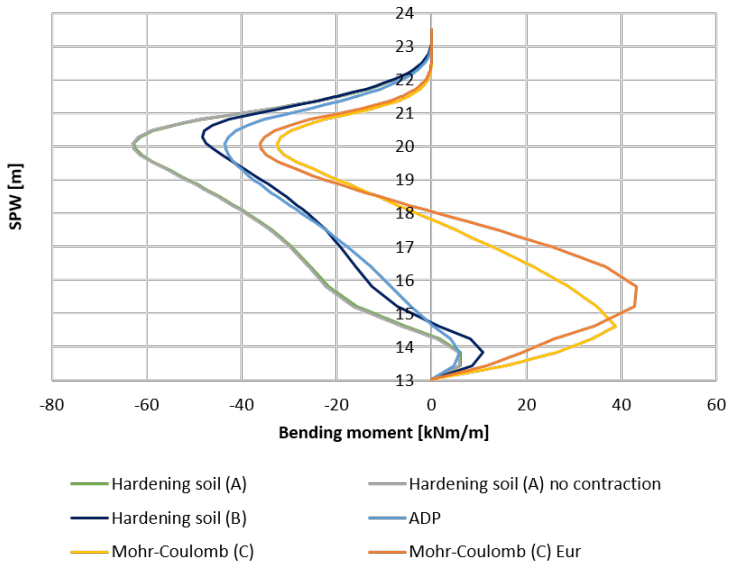


---

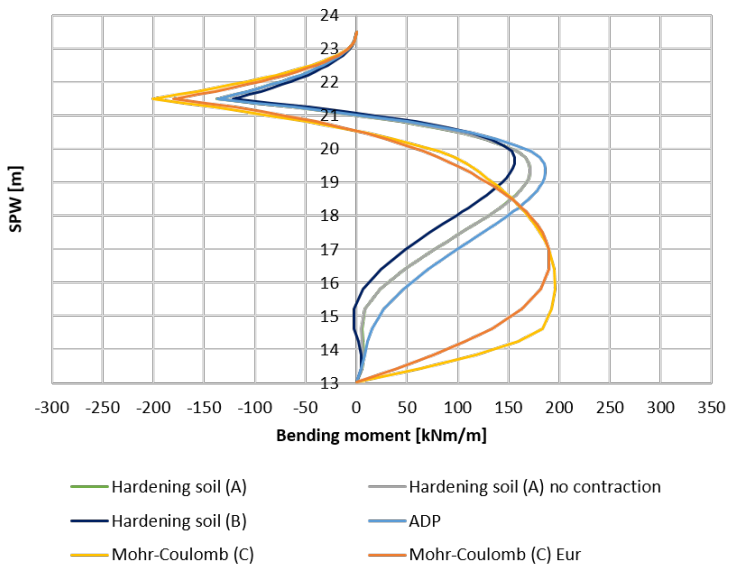
## E.2 Bending moment of SPW with full effect of LCC in PLAXIS



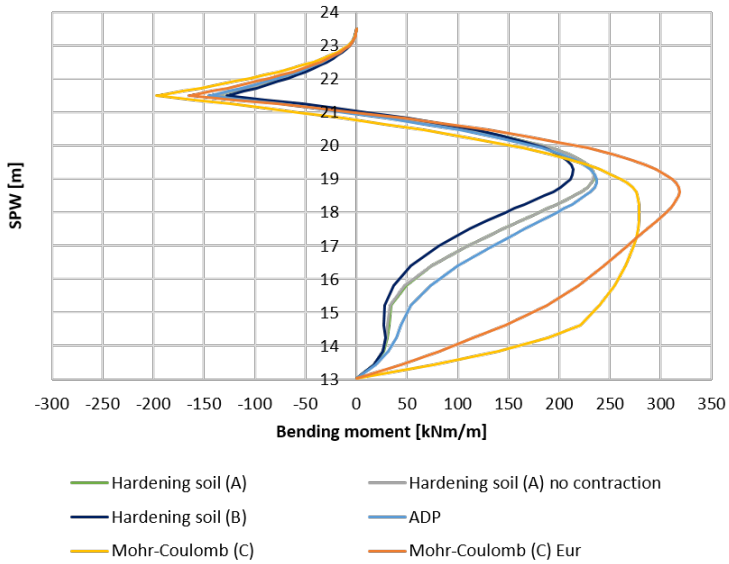
### Excavation +21



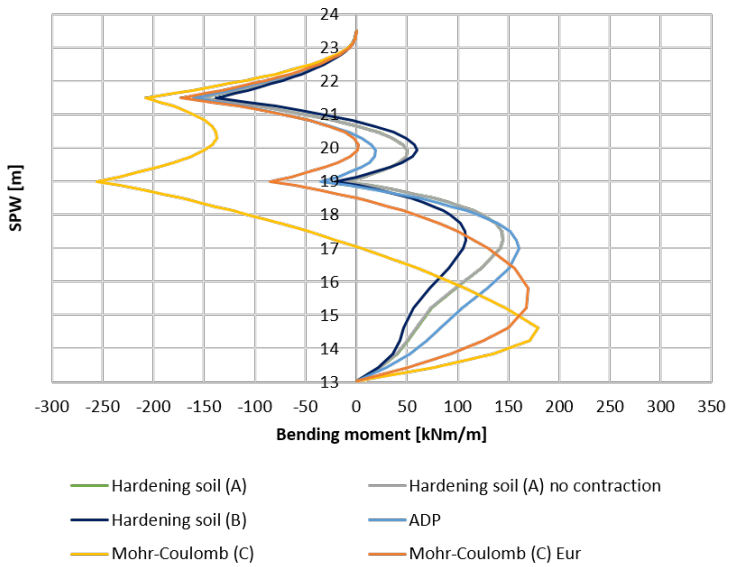
### Installation top anchor row



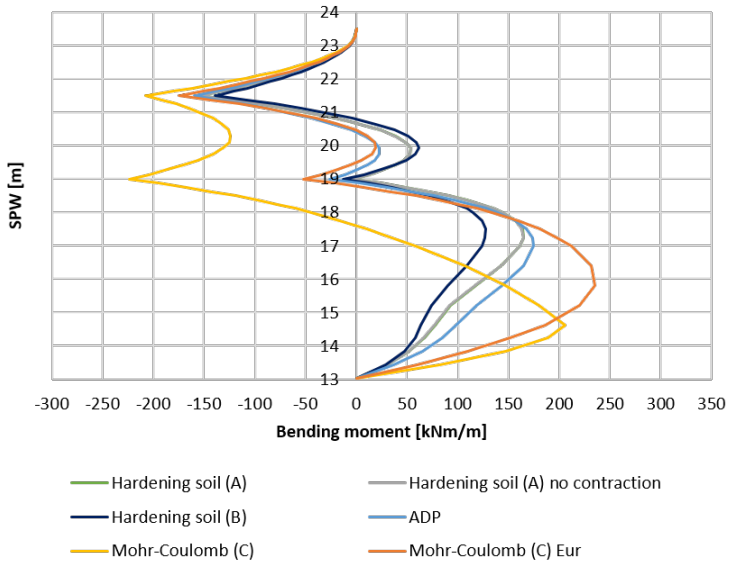
### Excavation +18.5



### Installation bottom anchor row

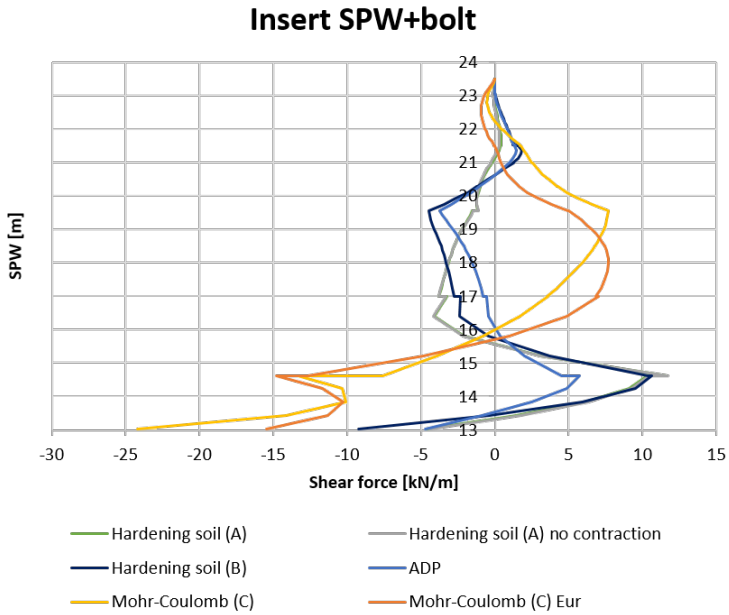


## Excavation +18

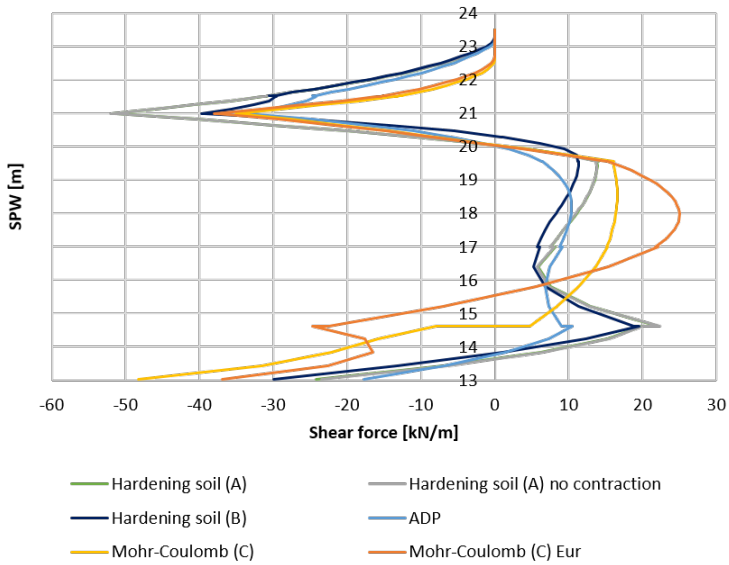


---

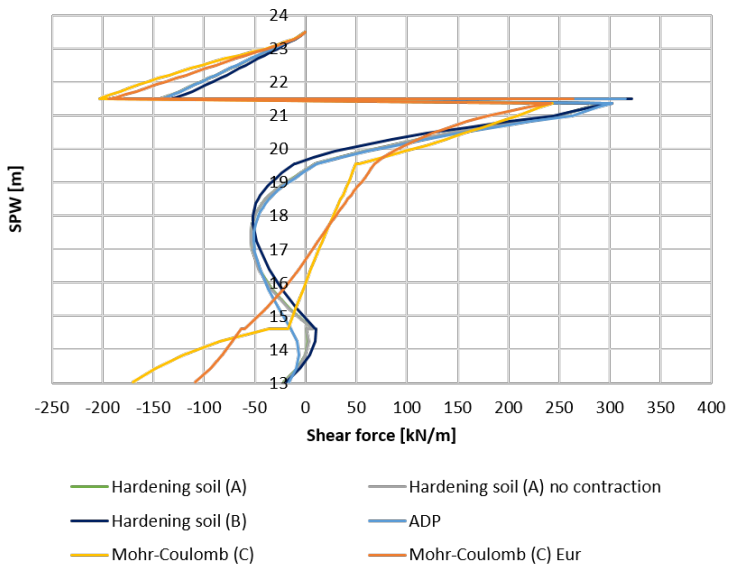
### E.3 Shear force of SPW with full effect of LCC in PLAXIS



### Excavation +21

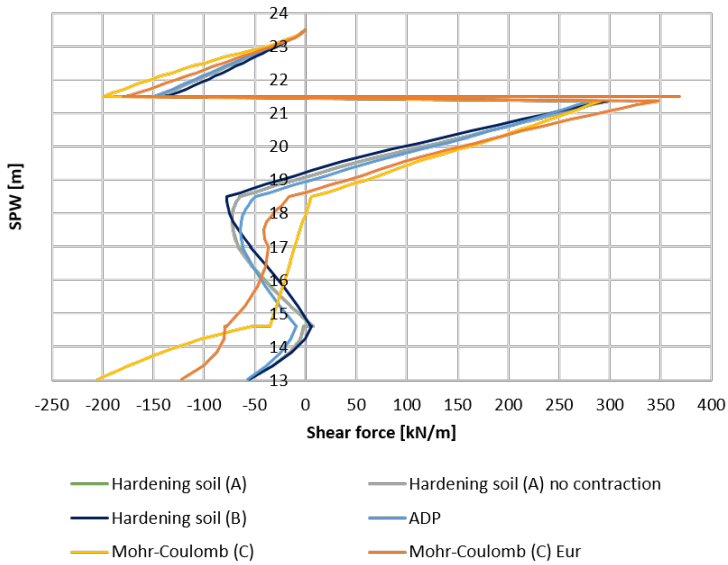


### Installation top anchor row

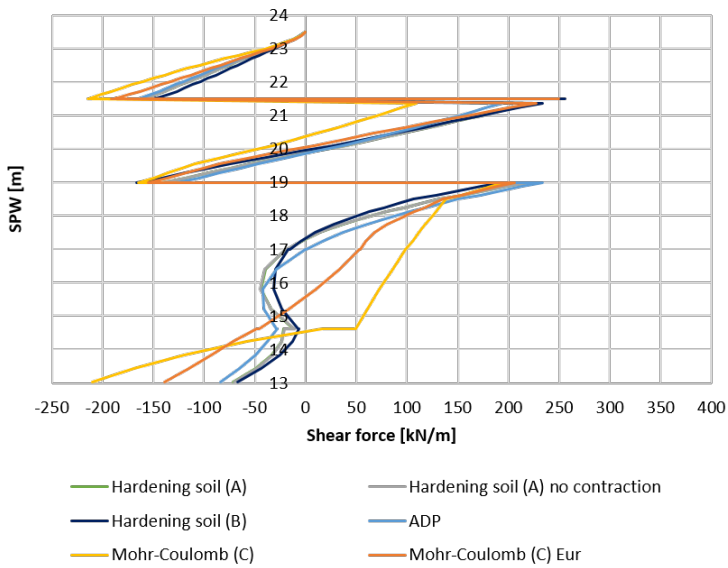




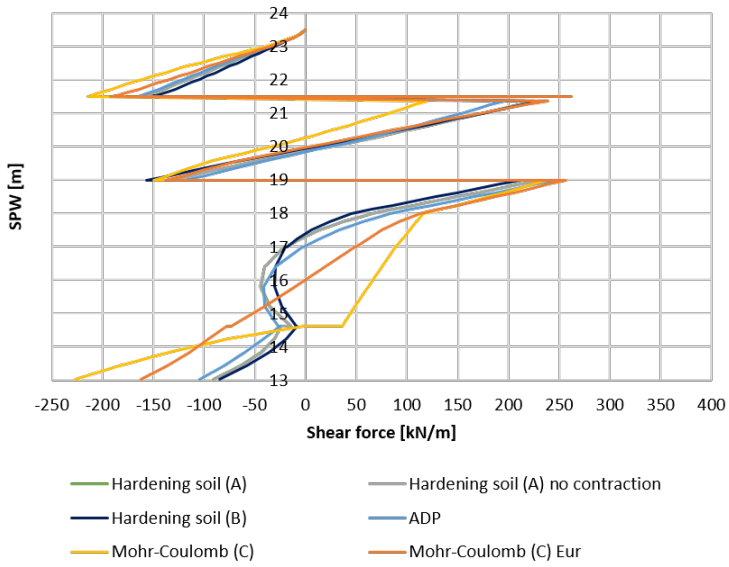
### Excavation +18.5



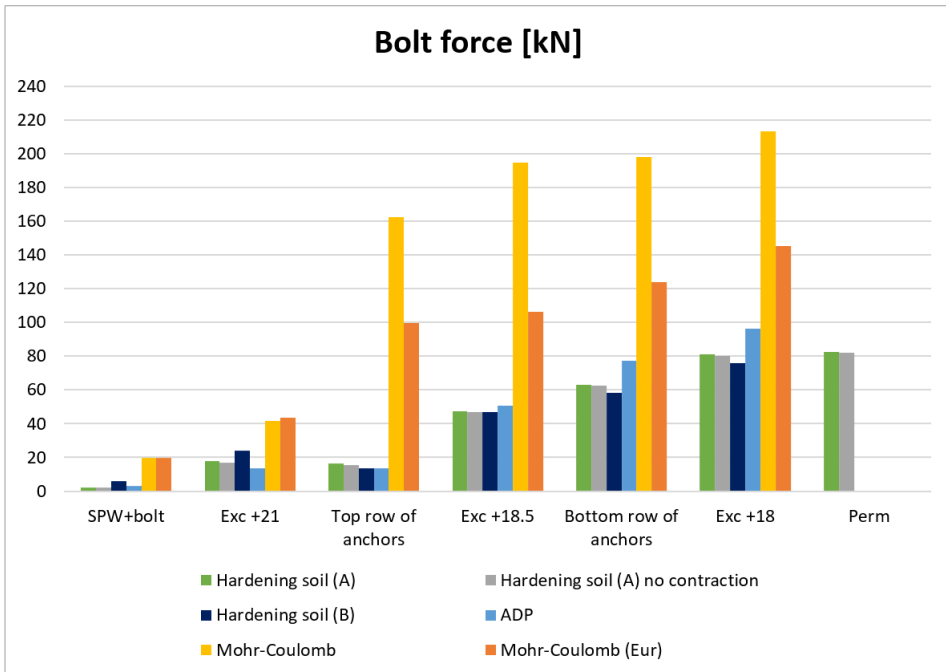
### Installation bottom anchor row



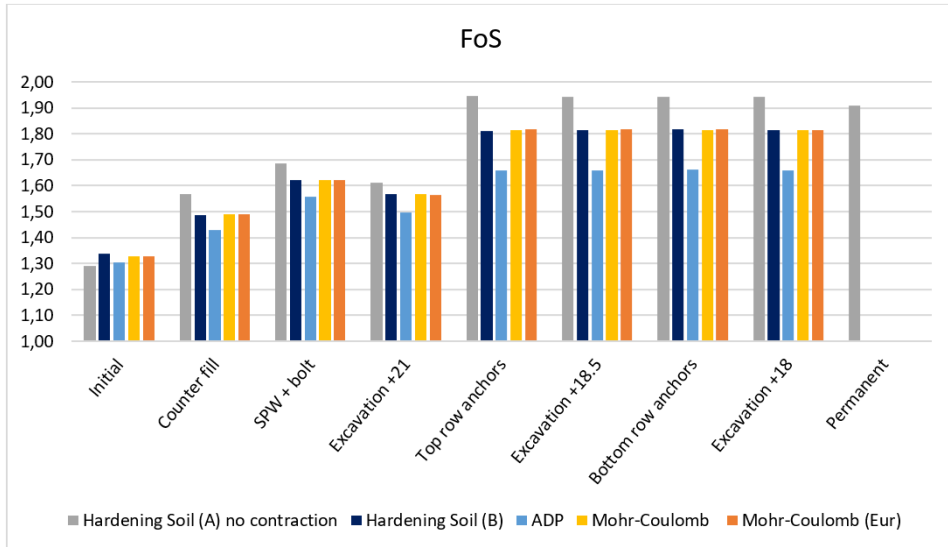
## Excavation +18



## F.4 Bolt force with full effect of LCC in PLAXIS

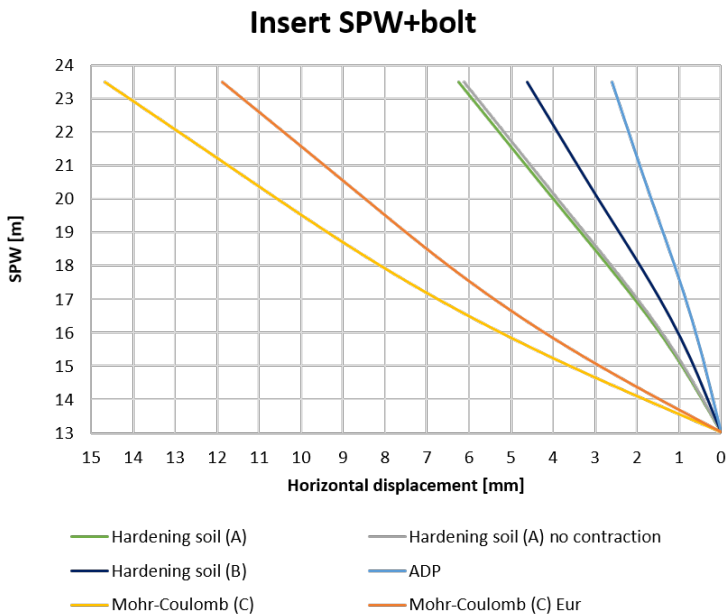


## E.5 FoS in all phases with full effect of LCC in PLAXIS

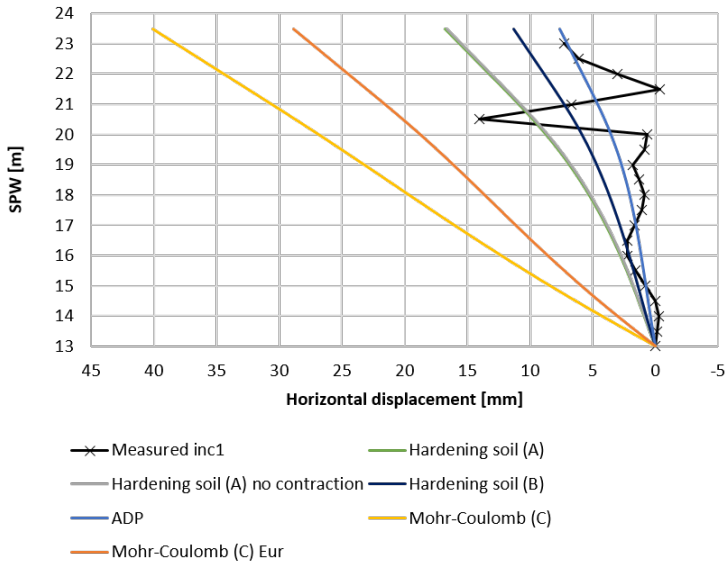


# PLAXIS modeled with partial effect of LCC results

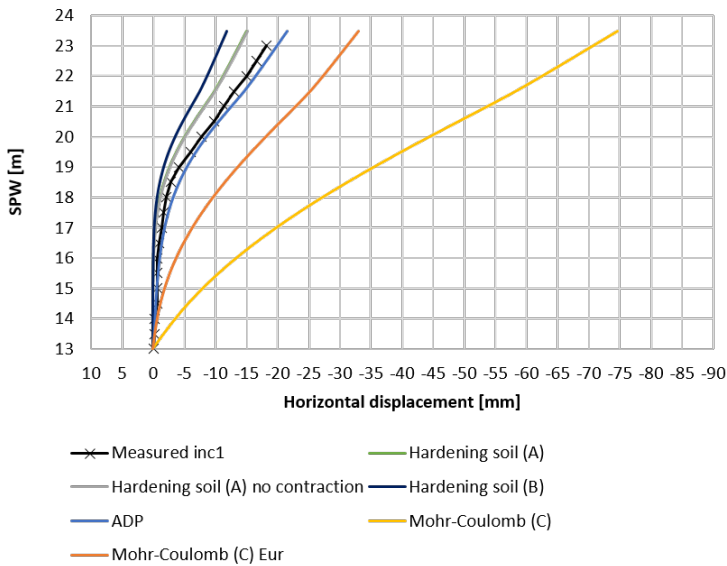
## G.1 Displacement of SPW with partial effect of LCC in PLAXIS



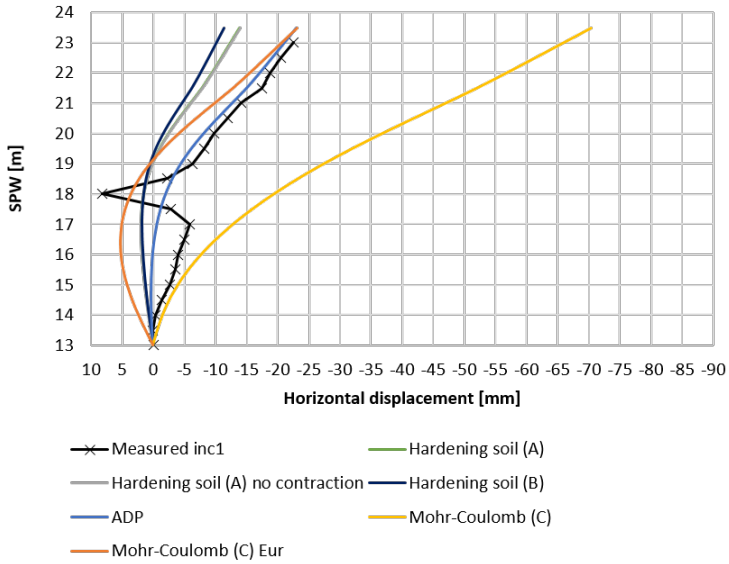
### Excavation +21



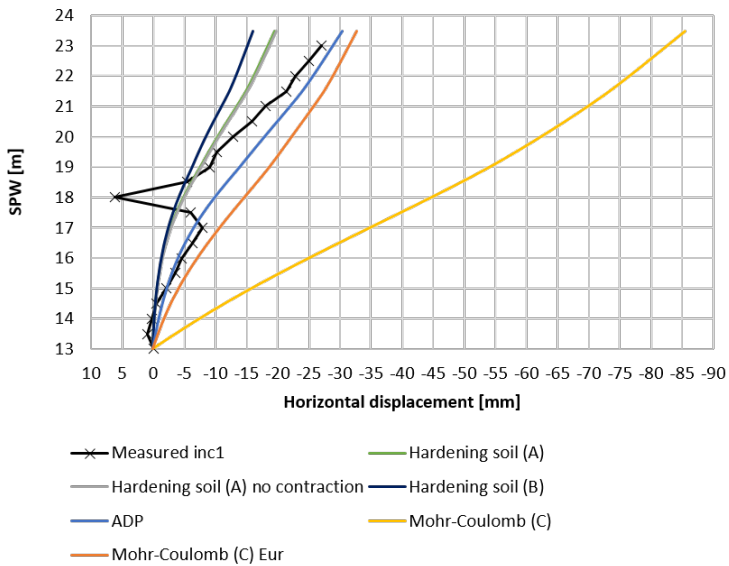
### Installation top anchor row



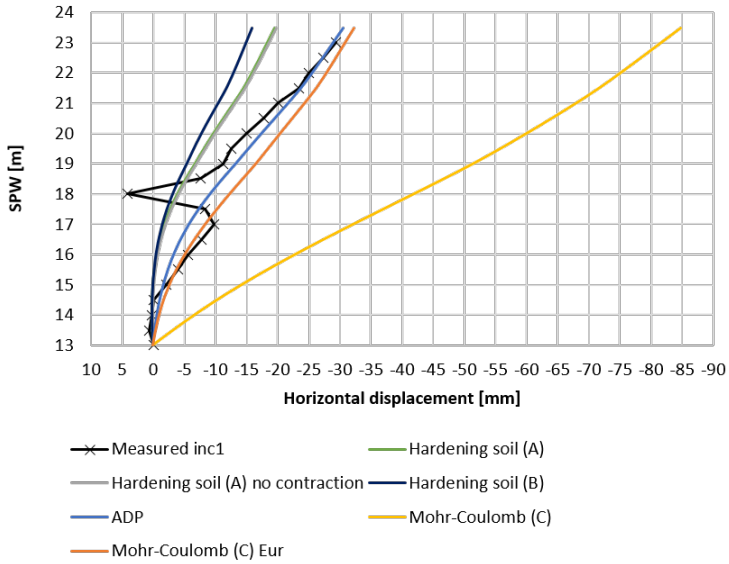
### Excavation +18.5



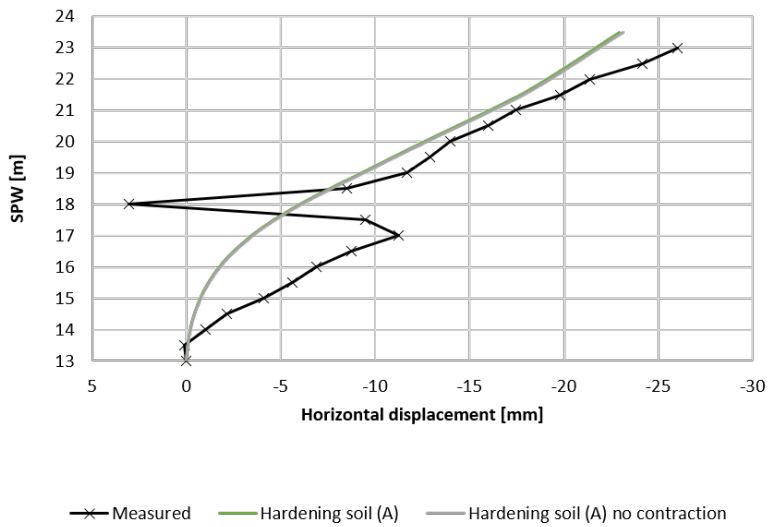
### Installation bottom anchor row



### Excavation +18



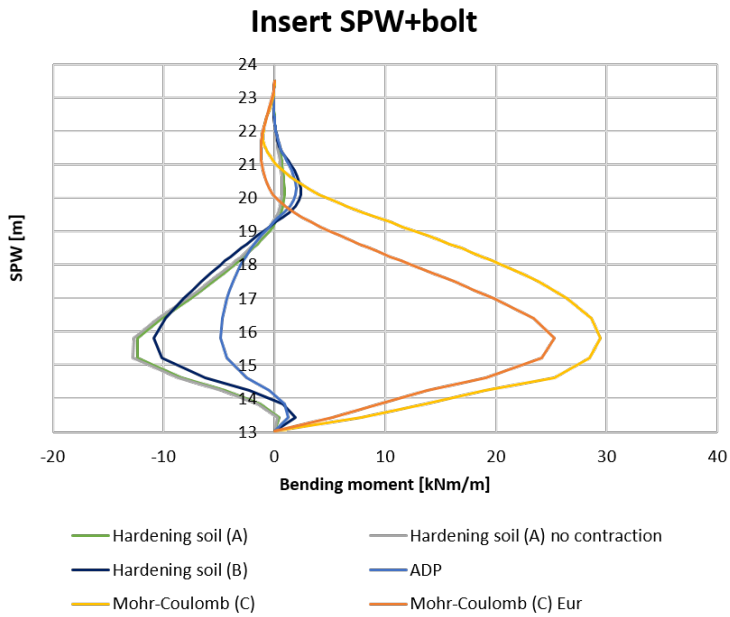
### Consolidation



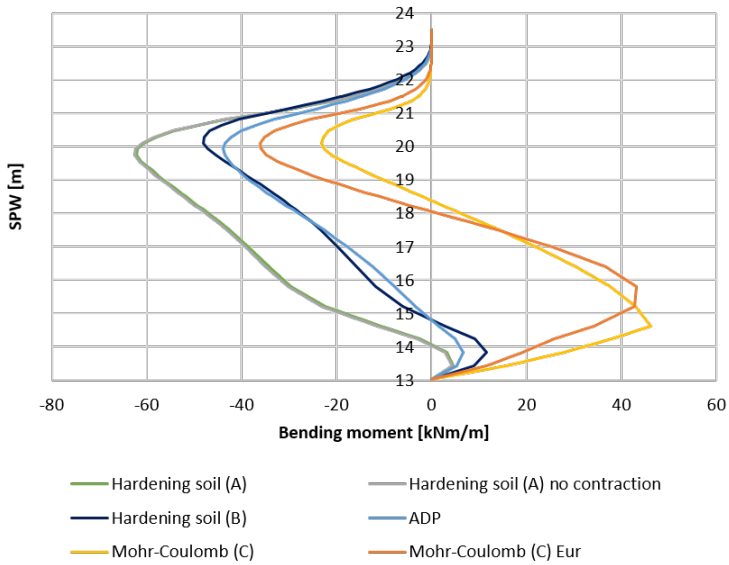


---

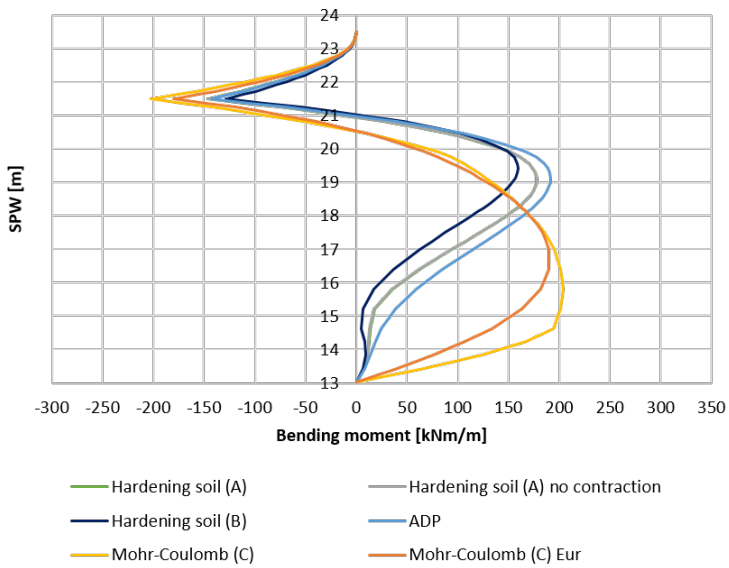
## G.2 Bending moment of SPW with partial effect of LCC in PLAXIS



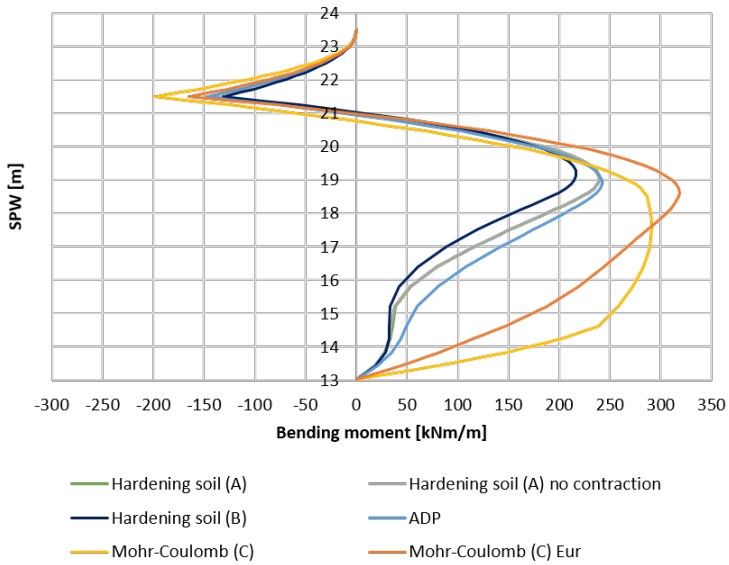
### Excavation +21



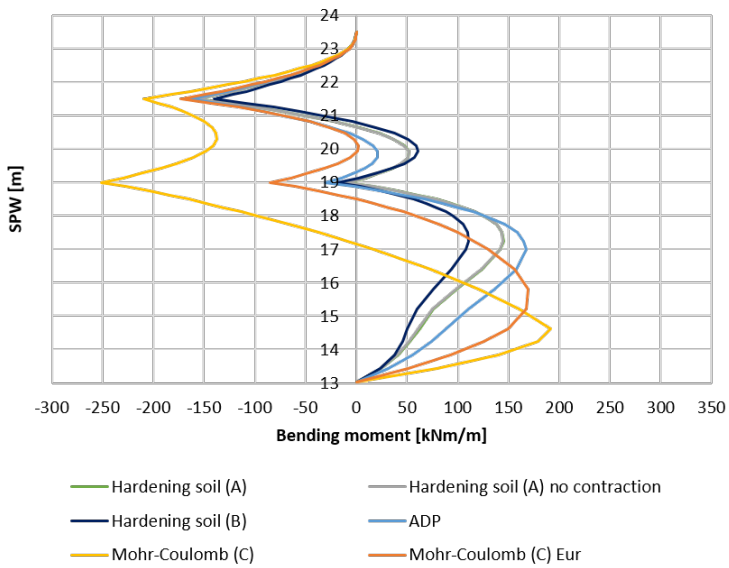
### Installation top anchor row



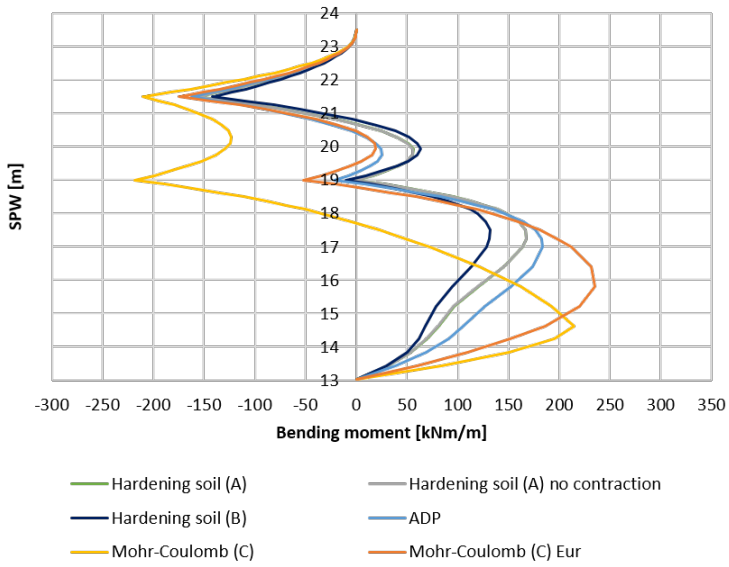
### Excavation +18.5



### Installation bottom anchor row

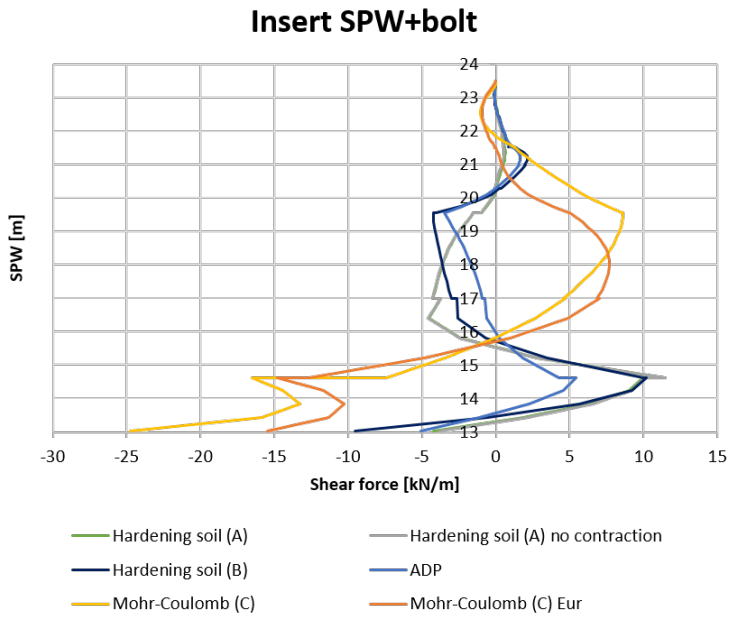


## Excavation +18

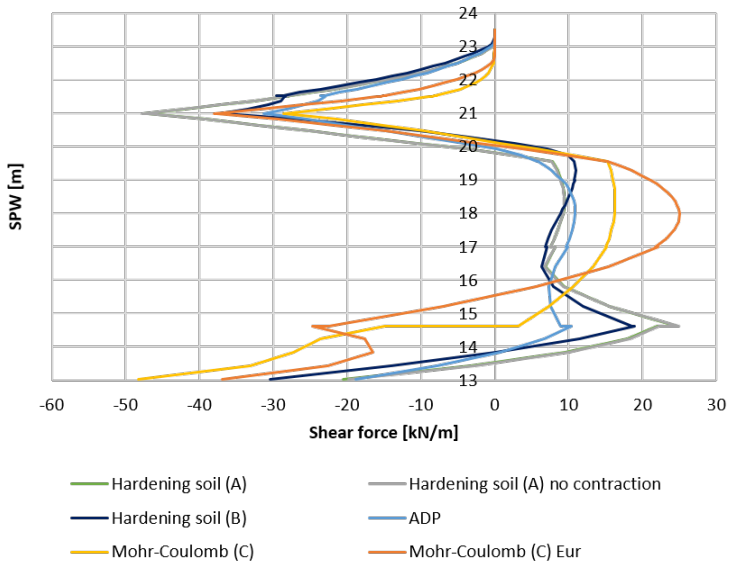


---

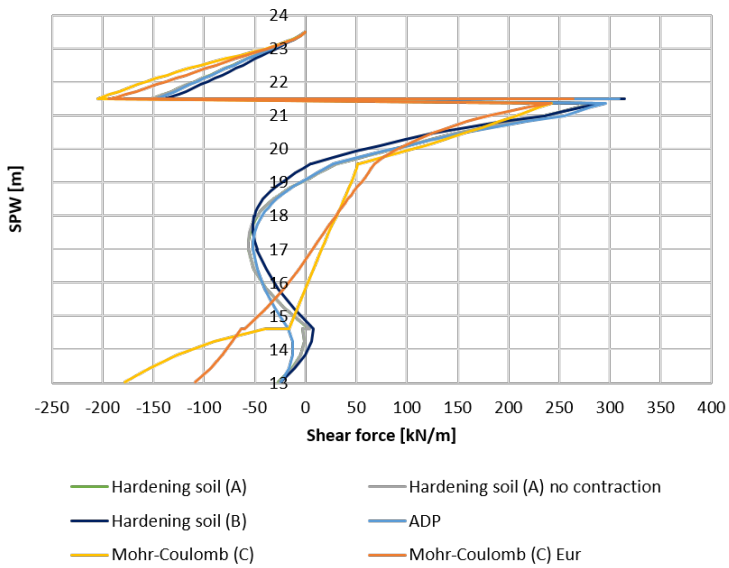
### G.3 Shear force of SPW with partial effect of LCC in PLAXIS



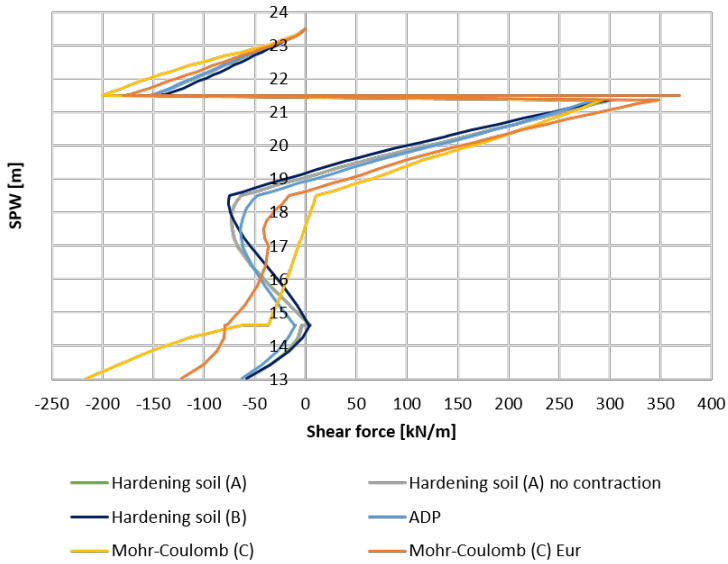
### Excavation +21



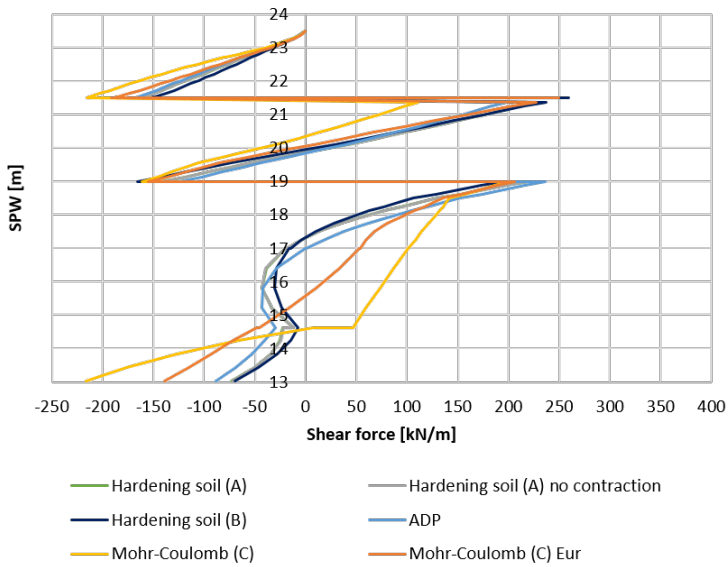
### Installation top anchor row



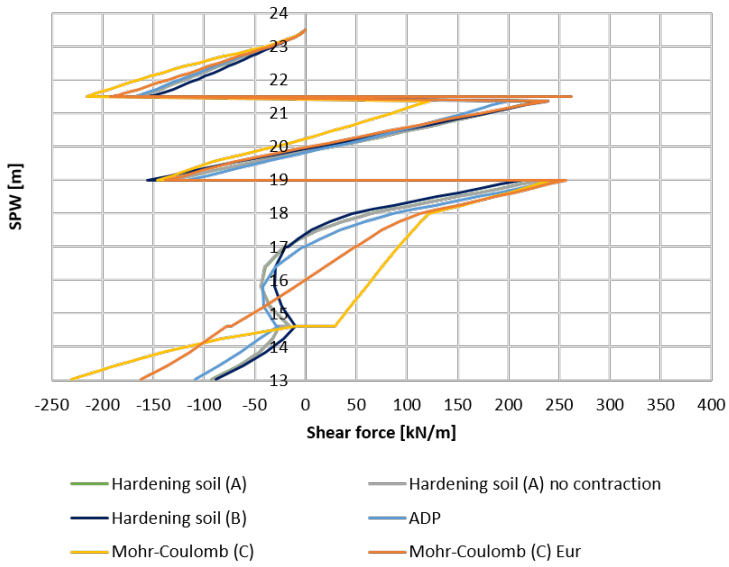
### Excavation +18.5



### Installation bottom anchor row

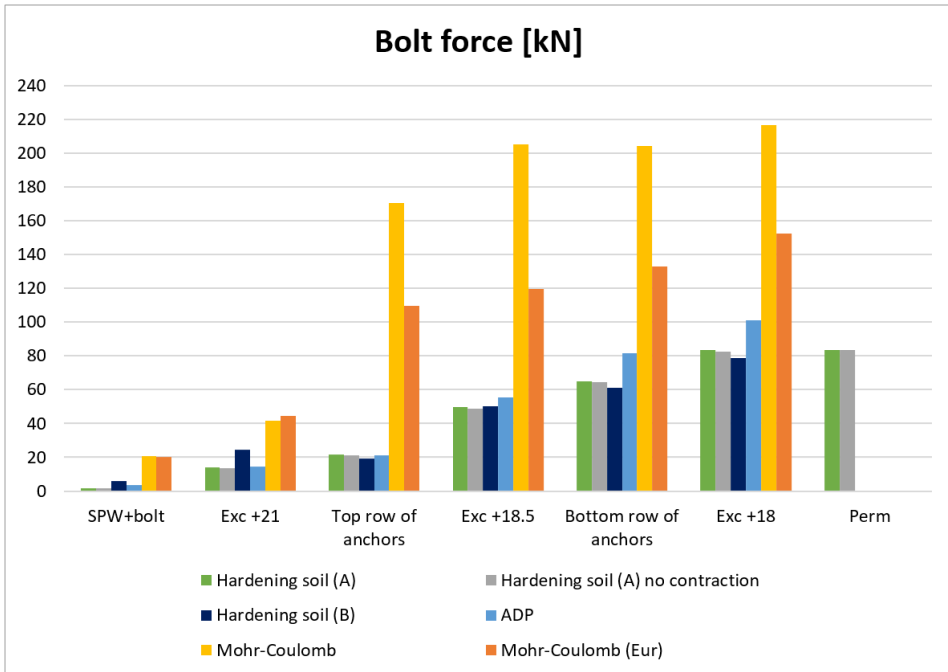


## Excavation +18

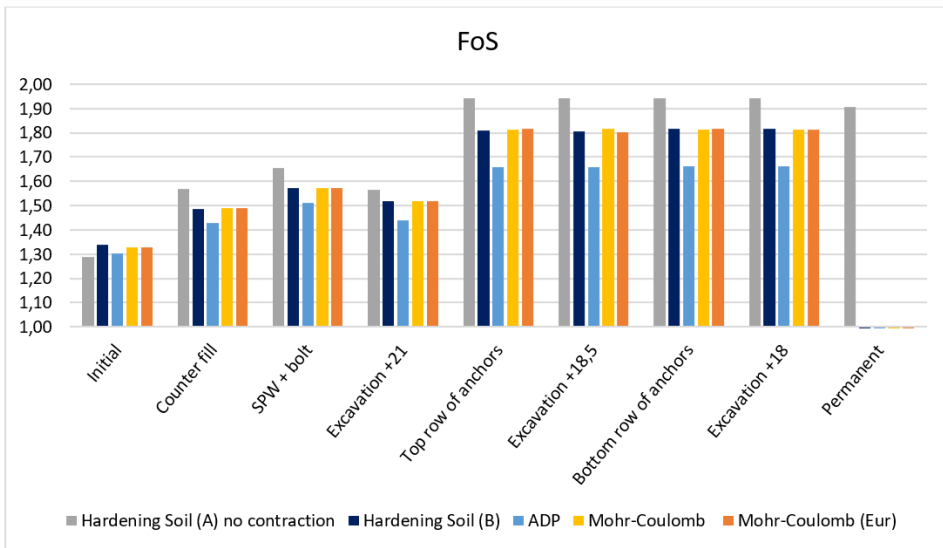




## G.4 Bolt force with partial effect of LCC in PLAXIS



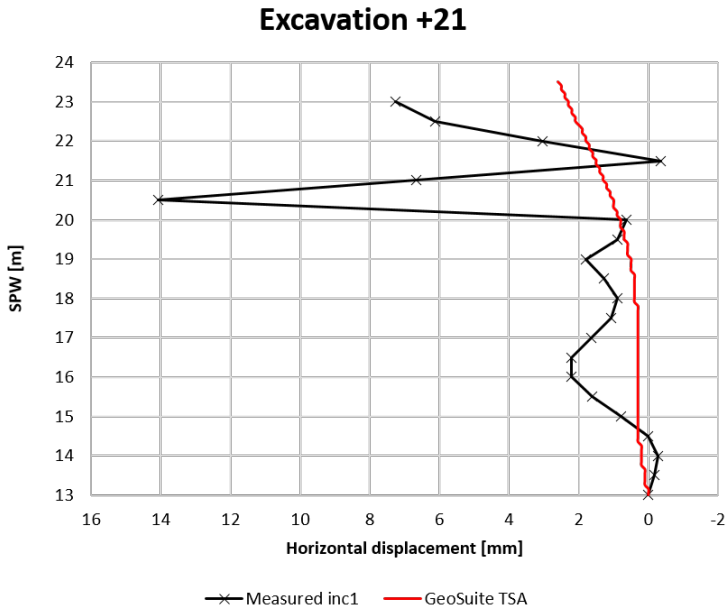
## G.5 FoS in all phases with partial effect of LCC in PLAXIS



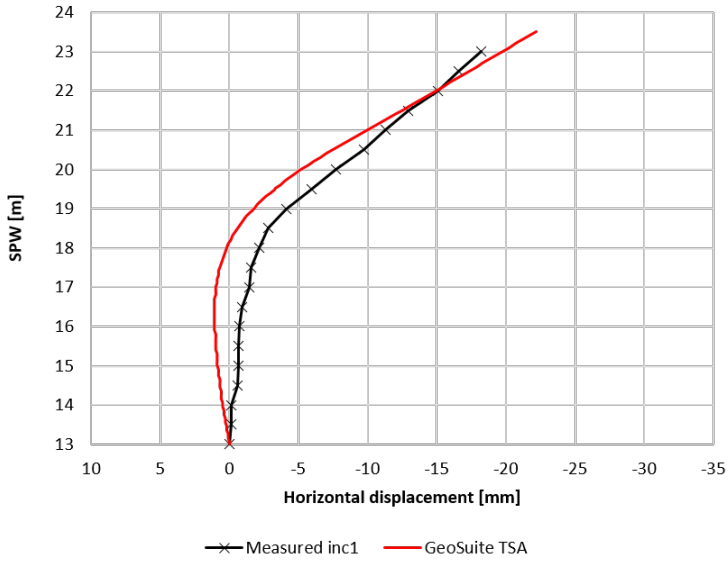
# Appendix H

## GS modeled with $r = 0.4$ results

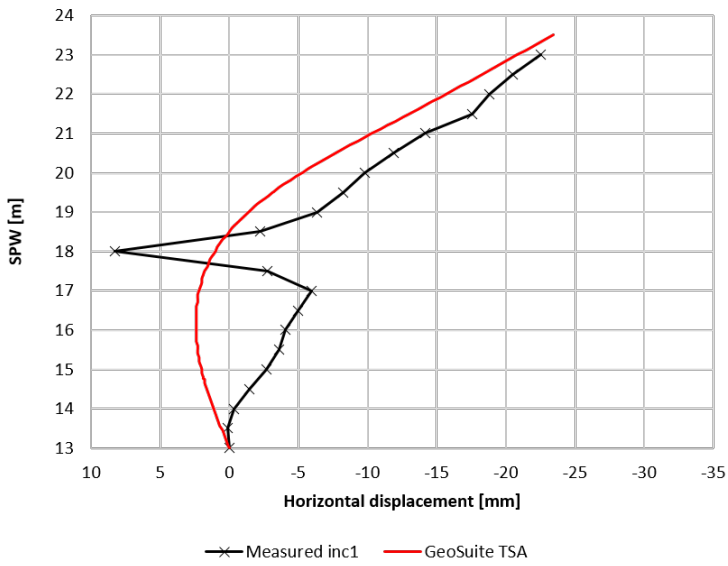
### H.1 Displacement of SPW for $r = 0.4$ in GeoSuite Excavation



### Installation top anchor row

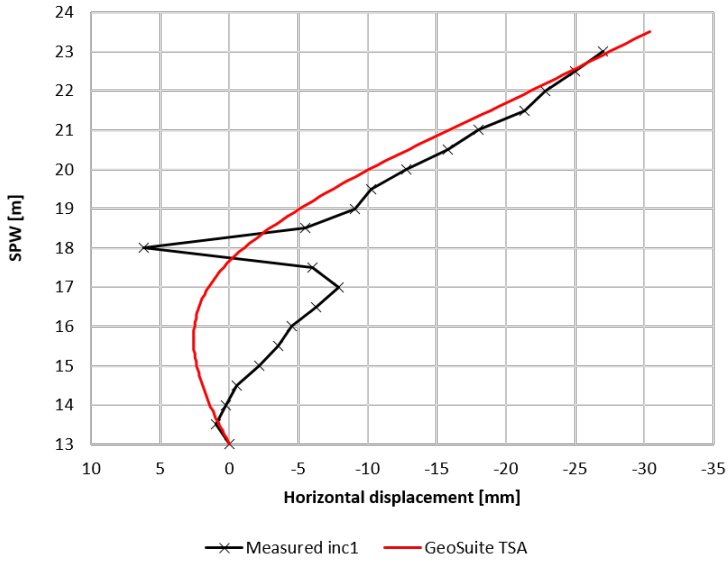


### Excavation +18.5

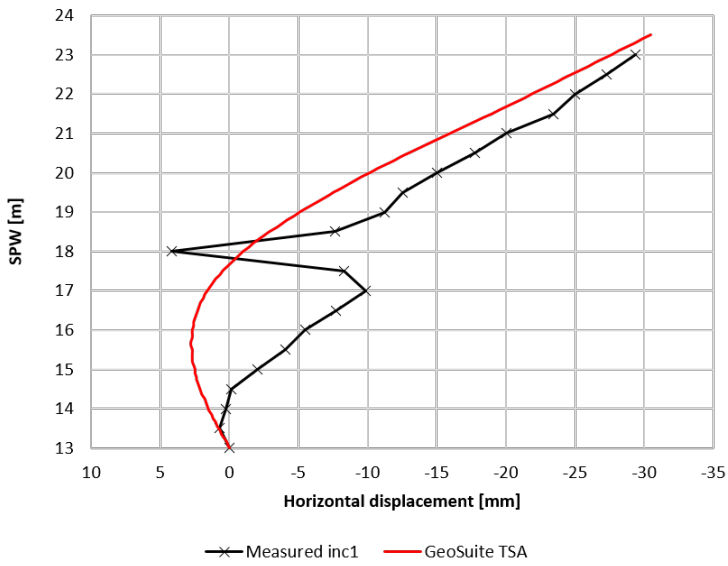


---

### Installation bottom anchor row

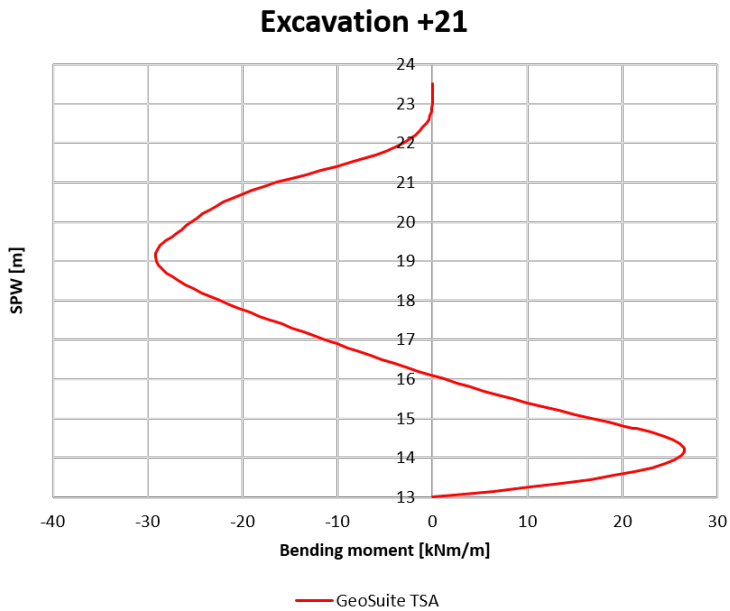


### Excavation +18



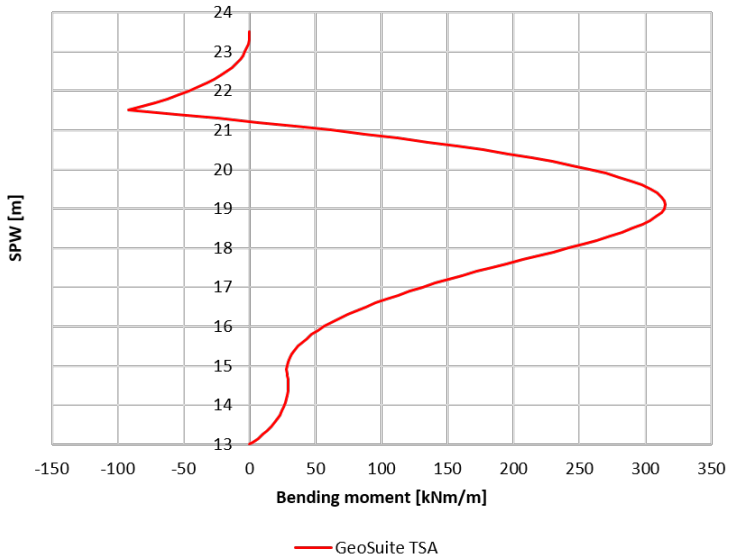
---

## H.2 Bending moment of SPW for $r = 0.4$ in GeoSuite Excavation

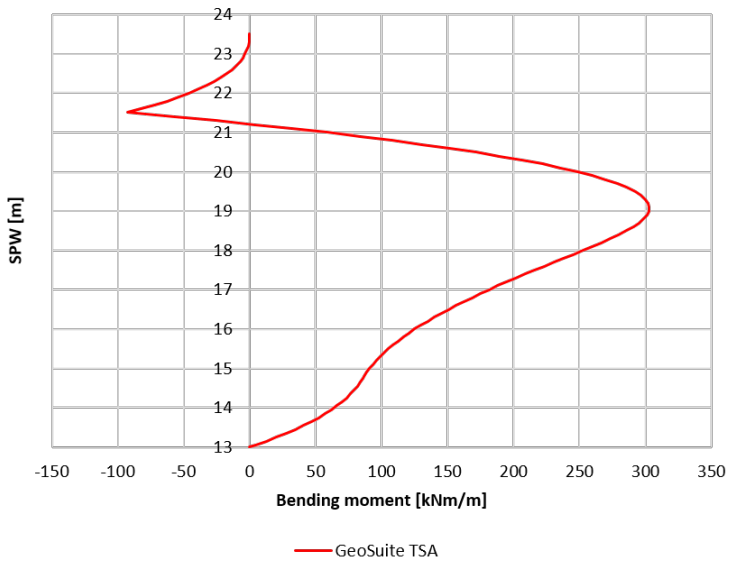


---

### Installation top anchor row

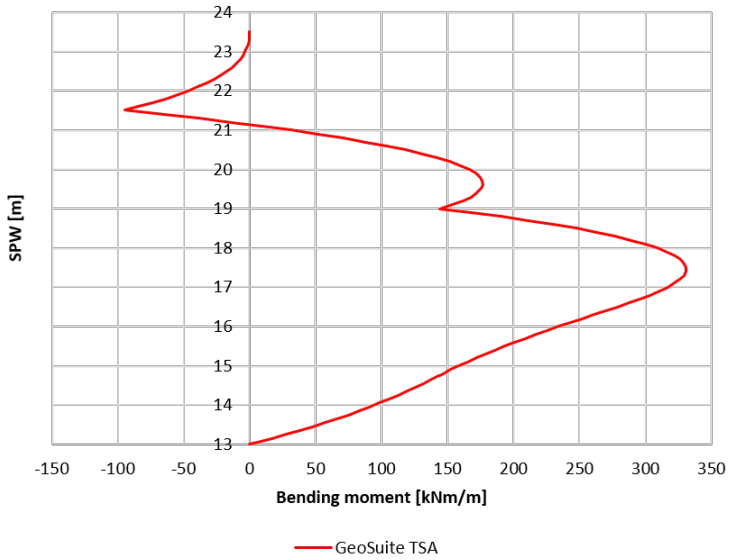


### Excavation +18.5

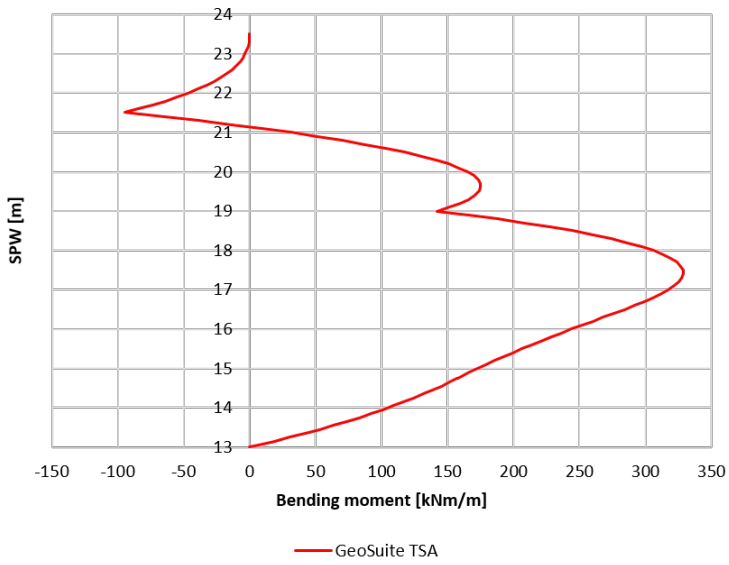


---

### Installation bottom anchor row



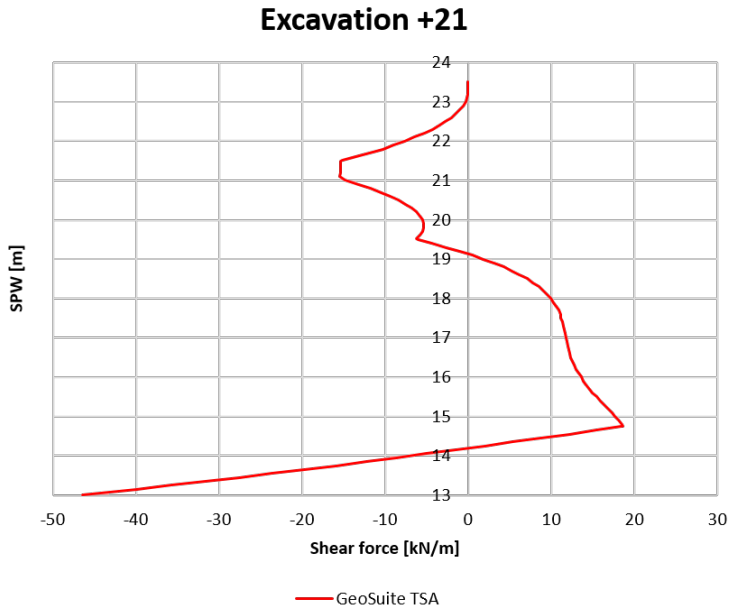
### Excavation +18



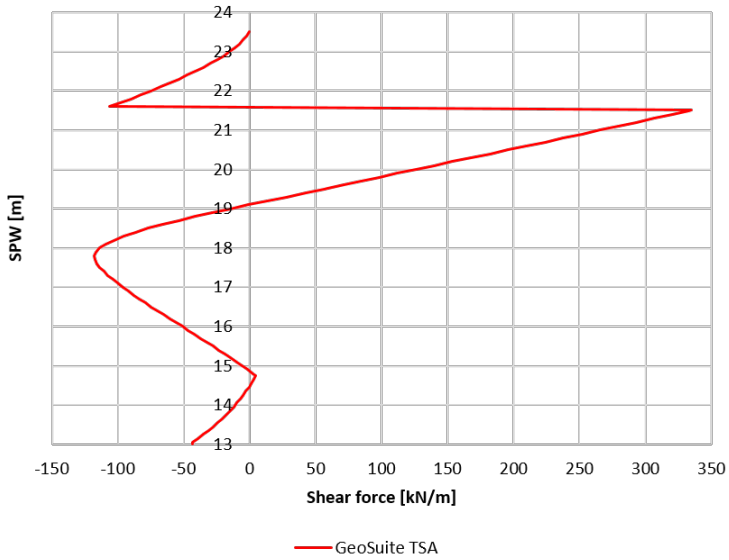


---

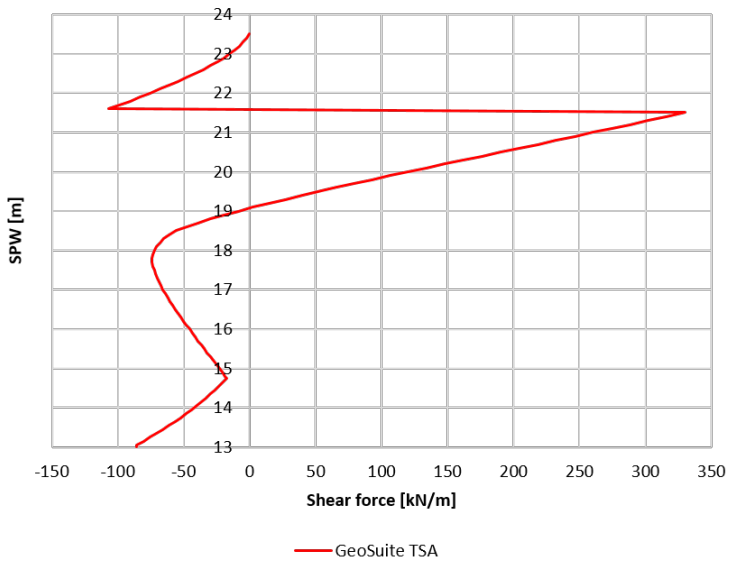
### H.3 Shear force of SPW for $r = 0.4$ in GeoSuite Excavation



### Installation top anchor row

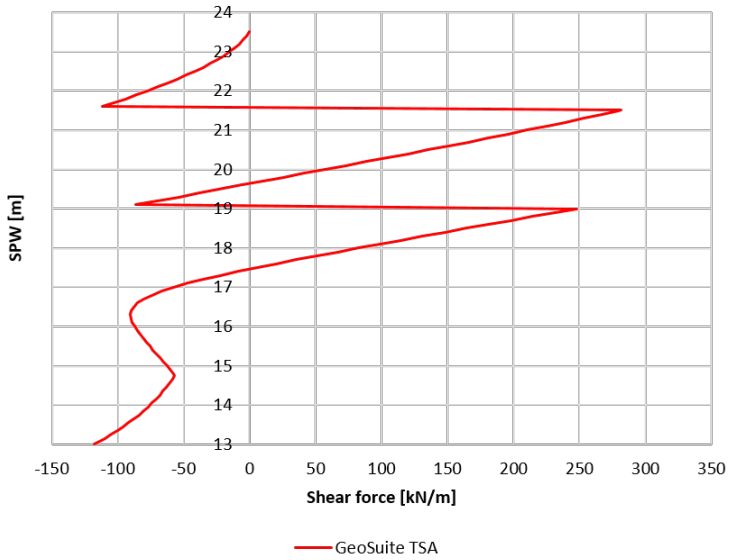


### Excavation +18.5

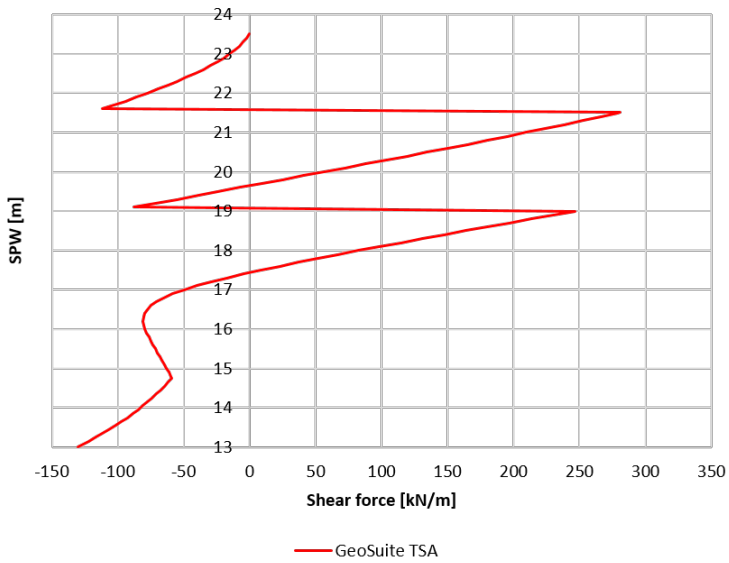


---

### Installation bottom anchor row



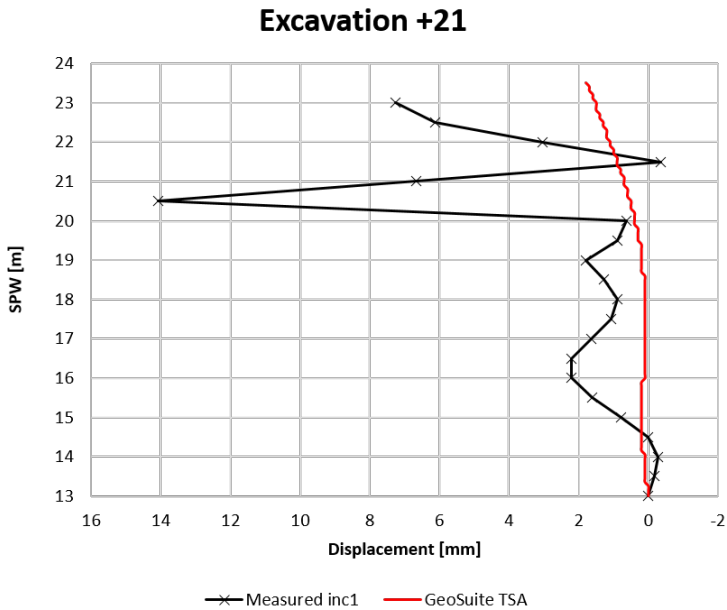
### Excavation +18





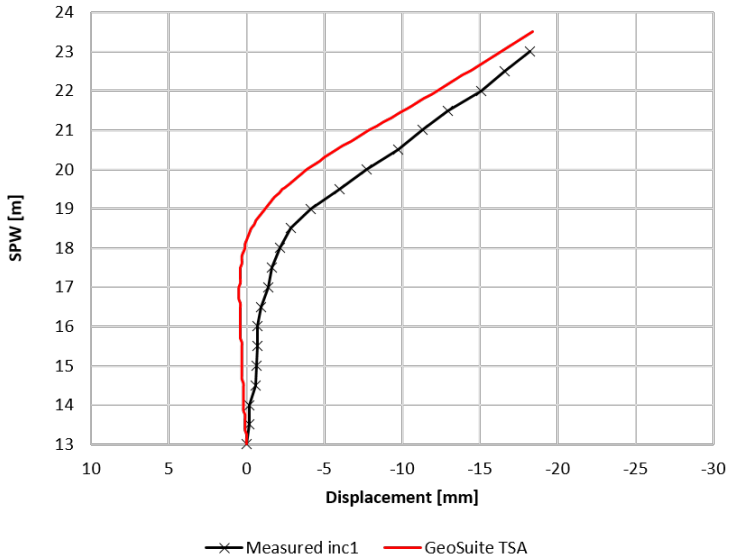
# GS modeled with full effect of LCC results

## I.1 Displacement of SPW with full effect of LCC in GS Excavation

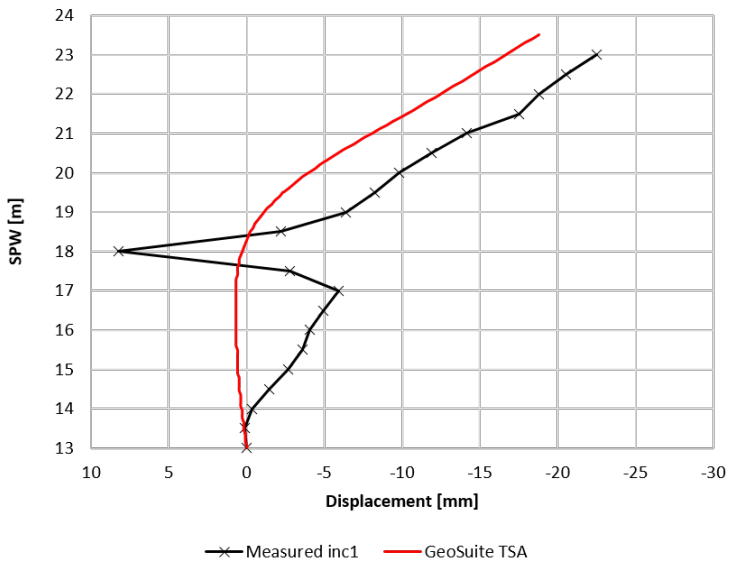


---

### Installation top anchor row

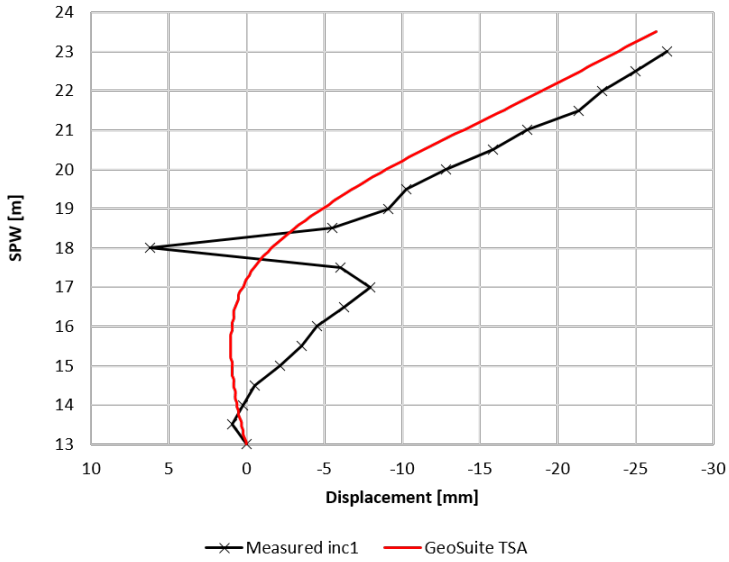


### Excavation +18.5

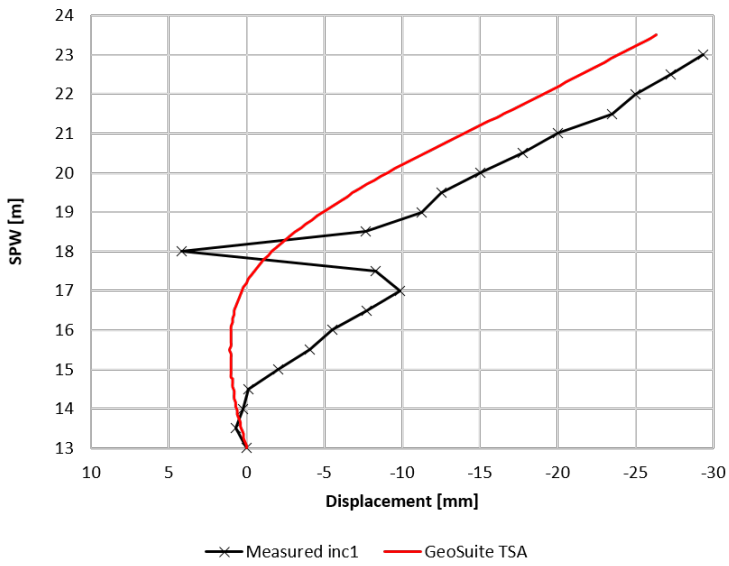


---

### Installation bottom anchor row

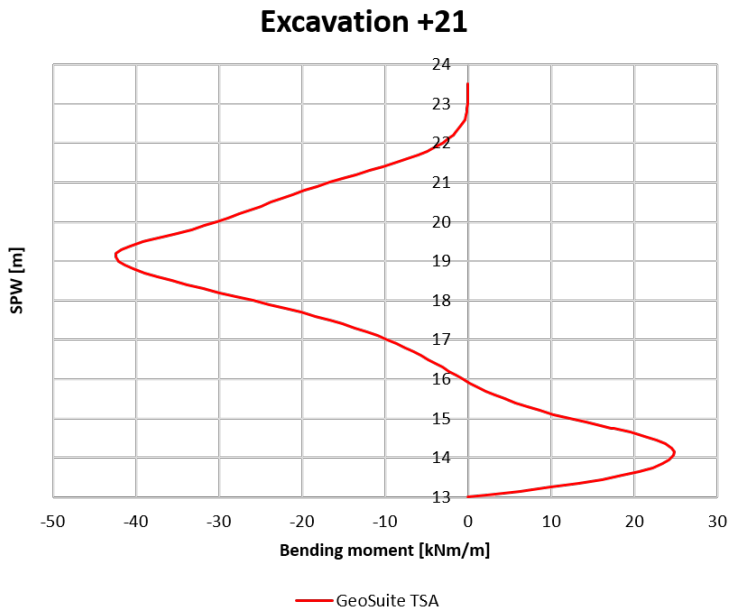


### Excavation +18



---

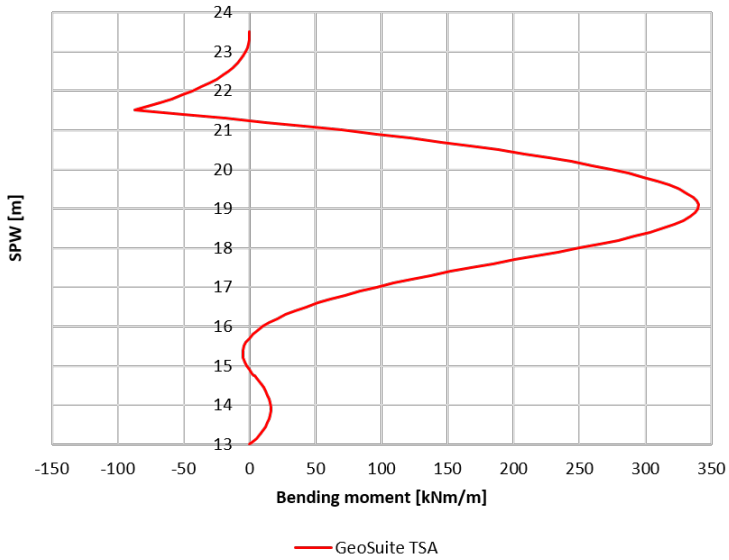
## I.2 Bending moment of SPW with full effect of LCC in GS Excavation



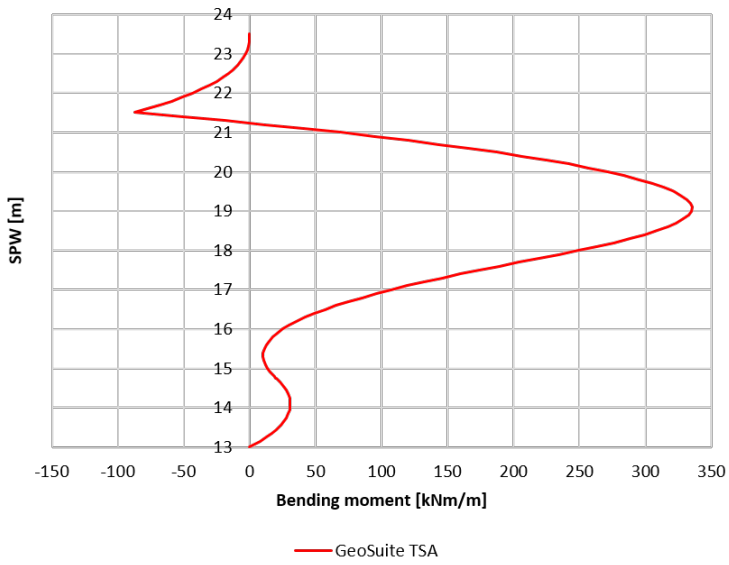


---

### Installation top anchor row

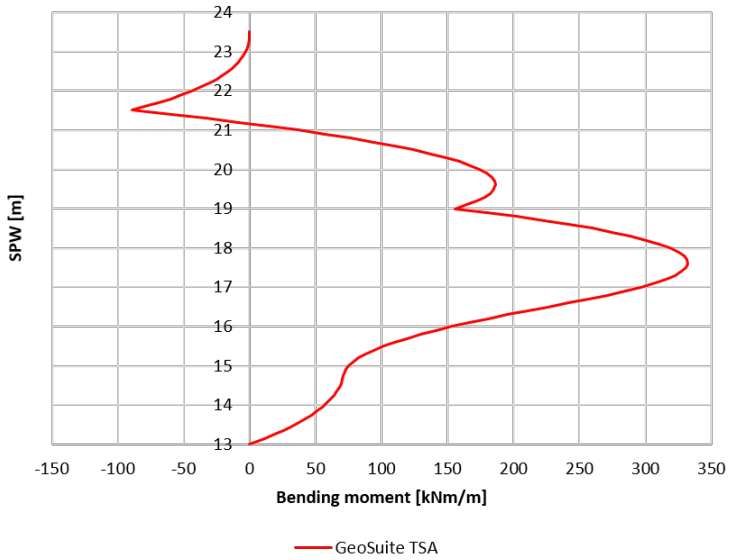


### Excavation +18.5

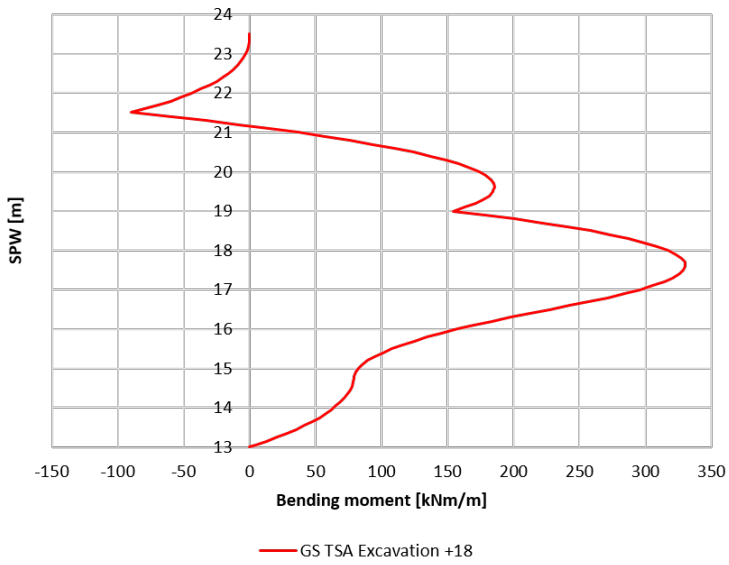


---

### Installation bottom anchor row

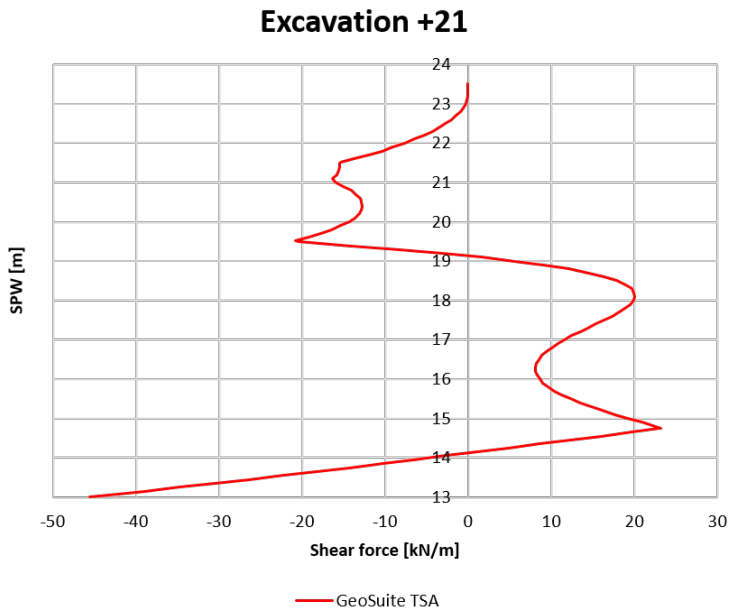


### Excavation +18

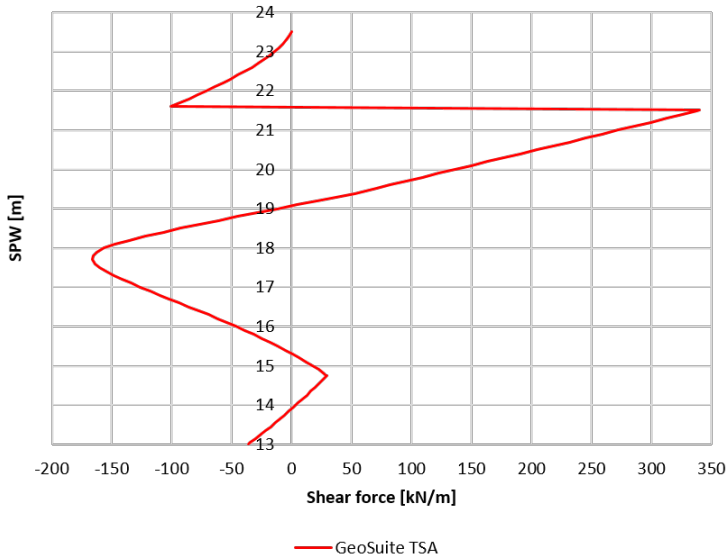


---

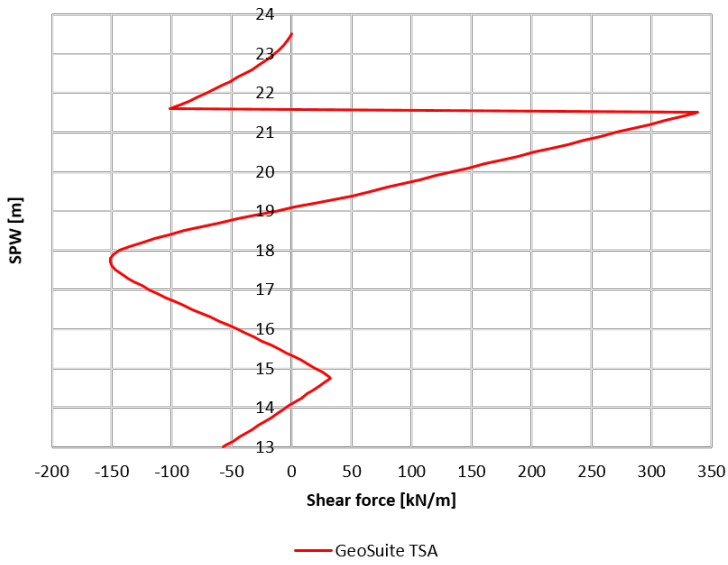
### I.3 Shear force of SPW with full effect of LCC in GS Excavation



### Installation top anchor row

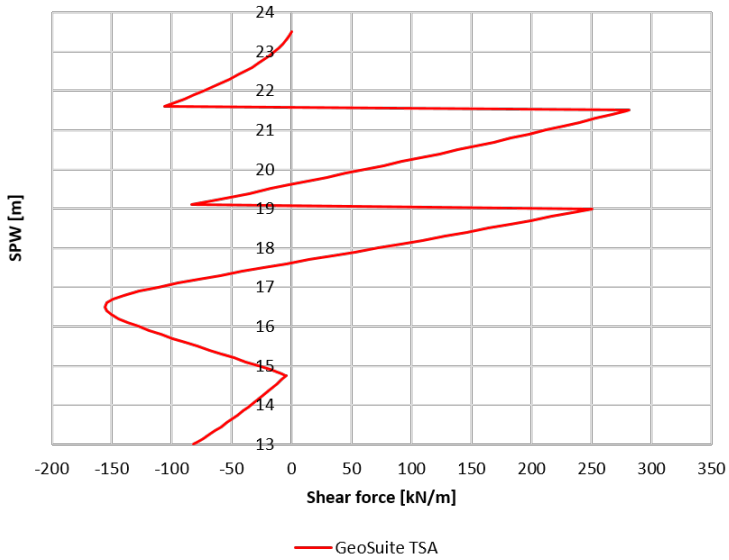


### Excavation +18.5

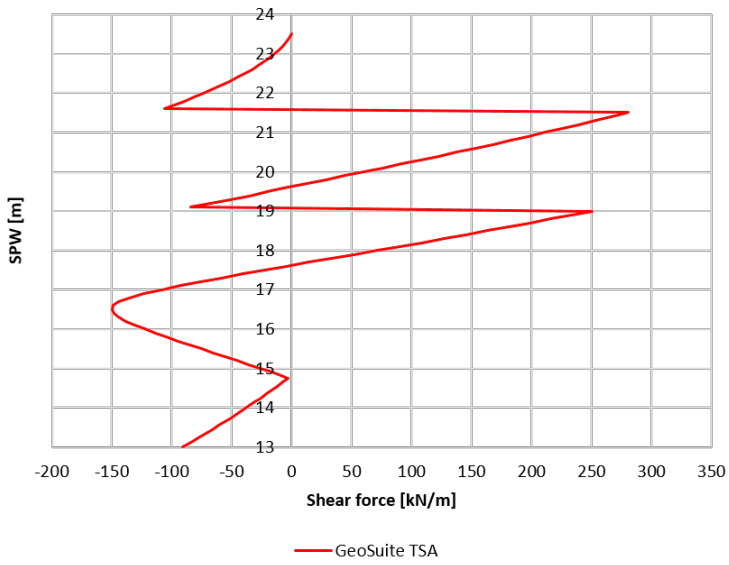


---

### Installation bottom anchor row



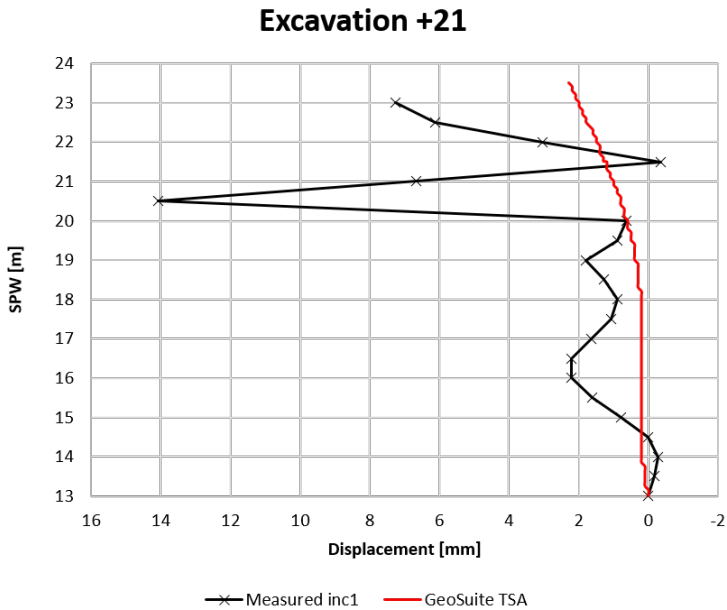
### Excavation +18



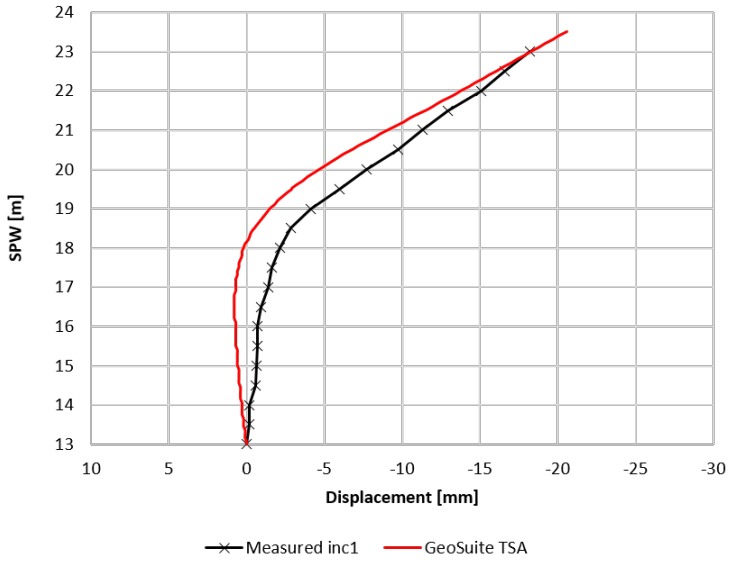


# GS modeled with partial effect of LCC results

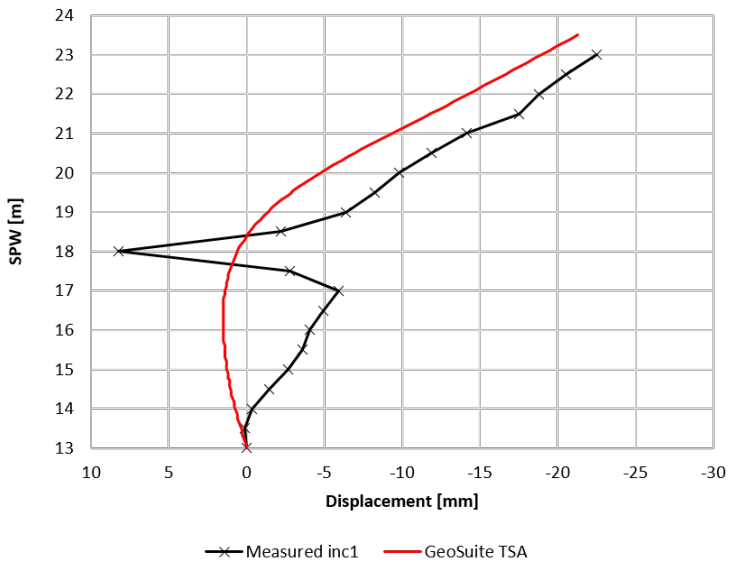
## J.1 Displacement of SPW with partial effect of LCC in GS Excavation



### Installation top anchor row



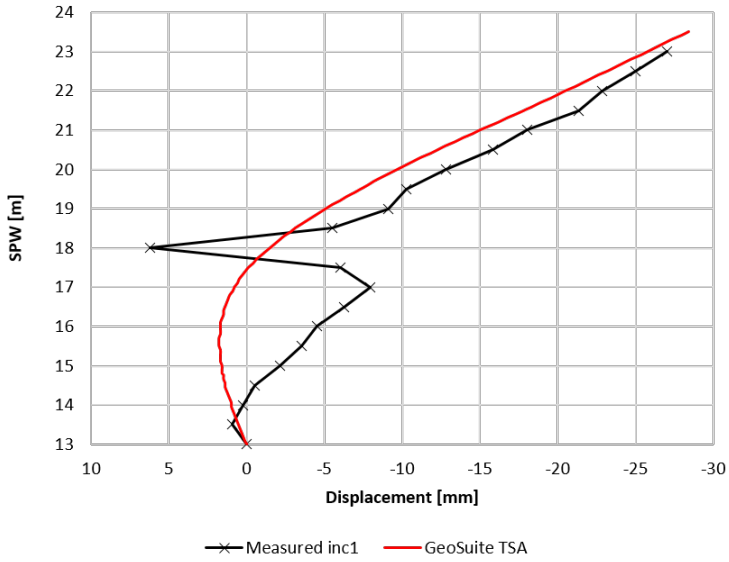
### Excavation +18.5



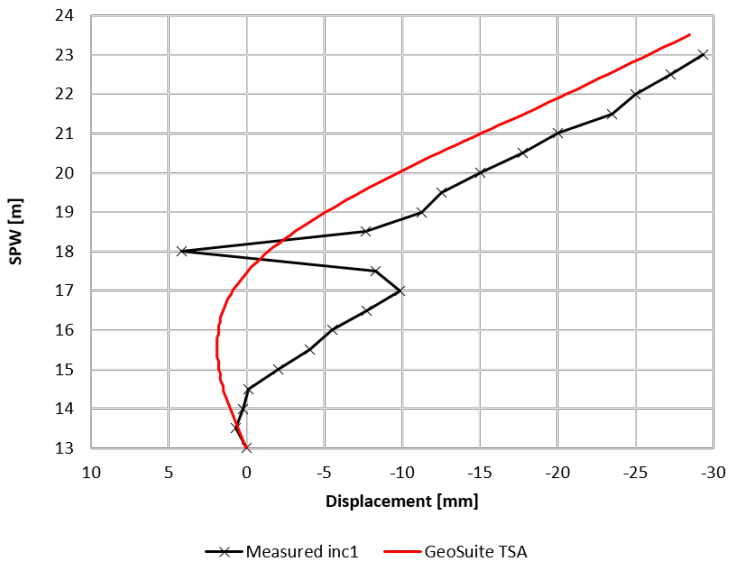


---

### Installation bottom anchor row

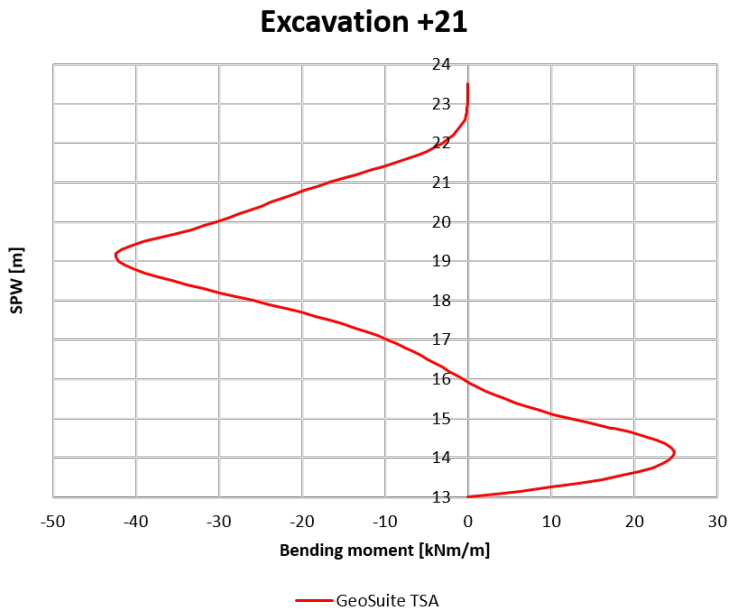


### Excavation +18



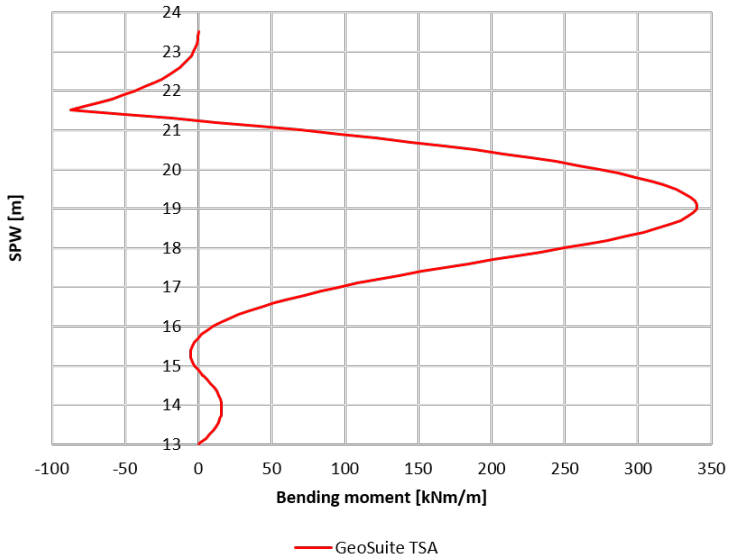
---

## J.2 Bending moment of SPW with partial effect of LCC in GS Excavation

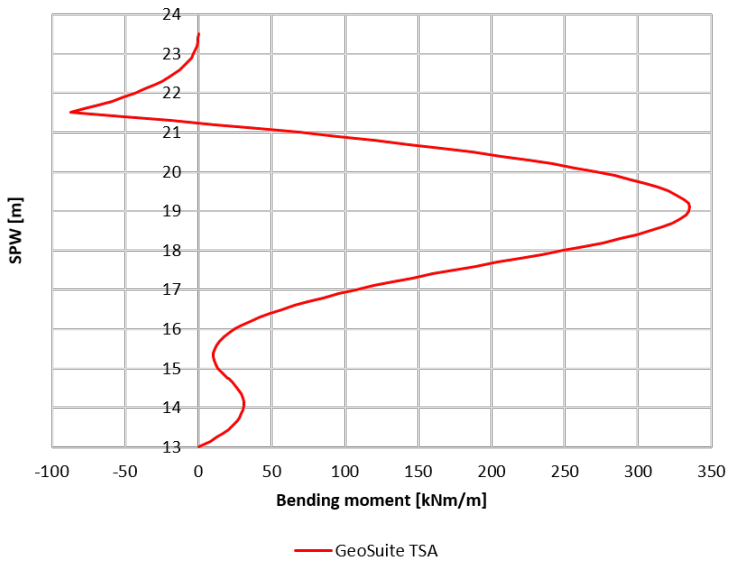


---

### Installation top anchor row

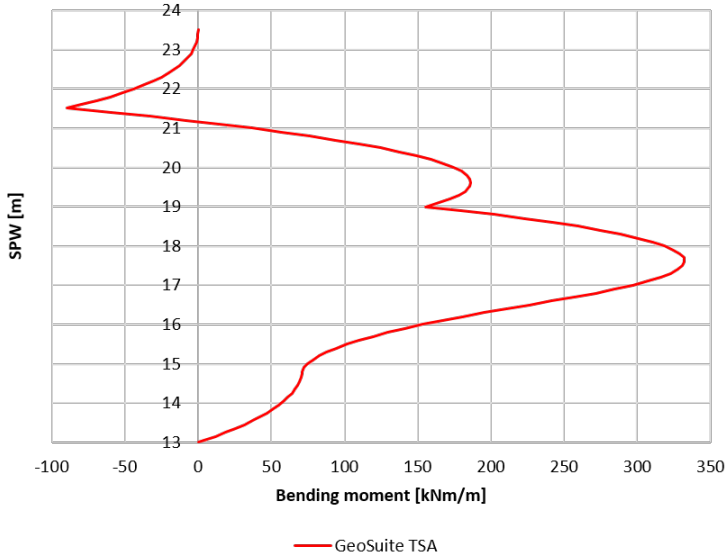


### Excavation +18.5

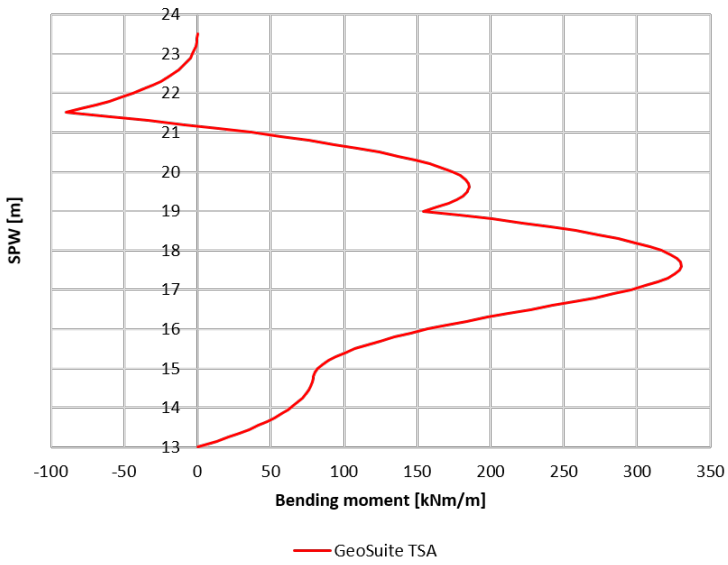


---

### Installation bottom anchor row

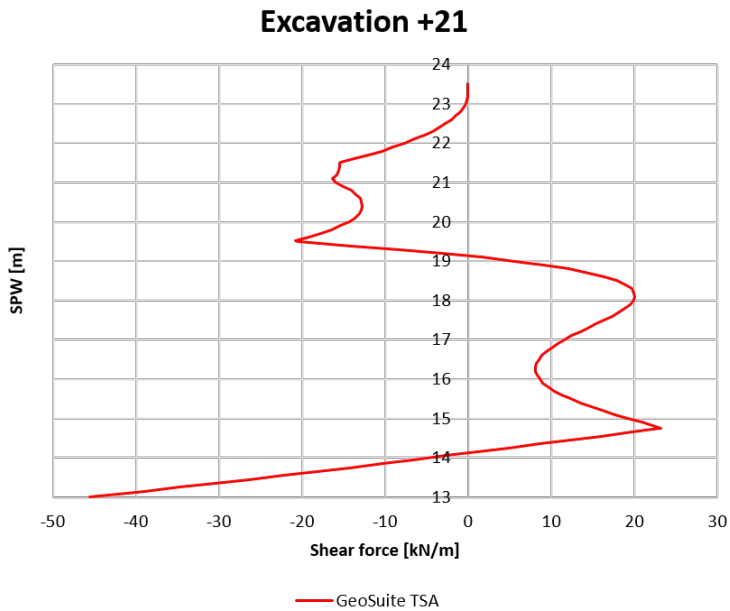


### Excavation +18



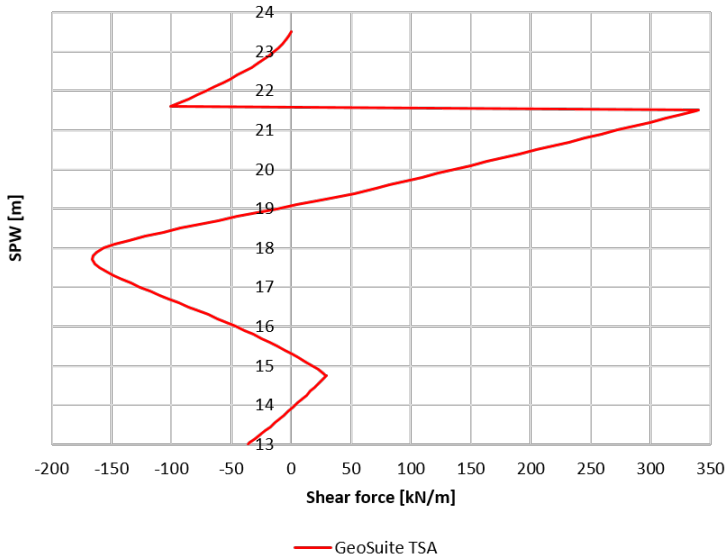
---

### J.3 Shear force of SPW with partial effect of LCC in GS Excavation

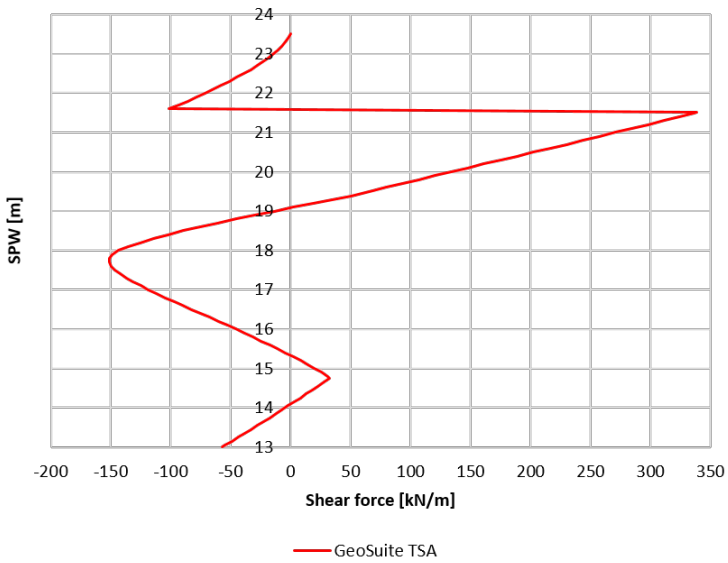


---

### Installation top anchor row

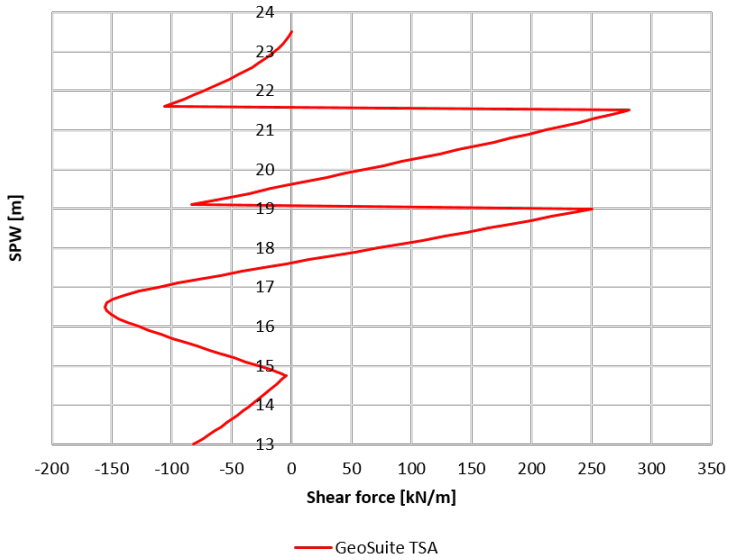


### Excavation +18.5

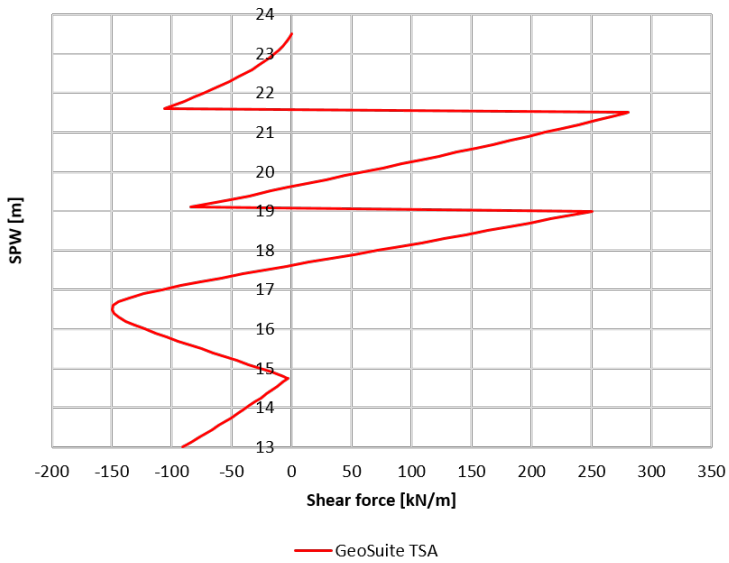


---

### Installation bottom anchor row



### Excavation +18







# Appendix **K**

## Hand calculation results

### K.1 Earth pressure calculation

<b>z [m]</b>	<b>Elevation [m]</b>	$p_v^a$ [kPa]	$p_a$ [kPa]	$p_v^p$ [kPa]	$p_p$ [kPa]
0.0	23.5	100	29	-	-
2.0	21.5	139	42	-	-
2.0	21.5	138	52	-	-
4.0	19.5	176	90	-	-
4.0	19.5	176	108	-	-
5.5	18.0	204	131	-	-
10.5	13.0	300	208	95	187